Vol. 188, October 31, 1986
Complete in one issue

ISSN 0003-2670

ANALYTICA CHIMICA ACTA

International journal devoted to all branches of analytical chemistry

ELSEVIER

ANALYTICA CHIMICA ACTA

International journal devoted to all branches of analytical chemistry
Revue internationale consacrée à tous les domaines de la chimie analytique
Internationale Zeitschrift für alle Gebiete der analytischen Chemie

PUBLICATION SCHEDULE FOR 1986

	J	F	M	A	M	J	J	A	S	O	N	D
Analytica Chimica Acta	179	180	181	182	183	184	185	186	187	188	189	190 191

Scope. *Analytica Chimica Acta* publishes original papers, short communications, and reviews dealing with eve aspect of modern chemical analysis both fundamental and applied.

Submission of Papers. Manuscripts (three copies) should be submitted as designated below for rapid and efficie handling:

Papers from the Americas to: Professor Harry L. Pardue, Department of Chemistry, Purdue University, West Lafayet IN 47907, U.S.A.

Papers from all other countries to: Dr. A. M. G. Macdonald, Department of Chemistry, The University, P.O. Box 36 Birmingham B15 2TT, England. Papers dealing particularly with computer techniques to: Professor J. T. Cle Universität Bern, Pharmazeutisches Institut, Baltzerstrasse 5, CH-3012 Bern, Switzerland.

Submission of an article is understood to imply that the article is original and unpublished and is not being consider for publication elsewhere. Upon acceptance of an article by the journal, authors will be asked to transfer the copyrig of the article to the publisher. This transfer will ensure the widest possible dissemination of information.

Information for Authors. Papers in English, French and German are published. There are no page charge Manuscripts should conform in layout and style to the papers published in this Volume. Authors should cons Vol. 170 for detailed information. Reprints of this information are available from the Editors or from: Elsevier Editor Services Ltd., Mayfield House, 256 Banbury Road, Oxford OX2 7DH (Great Britain).

Reprints. Fifty reprints will be supplied free of charge. Additional reprints (minimum 100) can be ordered. An ord form containing price quotations will be sent to the authors together with the proofs of their article.

Advertisements. Advertisement rates are available from the publisher.

Subscriptions. Subscriptions should be sent to: Elsevier Science Publishers B.V., Journals Department, P.O. B 211, 1000 AE Amsterdam, The Netherlands. Tel: 5803 911, Telex: 18582.

Publication. *Analytica Chimica Acta* appears in 13 volumes in 1986. The subscription for 1986 (Vols. 179–191) Dfl. 2730.00 plus Dfl. 312.00 (p.p.h.) (total approx. US $1192.94). All earlier volumes (Vols. 1–178) except Vols. 2 and 28 are available at Dfl. 231.00 (US $90.59), plus Dfl. 15.00 (US $5.88) p.p.h., per volume.

Our p.p.h. (postage, packing and handling) charge includes surface delivery of all issues, except to subscribers in t U.S.A., Canada, Japan, Australia, New Zealand, P.R. China, India, Israel, South Africa, Malaysia, Thailand, Singapo South Korea, Taiwan, Pakistan, Hong Kong, Brazil, Argentina and Mexico, who receive all issues by air delive (S.A.L. — Surface Air Lifted) at no extra cost. For the rest of the world, airmail and S.A.L. charges are available up request.

Claims for issues not received should be made within three months of publication of the issues. If not they cannot b honoured free of charge.

For further information, or a free sample copy of this or any other Elsevier Science Publishers journal, readers in t U.S.A. and Canada can contact the following address: Elsevier Science Publishing Co. Inc., Journal Informatic Center, 52 Vanderbilt Avenue, New York, NY 10017, U.S.A., Tel: (212) 916-1250.

0003-2670/86/$03.

Printed in The Netherlands

ANALYTICA CHIMICA ACTA
VOL. 188 (1986)

ANALYTICA CHIMICA ACTA

International journal devoted to all branches of analytical chemistry

ELSEVIER Amsterdam–Oxford–New York–Tokyo

Anal. Chim. Acta, Vol. 188 (1986)

0003-2670/86/$03.50

PRINTED IN THE NETHERLANDS

Analytica Chimica Acta, 188 (1986) 1—7
Elsevier Science Publishers B.V., Amsterdam — Printed in The Netherlands

DETERMINATION OF TRACE AMOUNTS OF VANADIUM(IV) AND (V) IN WATER BY ENERGY-DISPERSIVE X-RAY FLUORESCENCE SPECTROMETRY COMBINED WITH PRECONCENTRATION AND SEPARATION

KAZUO HIRAYAMA[a] and D. E. LEYDEN*
Department of Chemistry, Colorado State University, Fort Collins, CO 80523 (U.S.A.)
(Received 28th February 1986)

SUMMARY

A method is described for the separation, preconcentration and quantitation of V(IV) and V(V) in water. Vanadium(V) is precipitated with diethyldithiocarbamate (DDTC) at pH 1.8 and V(IV) is precipitated with DDTC at pH 4. The precipitates are collected by vacuum filtration on a membrane filter for quantitation by energy-dispersive x-ray fluorescence spectrometry. Multi-element and single-element calibration curves are prepared and used to evaluate the matrix and mass effects of diverse ions such as Fe(III), Co(II), Ni(II), Cu(II), Zn(II) and Pb(II). The total amount of metal ions should not exceed about 100 μg. The V(IV) and V(V) are separated completely and recovered quantitatively.

Increasing attention has been given to energy-dispersive x-ray fluorescence (e.d.x.r.f.) spectrometry for the determination of trace elements in water when combined with preconcentration techniques [1—5]. Precipitation with chelating reagents provides a specimen well suited for e.d.x.r.f. and a convenient procedure for collecting trace metal ions from water. Many reagents such as 8-quinolinol [6], ammonium pyrrolidinedithiocarbamate [7], immobilized dithiocarbamate [8], dibenzyldithiocarbamate [9] and sodium diethyldithiocarbamate (DDTC) [10] have been used. Most of these methods recover only specific oxidation states of metal ions. When there is only one oxidation state of significant concentration, these methods may be acceptable. However, several elements exist in more than one oxidation state in nature. Vanadium is a typical element with many stable oxidation states.

Vanadium exists as V(IV) and V(V) in well-aerated natural and industrial waters. Cole et al. [11] reported that the oxidation state of vanadium changes in aqueous solution, and a standard solution of vanadium will contain mixtures of V(IV) and V(V) which change with time. It is essential to be able to differentiate between the two oxidation states in water because of their different toxicity and nutritional properties [12—14]. But many

[a]Present address: Department of Industrial Chemistry, College of Engineering, Nihon University, Koriyama, Fukushima 963, Japan.

0003-2670/86/$03.50

analytical methods reported in the literature determine total vanadium without regard to its oxidation state [15, 16].

This paper describes a procedure for the separation of V(IV) from V(V) in acidic medium using DDTC, and quantitation of these species by e.d.x.r.f. V(V) is precipitated quantitatively by DDTC at pH 1.6—2 and V(IV) is subsequently precipitated at pH 4. Matrix and mass effects as well as the effect of diverse ions are discussed. The method is simple, rapid and has adequate sensitivity for practical applications.

EXPERIMENTAL

Reagents

Analytical-grade reagents and deionized/distilled water were used. Commercial atomic absorption standard solutions (Fisher Scientific) containing 1000 mg l^{-1} of V(V), Fe(III), Co(II), Ni(II), CU(II), Zn(II), Mn(II), or Pb(II) were used. Standard V(IV) solution (1000 mg l^{-1}) was prepared by dissolving vanadyl sulfate in 0.01 M hydrochloric acid (Ultrex, J. T. Baker). Working solutions were prepared by diluting the standard solutions with water and adjusting the nitric acid concentration to 0.01 M with Ultrex nitric acid. Potassium hydrogenphthalate (KHP) (2% w/v) was used to adjust the pH to 4.0 ± 0.5. The DDTC solution (1% w/v) was prepared by dissolving sodium diethyldithiocarbamate in water; the solution is stable for at least one month at room temperature.

Apparatus

All x-ray measurements were made using a TX5000 energy-dispersive x-ray spectrometer (Tracor Xray, Mountain View, CA). A rhodium target tube operated at 20 and 30 kV was used for vanadium and multi-element determinations, respectively. A 0.127-mm thick aluminum or a 0.05-mm thick rhodium filter was used to reduce spectral background for the tube voltages of 20 and 30 kV, respectively. The tube current was adjusted to give slightly less than 50% deadtime. The intensities of the *K*-lines of metals except Pb (*L*-lines) were extracted using the vendor program, XML. The x-ray net counts are the integrated peak counts minus background counts for the combined K_α and K_β lines, except L_α and L_β lines for lead. All samples were irradiated for 100 s.

Procedures

Preconcentration and separation of V(IV) and V(V). To precipitate V(V), a 100-ml aliquot of sample was placed in a 250-ml beaker and the pH was adjusted to 1.8 ± 0.1 with 0.1 M hydrochloric acid. Then, 4 ml of the 1.0% DDTC solution were added and the solution was stirred for 1 min using a magnetic stirrer. The solution was filtered under vacuum through a 25-mm diameter, 0.45-μm pore size membrane filter (Millipore, Type HA, Cat. No. HAPP02500). The filter was air-dried, and then mounted between 1/4-mil Mylar films on a Chemplex (Eastchester, NY) sample cup.

To precipitate V(IV), the pH of the filtrate from the previous step was adjusted to 4.0 ± 0.5 were 0.1 M potassium hydroxide and KHP, and 4 ml of the DDTC solution was added. Then, the solution was stirred for 10 min and filtered as described above.

Preparation of calibration curves. The pH of the standard solution was adjusted to 4.0 ± 0.5 which is optimum to precipitate both V(IV) and V(V) and other elements for multi-element calibration curves. Single-element calibration curves were obtained using standard solutions for each element. The concentration of vanadium in the standard solutions ranged from 0 to 100 μg/100 ml.

RESULTS AND DISCUSSION

Effect of pH

The effect of pH on the precipitation of V(V) and V(IV) with DDTC, and other metal ions such as Fe(III), Co(II), Ni(II), Cu(II), Zn(II) and Pb(II) was investigated. Figure 1 shows the effect of pH on the intensities of *K*-lines of vanadium for samples prepared from V(IV) and V(V). The intensities of the K_α and K_β lines of V(V) remained constant within the pH range 1.6—5.0, as did those of Cu(II), Ni(II) and Co(II). The intensities of the lines of Fe(III), Zn(II) and Pb(II) were constant over the pH range 3.5—5.0. The intensity of the line for V(IV) remained constant in the pH range 3.0—5.0, whereas V(IV) did not precipitate below pH 2.0. The filtrate from the pH 1.8 precipitation step was treated with 1.0 ml of potassium permanganate (0.2% w/v) to oxidize any vanadium that might have been reduced to V(IV). The solution was then treated with DDTC at pH 1.8 as before. As the concentration of V(V) in the second precipitation step was negligible, the recovery of 40 μg of V(V) in the initial precipitation was calculated to be 98.0 ± 2.5% (n = 5).

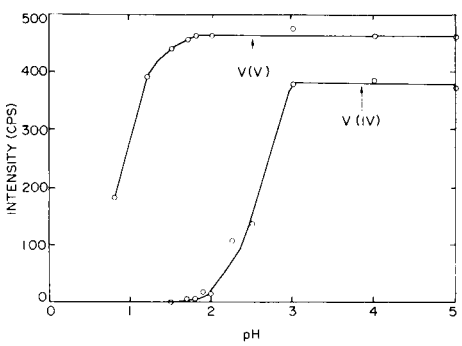

Fig. 1. X-ray intensity vs. pH for V(IV) and V(V).

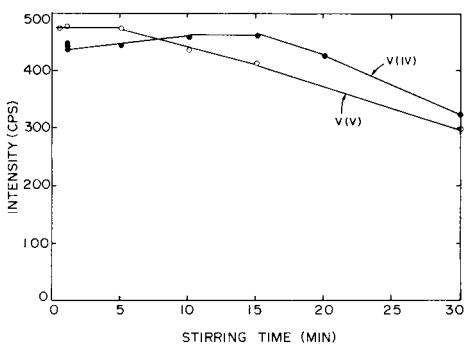

Fig. 2. X-ray intensity vs. stirring time before filtration for V(IV) and V(V).

Effect of stirring time

Most metal-DDTC precipitates are stable in acidic solution, and, to be sure of complete reaction, a stirring time of 15 min is recommended. However, some metal dithiocarbamates such as manganese(II)—DDTC [1], and zinc(II) dibenzyldithiocarbamate [9] redissolve during stirring. Iwasaki and Tanaka [16] reported that the V(V)—DDTC precipitate formed at pH 5 was stable for at least 1 h in the standing solution, but the effect of stirring time was not shown. For the precipitation of vanadium(V) pyrrolidinedithiocarbamate, Cole et al. [11] swirled the mixture for 15 s, which is a very short time compared to other studies. In a preliminary study, it was shown here that the V(V)—DDTC complex would redissolve if stirred for more than 15 min at pH 1.8, which is optimum to separate V(V) and V(IV).

The effect of stirring time on the precipitation of V(V) at pH 1.8 and V(IV) at pH 4.0 was examined. Figure 2 shows the intensities of K_α and K_β lines from 40 μg of V(V) and 34 μg of V(IV) at different stirring times. Each sample was allowed to stand for 5 min after stirring was stopped. At pH 1.8, the V(V)—DDTC precipitate formed, and then dissolved gradually with stirring. However, the loss is not significant for times between 15 s and 5 min. The V(IV)—DDTC complex was stable for stirring times up to 15 min. Therefore, 1 min and 10 min stirring times were selected for the precipitation of V(V)—DDTC and V(IV)—DDTC, respectively.

Calibration data

Single-element and multi-element calibration curves for vanadium were prepared. The pH of the standard solutions was maintained at 4 so that both V(IV) and V(V) that may exist in the standard solution can be quantitatively precipitated. Table 1 shows the linear regression calibration data for vanadium. The x-ray emission intensity was linearly related to the amount of vanadium up to 100 μg. The sensitivity in the range 0—40 μg for multi-element

TABLE 1

Linear regression of calibration data for vanadium

Tube voltage (kV)	Slope (cps/μg)	Intercept (cps)	Number of points	Std. error of estimate	Calibration range (μg)
20	11.6 ± 0.1[a]	−1.0 ± 4.5	14	8.1	0—100[c]
20	10.8 ± 0.2[a]	−0.6 ± 5.0	13	12.4	0—80[c]
20	11.4 ± 0.1[b]	−8.8 ± 2.9	12	6.3	0—40[c]
30	1.04 ± 0.02[a]	−0.72 ± 0.76	9	1.42	0—100
30	0.96 ± 0.01[b]	−0.06 ± 0.41	13	1.07	0—80
30	1.01 ± 0.01[b]	−0.71 ± 0.41	20	0.75	0—40

[a]Single-element standards. [b]Multi-element standards. [c]In each case, the lower limit of detection is 1.1—1.5 μg, based on a positive signal exceeding 3 times the standard deviation of the intercept of the linear regression calibration graph.

standards is in good agreement with that for single-element standards. But in the range 0—80 μg, the sensitivity decreased.

The ions Fe(III), Co(II), Ni(II), Cu(II), Zn(II) and Pb(II) were present in the multi-element standards in amounts ranging from 0 to 200 μg. These samples were irradiated using a 30-kV x-ray tube potential. As shown in Table 1, the sensitivity of the vanadium x-ray line decreases at 30 kV because of reduced excitation efficiency. Additionally, high vanadium concentration and/or the presence of other ions reduces the sensitivity for vanadium. This is undoubtedly a result of x-ray absorption by the increased mass of the precipitate. The correlation between the x-ray intensities for the concomitant elements and their concentration was excellent, indicating quantitative recovery by the reagent [5].

Preconcentration and separation of V(V) and V(IV)

There are two ways to quantify V(IV) in the filtrate from the first precipitation step. One is to oxidize V(IV) to V(V) with permanganate followed by precipitation at pH 1.8. Another is to change the pH of the filtrate to 4.0 ± 0.5 so that the V(IV)—DDTC chelate precipitates. Although both methods could be used to quantify V(IV), the latter was chosen because of its simplicity. When solutions containing different ratios of V(IV) and V(V) were processed by the present method, good correlation between the added and found concentration was obtained. Table 2 shows the slope and intercept of the linear regression line which indicates that V(V) and V(IV) can be separated and recovered quantitatively.

The effect of diverse ions on the separation and precipitation of V(IV) and (V) was investigated at pH 1.8. Table 3 shows that 20-μg amounts of Cr(III), Fe(III), Co(II), Ni(II), Cu(II), Zn(II), Mn(II) and Pb(II) did not interfere with the precipitation of V(V) with DDTC. Recoveries of 20 μg of V(V) in the presence of 20 μg of each metal were 93—99% complete; an average error of +0.8 μg for V(IV) was observed which corresponded to 4% of the

TABLE 2

Linear regression of V(V) and V(IV) concentration found and added

Ion	Slope	Intercept	Number of points	Std. error of estimate	Range (μg)
V(V)[a]	0.98 ± 0.01	0.78 ± 0.42	13	1.10	0—100
V(IV)[a]	0.91 ± 0.02	0.88 ± 0.30	13	0.80	0—34
V(V)[b]	0.85 ± 0.02	1.09 ± 0.53	15	1.28	0—40
V(IV)[b]	0.73 ± 0.07	2.68 ± 0.62	15	1.87	0—20
V(IV) + V(V)[c]	1.01 ± 0.02	−0.32 ± 0.39	15	1.00	—

[a]Single-element standards of only one vanadium oxidation state. [b]Either oxidation state of vanadium present as well as 0—40 μg of concomitant ions. [c]Both oxidation states of vanadium in the presence of concomitant ions.

TABLE 3

Effect of diverse ions

Metal ion	Added (μg)		Found (μg)	
	V(V)	V(IV)	V(V)	V(IV)
Cr(III)	20	0.0	19.4	0.5
	0	18.6	0.8	18.2
Fe(III)	20	0.0	19.6	1.4
	0	18.6	1.0	17.4
Co(II)	20	0.0	19.8	0.9
	0	18.6	1.5	16.0
Ni(II)	20	0.0	19.8	0.9
	0	18.6	0.5	17.5
Cu(II)	20	0.0	18.6	0.9
	0	18.6	1.6	16.4
Zn(II)	20	0.0	19.6	0.6
	0	18.6	0.7	18.0
Mn(II)	20	0.0	19.2	0.9
	0	18.6	0.5	19.0
Pb(II)	20	0.0	18.7	0.6
	0	18.6	0.7	17.7

[a]20 μg/100 ml was added in each case.

amount of V(V) present. Vanadium(IV) remained in the filtrate even when 20 μg of each metal was present and 86—102% of residual V(IV) was recovered in the second precipitation step. To evaluate the procedure for determining V(IV) and V(V) species in mixtures containing other elements, synthetic mixtures were prepared. The good correlation between the concentration of V(IV) and V(V) added and found even in the presence of concomitant ions (Table 2) shows that the two species can be separated and quantified. However, when large amounts of diverse ions were present, V(V) was not recovered quantitatively and V(IV) was detected even when it was not added. To check the oxidation state of vanadium in the filtrate, two of the standard mixtures were oxidized by potassium permanganate before V(V) was precipitated with DDTC. The positive error for V(IV) decreased which suggests that V(V) changes oxidation state in the presence of high concentration of some foreign ions. The high intercept for V(IV) as well as the excellent correlation for total vanadium confirm these conclusions.

The authors express their appreciation to TRACOR XRAY, INC. for supplying the x-ray spectrometer and a gift to support this research. K. H. acknowledges Nihon University for funding a sabbatical leave.

REFERENCES

1 C. L. Luke, Anal. Chim. Acta, 41 (1968) 237.
2 R. Van Grieken, Anal. Chim. Acta, 143 (1982) 3.
3 A. T. Ellis, D. E. Leyden, W. Wegscheider, B. B. Jablonski and W. B. Bodnar, Anal. Chim. Acta, 142 (1982) 73.
4 A. T. Ellis, D. E. Leyden, W. Wegscheider, B. B. Jablonski and W. B. Bodnar, Anal. Chim. Acta, 142 (1982) 89.
5 D. E. Leyden and W. Wegscheider, Anal. Chem., 53 (1981) 1059a.
6 B. M. Vanderborght and R. E. Van Grieken, Anal. Chem., 49 (1977) 311.
7 J. F. Elder, S. K. Perry and F. P. Brady, Environ. Sci. Technol., 9 (1975) 1039.
8 D. E. Leyden and G. H. Luttrell, Anal. Chem., 47 (1976) 97.
9 H. Linder, H. Selter and B. Schreiber, Anal. Chem., 50 (1978) 896.
10 H. Watanabe, S. Berman and D. S. Russell, Talanta, 19 (1972) 1363.
11 P. C. Cole, J. M. Eckert and K. L. Williams, Anal. Chim. Acta, 153 (1983) 61.
12 F. W. Oehme, Toxicity for Heavy Metals in the Environment, Part 2, Marcel Dekker, New York, 1979, p. 745.
13 L. Friberg, G. F. Nordberg and V. B. Vouk, Handbook on the Toxicology of Metals, Elsevier, Amsterdam, 1979, p. 659.
14 G. H. Morrison, CRC Critical Reviews in Anal. Chem., 8(3) (1979) 287.
15 G. Himworth, Analyst, 100 (1975) 186.
16 K. Iwasaki and K. Tanaka, Anal. Chim. Acta, 136 (1982) 293.

Analytica Chimica Acta, 188 (1986) 9—14
Elsevier Science Publishers B.V., Amsterdam — Printed in The Netherlands

SIMULTANEOUS DETERMINATION OF LANTHANIDES BY RADIOISOTOPE X-RAY FLUORESCENCE SPECTROMETRY BASED ON CHARACTERISTIC *K*-RADIATION

J. J. LABRECQUE*,[a], P. A. ROSALES and G. MEJÍAS

Instituto Venezolano de Investigaciones, Científicas (I.V.I.C.), Apartado 1827, Caracas 1020-A (Venezuela)

(Received 27th January 1986)

SUMMARY

The use of radioisotope-induced x-ray fluorescence is examined for the determination of lanthanides via their characteristic *K* x-ray lines. Various synthetic mixtures of barium and 14 rare-earth elements were prepared and their homogeneity was checked. The intensity from each mixture was measured for 10 min with excitation by the 88-keV γ-ray from a 3.5-mCi cadmium-109 source or by direct β-particles from a 100-μCi promethium-147 source. Typical spectra and their corrected peak intensities are presented. The spectral backgrounds produced by ^{147}Pm and ^{109}Cd are considered.

In some studies, it is important to quantify the content of individual rare-earth elements rather than the total content. One such situation [1] is the development of a model to predict the mobilization of thorium from an estimated 20 000 metric ton lateritic deposit in Morro de Ferro, Brazil. Another important situation is the investigation of the tropical weathering process on the formation of lateritic material such as the deposit at Cerro Impacto, Venezuela [2] which is highly enriched in rare-earth elements as well as in niobium and thorium.

The determination of rare-earth elements (lanthanides) is one of the more difficult tasks in inorganic quantitative chemistry because of their similar chemical properties. Therefore, many of the existing classical methods [3] have been superseded by physical techniques, including spectroscopic methods. For concentration levels greater than 0.1%, conventional wavelength-dispersive x-ray fluorescence is probably still considered the most versatile technique. For simultaneous multi-element determination of lanthanides at lower concentrations, flame emission, atomic absorption, direct-current arc and more recently plasma spectrometry have been used. However, the earlier of these methods are not completely satisfactory [4]. Activation by neutrons would probably be the technique of choice with the new lower-

[a]Present address: International Atomic Energy Agency, Wagramerstrasse-5, P.O. Box 100, A-1400 Vienna, Austria.

0003-2670/86/$03.50

energy photon detectors if the technique did not depend on a high neutron flux, resulting in a costly and sometimes time-consuming procedure.

When rare-earth elements are determined by conventional wavelength-dispersive x-ray fluorescence, the low-energy L x-rays are generally used because the conventional x-ray tube excitation system does not sufficiently excite the high-energy K x-rays. The same L x-rays are used with secondary-target excitation or direct excitation by an x-ray tube coupled to an energy-dispersive x-ray fluorescence system. The major limitation of using the L x-rays from the lanthanides is that they are strongly overlapped by the low-energy K x-rays from elements with low atomic numbers. This problem is partly overcome in the wavelength-dispersive system because of its high spectral resolution while it is compensated in the energy-dispersive system with computer programs [5—7]. However, in some cases, such as lateritic samples [8] in which the titanium and iron contents are orders of magnitude higher than the rare-earth elements, these procedures are less acceptable.

To excite high-energy ($\geqslant$32 keV) x-rays, various radioisotopes such as cobalt-57, gadolinium-153, thulium-170, and americium-241 [9] have been used. However, only the ^{57}Co radionuclide can excite and quantify all the rare-earth elements with its 122-keV γ-ray. The limitation of ^{57}Co, in addition to having a short half-life and being costly, is that the source itself has spectral peaks that interfere with the Fe K-radiation as well as the 14-keV γ-ray. In this work, the possibilities of using two other radionuclides for the excitation of the various high-energy K x-rays from the lanthanides were examined; cadmium-109 was tested by means of its 88-keV γ-ray, which is closer to the absorption edges of the K x-rays of the lanthanides, and promethium-147 by its direct β-particles (continuous to 244 keV).

EXPERIMENTAL

Preparations of lanthanide mixtures and the ^{147}Pm source mixture

Various synthetic mixtures of barium oxide and the rare-earth oxides were prepared by mixing the appropriate amounts of the oxides (analytical-grade; 99.9%) which were previously ground to less than 63-μm particle size (200-mesh sieve) and oven-dried at 102 ± 2°C. Because the amounts were small (100—200 mg) they were carefully transferred to a plastic vial (~7 ml) with eight plastic balls for homogenization in a SPEX 8000 mill/mixer for three 10-min periods with 30 min of cooling between each period. The homogeneity was checked by transferring separate portions (ca. 20 mg) to ten different sample holders. These sub-portions were then quantified by the x-ray fluorescence methods described herein and the relative intensities of the K_α peaks for the elements present were compared. Because the standard deviations for the different relative intensities were small (<3%) in most cases, it was assumed that the mixtures were homogeneous. For these mixtures, the same sample holder was used for excitation by the cadmium-109 source (ca. 3.5 mCi).

For preparation of the ^{147}Pm source mixture, a small portion of the mixture (about 20 mg) was transferred to a 1-cm diameter aperture (covered with Scotch tape) in a 2 × 6-cm piece of IBM card. The 50 μl of a 2 mCi ml^{-1} solution of ^{147}Pm was added to the center from an Eppendorf pipette. After the source mixture had dried overnight, a second piece of Scotch tape was used to secure the sample in place.

Energy-dispersive x-ray fluorescence instrumentation

The characteristic *K* x-rays from the synthetic mixtures excited by the 88-keV γ-ray from the ^{109}Cd annular source, or the β-particles from the ^{147}Pm (100 μCi) source mixtures, were collected by a planar high purity germanium detector (Canberra) with a measured energy resolution of 230 eV (FWHM) at 5.9 keV from iron-55 and 740 eV at 122 keV from cobalt-57. The window was 0.15-mm thick beryllium.

The data acquisition and processing were done with an Apple IIe microprocessor with 64K of memory and a 1024-channel ADC card from the Nucleus (Oak Ridge, TN). The hardware of this system has been described elsewhere [10, 11] and the software was supplied by Dapple Systems (Sunnyvale, CA).

The *K* x-ray peaks were integrated by summing all counts in the peak within 0.6 FWHM from the peak maximum. Corrected peak intensities were calculated by subtracting the appropriate background.

RESULTS AND DISCUSSION

The corrected peak intensities for the characteristic *K* x-rays for barium and the lanthanides from three of the synthetic mixtures are presented in Table 1 for 10-min measurement times. It can be seen that, for direct excitation by β-particles from ^{147}Pm, the corrected peak intensities for the equal-weight mixture of barium and 14 rare-earth elements (6.67% of each oxide) decrease with increasing atomic number (increasing x-ray energy); this is typical of electron excitation. The background associated with the use of promethium-147 as a direct β-particle excitation source can be seen in Figs. 1—3; it is a continuum shape similar to the backgrounds from electron excitation and bremsstrahlung spectra. Further, the ^{147}Pm source itself also contributes to the samarium *K* x-ray peaks, especially for mixtures in which no samarium was present. From previous studies, it appears that the contribution of the samarium *K*-radiation depends on the decay of ^{147}Pm to ^{147}Sm and so depends on the age of the promethium solution. It can be concluded that this type of excitation is more efficient for the lower atomic-number lanthanides although the associated background is higher.

The corrected intensities for the different elements excited with ^{109}Cd (ca. 3.5 mCi) are similar (see Table 1 and Figs. 1—3). The peak intensities are slightly higher at lower energies. It was expected that *K*-radiation with higher energies would be excited more because their respective *K* x-ray absorption

TABLE 1

Corrected peak counts for K x-rays in three synthetic mixtures of barium and rare-earth oxides with 10-min counting times

Element	Corrected peak counts					
	TR-T[a]		TR-1S2[b]		TR-5S[c]	
	^{147}Pm	^{109}Cd	^{147}Pm	^{109}Cd	^{147}Pm	^{109}Cd
Ba	16724	6883	—			
La	12160	6930	30723	18175		
Ce	16014	8688	—		64090	27752
Pr	16601	9525	34830	21162		
Nd	13747	8328	—			
Sm	18150	5390	—			
Eu	7356	5635	—			
Gd	5779	4978	13811	17670	25785	21010
Tb	6944	4230	—			
Dy	9597	4788	13714	17118		
Ho	5194	4892	—			
Er	4265	5288	13535	20025		
Tm	5951	4743	—			
Yb	4900	4850	10323	19347		
Lu	3822	4503	—		11794	17520

[a]100 mg of the oxide of each element. [b]150 mg of the oxide for each element for which intensity is given. [c]200 mg of the oxide of each element for which intensity is given.

edges would be closer to the 88-keV γ-ray responsible for the excitation. However, it should be noted that the mixtures were of equal weight and not equal number of atoms; this may account for this small effect.

The major advantage of using the ^{109}Cd source for the determination of

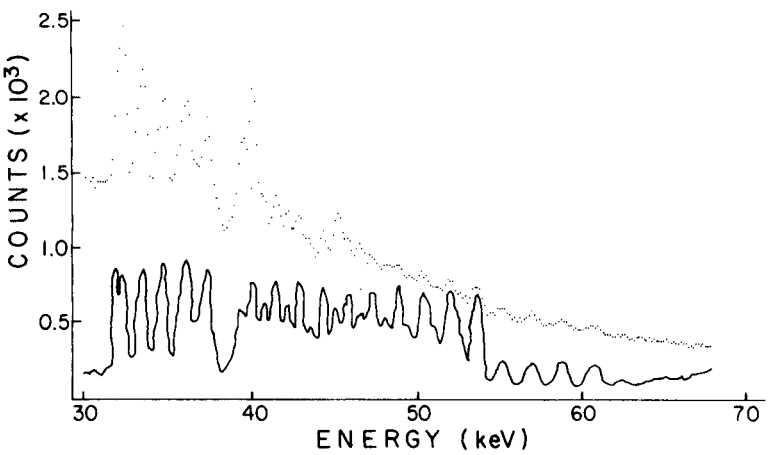

Fig. 1. Spectra of barium and the 14 lanthanides (TR-T) with 10-min measurement time: (—) cadmium-109 source; (···) promethium-147 source.

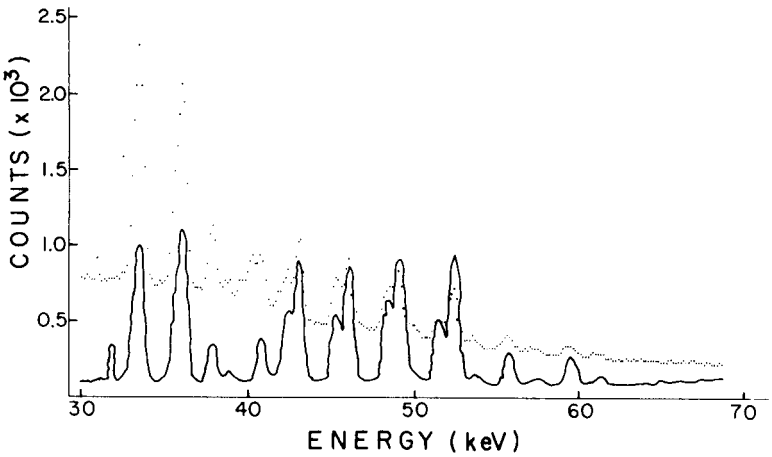

Fig. 2. Spectra of the TR-1S2 sample with 10-min measurement time. Symbols as for Fig. 1.

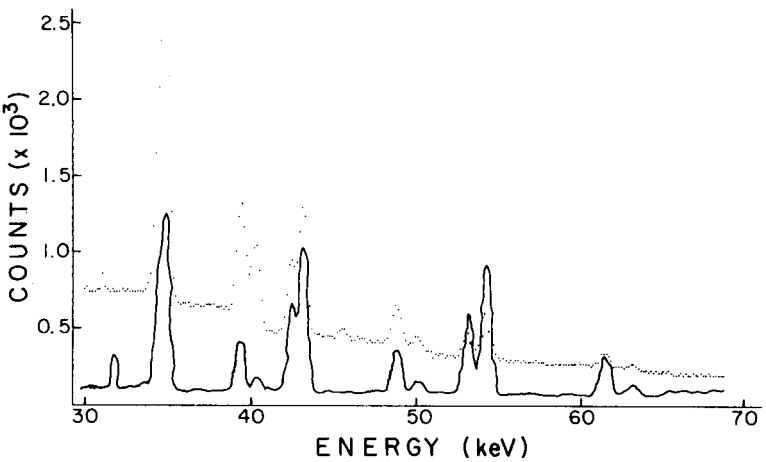

Fig. 3. Spectra of TR-5S with 10-min measurement time. Symbols as for Fig. 1.

the lanthanides is that the region for their respective K x-ray energies is free from spectral interferences. The background signals are small and flat, as can be seen in Figs. 2 and 3. Limits of detection of the lanthanide elements based on excitation of their K-radiation with 88-keV γ-rays from ^{109}Cd will be evaluated when a new source (25 mCi) is obtained.

This work was presented in part at the XIV Colloquium Spectroscopium Internationale, Garmisch-Partenkirchen, Federal Republic of Germany, September 1985.

REFERENCES

1 G. R. Laurer, J. Furfaro, M. Carlos, W. Lei, R. Ballard and J. J. Kneip, Adv. X-Ray Anal., 25 (1982) 201.
2 V. Garica and H. M. Aarden, Proc. 5th Congr. Geol. Venen., Caracas, Venezuela, 1977, p. 941.
3 C. L. Wilson and D. W. Wilson (Eds.), Comprehensive Analytical Chemistry, 6 vol., Elsevier, Amsterdam, 1962.
4 J. A. Bouman and J. B. Willis, Anal. Chem., 30 (1967) 1210.
5 P. Van Espen, H. Nullens and F. Adams, Nucl. Instrum. Methods, 143 (1977) 243.
6 P. Van Espen, L. Van t'Dack, F. Adams and R. E. Van Grieken, Anal. Chem., 51 (1979) 961.
7 P. M. Van Dyck and R. E. Van Grieken, Anal. Chem., 52 (1982) 1859.
8 J. J. LaBrecque, J. M. Beusen and R. E. Van Grieken, X-Ray Spectrosc., 15 (1986) 13.
9 J. J. LaBrecque, Prog. Anal. At. Spectrosc., 4 (1981) 191.
10 D. Hale, J. C. Russ and D. E. Leyden, Microbeam Anal., (1982) 473.
11 K. Borowski, I. L. Priess, J. J. LaBrecque and C. Pauley, Computer-enhanced Spectrosc., 1 (1983) 99.

Analytica Chimica Acta, 188 (1986) 15—24
Elsevier Science Publishers B.V., Amsterdam — Printed in The Netherlands

ENERGY-DISPERSIVE X-RAY FLUORESCENCE SPECTROMETRY OF INDUSTRIAL PAINT SAMPLES

LEIF HØJSLET CHRISTENSEN*
Isotope Division, Risø National Laboratory, DK-4000 Roskilde (Denmark)
IVER DRABÆK
Danish Isotope Centre, Skelbækgade 2, DK-1717 Copenhagen V (Denmark)
(Received 29th August 1985)

SUMMARY

An energy-dispersive x-ray fluorescence method for the direct, simultaneous determination of major and minor elements in coatings is described. The method relies on the back-scatter/fundamental parameter concept and provides a general solution to matrix problems. The method has been implemented and verified on spectrometers based both on tube excitation and radioisotope excitation. Results demonstrating some performance characteristics are presented. Sample inhomogeneity problems that impede quantification of low-Z elements in some types of paint are discussed.

Technical demands as well as demands arising from environmental regulations have increased the need to quantify most components in coating products. Such products are complex mixtures of pigments, binders, fillers, solvents, etc., and the problem can be difficult. Structural information, which is by far the most important in paint research, is usually obtained by means of infrared spectroscopy, nuclear magnetic resonance spectroscopy, and x-ray diffraction. For quantitative analysis, the commonly used methods are atomic absorption spectrometry, titrimetry, and colorimetry [1] whereas x-ray fluorescence spectrometry (x.r.f.) is rarely used for anything but detection of elements. This is believed to be mainly due to the problems of the matrix effects inherent in x-ray fluorescence spectrometry. In most practical x.r.f. applications for coatings, both attenuation and enhancement effects are significant and have to be accounted for in a quantitative approach. Matrix correction calculations are further complicated by the fact that light elements not amenable to x.r.f. constitute a major and variable fraction (20—80%) of the bulk sample, and thus contribute significantly to the attenuation of the characteristic radiation.

Various experimental procedures have been proposed to compensate for, or alleviate, matrix effects in samples of paint [2—4]. However, none of these has provided a universal solution to the problem and, so far, the potential of the x.r.f. technique has not been fully exploited [5]; in particular, this is true for the energy-dispersive version of the technique.

0003-2670/86/$03.50

The aim of this work was twofold: to develop a generally applicable method for the direct determination of major and minor elements in different types of paint by energy-dispersive x.r.f. in combination with a back-scatter/fundamental parameter matrix correction algorithm, and to implement the proposed method on a fairly cheap spectrometer by using a radioisotope as primary excitation source.

The work reported here was based on six different types of paint with known formulations. The paint samples were delivered by the Danish painting industry. Preliminary results of this work have been presented [6, 7], but this paper discusses the definitive conclusions.

Quantitative method

The back-scatter/fundamental parameter (BFP) method of quantification proposed by Nielson [8] has proven to work successfully for samples containing variable amounts of light elements ($Z \leqslant 12$). The BFP method is advantageous for multi-element quantitation in unweighed samples of finite or infinite thickness and can handle solid as well as liquid samples. The light-element fraction of such samples is derived from the observed coherent and incoherent scattered characteristic radiation of the excitation source, e.g., Ag K_α radiation from a ^{109}Cd radioisotope (see Fig. 1) or Mo K_α radiation from a molybdenum secondary target.

The present approach closely follows that of Nielson and Sanders [9] and some of the key subroutines in their program were implemented in the present back-scatter algorithm. The differences, of only secondary importance, lie in the choice of calibration standards and the software option of using several secondary targets or radioisotopes for excitation of the sample.

The fluorescence equations are of the form

$$I_i = K_i A_i (1 + H_i) W_i \qquad (1)$$

where I_i is fluoresence intensity, K_i is a calibration factor, A_i is an attenuation factor, H_i is an enhancement factor, and W_i is the weight fraction.

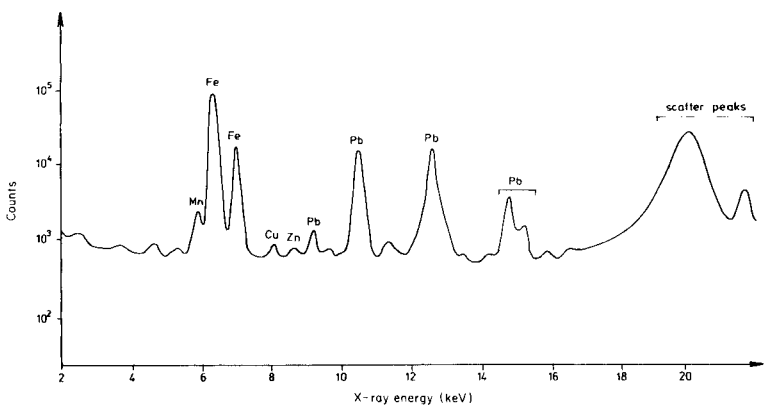

Fig. 1. X-ray fluorescence spectrum of a wood-preservative liquid obtained with the radioisotope-excited spectrometer.

The coherent and incoherent scatter equations have the form

$$I_S = K_S A_S(\sum W_j \sigma_{jS} + \sum W_i \sigma_{iS}) \quad (2)$$

where σ is the scatter cross-section, W_j refers to light elements and W_i refers to heavy elements.

The degrees of attenuation and enhancement and the amount of scatter depend on the composition of the sample, so that calculations have to progress in an iterative manner. The weight fractions of the directly observed elements quantified from the calibration factors and the fluorescence intensities, are first used to estimate the scatter these heavy elements have caused ($\Sigma W_i \sigma_{iS}$). The light element part of the sample matrix is represented by two light elements (e.g., carbon and oxygen) with weight fractions W_a and W_b. The scatter equations can be rearranged to yield two simultaneous equations with unknowns W_a and W_b, one for the coherent scatter

$$W_a \sigma_{aC} + W_b \sigma_{bC} = I_C K_C^{-1} A_C^{-1} - \sum W_i \sigma_{iC} \quad (3)$$

and a similar one for the incoherent scatter.

In each step of the iteration algorithm, the necessary matrix corrections as well as the individual scatter contributions are calculated, by using the weight fractions of all the elements, mass attenuation coefficients, scatter cross-sections and a number of other fundamental parameters all of which are tabulated in the literature. After convergence has been obtained, the weight fractions are normalized to unity.

EXPERIMENTAL

Instrumentation

X-ray tube excitation. The tube-excited system was a fully automated Kevex 0700 energy-dispersive spectrometer connected to a Nuclear Data ND680 multichannel analyzer/microcomputer system. The primary source of radiation was a low-powered rhodium anode x-ray tube. The spectrometer offers two modes of excitation, i.e., direct excitation and excitation by means of secondary targets. The direct excitation mode was used in combination with two or three secondary targets (Ti, Mo, and Ag) to provide optimum sensitivities for a broad range of elements.

Radioisotope excitation. The radioisotope system consisted of an Ortec Si(Li) detector, a laboratory-constructed annular source-holder/excitation chamber with interchangeable collimators, and a computer-controlled sample changer resembling that of the Kevex spectrometer. The annular source was a 370-MBq ^{109}Cd isotope providing Ag x-rays. The spectrometer was coupled to a Canberra S35 multi-channel analyzer. Data acquisition and spectrometer control were handled by a PDP11/23+ microcomputer (operating system RT11).

Neutron activation. For comparative purposes, most of the samples were subjected to instrumental neutron activation analysis (i.n.a.a.). Samples were

irradiated in the Danish 10-MW heavy-water-moderated reactor DR-3. The reactor provides two irradiation facilities with a neutron flux of 2.5 and 4.5×10^{17} n m^{-2} s^{-1}, respectively. The low-flux facility was used for short irradiations (1—5 min) and the high-flux facility for long irradiations (1—2 h).

Spectrum evaluation and quantitative calculations

For the Kevex system and the γ-spectrometers used for i.n.a.a., spectral information was extracted by using a standard non-linear least-squares Gaussian fitting routine supplied by Nuclear Data. For the radioisotope system, the spectrum evaluation program SAMPO-80 [10] was used. The intensities of the non-Gaussian back-scatter peaks were measured with the best precision by using fixed-energy windows.

Quantitative calculations were done using the program, MATRIX [11]. The program is coded in ALGOL and runs on a Burroughs B7800 mainframe computer. Quantitative neutron activation calculations were based on the single-comparator principle.

Sample preparation

In most cases, the sample preparation was straightforward. Samples of paint were thoroughly stirred and unweighed aliquots were poured into disposable Spectro-cups having a thin mylar window. For the Kevex system, the time required for counting was between 200 and 2000 s depending on concentration levels and the number of excitation sources required for complete elemental coverage, whereas 2000 s was used in the case of the radioisotope-excited system.

Calibration

Calibration of the spectrometers was accomplished with pure metal standards or standards of known total composition (i.e., pellets of analytical-grade chemical compounds). All the standards were of infinite thickness. For each excitation source, calibration curves like those shown in Fig. 2 were established. Similar but less accurate calibration curves could have been obtained with thin foils (e.g., 50—100 μg cm^{-2} elemental deposits on Nuclepore filters). Calibration factors for the two back-scatter peaks were evaluated by measuring pellets of NaCl, KCl, $CaSO_4$, and KH_2PO_4.

RESULTS AND DISCUSSION

Before actual results are presented, it is worth noting that a fundamental approach to the matrix correction calculations facilitates calibration of the spectrometer. In fact, fairly accurate relative calibration constants may even be calculated from basic x-ray physics [12]. Regardless of which way calibration is accomplished, it is not restricted to a particular application. For routine use of the spectrometer, only one reference sample is required. The count rate for this sample is used to monitor changes in the excitation flux from the x-ray tube or the decaying source.

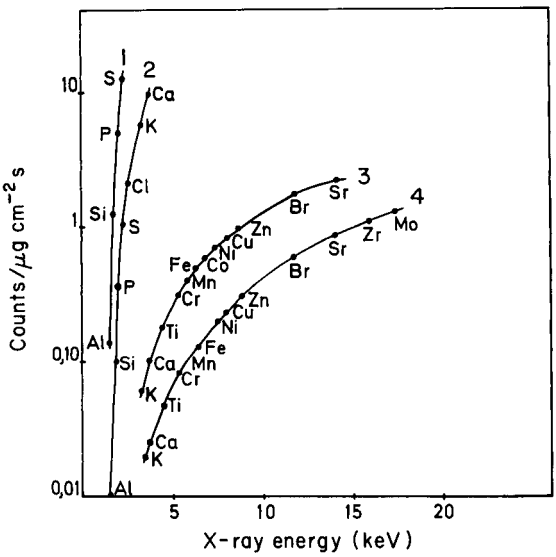

Fig. 2. Calibration curves for K_α lines for different modes of excitation: (1) direct excitation; (2) Ti secondary target; (3) Mo secondary target; (4) ^{109}Cd source.

The direct excitation, which in the calculations is regarded as a monochromatic source, is used to enhance the otherwise poor sensitivity for aluminium and silicon. The sensitivities for these two elements could be improved further by flushing the irradiation chamber with helium, an option which is not available with the present systems. The elemental coverage for the isotope-based system is limited in comparison to the Kevex system, but introduction of an ^{55}Fe source in addition to the ^{109}Cd source would improve the sensitivity for elements Ti—Al significantly. Depending on the concentration level, the cut-off in Z for the isotope-based system is around 20.

Tables 1—6 show the results together with the formulation values for the six paints. The results are calculated as the mean value of five replicates of a

TABLE 1

Results for an anti-fouling paint

Element	Mean content (g kg^{-1})[a]			Formulation
	E.d.x.r.f.[b]	E.d.x.r.f.[c]	I.n.a.a.[d]	
Cl	159 ± 9	162 ± 10	75 ± 3	74.7
Fe	1.32 ± 0.08	1.24 ± 0.07	—	—
Cu	323 ± 16	346 ± 17	354 ± 20	344
Zn	32.4 ± 1.6	35.8 ± 1.7	—	40.2
Sn	43 ± 2	47 ± 2	31 ± 2	36

[a]Mean of 5 replicates with overall standard deviation. [b]Tube-excited e.d.x.r.f. [c]Source-excited e.d.x.r.f. [d]I.n.a.a./short irradiation.

TABLE 2

Results for a zinc silicate paint[a]

Element	Mean content (g kg^{-1})[a]			Formulation
	E.d.x.r.f.[b]	E.d.x.r.f.[c]	A.a.s.[d]	
Si	249 ± 13	—	261	65.8
P	29.6 ± 1.5	—	—	21.7
K	1.1 ± 0.1	—	0.8	0.8
Ca	3.4 ± 0.3	4.2 ± 0.3	3.5	3.2
Mn	1.8 ± 0.1	1.6 ± 0.1	—	—
Fe	73 ± 4	73 ± 4	90	79.2
Zn	533 ± 27	499 ± 25	554	495

[a—c]See footnotes to Table 1. [d]Mean of duplicate results by a.a.s.

TABLE 3

Results for a wood preservative liquid

Element	Mean content (g kg^{-1})[a]			Formulation
	E.d.x.r.f.[b]	E.d.x.r.f.[c]	I.n.a.a.[d]	
Si	5.1 ± 0.7	—	—	9.3
Cl	2.6 ± 0.3	—	2.5 ± 0.2	2.4
Mn	0.41 ± 0.04	0.39 ± 0.04	0.42 ± 0.01	0.4
Fe	10.0 ± 0.8	11.7 ± 1.0	10.4 ± 0.2	16.3
Zn	0.008 ± 0.001	0.010 ± 0.002	—	—
Sn	5.4 ± 0.4	4.5 ± 0.3	5.8 ± 0.2	5.8
Pb	0.92 ± 0.08	0.88 ± 0.07	0.84 ± 0.01[e]	1.0

[a—c]See footnotes to Table 1. [d]Short and long irradiation. [e]ASTM D3335-78 (6 replicates).

TABLE 4

Results for an alkyd paint

Element	Mean content (g kg^{-1})[a]			Formulation
	E.d.x.r.f.[b]	E.d.x.r.f.[c]	I.n.a.a.[d]	
Al	51 ± 3	—	48 ± 2	41.6
Si	66 ± 3	—	—	63.0
K	2.0 ± 0.1	—	24 ± 0.1	1.2
Ca	0.45 ± 0.03	—	—	0.5
Ti	43 ± 2	40 ± 2	46 ± 2	44.1
Fe	11.8 ± 0.6	11.7 ± 0.6	12.3 ± 0.1	11.4
Cu	0.37 ± 0.02	0.38 ± 0.02	0.35 ± 0.03	0.34
Zn	0.48 ± 0.03	0.54 ± 0.03	0.49 ± 0.01	—
Zr	0.23 ± 0.02	—	—	0.21
Pb	3.0 ± 0.2	3.4 ± 0.2	3.00 ± 0.07[e]	3.5

[a—d]See footnotes to Table 3. [e]ASTM D3335-78 (3 replicates).

TABLE 5

Results for an emulsion paint

Element	Mean content (g kg^{-1})[a]			Formulation
	E.d.x.r.f.[b]	E.d.x.r.f.[c]	I.n.a.a.[d]	
Al	11.0 ± 1.0	—	10.3 ± 0.4	8.9
Si	26.9 ± 1.4	—	—	28.8
K	1.1 ± 0.1	—	0.8 ± 0.1	0.4
Ca	73 ± 4	96 ± 5	74.9 ± 0.6	76.3
Ti	5.9 ± 0.3	5.9 ± 0.3	5.5 ± 0.2	4.4
Fe	39 ± 2	42 ± 2	37.7 ± 0.7	37.0
Cu	2.3 ± 0.1	2.4 ± 0.1	2.1 ± 0.1	2.5

[a—d]See footnotes to Table 3.

TABLE 6

Results for an alkyd zinc chromate primer

Element	Mean content (g kg^{-1})[a]			Formulation
	E.d.x.r.f.[b]	E.d.x.r.f.[c]	I.n.a.a.[d]	
K	25.1 ± 1.3	35.6 ± 1.5	23.9 ± 0.9	—
Ti	54 ± 3	57 ± 3	45 ± 2	35
Cr	76 ± 4	77 ± 4	67 ± 3	54
Fe	3.7 ± 0.2	3.7 ± 0.2	—	—
Zn	168 ± 8	182 ± 9	164 ± 7	154
Pb	6.0 ± 0.3	6.5 ± 0.4	—	2.9

[a—d]See footnotes to Table 1.

particular paint. The quoted overall uncertainty, $\hat{\sigma}_{xrf}$, includes variance contributions from the calibration, sample preparation, and counting statistics. The main contribution to the uncertainties of the x-ray fluorescence results comes from the back-scatter calibration, which amounts to 5% relative. The reproducibility of the sample preparation procedure is about 1—2% in most cases. The chosen time of measurement assured good counting statistics for most elements.

In general, the results obtained by means of the two x-ray fluorescence spectrometers agree well and so do the x-ray fluorescence results and those obtained by i.n.a.a. In some cases, which will be discussed below, the observed differences are statistically significant (5% significance level). With a single-isotope system, the sensitivities for potassium and calcium are not adequate for concentration levels below 100 g kg^{-1}. The lack of agreement between the two x-ray fluorescence results is attributed to this fact and is not further discussed. Comparisons with the formulations also show significant differences in some cases. However, the formulation values should only be con-

sidered indicative, as they were calculated on the basis of the raw materials which were often poorly characterized.

One of the more obvious discrepancies found is related to the determination of chlorine in the anti-fouling paint (Table 1). The x.r.f. results are more than a factor of two higher than the results obtained by i.n.a.a., but the latter results agree with the formulation. X-ray mapping provided by a scanning electron microscope, however, disclosed an uneven distribution of copper and chlorine in the sample. Figure 3 reveals copper-depleted areas and corresponding chlorine-enriched areas yielding much less attenuated Cl K_α radiation. It is therefore believed that the discrepancy is due to this problem of sample inhomogeneity. The results for the other elements emitting higher-energy radiation are not affected. Homogenization of a dried aliquot of the paint has not been tried.

The BFP method was originally developed for biological and geological samples with a mean Z in the range 6—12. For a zinc silicate paint, the results of which are presented in Table 2, the mean Z is approximately 22. Such a sample represents an extreme case in the calculations. Despite that, the agreement between the majority of e.d.x.r.f. results and those obtained by a.a.s. and/or those of the formulation is good. The exception is silicon. A wet-chemical method involving sample destruction support the apparently very high content of silicon contrary to what is indicated by the formulation. At present the problem remains unsolved.

Concerning the wood preservative (Table 3), the evaporation rate is significant compared to the required time of counting. Therefore, in this case, aliquots of the paint were allowed to dry before measurement and the results were afterwards corrected to wet weight. With one exception, i.e., iron, the i.n.a.a. results agree with the formulation. However, the findings for iron are substantiated by the two e.d.x.r.f. results. The determination of tin is of particular interest for this wood preservative. Whereas agreement between the results by the two different techniques and the formulation is good for

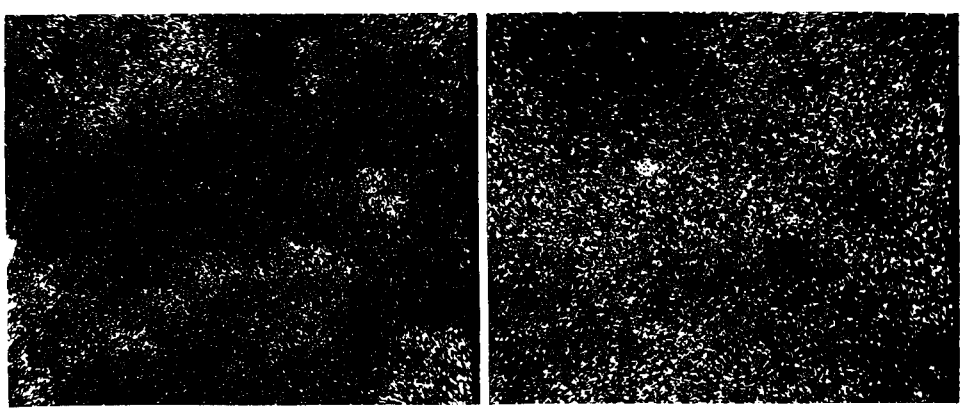

Fig. 3. Distribution of copper (left) and chlorine (right) as revealed by the x-ray mapping facility of a scanning electron microscope.

chlorine, the x-ray fluorescence results for tin based on the Sn L_α line were found to be significantly lower than the formulation value. With the more penetrating Sn K_α/K_β radiation, satisfactory agreement is observed, especially regarding the result obtained with the tube-excited system. In this case, a gadolinium secondary target was used for excitation. The reason for the rather low value obtained with the source-excited system is not known.

The results shown in Tables 4 and 5 for an alkyd paint and an emulsion paint demonstrate that it is possible to obtain satisfactory data by e.d.x.r.f. for low-Z elements like aluminium and silicon. However, confidence in x-ray fluorescence results for elements emitting characteristic x-rays, K_α/L_α, in the energy region of 1—4 keV should be based on experience. Sample homogeneity and particle-size effects are of particular importance in this energy region.

In two cases (see Tables 3 and 4), the results for lead were verified by a standard method (ASTM D3335-78). However, with this method it was impossible to obtain reproducible results for lead in the alkyd zinc chromate primer within the allocated time. Although the e.d.x.r.f. results for this primer are twice that of the formulation, there is no reason to believe they should be wrong.

The results presented in Tables 1—6 emphasize the versatility of the energy-dispersive x-ray fluorescence technique. Direct and simultaneous determination of a number of important constituents in a variety of paint types can be achieved with the same set of calibration factors. The backscatter/fundamental parameter method of quantification easily spans four decades in concentration, e.g., zinc in Tables 2 and 3.

A spectrometer suitable for this application, with a radioisotope-based system could be assembled for U.S. $35 000 or less. Work is under way to implement the necessary software for spectrum deconvolution and matrix-correction calculations on a personal computer (e.g., IBM PC/XT or DEC PC/350). The same computer could be used for automatic control of the spectrometer and as a multichannel analyzer, thus allowing data accumulation and quantitative calculations to take place simultaneously.

This work was supported by the Danish National Council of Technology, the Thomas B. Thrige Foundation, Sadolin & Holmblad, Ltd., Hempel Technology, Ltd., and Dyrup & Co., Ltd. We thank Poul Pheiffer Madsen for his comments on the preparation of the paper, J. B. Bilde-Sørensen for providing the scanning microscope pictures, and P. Solgaard and S. Hvilsted for the a.a.s. results.

REFERENCES

1 D. G. Anderson and J. T. Vanderberg, Anal. Chem., 55 (1983) 1R.
2 F. H. Chung, A. J. Lorentz and R. W. Scott, X-Ray Spectrom., 3 (1974) 172.
3 G. P. Cunningham, Adv. Org. Coat. Sci. Technol., 5 (1979) 261.
4 G. S. Kunz and R. L. R. Towns, J. Coat. Technol., 54 (1982) 63.

5 P. Kamarchik, Jr. and G. P. Cunningham, Prog. Org. Coat., 8 (1980) 81.
6 L. H. Christensen and I. Drabæk, Adv. X-Ray Anal., 26 (1983) 377.
7 L. H. Christensen and I. Drabæk, Proc. XVIIth Fatipec Congress, Lugano, Vol. I, Interconvention AG Zurich, Switzerland, 1984, p. 327.
8 K. K. Nielson, Anal. Chem., 49 (1977) 641.
9 K. K. Nielson and R. W. Sanders, U.S. DOE Report PNL-4173, 1982.
10 M. J. Koskelo, P. A. Aarnio and J. T. Routti, Nucl. Instrum. Methods, 190 (1981) 89.
11 L. H. Christensen and N. Pind, X-Ray Spectrom., 10 (1981) 156.
12 M. O. Krause, E. Ricci, C. J. Sparks, Jr. and C. W. Nestor, Adv. X-Ray Anal., 21 (1978) 119.

Analytica Chimica Acta, 188 (1986) 25—35
Elsevier Science Publishers B.V., Amsterdam — Printed in The Netherlands

X-RAY FLUORESCENCE ANALYSIS OF MULTIPLE-LAYER FILMS

M. MANTLER[a]
IBM Research Laboratories San Jose, San Jose, CA 95193 (U.S.A.)
(Received 29th August 1985)

SUMMARY

Theoretical equations for fluorescent count rates from bulks, single-layer films, and multiple-layer film specimens, based on fundamental parameter models, are developed. Absorption and secondary enhancement within each layer, between layers, and between layers and substrate are considered. A computer program is used to predict count rates as well as for simultaneous back-calculation of concentrations and thicknesses. Standards can be bulks, single films, or multiple films in any combination; pure-element standards as well as those containing additional elements are suitable. Evaluation of experimental data from two- and three-layer films (by using bulk pure-element standards) by the proposed method shows agreement within $<0.3\%$(absolute) for concentrations and $<5\%$(relative) for thicknesses compared to results from single-layer reference specimens prepared under identical conditions.

Determination of the chemical compositions and thicknesses of single-layer films and of multiple-layer films is of growing importance in industrial and scientific laboratories. Examples of applications are multiple coatings of sheet metals for corrosion protection, gold layers (usually on sublayers) on electrical contact pins, and the complicated multilayer set-up on silicon wafers in the electronics industries. X-ray fluorescence spectrometry offers several advantages for this kind of application. It is generally nondestructive and a wide range of elements can be quantified. It is possible to determine concentrations and film thicknesses simultaneously, even in the case of multiple-layer films (with some restrictions). Quantification time is relatively short compared to other methods, and specimen preparation is simple.

In this paper, theoretical equations are developed for the prediction of count rates from elements in multiple film layers based on fundamental parameter models. Calculation of concentrations as well as of the individual thicknesses are possible by iterative methods if the qualitative composition of each layer is known. The fundamental parameter equations for multiple films are based on Sherman's theory [1] and include interactions (absorption and secondary enhancement) between all elements within each layer as well as between all other layers and with the substrate.

---

[a]Permanent address: Institut für Angewandte und Technische Physik, Technical University, Karlsplatz 13, A-1040 Vienna, Austria.

0003-2670/86/$03.50

THEORY

Basic assumptions

'Primary radiation' is the radiation from the selected radiation source used to excite fluorescent radiation in a specimen. It may be radiation from an x-ray tube, radioactive source, or any other electromagnetic radiation of sufficient energy. 'Primary fluorescent radiation' is fluorescent radiation directly excited by the primary radiation. 'Secondary fluorescent radiation' is excited by primary fluorescent photons of other atoms in the same specimen.

The primary radiation is assumed to have a cross-section of 1 cm^2. The spectral distribution of the photons in the primary radiation is defined by a function $\mathbf{x}(E)$ in such a way, that $\mathbf{x}(E)\,dE$ is the number of photons with energies between E and $E + dE$ passing the cross-section of the primary beam (1 cm^2) per second. The lateral dimensions of the specimen are large compared to the pathlengths of the photons within the specimen. This avoids problems arising from photons entering the specimen or emerging from it through side faces.

A short review of the equations for bulk samples and single-layer films is also given. This makes it possible to show the development of the film equations in the multiple film case by simple analogy to bulk and single-film

TABLE 1

Symbols and definitions

Symbol	Definition
$\mu_i(E)$	Mass absorption coefficient for radiation energy E in element i. Linear absorption coefficients are indicated by an asterisk
$\mu(E)$	Mass absorption coefficient for energy E in a sample
$\mu_{[m]}(E)$	Mass absorption for energy E in film m
$\mu(\mathrm{i})$	Mass absorption coefficient for analyte line i
τ	Photoabsorption coefficient
T, $T_{[m]}$	Film thicknesses (m indicates layer)
c_i	Weight fraction of element i
$c_{[m],i}$	Weight fraction of element i in film m
ψ_1	Angle at which primary radiation illuminates the specimen
ψ_2	Take-off angle of fluorescent radiation
ϕ	See Fig. 1(d)
p_i	Probability of the required electron transition compared to all transitions to the considered shell
P_i'	Probability of photoabsorption in element of interest
P_i	Probability of emission of a photon contributing to the line of interest after excitation of an analyte atom
w_i	Fluorescent yield
S_i	Absorption edge jump
L	Number of films (substrate counts as a film with infinite thickness)
Ω	Solid angle at which radiation is detected
$\mathrm{x}(\mathrm{i})$	Detector efficiency for analyte line i
ρ, $\rho_{[m]}$	Density of specimen or (with index) of film
η	Factor combining the geometrical acceptance probability of the detector and the detector efficiency

layers, and to present the complete theory in a coherent notation. Symbols used in equations are summarized in Table 1.

Primary excitation in bulk materials

The specimen is irradiated by the primary beam under an angle ψ_1. The contribution from an infinitesimally thin layer of depth t below the surface to the fluorescent radiation (Fig. 1) is considered. The number of photons arriving per second at the layer is

$$dn_{E,\mathrm{arr}} = \mathrm{x}(E)dE \exp\left[-(t/\sin\psi_1)\,\mu^*(E)\right] \tag{1}$$

The number of photons absorbed in the layer is

$$d^2n_{E,\mathrm{abs}} = dn_{E,\mathrm{arr}}\,(dt/\sin\psi_1)\,\mu^*(E) \tag{2}$$

The probability that this is photo-absorption in the element of interest, i, (and not absorption by scattering or photo-absorption in any other element) is

$$P_i' = c_i\,[\tau_i(E)/\mu(E)] = c_i\,[\tau_i(E)/\mu^*(E)]\,\rho \tag{3}$$

A photon contributing to the line of interest will be excited, if the atom has been ionized in the proper shell (probability: $(S_i - 1)/S_i$), if the proper transition fills the vacancy (probability: p_i), and if the photon actually leaves the atom without Auger effect (probability = fluorescent yield: w_i).

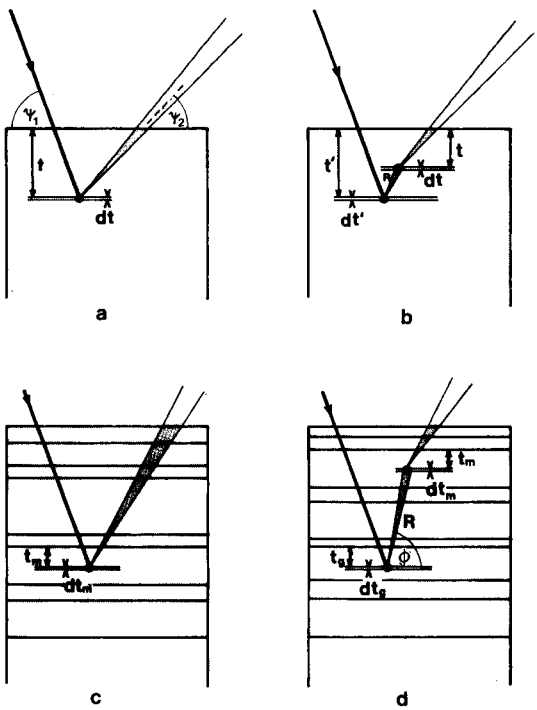

Fig. 1. Geometry for different models: (a) bulk, primary fluorescence excitation; (b) bulk, secondary fluorescence excitation; (c) multiple-layer film, primary fluorescence excitation; (d) multiple-layer film, secondary fluorescence excitation.

It is convenient to summarize all factors affecting the conversion of the absorbed photon into a fluorescent photon of interest by a conversion constant P_i,

$$P_i = p_i w_i \left[(S_i - 1)/S_i\right] \tag{4}$$

There is no preference of direction in which fluorescent radiation is emitted. It is assumed that the solid angle, Ω, under which the detector appears to the fluorescent radiation is the same from all points within the specimen, and that therefore the fraction of radiation emitted in this direction is constant:

$$d^2 n_{i,em} = d^2 n_{i,abs} P_i c_i (\Omega/4\pi) \tau_i(E) \rho \tag{5}$$

The total number of photons per second entering the detector window is therefore (accounting also for absorption of the fluorescent radiation on the pathlength between layer dt and the detector):

$$n_i' = c_i (\Omega/4\pi) P_i (\rho/\sin\psi_1) \int_{E_i}^{E_0} \int_0^{\infty} \mathbf{x}(E) \tau_i(E) \exp\left\{-t\left[\frac{\mu^*(E)}{\sin\psi_1} + \frac{\mu^*(i)}{\sin\psi_2}\right]\right\} dt\, dE \tag{6}$$

The number of actually detected photons (registered counts for the line) differs from that above because of the limited detector efficiency, $\chi(E)$. This factor, χ, is combined with that for the geometrical acceptance angle of the detector: $\eta(i) = \chi(i)\,(\Omega/4\pi)$. Inclusion of this factor and integration over all layers, dt, yields the total number of fluorescent photon counts per second for a given elemental line:

$$n_i = c_i P_i \eta(i) (1/\sin\psi_1) \int_{E_i}^{E_0} \frac{\mathbf{x}(E)\, \tau_i(E)}{\dfrac{\mu(E)}{\sin\psi_1} + \dfrac{\mu(i)}{\sin\psi_2}} dE \tag{7}$$

Secondary enhancement

It is now assumed that there is a second element, j, in the specimen which emits fluorescent radiation of an energy higher than the absorption edge of the element, i, to be quantified. The energy of the primary radiation must be sufficiently high to excite this j-radiation. Radiation j is excited in layer dt' and emitted in all directions. A fraction, $d\Omega'/4\pi = 1/2 \cos\phi\, d\phi$ is emitted in the direction under consideration and reaches the layer dt, where the i-radiation is excited, after a pathlength $R = |t - t'|/\sin\phi$. The number of j-photons emitted in all directions from layer dt' is

$$d^2 n_{j,em} = \mathbf{x}(E) \exp\left[-\frac{t'}{\sin\psi_1} \mu^*(E)\right] P_j c_j \rho \frac{dt'}{\sin\psi_1} \tau_j(E) dE \tag{8}$$

and the number of j-photons absorbed in dt is

$$d^3n_{j,abs} = d^2n_{j,em}\,\frac{d\Omega}{4\pi}\exp\left[-\frac{|t-t'|}{\sin\phi}\,\mu^*(j)\right]\frac{dt}{\sin\phi}\,\mu^*(j) \tag{9}$$

$d^3_{i,em}$ i-photons are thereby excited and emitted in all directions:

$$d^3n_{i,em} = d^3n_{j,abs}\,\frac{\tau_i(j)}{\mu^*(j)}\,c_iP_i\rho \tag{10}$$

The number of secondary i-photons registered in the detector is obtained by accounting for absorption on the way to the detector and the fractional factor of radiation accepted and registered by the detector:

$$d^3n_i = d^3n_{i,em}\,\exp\left[-\frac{t}{\sin\psi_2}\,\mu^*(i)\right]\eta(i) \tag{11}$$

The total number of all secondary i-photons is obtained by simultaneous integration over all layers dt and dt' (dt' may be above or below the layer dt), and all directions as follows:

$$n_{i,sec} = \frac{\eta(i)}{2\sin\psi_1}\,c_ic_j\,P_iP_j\int_{E_j}^{E_0}\frac{\mathbf{x}(E)\tau_i(j)\tau_j(E)}{\dfrac{\mu(E)}{\sin\psi_1}+\dfrac{\mu(i)}{\sin\psi_2}}$$

$$\left\{\frac{\sin\psi_1}{\mu(E)}\,\ln\left[1+\frac{\mu(E)}{\mu(j)\sin\psi_1}\right]+\frac{\sin\psi_2}{\mu(i)}\,\ln\left[1+\frac{\mu(i)}{\mu(j)\sin\psi_2}\right]\right\}dE \tag{12}$$

Films

Free-standing single layer: primary fluorescent counts. The equation for primary fluorescent counts is developed similarly to that for the bulk material; the only difference being the integration interval for the thickness dt. Instead of an infinite upper limit, the actual thickness, T, has to be substituted:

$$n_i = c_i\,P_i\,\eta(i)\,\frac{1}{\sin\psi_1}\int_{E_i}^{E_0}\frac{\mathbf{x}(E)\,\tau_i(E)}{\dfrac{\mu(E)}{\sin\psi_1}+\dfrac{\mu(i)}{\sin\psi_2}}$$

$$\left\{1-\exp\left[-T\,\rho\left(\frac{\mu(E)}{\sin\psi_1}+\frac{\mu(i)}{\sin\psi_2}\right)\right]\right\}dE \tag{13}$$

Free-standing single layers: secondary enhancement. One difference in the derivation of the equation for bulk material and that for a film is again the interval for the thickness integration. In addition, the integral over the angle cannot be solved to give an analytical function and numerical integration has to be applied [2]. The resulting equation is

$$n_{i,sec} = \frac{\eta(i)}{2 \sin \psi_1} c_i c_j P_i P_j \int_{E_j}^{E_0} \mathbf{x}(E) \tau_i(j) \tau_j(E) \int_{\phi=0}^{\pi/2} \frac{\cos \psi}{\sin \phi} \, dE \, d\phi$$

$$\left\{ \frac{1 - \exp\left[-T\rho\left(\frac{\mu(E)}{\sin \psi_1} + \frac{\mu(j)}{\sin \phi}\right)\right]}{\left(\frac{\mu(E)}{\sin \psi_1} + \frac{\mu(j)}{\sin \phi}\right)\left(\frac{\mu(i)}{\sin \psi_2} - \frac{\mu(j)}{\sin \phi}\right)} - \frac{1 - \exp\left[-T\rho\left(\frac{\mu(E)}{\sin \psi_1} + \frac{\mu(i)}{\sin \psi_2}\right)\right]}{\left(\frac{\mu(E)}{\sin \psi_1} + \frac{\mu(i)}{\sin \psi_2}\right)\left(\frac{\mu(i)}{\sin \psi_2} - \frac{\mu(j)}{\sin \phi}\right)} + \right.$$

$$\frac{1 - \exp\left[-T\rho\left(\frac{\mu(E)}{\sin \psi_1} + \frac{\mu(i)}{\sin \psi_2}\right)\right]}{\left(\frac{\mu(i)}{\sin \psi_2} + \frac{\mu(j)}{\sin \phi}\right)\left(\frac{\mu(E)}{\sin \psi_1} + \frac{\mu(i)}{\sin \psi_2}\right)} -$$

$$\left. \frac{\exp\left[-T\rho\left(\frac{\mu(i)}{\sin \psi_2} + \frac{\mu(j)}{\sin \phi}\right)\right] - \exp\left[-T\rho\left(\frac{\mu(E)}{\sin \psi_1} + \frac{\mu(i)}{\sin \psi_2}\right)\right]}{\left(\frac{\mu(i)}{\sin \psi_2} + \frac{\mu(j)}{\sin \phi}\right)\left(\frac{\mu(E)}{\sin \psi_1} - \frac{\mu(j)}{\sin \phi}\right)} \right\} \quad (14)$$

Multilayer films: primary fluorescence. The fluorescent counts from an element, i, are the sum of all counts from all layers containing element i. Primary radiation has to penetrate all layers above the one under consideration and will be partially absorbed. Similarly, the fluorescent radiation from this layer has to penetrate all those above on its way to the detector and again absorption has to be accounted for. Modification of Eqn. 13 to include this absorption effect yields the contribution of layer m:

$$n_{[m],i} = c_{[m],i} P_i \frac{\eta(i)}{\sin \psi_1} \int_{E_i}^{E_0} \frac{\mathbf{x}(E) \, \tau_i(E)}{\frac{\mu_{[m]}(E)}{\sin \psi_1} + \frac{\mu_{[m]}(i)}{\sin \psi_2}}$$

$$\exp\left\{ - \sum_{k=1}^{m-1} \left[T_{[k]} \, \rho_{[k]} \left(\frac{\mu_{[k]}(E)}{\sin \psi_1} + \frac{\mu_{[k]}(i)}{\sin \psi_2} \right) \right] \right\}$$

$$\left\{ 1 - \exp\left[-T_{[m]} \, \rho_{[m]} \left(\frac{\mu_{[m]}(E)}{\sin \psi_1} + \frac{\mu_{[m]}(i)}{\sin \psi_2} \right) \right] \right\} dE \quad (15a)$$

and for the fluorescent radiation from all layers:

$$n_i = \sum_{m=1}^{L} n_{[m],i} \quad (15b)$$

Indices in brackets indicate the layers. The numbering of layers in such that the 'top layer', which is that closest to air (and to the detector), has the index 1.

Multilayer films: secondary enhancement within the same layer. The same type of correction as above has now to be applied to Eqn. 14:

$$n_{[m],\mathrm{i,sec}} = \frac{\eta(\mathrm{i})}{2\sin\psi_1}\, c_{[m],\mathrm{i}}\, c_{[m],\mathrm{j}}\, P_\mathrm{i} P_\mathrm{j} \int_{E_\mathrm{j}}^{E_0} \mathrm{x}(E)\tau_\mathrm{i}(\mathrm{j})\tau_\mathrm{j}(E)$$

$$\exp\left\{-\sum_{k=1}^{m-1}\left[T_{[k]}\,\rho_{[k]}\left(\frac{\mu_{[k]}(E)}{\sin\psi_1}+\frac{\mu_{[k]}(\mathrm{i})}{\sin\psi_2}\right)\right]\right\}\int_{\phi=0}^{\pi/2}\frac{\cos\phi}{\sin\phi}$$

$$\left\{\frac{1-\exp\left[-T_{[m]}\rho_{[m]}\left(\frac{\mu_{[m]}(E)}{\sin\psi_1}+\frac{\mu_{[m]}(\mathrm{j})}{\sin\phi}\right)\right]}{\left(\frac{\mu_{[m]}(E)}{\sin\psi_1}+\frac{\mu_{[m]}(\mathrm{j})}{\sin\phi}\right)\left(\frac{\mu_{[m]}(\mathrm{i})}{\sin\psi_2}-\frac{\mu_{[m]}(\mathrm{j})}{\sin\phi}\right)}\right.$$

$$-\frac{1-\exp\left[-T_{[m]}\rho_{[m]}\left(\frac{\mu_{[m]}(E)}{\sin\psi_1}+\frac{\mu_{[m]}(\mathrm{i})}{\sin\psi_2}\right)\right]}{\left(\frac{\mu_{[m]}(E)}{\sin\psi_1}+\frac{\mu_{[m]}(\mathrm{i})}{\sin\psi_2}\right)\left(\frac{\mu_{[m]}(\mathrm{i})}{\sin\psi_2}-\frac{\mu_{[m]}(\mathrm{j})}{\sin\phi}\right)}$$

$$+\frac{1-\exp\left[-T_{[m]}\rho_{[m]}\left(\frac{\mu_{[m]}(E)}{\sin\psi_1}+\frac{\mu_{[m]}(\mathrm{i})}{\sin\psi_2}\right)\right]}{\left(\frac{\mu_{[m]}(\mathrm{i})}{\sin\psi_2}+\frac{\mu_{[m]}(\mathrm{j})}{\sin\phi}\right)\left(\frac{\mu_{[m]}(E)}{\sin\psi_1}+\frac{\mu_{[m]}(\mathrm{i})}{\sin\psi_2}\right)}$$

$$-\left(\exp\left[-T_{[m]}\rho_{[m]}\left(\frac{\mu_{[m]}(\mathrm{i})}{\sin\psi_2}+\frac{\mu_{[m]}(\mathrm{j})}{\sin\phi}\right)\right]+\exp\left[-T_{[m]}\rho_{[m]}\left(\frac{\mu_{[m]}(E)}{\sin\psi_1}\right.\right.\right.$$

$$\left.\left.\left.+\frac{\mu_{[m]}(\mathrm{i})}{\sin\psi_2}\right)\right]\right)\Big/\left(\frac{\mu_{[m]}(\mathrm{i})}{\sin\psi_2}+\frac{\mu_{[m]}(\mathrm{j})}{\sin\phi}\right)\left(\frac{\mu_{[m]}(E)}{\sin\psi_1}-\frac{\mu_{[m]}(\mathrm{j})}{\sin\phi}\right)\Bigg\}\,\mathrm{d}\phi\,\mathrm{d}E \qquad (16)$$

Multilayer films: secondary enhancement between different layers. The derivation of the equation for contributions from layers above is similar to that for secondary enhancement in the bulk material.

Radiation j is excited in layer $\mathrm{d}t_{[g]}$ by primary tube radiation. The number of photons arriving and the number of emitted j-photons, respectively, are

$$\mathrm{d}n_{[g],E,\mathrm{arr}} = \mathrm{x}(E)\,\mathrm{d}E\,\exp\left\{-\frac{1}{\sin\psi_1}\sum_{k=1}^{g-1} T_{[k]}\,\rho_{[k]}\,\mu_{[k]}(E)\right\}\times$$

$$\exp\left[-t_{[g]}\,\rho_{[g]}\,\mu_{[g]}\,\frac{1}{\sin\psi_1}\right] \qquad (17)$$

$$\mathrm{d}^2 n_{[g],\mathrm{j,em}} = \mathrm{d}n_{[g],E,\mathrm{arr}}\, c_{[g],\mathrm{j}}\, P_\mathrm{j}\,\rho_{[g]}\,\tau_\mathrm{j}(E)\,\frac{\mathrm{d}t_{[g]}}{\sin\psi_1} \qquad (18)$$

A fraction $\Omega'/4\pi = 1/2 \cos\phi \, d\phi$ is emitted in the direction under consideration and reaches the layer $dt_{[m]}$, where the i-radiation is excited, after a pathlength R:

$$R = \frac{1}{\sin\phi}\left\{\sum_{k=g}^{m-1} T_{[k]} + t_{[m]} - t_{[g]}\right\} \tag{19}$$

Then $d^3n_{[m],j,arr}$ photons arrive at layer $dt_{[m]}$:

$$d^3n_{[m],j,arr} = d^2n_{[g]j,em}\ 1/2\cos\phi\, d\phi \exp\left\{-\frac{1}{\sin\phi}\left[\sum_{k=g}^{m-1} T_{[k]}\,\rho_{[k]}\,\mu_{[k]}(j) + t_{[m]}\,\rho_{[m]}\,\mu_{[m]}(j) - t_{[g]}\,\rho_{[g]}\,\mu_{[g]}(j)\right]\right\} \tag{20}$$

Then $d^4n_{[m],i,em}$ is the number of i photons emitted from layer $dt_{[m]}$ in all directions:

$$dn^4_{[m],i,em} = d^3n_{[m],j,arr}\ c_{[m],i}P_i\,\tau_i(j)\,\rho_{[m]}\,\frac{dt_{[m]}}{\sin\phi} \tag{21}$$

The number of photons arriving at the detector is

$$d^4n_i = \frac{\eta(i)}{2\sin\psi_1}\, c_{[g],j}\, c_{[m],i} P_i P_j \rho_{[m]}\,\rho_{[g]} \int_{E_j}^{E_0} x(E)\,\tau_j(E)\,\tau_i(j)$$
$$\frac{\cos\phi}{\sin\phi}\exp\left\{-\frac{1}{\sin\psi_1}\left[\sum_{k=1}^{g-1} T_{[k]}\,\rho_{[k]}\,\mu_{[k]}(E) + t_{[g]}\,\rho_{[g]}\,\mu_{[g]}(E)\right]\right.$$
$$-\frac{1}{\sin\phi}\left[\sum_{k=g}^{m-1} T_{[k]}\,\rho_{[k]}\mu_{[k]}(j) - t_{[g]}\,\rho_{[g]}\mu_{[g]}(j) + t_{[m]}\,\rho_{[m]}\,\mu_{[m]}(j)\right]$$
$$\left.-\frac{1}{\sin\psi_2}\left[\sum_{k=1}^{m-1} T_{[k]}\,\rho_{[k]}\,\mu_{[k]}(i) + t_{[m]}\,\mu_{[m]}(i)\,\rho_{[m]}\right]\right\} d\phi\, dE\, dt_{[k]}\, dt_{[m]} \tag{22}$$

The number of photons registered per second by the detector is obtained by integration over the layer thicknesses (which is possible in an analytical way) and over the angle ϕ and the energies of the primary radiation (which must be done numerically):

$$d^2n_i = \frac{\eta(i)}{2\sin\psi_1}\, c_{[g],j}\, c_{[m],i} P_j P_i \int_{E_j}^{E_0} x(E)\,\tau_j(E)\,\tau_i(j) \int_{\phi=0}^{\pi/2} \frac{\cos\phi}{\sin\phi}$$
$$\exp\left\{-\frac{1}{\sin\psi_1}\sum_{k=1}^{g-1} T_{[k]}\,\rho_{[k]}\,\mu_{[k]}(E) - \frac{1}{\sin\phi}\sum_{k=g}^{m-1} T_{[k]}\,\rho_{[k]}\,\mu_{[k]}(j)\right.$$
$$\left.-\frac{1}{\sin\psi_2}\sum_{k=1}^{m-1} T_{[k]}\,\rho_{[k]}\,\mu_{[k]}(i)\right\}$$

$$\left\{1-\exp\left[-\frac{1}{\sin\psi_2}\,T_{[m]}\,\rho_{[m]}\,\mu_{[m]}\,(\mathrm{i})-\frac{1}{\sin\phi}\,T_{[m]}\,\rho_{[m]}\,\mu_{[m]}\,(\mathrm{j})\right]\right\}$$

$$\left\{1-\exp\left[\frac{1}{\sin\phi}\,T_{[g]}\,\rho_{[g]}\,\mu_{[g]}\,(\mathrm{j})-\frac{1}{\sin\psi_1}\,T_{[g]}\,\rho_{[g]}\,\mu_{[g]}(E)\right]\right\}$$

$$\left[\left(\frac{\mu_{[g]}\,(E)}{\sin\psi_1}-\frac{\mu_{[g]}\,(\mathrm{j})}{\sin\phi}\right)\left(\frac{\mu_{[m]}\,(\mathrm{j})}{\sin\phi}+\frac{\mu_{[m]}\,(\mathrm{i})}{\sin\psi_2}\right)\right]^{-1}\mathrm{d}\phi\,\mathrm{d}E \tag{23}$$

The equations for the secondary enhancement by underlying layers are similar to those above. For the derivation, only a few differences in the geometry have to be considered (Fig. 1). The result is

$$\mathrm{d}^2n_i=\frac{\eta(\mathrm{i})}{2\sin\psi_1}\,c_{[g],\mathrm{j}}c_{[m],\mathrm{i}}P_\mathrm{j}P_\mathrm{i}\int_{E_\mathrm{j}}^{E_0}\mathbf{x}(E)\,\tau_\mathrm{j}(E)\,\tau_\mathrm{i}(\mathrm{j})\int_{\phi=0}^{\pi/2}\frac{\cos\phi}{\sin\phi}$$

$$\exp\left\{-\frac{1}{\sin\psi_1}\sum_{k=1}^{g-1}T_{[k]}\,\rho_{[k]}\,\mu_{[k]}\,(E)-\frac{1}{\sin\phi}\sum_{\mathrm{k}=m}^{g-1}T_{[k]}\,\rho_{[k]}\,\mu_{[k]}\,(\mathrm{j})\right.$$

$$\left.-\frac{1}{\sin\psi_2}\sum_{k=1}^{m-1}T_{[k]}\,\rho_{[k]}\,\mu_{[k]}\,(\mathrm{i})\right\}$$

$$\left\{1-\exp\left[-\frac{1}{\sin\psi_2}\,T_{[m]}\,\rho_{[m]}\,\mu_{[m]}\,(\mathrm{i})+\frac{1}{\sin\phi}\,T_{[m]}\,\rho_{[m]}\,\mu_{[m]}\,(\mathrm{j})\right]\right\}$$

$$\left\{1-\exp\left[-\frac{1}{\sin\phi}\,T_{[g]}\,\rho_{[g]}\,\mu_{[g]}\,(\mathrm{j})-\frac{1}{\sin\psi_1}\,T_{[g]}\,\rho_{[g]}\,\mu_{[g]}(E)\right]\right\}$$

$$\left[\left(\frac{\mu_{[g]}\,(E)}{\sin\psi_1}+\frac{\mu_{[g]}\,(\mathrm{j})}{\sin\phi}\right)\left(\frac{\mu_{[m]}\,(\mathrm{i})}{\sin\psi_2}-\frac{\mu_{[m]}\,(\mathrm{j})}{\sin\phi}\right)\right]^{-1}\mathrm{d}\phi\,\mathrm{d}E \tag{24}$$

Contributions from a bulk substrate

Equation 24 can easily be modified to provide information about the effect of secondary enhancement by the substrate. Only the thickness of the substrate layer (index g) has to be set to infinity, which simplifies the formula slightly.

The special case for secondary enhancement of a single layer by a substrate is also easily derived:

$$\mathrm{d}^2n_\mathrm{i}=\frac{\eta(\mathrm{i})}{2\sin\psi_1}\,c_{[g],\mathrm{j}}c_{[m],\mathrm{i}}P_\mathrm{j}P_\mathrm{i}\int_{E_\mathrm{j}}^{E_0}\mathbf{x}(E)\,\tau_\mathrm{j}(E)\,\tau_\mathrm{i}(\mathrm{j})\int_{\phi=0}^{\pi/2}\frac{\cos\phi}{\sin\phi}$$

$$\exp\left\{-\frac{1}{\sin\psi_1}\,T_{[m]}\,\rho_{[m]}\,\mu_{[m]}\,(E)\right\}$$

$$\left\{ 1 - \exp\left[-\frac{1}{\sin\psi_2} T_{[m]}\, \rho_{[m]}\, \mu_{[m]}\,(\mathrm{i}) + \frac{1}{\sin\phi} T_{[m]}\, \rho_{[m]}\, \mu_{[m]}\,(\mathrm{j}) \right] \right\}$$

$$\left[\left(\frac{\mu_{[g]}(E)}{\sin\psi_1} + \frac{\mu_{[g]}(\mathrm{j})}{\sin\phi} \right) \left(\frac{\mu_{[m]}(\mathrm{i})}{\sin\psi_2} - \frac{\mu_{[m]}(\mathrm{j})}{\sin\phi} \right) \right]^{-1} \mathrm{d}\phi\, \mathrm{d}E \qquad (25)$$

DISCUSSION OF THE THEORETICAL FORMULAE

If the exponential term in Eqn. 25 is very small (i.e., $\ll 1$), the approximation $e^{-\Delta} \approx 1 - \Delta$ is valid. In such cases, the intensity is proportional to concentration and the interelement effects are negligibly small. In addition, the intensity of the analyte lines increases linearly with film thickness. Several published methods are based on such linear relationships and resulting calibration curves [3—5]. It has also been shown that the specimen need not be flat or specially shaped, and successful applications to coated wires and filaments have been reported [6].

In the case of general multiple film samples, prediction of intensities is possible if the qualitative and quantitative composition of each individual film as well as their thicknesses are known. Simultaneous back-calculation of concentrations and thicknesses requires that the qualitative composition of each film be known and that the weight fractions add up to 1 within each layer. An additional limitation is that any chemical element can be contained in only one layer; this is a purely mathematical condition because otherwise the number of unknowns exceeds the number of equations.

In specimens for which chemical elements appear in more than one layer, additional information must be supplied. This may be the case, for example, if one of the film thicknesses is known, if stoichiometric relationships exist between certain elements, if the quantitative composition of one layer is known, or if more than one line (with a quite different absorption characteristic in the specimen) of an element has been measured. From a practical and numerical point of view, this additional condition must have a significant relationship with the measured intensity of the pertinent analyte line.

In practical applications, the density of films is strongly dependent on the manufacturing process and the thickness and may be considerably lower than that of the bulk. The geometrical (optical) thickness, T, should therefore be replaced by the 'mass thickness' (mass per unit area), $T_i = m_i/A\,\rho_i$. Most thickness monitors in evaporation apparatus, like quartz oscillators, measure mass thicknesses rather than geometrical thicknesses; interferometric procedures or devices based on a mechanical stylus, however, measure geometrical thicknesses.

Numerical considerations

The rather complex structure of the equations presented required sophisticated computer methods for numerical evaluations [7]. The algorithms do not require any initial values, but accept known parameters (concentrations and/or thickness(es)) as input. These known parameters are then not included

in the iteration procedure. Any number of standards can be used with arbitrary compositions; if more than one intensity value is provided as standard for an analyte line, least-square methods are applied. In such a way, any information supplied by an unlimited number of standards contributes to the accuracy of the result.

Iteration loops for simultaneous concentration and thickness determination (back-calculation) start with the uppermost layer (closest to air), where intensities are not affected by absorption in other layers, and continue downwards. Several refinement cycles, each looping through all layers, are allowed. In three-layer films with a total of six elements, between 4 and 15 overall cycles are generally required before meeting the cut-off condition (i.e., no individual relative value changes by more than 0.0001 compared to the previous iteration step).

REFERENCES

1 J. Sherman, Spectrochim. Acta, 7 (1955) 283.
2 G. Pollai, M. Mantler and H. Ebel, Spectrochim. Acta, Part B, 26 (1971) 747.
3 S. K. Jain, P. P. Gupta and A. C. Eapen, X-Ray Spectrom., 8 (1979) 11.
4 N. S. Saleh and A. B. Hallak, X-Ray Spectrom., 12 (1983) 170.
5 F. H. Chung, A. J. Lentz and R. W. Scott, X-Ray Spectrom., 3 (1974) 172.
6 J. L. Ponchon, P. Bourrain and A. Palsky, X-Ray Spectrom., 12 (1983) 79.
7 M. Mantler, Adv. X-Ray Anal., 27 (1984) 433.

Analytica Chimica Acta, 188 (1986) 37—50
Elsevier Science Publishers B.V., Amsterdam — Printed in The Netherlands

A FUNDAMENTAL PARAMETERS APPROACH INCLUDING SCATTERED RADIATION FOR MONO-ENERGETICALLY EXCITED SAMPLES IN ENERGY-DISPERSIVE X-RAY FLUORESCENCE SPECTROMETRY

ALESSANDRA RACHETTI and WOLFHARD WEGSCHEIDER*

Institut für Analytische Chemie, Mikro- und Radiochemie, Technische Universität Graz, Technikerstraße 4, A-8010 Graz (Austria)

(Received 12th November 1985)

SUMMARY

A fundamental parameters approach that incorporates data on scattered radiation is shown to be a useful tool for the determination of trace elements in light matrices. For thick, transparent samples, a computer program is developed that uses differential intensity equations adjusted for decreasing geometric efficiency. Various organic and biological reference materials are analysed to assess the reliability of the procedure. A nested design for analysis of variance shows that major errors can originate from the deconvolution process and sample inhomogeneities in many cases. For loose powders, great care must be exercised to avoid errors caused by scatter from the sample cups. The program is also useful for alloys.

Recently, an increasing number of calibration methods that rely on fundamental physical parameters has been developed. Among other advantages, these procedures have introduced corrections that permit reasonably accurate determinations by x-ray fluorescence spectrometry (x.r.f.) on less than ideal samples without matching standards being required. The extension of this approach to samples with significant concentrations of light elements is very desirable for agricultural and environmental purposes. The sum of these light elements can be regarded as a "residual matrix" defined to denote those components of a sample that do not give signals from K, L or M lines under the experimental conditions used. For energy-dispersive (e.d.) x.r.f. on loose powders, this may well include the light elements up to chlorine.

Early work [1] showed that scattered radiation provides analytically valuable information. However, it took much longer and required the use of a pseudo-monochromatic excitation source to incorporate scatter coefficients into a fundamental parameter approach [2]. Refinements that have taken place since then include estimation of effective sample weight [3, 4], processing of samples with widely varying thicknesses [5], consideration of more than one excitation mode [6] and others [7, 8]. Despite the reported advantages of incorporating scatter in fundamental parameters calculations,

0003-2670/86/$03.50

practical limitations are not clear from literature data and experience seems to be limited to two research groups. One group advocates the approximation of the residual matrix by one element only [3, 5], while the other recommends the use of two elements [2] that involves some uncertainty in the selection procedure [8].

This paper describes a fundamental parameters approach based on coherently and incoherently scattered radiation. Its performance is tested on a variety of samples, including botanical material, sewage sludge and alloys. The method is similar to Nielson's approach [2] in that it relies on two elements for the definition of the residual matrix, but it avoids some of the ambiguity in the selection process. Additionally, the energy range is expanded over previous work by exciting with samarium K radiation. As this causes the approximation of constant geometry to fail for thick transparent samples, the differential forms of the fundamental parameters equations are used.

THEORY AND COMPUTATIONS

Scattered radiation in x.r.f. is composed of contributions from all elements in a sample if care is exercised to ensure that the sample support and the spectrometer chamber do not cause radiation to be observed. In quantitative terms, the scattered intensity can be described as a weighted sum of single element contributions, weighted both for the area weight of the element in the sample and for the scatter cross-section of this element [2, 3]:

$$I(\mathrm{co}) = k(\mathrm{co}) \sum w(\mathrm{i})\, \sigma(\mathrm{co}, \mathrm{i}) \tag{1}$$

$$I(\mathrm{in}) = k(\mathrm{in}) \sum w(\mathrm{i})\, \sigma(\mathrm{in}, \mathrm{i}) \tag{2}$$

where $I(\mathrm{co})$ and $I(\mathrm{in})$ are the observed absorption-corrected intensities of coherent and incoherent scatter, $w(\mathrm{i})$ is the area weight of element i (in g cm^{-2}) and the σ's are the cross-sections available from literature [9]. The parameters $k(\mathrm{co})$ and $k(\mathrm{in})$ are evaluated experimentally from standard samples. As $\sigma(\mathrm{co})$ increases and $\sigma(\mathrm{in})$ decreases with increasing atomic number, the system described by Eqns. 1 and 2 is well conditioned and the area weight of two elements of the residual matrix is thus defined. For more than two elements in the residual matrix, the relationships are approximate only. Contributions of elements quantified through their characteristic radiation are subtracted from $I(\mathrm{co})/k(\mathrm{co})$ and $I(\mathrm{in})/k(\mathrm{in})$ before the area weight of the light elements is computed.

Absorption and enhancement corrections are applied in the usual manner [10]. Thick transparent samples, however, have to be subjected to the differential correction procedure:

$$\mathrm{d}I(\mathrm{i}) = \exp\{-\rho \times [\mu(E^0)\ \mathrm{cosec}\ \psi_1 + \mu(E_\mathrm{i})\ \mathrm{cosec}\ \psi_2]\}\ c(\mathrm{i})\rho I(E^0)\, F(\mathrm{i})\ \epsilon(E_\mathrm{i})$$
$$\times\ \mathrm{cosec}\ \psi_2\ [\mathrm{d}\Omega(x)/4\pi]\ \mathrm{d}x \tag{3}$$

where $dI(i)$ is the intensity of the fluorescence radiation from element i emerging from a sample depth interval dx, the exponential term is the well known expression for absorption correction, $c(i)$ is the relative amount of element i in the sample, ρ is the density of the sample, $I(E^0)$ is the intensity of the exciting radiation, $F(i)$ is a factor dependent on the physical constants (photoelectric cross-section, absorption jump ratio, fluorescence yield, intensity fraction $K\alpha/(K\alpha + K\beta)$), $\epsilon(E_i)$ is the detector efficiency for the characteristic radiation and $[d\Omega(x)/4\pi]$ is the depth-dependent geometric constant that is determined experimentally from a separate set of experiments. The total intensity, $I(i)$, is obtained by summing over all depth elements, dx, in steps of 0.5 mm. This, however, presupposes knowledge of the total sample depth, d, and Eqns. 1 and 2 have to be rewritten as

$$I(\mathrm{co})/\int_d k(\mathrm{co}, x) = \sum w(\mathrm{i})\, \sigma(\mathrm{co}, \mathrm{i}) \tag{4}$$

$$I(\mathrm{in})/\int_d k(\mathrm{in}, x) = \sum w(\mathrm{i})\, \sigma(\mathrm{in}, \mathrm{i}) \tag{5}$$

A flow chart of the program is given in Fig. 1. Basic data, such as target, intensities, etc., are provided and one of the program options is selected. Currently available are options for thin and thick pressed organic samples that differ in that thick samples are corrected for the volume effect by Eqn. 3, and an option for thin and thick inorganic samples that operates without the scatter-correction procedure. For loose powders, the appropriate option corrects for the scattered radiation from the mylar. For thick inorganic samples, the area weight is not calculated but set up to a value beyond infinite thickness. Blank counts are subtracted according to a scheme that accounts for the increase of the spectrometer blank with increased sample weight. Next, a first estimate of the "heavy" elements from stored calibration factors is computed for one of the following secondary targets: titanium, zirconium or samarium. Depending on the option previously chosen, a light element mass may or may not be estimated. These data are then converted to concentrations and the appropriate absorption and enhancement factors are calculated. From Eqn. 3, a volume correction factor is then derived from the given composition and the input thickness. These calculations are repeated iteratively until convergence to constant concentration values is achieved or for fifteen iterations, whichever is shorter. The output is optionally in $\mu g\ cm^{-2}$ or as percentage. Light element masses are given where applicable.

EXPERIMENTAL

Apparatus

All x-ray measurements were made on an energy-dispersive system (Philips/Edax EXAM VI) equipped with an x-ray generator (PW 1140), and a secondary target turret with Ti, Zr and Sm. The targets were excited by a tungsten side-window tube; the Si(Li)-detector had a resolution of 180 eV. For

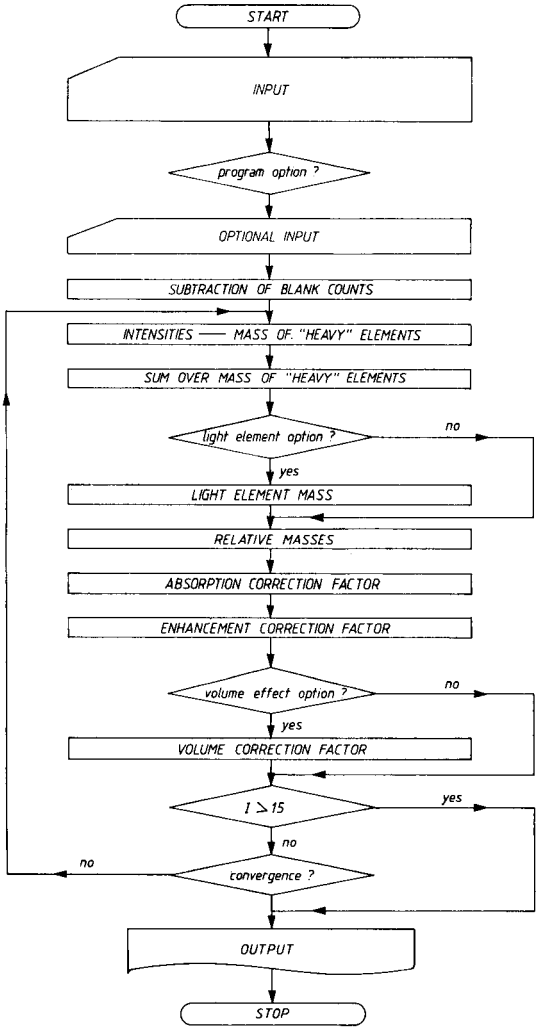

Fig. 1. Flow chart of computer program. The input includes atomic numbers, energy of fluorescence lines, intensities of fluorescence lines and scattered radiation, mA, time of measurement, program option. Optional input includes thickness, weight and fixed light element.

deconvolution, a previously described program [11] gave net intensities for the characteristic radiation and the background radiation. Integration over the channels calibrated to contain scattered radiation yielded gross intensities of Rayleigh and Compton scatter. The system was calibrated with metal foils for the elements of Al, Ti, Fe, Co, Ni, Cu, Zn, Nb, Mo, Sn, Ta, W, Au and Pb (Goodfellow Metals, Cambridge, England) with thicknesses ranging from 9 to 25 μm and with suitable compounds deposited on Whatman 541

cellulose filters (area weight ca. 8 mg cm^{-2}) for the elements P, S, Cl, K, Ca, As, Br, Sr, Cd and Sb (Columbia Scientific Industries Corp., Austin, TX). The absorption-corrected data given in Fig. 2 show that no difference is discernible between the metal foils and filter paper standards.

To evaluate the calibration factors for the coherently and incoherently scattered radiation, scatter from the metal foils was corrected for absorption and normalized to the respective scatter cross-section. Additional measurements were taken on S/C-pellets. The relative standard deviations of the calibration factor were 14% for the coherent scatter and 25% for the incoherent scatter.

Samples

To assess accuracy and precision, standard reference materials were processed. The following materials were obtained from the National Bureau of Standards (Washington, DC): SRM 1566 Oyster Tissue, SRM 1570 Spinach, SRM 1571 Orchard Leaves, SRM 1572 Citrus Leaves, SRM 1573 Tomato Leaves, SRM 1575 Pine Needles, SRM 1577 Bovine Liver, SRM 1632a Bituminous Coal, SRM 1635 Subbituminous Coal, SRM 1646 Estuarine Sediment, SRM 1198 Incoloy, SRM 1201 Hastelloy, SRM 1102 Brass, SRM 1119 Aluminium Brass. Aquatic Plant, Aquatic Moss and Sewage Sludge were purchased from the Bureau of Reference (BCR, Brussels). The loose samples were either pressed at 168 MPa or processed as powders in a Spectro-Cup (Somar) covered with a 6-μm mylar foil. A spectrum of mylar is subtracted before running the fundamental parameters program.

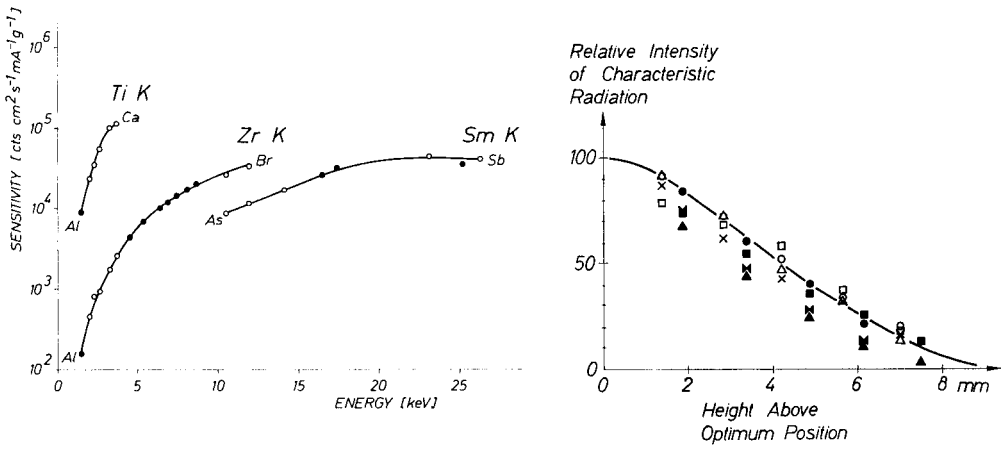

Fig. 2. Results of the calibration of the x-ray spectrometer: (•) for pure metal foils; (○) for compounds on filter paper.

Fig. 3. Depth dependence of the fluorescent intensities for various elements and targets (in parentheses): (△) Pb(Zr); (×) Pb(Sm); (○) Cu(Zr); (□) Sn(Sm); (▲) S(Ti); (⋈) K(Ti); (•) K(Zr); (▪) Sr(Zr).

Nested design

Because good sample homogeneity is a prerequisite for the direct analysis of materials by e.d.x.r.f., a separate set of experiments was conducted to discriminate between errors inherent in physical assumptions of the data reduction scheme and errors from sample imperfections. Five separate pellets (ca. 0.3 g cm^{-2}) were pressed from NBS SRM 1570 Spinach and processed twice from both sides yielding four spectra per pellet. The spectra were subjected to the deconvolution and the fundamental parameters regime; from the resulting concentration data, error contributions from sample preparation, front/back differences and the fundamental parameters procedure including those from deconvolution, were computed by analysis of variance. Poisson errors are given without regard to effects of overlap and background.

RESULTS AND DISCUSSION

Fairly thick pressed pellets of organic and biological SRM's were examined, with oxygen initially fixed as one of the elements defining the residual matrix. The other element was chosen to give the best match between the observed ratio of scattered radiation and the theoretical ratio calculated from scatter cross-sections. The program automatically switches from oxygen to another element if the incoherent/coherent ratio cannot be accommodated by either of the two extremes, H/O or F/O. Data for the light elements are given along with the main results in Table 1. Problems exist mainly for light elements and are attributed to incorrect deconvolution. This is also supported by the results given on alloys (see below). It is also clear that inhomogeneities would cause this method to fail; potential indicators are Ca and Zn in Oyster Tissue or Fe and Cu in Bovine Liver. For these two materials, a second pellet was processed and the averaged data are given. Calcium in Oyster tissue is consistently low. To decide how serious this problem is, several other reference materials were examined (Table 2). As expected, appreciable errors from deconvolution of light element intensities and errors from overlap of a trace element with a major element (e.g., Cr and Mn in Bituminous Coal and Subbituminous Coal) were observed; Mn and Zn in Aquatic Plant and Cu and Ni in Estuarine Sediment, however, seem to be affected by inhomogeneities.

For SRM 1570 (Spinach), a factorial design was run to assess the relative sizes of the errors because some elements showed systematic deviations. The data are given in Table 3. The Poisson error was derived as a first approximation from the square root of the net intensities and is significant for the elements Cr, Mn, Fe, Ni, Cu, Zn and Br. For the elements Si, P, S, K, Cr and Pb, the error from replicate measurements on the same pellet from the same side is 10% or more. Small scale inhomogeneities are indicated by the differences in results between both sides of the pellet and are important for Si, Ca, Ni and Cu, while they are similar to larger scale inhomogeneities for sulphur. Systematic deviations for Ca and Pb may be caused by a mineralogical effect.

For thick samples, the observed fluorescence yield may be less than expected from the calibration procedure because calibration was done with relatively thin samples, the depths of which were negligible relative to the sample-to-detector distance. This phenomenon is caused by a change of the effective solid angle and can be dealt with in different ways [12, 13]. Here, some of the metal foils used for calibration were measured at different distances from the detector and the intensities were normalized to the maximal intensity at the smallest distance. Figure 3 gives this dependence that served as a basis for model calculations to assess the importance of this effect. The results showed, in accordance with data given by Weber [13], that the intensity loss would be particularly large for trace elements with higher atomic weights in light matrices, such as strontium in coal (18% less intensity for excitation with the Zr target), barium in silica (22% less intensity for Sm excitation), and barium in cellulose (50% less intensity for Sm excitation). All of these data refer to infinite thickness. The data from Fig. 3 were then used to adjust the calibration factors in the differential calculation scheme (Eqn. 3). Cellulose powder was mixed with tin powder at a nominal concentration of 1% tin; four pellets ranging from 190 to 1400 mg cm^{-2} were prepared and the tin content was determined by excitation with the Sm target. The apparent content decreased from 0.96 to 0.60% without depth correction, while it stayed constant if the differential depth correction was applied (0.92 ± 0.08%). Although BCR Sewage Sludge is not strictly a light matrix, the mean for cadmium increased on the same set of measurements from 70 to 76 $\mu g\ g^{-1}$ (r.s.d. < 10%) close to the certified value of 77.7 ± 2.6 $\mu g\ g^{-1}$.

Because one of the aims of fundamental parameters quantitation is to keep sample preparation as simple as possible, the influence of different preparation procedures was tested. A powdered sample, either pressed to a pellet or as loose powder was processed in a Spectro-Cup covered with mylar. The results are given in Table 4. The area weight was varied from 81 to 620 mg cm^{-2} in seven steps and two program options are contrasted in the Table: one, for which the area weight is explicitly included in the calculation ("fixed weight") to provide for depth correction, and one for which the weight is determined by a calculation first described by Van Espen et al. [3]. It can be seen that, overall, the standard deviation is similar in both instances, but the "fixed weight" option gives better accuracy. The numbers for the thinnest and thickest samples are provided because they show larger differences for the "fixed weight" than for the "free weight" option. Clearly, for the thinnest sample, the results are not very different. Because this tabular summary of results does not give the entire picture, Fig. 4 details the depth dependence. For all elements, there is a discontinuity between 163 and 240 mg cm^{-2} caused by a change in the selection of the elements used to define the residual matrix, which in turn is brought about by a drop of the incoherent/coherent ratio from about 1.15 to 0.99 (Fig. 4D). Although the higher ratio is best accommodated by the element combination of hydrogen and oxygen, the lower ratio is best accommodated by hydrogen and fluorine.

TABLE 1

Results for organic and biological reference materials[a]

Element	Oyster tissue[b]		Orchard leaves[c]		Citrus leaves[c]	
	Certified	Found	Certified	Found	Certified	Found
Mg[d]			0.62 /0.02	0.57 /0.09	0.58 /0.03	0.47 /0.03
Al[d]		0.48 /0.15				
Si[d]						
P[d]	(0.81)	0.57 /0.12	0.21 /0.01	0.26 /0.03	0.13 /0.02	0.25 /0.02
S[d]	(0.76)	0.73 /0.01	(0.19)	0.23 /0.05	0.407 /0.009	0.46 /0.05
Cl[d]	(1.0)	0.75 /0.06	(0.069)	0.059 /0.006	(0.041)	0.020 /0.004
K[d]	0.965 /0.005	0.82 /0.05	1.47 /0.03	1.66 /0.13	1.82 /0.06	1.84 /0.23
Ca[d]	0.15 /0.02	0.10 /0.04[e]	2.09 /0.03	2.03 /0.15	3.15 /0.1	3.2 /0.4
Mn	17.5 /1.2	17.3 /6.3	91 /4	102 /12	23 /2	32 /6
Fe	195 /34	195 /6.8[e]	300 /20	300 /34	90 /10	76 /9
Ni	1.3 /0.19	2.8 /0.8	1.3 /0.2	3 /1	0.6 /0.3	2.5 /1.0
Cu	63 /3.4	58.5 /1.8	12 /1	15 /2	16.5 /1.0	17.5 /2.0
Zn	852 /14	775 /23	25 /3	28 /2	29 /2	30 /5
Br	(55)	57.5 /2	(10)	10 /1	(8.2)	7.9 /0.6
Pb	0.48 /0.04		45 /3	53 /3	13.3 /2.4	14.4 /1.0
Light elem.		96.4 /0.6		93.2 /0.4		91.6 /0.9

	Pine needles[c]		Bovine liver[b]	
	Certified	Found	Certified	Found
Mg[d]				0.14 /0.04
Al[d]	0.0545 /0.0003	0.33 /0.04		0.53 /0.03
Si[d]		0.082 /0.024	(0.0017)	
P[d]	0.12 /0.02	0.09 /0.02	(1.1)	0.91 /0.07
S[d]		0.11 /0.01		0.64 /0.06
Cl[d]		0.017 /0.005	(0.27)	0.21 /0.02
K[d]	0.37 /0.02	0.35 /0.02	0.97 /0.06	0.83 /0.11
Ca[d]	0.41 /0.02	0.42 /0.02	0.0124 /0.006	0.0088 /0.0020
Mn	675 /15	626 /61	10.3 /1	9.1 /7.2
Fe	200 /10	168 /10	268 /8	236 /29[e]
Ni	(3.5)	3.9 /0.5		1.5 /1.8
Cu	3.0 /0.3	2.7 /0.4	193 /10	197 /22[e]
Zn		57.3 /4.0	130 /13	121 /14
Br	(9)	8.2 /0.7		10 /1
Pb	10.8 /0.2	11.2 /0.9	0.34 /0.08	0.1 /0.1
Light elem.		98.5 /0.1		96.7 /0.3

[a]Results are given as $\mu g\ g^{-1}$ except where indicated, with standard deviations. Certified values in parentheses are tentative only. [b]For $N = 4$. [c]For $N = 3$. [d]Results given as percentage. [e]Average of duplicate pellets.

TABLE 2

Results for single samples of reference materials[a]

Element	Aquatic plant		Aquatic moss		Estuarine sediment		Bituminous coal		Subbituminous coal	
	Certified	Found	Certified	Found	Certified	Found	Certified	Found	Certified	Found
Al[d]	(0.614)	1.6	(1.71)	1.54	6.25 /0.20	8.72	(3.1)	3.9	(0.32)	0.36
Si[d]	(2.85)	3.0	(7.5)	5.05	(31)	36	& 5.8	6.8		0.69
P[d]	(0.515)	0.7	(0.92)	1.03	0.054 /0.005	0.23		0.16		
S[d]	(0.52)	0.75	(0.23)	0.34	(0.96)	1.46	1.62 /0.03	1.75	0.33 /0.03	0.44
Cl[d]	(1.0)	1.1	(0.23)	0.24		1.97	0.079 /0.002	0.095	0.0026 /0.0004[f]	0.0025
K[d]	(1.14)	2.3	(1.24)	1.27	(1.4)	2.3	0.42 /0.02	0.42	0.012 /0.001[f]	0.012
Ca[d]	(3.09)	2.9	(1.69)	1.87	0.83 /0.03	1.05	0.23 /0.03	0.26	0.57 /0.07[f]	0.79
Cr	(532)	496	(532)	469	76 /3	88	34.4 /1.5	15.7	2.5 /0.03	n.d.
Mn	1759 /51	2120	3771 /78	3709	375 /20	322	28 /2	n.d.	21.4 /1.5	14.2
Fe	(2380)	2520	(9303)	8100	3.35 /0.10[d]	3.94[d]	1.11 /0.02[d]	1.09[d]	2390 /5	2300
Ni	(40)	46.8	(420)	458	32 /3	43[e]	19.4 /1.0	36.7	1.74 /0.1	7.2
Cu	51.2/1.9	50.1	720 /31	685	18 /3	17[e]	16.5 /1	20.6	3.6 /0.3	4.4
Zn	313 /8	352	566 /13	565	138 /6	151	28 /2	32	4.7 /0.5	5.4
Br	(20)	18	(22)	17.5		144	41 /4	55	1.6 /0.3[f]	
Pb	63.8/3.2	71	64 /3.5	67.1	28.2 /1.8	26.7	12.4 /0.6	8.9	1.9 /0.2	

[a]Footnotes as for Table 1; n.d. means not deconvoluted. [f]Data from [15].

TABLE 3

Error analysis for NBS SRM 1570 Spinach

Element	Certified		Mean	Error from				Total error
	Mean	Error		Pellet	Front/back	Replication	Poisson	
Si[a]	—		0.18	—	0.03	0.04	0.002	0.05
P[a]	0.55	/0.02	0.51	—	—	0.06	0.014	0.07
S[a]	—		0.50	0.01	0.01	0.05	0.010	0.07
Cl[a]	—		0.80	—	—	0.06	0.008	0.08
K[a]	3.56	/0.03	3.96	—	—	0.32	0.010	0.38
Ca[a]	1.35	/0.03	0.84	—	0.09	0.06	0.008	0.12
Cr[b]	4.6	/0.3	2.30	—	—	4.40	0.70	3.80
Mn[b]	165	/6	165.0	—	—	19	9	19
Fe[b]	550	/50	541.0	—	—	48	13	53
Ni[b]	(6)		6.1	—	0.7	0.9	1.1	1.3
Cu[b]	12	/2	12.5	—	0.6	1.0	0.8	1.5
Zn[b]	50	/2	52.1	—	—	3.7	1.9	4.5
Br[b]	(54)		64.0	—	—	4.0	1.0	4.0
Pb[b]	1.2	/0.2	5.3	—	—	1.3	0.14	1.3

[a]Data as %. [b]Data as $\mu g\ g^{-1}$.

Also seen from Fig. 4 is the asymptotic rise of results typical for thin transparent samples; the mean atomic number of the residual matrix is underestimated because significant scatter from the polypropylene sample cup is detected up to about 200 mg cm^{-2}. This is also supported by the data for pressed pellets in Table 4 with area weights ranging from 121 to 620 mg cm^{-2}. Because the correction for thickness is less important here, the "free weight" option uniformly gives better values in all respects, including smaller range and better accuracy and precision.

For alloys, the fundamental parameters program NRLXRF [14] has found wide acceptance. With the incorporation of corrections for the enhancement effect, the described program should in principle be suitable for this application also. For alloys, the scatter data are ignored; instead, a scaling of the results to 100% can be done if justified. Results are presented in Table 5 and compared to those obtained by NRLXRF. The latter was calibrated by data from Incoloy for Hastelloy and from Brass for Aluminium Brass. The calibration with similar alloys, along with the "SUM-100" mode, works well as long as there is no calibration error such as seen for aluminum in Brass, leading to erratic results for aluminum in Aluminum Brass. If the concentration of aluminum is supplied (fixed), the data improve considerably. Because the calibration in the present program is done independently, it works better in cases for which the calibration with intensities from similar alloys is unreliable and less well in other situations. This is not surprising because the calibration with pure elements requires higher accuracy of the physical model.

TABLE 4

Effect of sample preparation on results for SRM Tomato leaves[a]

Element	Certified	Loose powder (81—620 mg cm^{-2})[b]				Pressed pellets (122—620 mg cm^{-2})[c]			
		Fixed weight		Free weight		Fixed weight		Free weight	
		Range[d]	Mean	Range[d]	Mean	Range[d]	Mean	Range[d]	Mean
K (%)	4.46 /0.03	3.9—4.7	4.46 /0.40	3.9—4.0	4.14 /0.34	4.3—4.8	4.71 /0.24	4.5—4.5	4.48 /0.04
Ca (%)	3.00 /0.03	2.6—3.1	2.98 /0.24	2.6—3.0	2.78 /0.22	3.5—3.8	3.80 /0.18	3.7—3.7	3.70 /0.06
Mn	238 /7	209—261	240 /27	210—222	220 /14	284—256	282 /15	305—251	276 /17
Fe	690 /25	565—666	639 /52	563—563	584 /57	725—673	713 /37	776—657	694 /45
Cu	11 /1	11.2—11.8	11.0 /0.7	11.2—9.8	10 /1.5	11.4—9.6	11.7 /1.4	12.1—9.3	11.4 /1.2
Zn	62 /6	54—65	63 /5	54—54	56 /5	66—69	71 /4	69—67	68 /1
Br	(26)	21—28	25 /3	25—24	23 /1	30—28	30 /3	28—27	28 /2
Rb	16.5 /0.1	16—16	21 /6	18—14	19 /5	20—28	25 /4	18—27	23 /2
Pb	6.3 /0.3	4.5—9.5	6.5 /2	5—8	6 /2	9.2—7.2	7.8 /1	8.5—6.9	7.3 /1

[a]Data given as $\mu g\ g^{-1}$ (except where indicated) with standard deviation. [b]$N = 7$. [c]$N = 6$. [d]Data for thinnest and thickest sample, respectively.

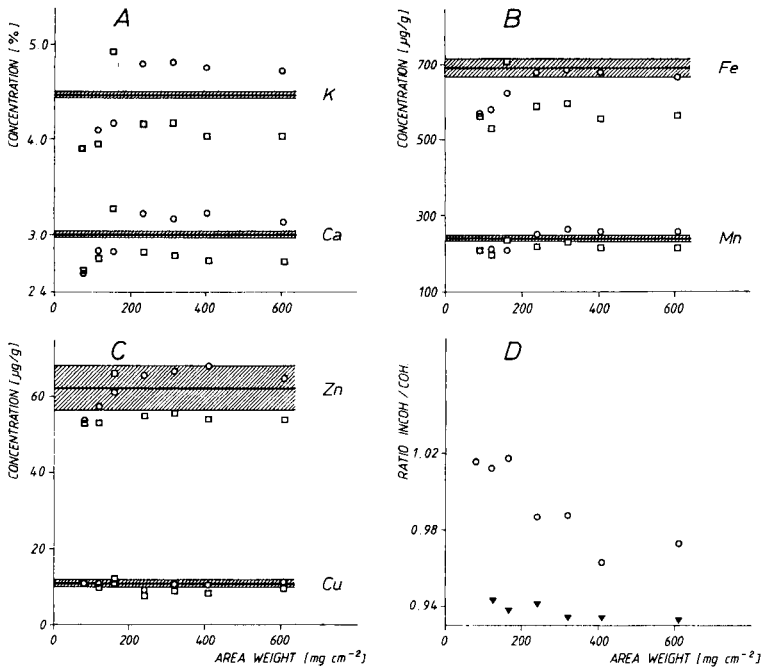

Fig. 4. Variation of results and incoherent/coherent ratios as a function of area weight. For A—C: (○) loose powders, fixed weight; (□) loose powders, free weight. For D: (○) variation of incoherent/coherent ratio for loose powders; (▼) variation of this ratio for pressed pellets.

TABLE 5

Results for alloys (all results in %)

Elements	Incoloy		Hastelloy			Brass		Aluminum Brass		
	Cert.	This work	Cert.	This work	NRLXRF	Cert.	This work	Cert.	This work	NRLXRF
Al	0.24	0.76	—	0.26	0.08	0.0007	0.68	2.1	2.0	0.002 (fixed)
Si	0.38	0.38	0.54	0.74	0.74					
Ti	2.59	2.43								
Cr	12.9	11.5	20.7	18.7	21.5					
Mn	0.49	0.65								
Fe	36.2	33.4	23.2	21.0	24.2	0.011	0.032	0.03	0.02	0.01
Co	0.70	1.10	0.56	0.79	0.53					
Ni	40.1	42.2	45.7	47.8	46.0	0.005	0.003			
Cu						72.8	72.9	77.1	78.2	79.9 (78.4)
Zn						27.10	25.4	20.5	19.7	21.3 (20.8)
Zr	0.014	0.020								
Mo	6.0	7.6	9.18	10.5	8.50					
Ag						0.001	0.025			
Sn						0.006	0.011			
Sb						0.005	0.005	0.05	0.08	0.05

This research was supported in part by a grant from the Fonds zur Förderung der wissenschaftlichen Forschung, Vienna (Project P5200).

REFERENCES

1 G. Andermann and J. W. Kemp, Anal. Chem., 30 (1958) 1306.
2 K. K. Nielson, Anal. Chem., 49 (1977) 641.
3 P. Van Espen, K. Van't Dack, F. Adams and R. Van Grieken, Anal. Chem., 51 (1979) 961.
4 H. Kubo and W. R. Smythe, Anal. Chem., 51 (1979) 1194.
5 P. M. Van Dyck and R. E. Van Grieken, Anal. Chem., 52 (1980) 1859.
6 R. W. Sanders, K. B. Olsen, W. C. Weimer and K. K. Nielson, Anal. Chem., 55 (1983) 1911.
7 K. K. Nielson and R. W. Sanders, Adv. X-Ray Anal., 26 (1983) 385.
8 K. K. Nielson and V. C. Rogers, Adv. X-Ray Anal., 27 (1984) 449.
9 W. H. McMaster, N. Delgrande, J. H. Mallet and J. H. Hubbell, Compilation of X-ray Cross-Sections, Report UCRL-50174 University of California, Lawrence Livermore Radiation Laboratory, 1969.
10 R. Tertian and F. Claisse, Principles of Quantitative X-Ray Fluorescence Analysis, Heyden, London, 1982.
11 E. Marageter, W. Wegscheider and K. Müller, Nucl. Instrum. Methods, B1 (1984) 137.
12 K. Weber, X-Ray Spectrom., 3 (1974) 159.
13 A. Weber, X-Ray Spectrom., 12 (1983) 11.
14 J. W. Criss, L. S. Birks and J. V. Gilfrich, Anal. Chem., 50 (1978) 33.
15 M. S. Germani, Inci Gökmen, A. C. Sigleo, G. S. Kowalczyk, Ilhan Olmez, A. M. Small, D. L. Anderson, M. P. Failey, M. C. Gulovali, C. E. Choquette, E. A. Lepel, G. E. Gordon and W. H. Zoller, Anal. Chem., 52 (1980) 240.

Analytica Chimica Acta, 188 (1986) 51—57
Elsevier Science Publishers B.V., Amsterdam — Printed in The Netherlands

MULTILAYERED STRUCTURES AS DISPERSING DEVICES IN X-RAY SPECTROMETRY

JOHN V. GILFRICH
Naval Research Laboratory, Washington, DC 20375-5000 (U.S.A.)
(Received 25th November 1985)

SUMMARY

Artificial Bragg diffractors (multilayers) are useful dispersing devices for the quantification of boron to silicon (atomic numbers 5—14). This paper describes the preparation, characterization and recent efforts to use such devices in that application, particularly where dispersing crystals of appropriate spacings for wavelength-dispersive spectrometers are not available.

For over fifty years, attempts have been made to produce alternating layers of different materals for use as dispersing media in x-ray spectrometers [1]. Success came slowly, culminating in the production of usable devices by evaporation or sputtering a few years ago [2—4]. The history of these efforts has been reviewed [5]. The development of these multilayered structures (or layered synthetic microstructures) demonstrated the importance of substrate smoothness and exceptional control of the deposition process. More recently, the techniques for producing multilayers engineered for x-ray spectrometer optics have been refined, making it possible to produce them commercially with optimum layer compositions and thickness (ECD; Energy Conversion Devices, Troy, MI). The major advantage of multilayers is illustrated in Fig. 1, which shows the way in which the continuous variability of layer spacing fills in the gap between conventional crystals and gratings as dispersing devices. While it is true that multilayers prepared by the Langmuir-Blodgett technique, such as lead octadecanoate (stearate), also have layer spacings in the same range, they are limited to discrete values and are not particularly efficient diffractors. In contrast, the multilayers being considered here can be tailored to have larger diffraction efficiencies than any other wavelength-dispersive device for intermediate wavelengths.

The principle of efficient diffraction of x-ray photons by these multilayers depends on electron-density contrast between the alternating layers, i.e., layers of high electron density separated by layers of low electron density. For the multilayers produced at Stanford University and examined at the Naval Research Laboratory (NRL), the layer with low electron density was always carbon, while the layers with high electron density were transition metals of widely different atomic numbers, specifically titanium, niobium or molybdenum, and tungsten.

0003-2670/86/$03.50

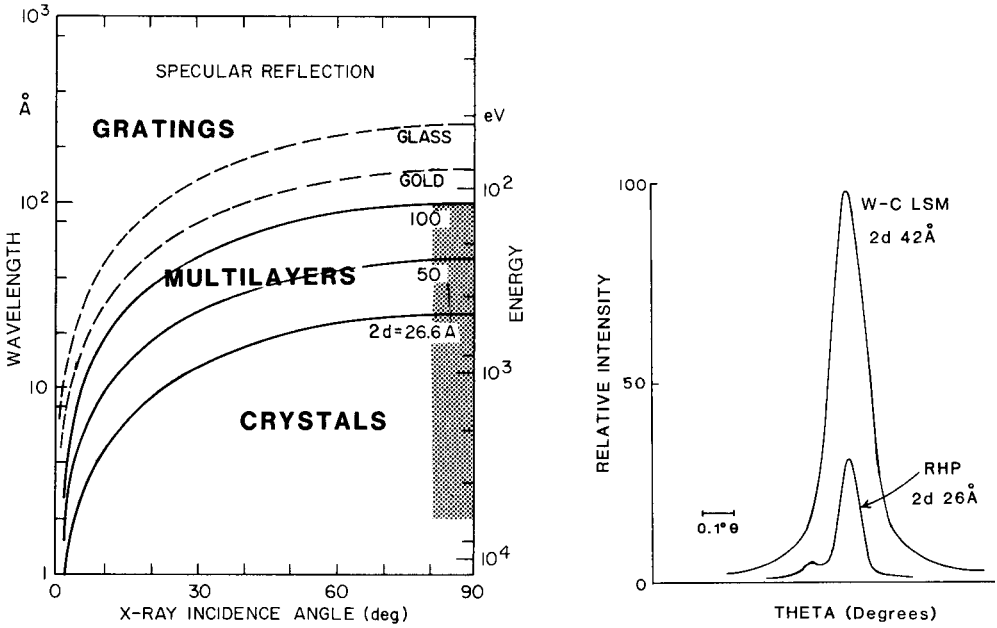

Fig. 1. Photon wavelength and energy versus incidence (and diffraction) angle θ for a variety of dispersion devices used in wavelength-dispersive spectrometers, showing how multilayers span the gap between crystals and gratings. (Reproduced with permission [7].)

Fig. 2. Al K_α (8.34 Å) dispersed with a 42 Å W—C multilayer and a RHP crystal. (Reproduced with permission [5].)

PREPARATION OF MULTILAYERS

Over the years, since 1930, attempts to produce multilayers have been based on electrodeposition and evaporation techniques. More recently, both evaporation and sputtering have produced devices having exceptional properties. The particular multilayers which were evaluated at NRL [5] were produced in a facility at Stanford University [6]. In this technique, magnetron-sputter deposition sources were used to deposit layers on thin, highly polished silicon wafers which were held on a rotatable table, controlled to reside under elemental sources for appropriate deposition of the alternating layers. It is also possible (and has been demonstrated) that multilayers can be prepared on any substrate that approaches atomic dimensions in smoothness. The facility at Stanford University has successfully produced multilayers on mica (where it is possible to observe diffraction from the multilayer and the mica) [7] and on quartz optical flats. Also, they have been deposited on curved or curvable substrates for focussing optics [8, 9]. In addition, it is possible to vary the layer thickness, either in depth or laterally along the surface for specific purposes [7].

CHARACTERIZATION

Generally speaking, the multilayers have wide rocking curves and large diffraction efficiencies, providing increased intensities in wavelength-dispersive x-ray emission spectrometers. However, they have relatively poor resolution. The poor resolution becomes less important when the multilayer device is used in a single-crystal spectrometer because of the predominance of the collimator divergence. Figure 2 illustrates the diffraction peak for Al K_α recorded with a multilayer and a high-resolution rubidium hydrogenphthalate (RHP) crystal, and fine collimation, demonstrating a difference of only a factor of two in resolution (full width at half maximum).

At the Stanford facility, a diffractometer based on a copper x-ray tube and 12-μm source and detector slits is used to evaluate the multilayers after production [7]. At NRL, extensive measurements were made over a wavelength range of 3—15 Å [5]. And, in a collaborative effort with the commercial manufacturer (ECD), Nicolosi and Jenkins [10] evaluated a number of the commercial products over a range of 7 to 67 Å.

Measurements based on Cu K_α at Stanford indicated that the peak diffraction efficiency varied from $<10\%$ to $>50\%$. Measurements at NRL in the longer wavelength region demonstrated integral reflection coefficients (R values) ranging from 3×10^{-4} to 3×10^{-3} radians, depending on the atomic number of the transition metal and the layer spacing. Figures 3 and 4 show the way in which the R values vary with wavelength and material in comparison to lead octadecanoate [11], potassium hydrogenphthalate (KHP) [12] and rubidium hydrogenphthalate [5]. As can be seen, the R value at 10 Å is 4.2×10^{-4} radians for Ti—C, 1.2×10^{-3} radians for Nb—C and 2.4×10^{-3} radians for W—C, all having $2d$ spacings of about 100 Å; for W—C multilayers, again at 10 Å, the R value is 7.0×10^{-4} at a $2d$ spacing of 42 Å, 1.0×10^{-3} at 61 Å and 2.4×10^{-3} radians at 120 Å. This variation agrees reasonably well with the theoretical treatment which says that the R value should vary linearly with the layer spacing and linearly with the difference in atomic number.

The work reported by Nicolosi and Jenkins [10] was primarily aimed at evaluation in the x-ray spectrometer products manufactured by Philips. They examined several devices each of two types, identified by the commercial source (ECD) as PX-1, $2d = 50$ Å and PX-2, $2d = 120$ Å, using the flat-crystal optics of the PW1400 x-ray spectrometer. The results, illustrated in Fig. 5, show about a 10% variation among the several specimens of each type, and indicate that PX-1 diffracted about 4.5 times as much intensity as a thallium hydrogenphthalate crystal over the element range from oxygen to silicon (wavelengths of 24 to 7 Å) and that PX-2 was up to 6 times more efficient than lead octadecanoate for boron to fluorine (67—18 Å). These data illustrate the uniformity and utility of the commercial products.

The diffraction peak of these multilayers, as measured in a single-crystal spectrometer, can be fairly broad, being as large as one degree 2θ. This can

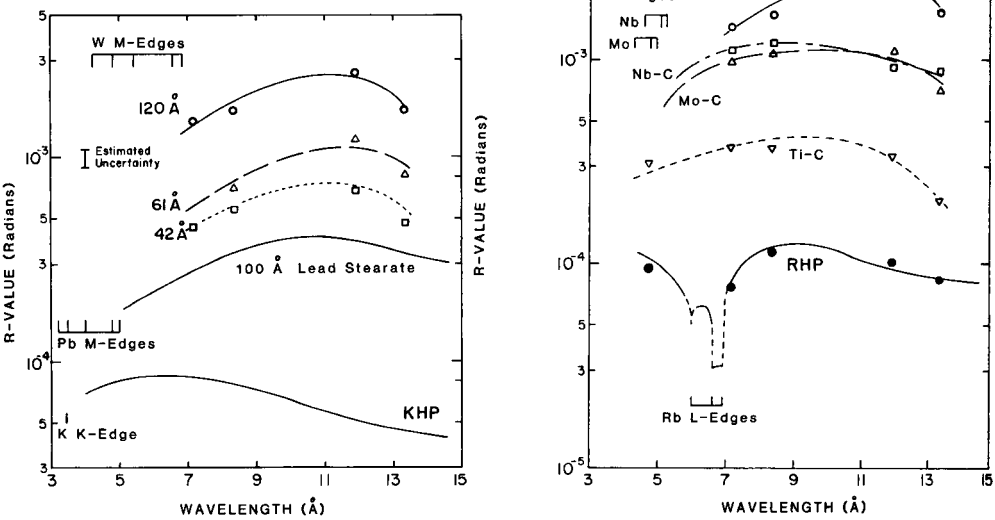

Fig. 3. Variation of integral reflection coefficient with wavelength for W—C multilayers of different $2d$ spacing. (Reproduced with permission [5].)

Fig. 4. Variation of integral reflection coefficient with wavelength for multilayers of approximately 100 Å $2d$ spacing with different transition metal components. (Reproduced with permission [5].)

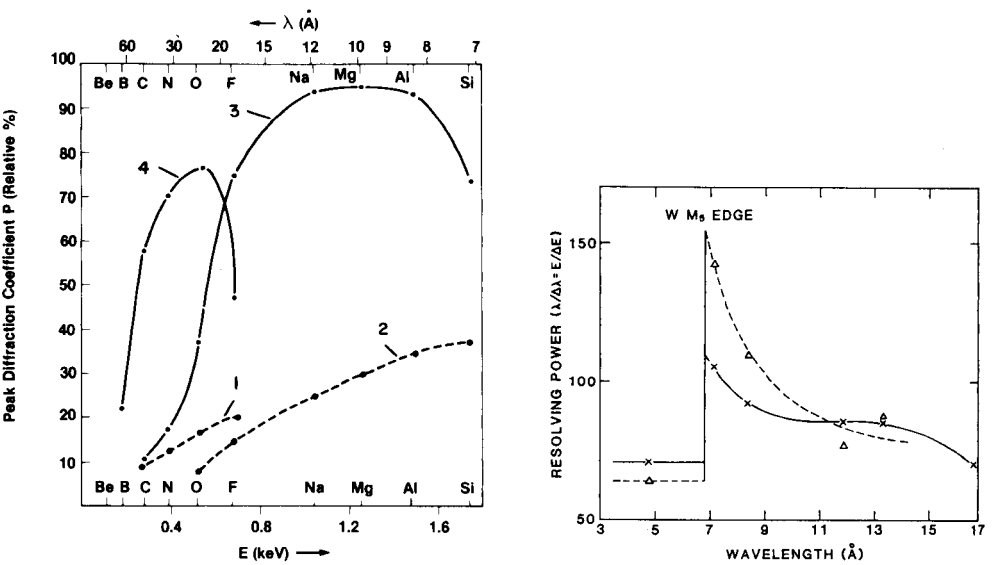

Fig. 5. Comparison of peak diffraction coefficients: (1) lead octadecanoate; (2) thallium hydrogenphthalate; (3) PX-1; (4) PX-2. (Reproduced with permission [10].)

Fig. 6. Resolving power of a W—C multilayer: (×) theoretical; (△) measured.

produce a resolution problem when nearest-neighbor elements are present in the sample. The diffraction peak width, of course, is a convolution of the collimator broadening, the natural line width and the rocking curve of the multilayer. If one assumes that the diffraction peak can be represented as a Voigt curve, an adequate numerical approximation can be used to extract the rocking curve width [13], permitting an estimation of the resolving power, $\lambda/\Delta\lambda$. Figure 6 shows the results of that exercise for a W—C multilayer ($2d$ = 42 Å). In general terms, the resolving power of multilayers is about 10 times poorer than that of the hydrogenphthalates in the 5 to 15 Å region.

APPLICATIONS

For analytical purposes, x-ray fluorescence spectrometry has become a workhorse for multi-element determinations. One of the drawbacks of even more general application of this technique has been the difficulty of quantifying elements below fluorine (Z = 9) in atomic number. Coupled with the inefficiency of exciting these low atomic numbers and the low fluorescence yield, has been the lack of efficient dispersing elements for the long-wavelength radiation. While inefficient excitation and low fluorescence yield are facts of life, the multilayers discussed above provide efficient dispersing devices which facilitate quantitation of elements with low atomic numbers.

Nicolosi and Jenkins [10] tested the use of multilayers as dispersing elements on two types of samples: "MATRIX", a mixture of all the elements in the range of the diffracting structure (nominally 2% in each of Na, Mg, Al and Si with 9% F and 75% O), and "PURE" in which at least one adjacent element was absent and there were no overlapping spectra (but the sample also included nitrogen and carbon). This effort is perhaps the most definitive exercise in evaluating the application of multilayers to quantitative problems. Figure 7 [10] illustrates their results, which indicate an improvement in the lower limit of detection of factors from two to three for elements from boron to silicon in the "PURE" samples, and from boron to sodium in the "MATRIX" samples. This improvement degrades for magnesium, aluminum and silicon in the "MATRIX" samples because of interference from overlapping spectra as a result of the relatively poor resolution.

Other applications demonstrated for these devices include plasma diagnostics and x-ray astronomy [14], but these applications are outside the scope of this discussion.

Conclusion

This brief survey of the applications of multilayers to x-ray spectrometry is intended to introduce a wider audience to these devices which show considerable promise for determination of the light elements that have been difficult to quantify by x-ray measurements. It has been demonstrated that they can be produced commercially with the same desirable properties avail-

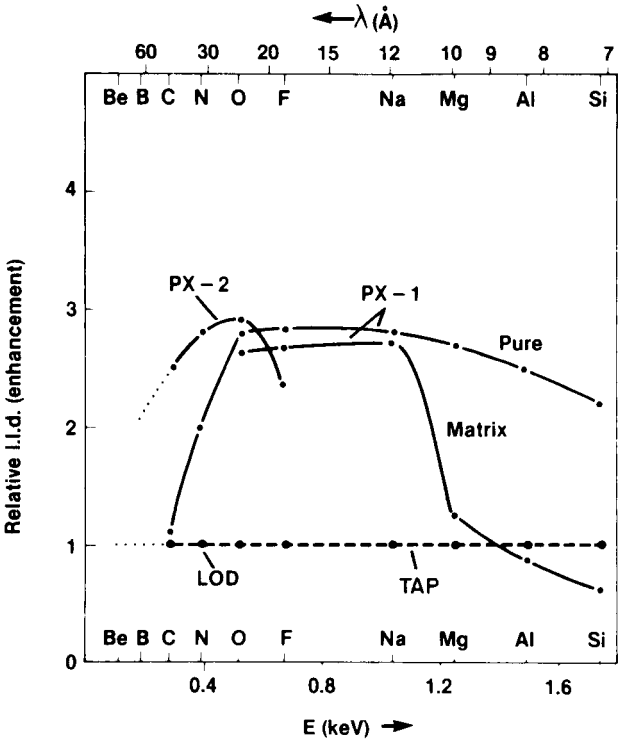

Fig. 7. Relative low limits of detection (l.l.d.) with the multilayers, PX-1 and PX-2, for "PURE" and "MATRIX" samples scaled to THP and lead octadecanoate (LOD). Dotted lines indicate projections. (Reproduced with permission [10].)

able from the devices produced under laboratory conditions. The increased intensity (for both signal and background) of a factor of about five, and improvements in lower limit of detection of between two and three, make it possible to use them in applications which have been impractical heretofore. It is expected that the situation will improve because of the increased effort being expended in understanding multilayers from the theoretical aspect. Experimental effort is also being directed toward the production of even more efficient devices.

REFERENCES

1 W. Deubner, Ann. Phys., 5 (1930) 261.
2 E. Spiller, Appl. Opt., 15 (1976) 2333.
3 T. W. Barbee, Jr. and D. C. Keith, in H. Winick and G. Brown (Eds.), Synthetic Structures Layered on the Atomic Scale, in Workshop on X-Ray Instrumentation for Synchrotron Radiation Research, Stanford Synchrotron Radiation Laboratory Report No. 78/04, May 1978, p. III-26.
4 E. Spiller, A. Segmuller, J. Rife and R. P. Haelbich, Appl. Phys. Lett., 37 (1980) 1048.
5 J. V. Gilfrich, D. J. Nagel and T. W. Barbee, Jr., Appl. Spectrosc., 36 (1982) 58.

6 T. W. Barbee, Jr., in D. T. Atwood and B. L. Henke (Eds.), Sputtered Layered Synthetic Microstructure (LSM) DIspersion Elements, in Proceedings of Topical Conference on Low Energy X-Ray Diagnostics, American Institute of Physics, New York, 1981.
7 D. J. Nagel, T. W. Barbee, Jr. and J. V. Gilfrich, SPIE, Vol. 315, Reflecting Optics for Synchrotron Radiation, 1982, p. 110.
8 J. H. Underwood and T. W. Barbee, Jr., Nature, 294 (1981) 429.
9 J. P. Henry, E. Spiller and M. Weisskopf, Appl. Phys. Lett., 40 (1982) 25.
10 J. A. Nicolosi and R. Jenkins, Norelco Rep., 31 (1984) 1.
11 B. L. Henke and M. A. Tester, Adv. X-Ray Anal., 18 (1975) 87.
12 J. V. Gilfrich, D. B. Brown and P. G. Burkhalter, Appl. Spectrosc., 29 (1975) 322.
13 B. L. Henke, R. C. Perera, E. M. Gullickson and M. L. Schattenburg, J. Appl. Phys., 49 (1978) 480.
14 J. V. Gilfrich, D. J. Nagel, N. G. Loter and T. W. Barbee, Jr., Adv. X-Ray Anal., 25 (1982) 355.

Analytica Chimica Acta, 188 (1986) 59—66
Elsevier Science Publishers B.V., Amsterdam — Printed in The Netherlands

USE OF SENSITIVITY AS A FUNCTION OF FLUORESCENT X-RAY ENERGY IN ENERGY-DISPERSIVE X-RAY SPECTROMETRY

W. WEGSCHEIDER

Institute of Analytical Chemistry, Micro- and Radiochemistry, Technical University Graz, Graz, A-8010 (Austria)

A. T. ELLIS[a], K. GOLDBACH and D. E. LEYDEN*

Department of Chemistry, Colorado State University, Fort Collins, CO 80523 (U.S.A.)

K. I. MAHAN

Department of Chemistry, University of Southern Colorado, Pueblo, CO 81001 (U.S.A.) (U.S.A.)

(Received 28th February 1986)

SUMMARY

The approximate linear relationship between the logarithm of the sensitivity and the logarithm of the energy of the observed characteristic x-ray emission is used to show the relative retention of elements during fusion with lithium tetraborate to form fused pellets, and the relative recovery of elements by preconcentration methods. Elements with atomic numbers ranging from 20 to 33 were investigated in fused pellets and/or filtered precipitated samples. Linear or nearly linear curves with slopes ranging from near two for infinitely thin samples to near six for infinitely thick samples are predicted if certain conditions of x-ray excitation are met.

Matsumoto and Fuwa [1] pointed out that with certain reasonable approximations, a linear relationship can be expected between log-sensitivity and log-energy of x-ray emission based on theoretical considerations. These authors showed several sets of experimental verifications. Previously, Takamatsu [2] had given experimental examples with no discussion of the theoretical basis. The expression for the fluorescent x-ray intensity for an infinitely thick sample [3] is

$$I_L = I_\phi \omega_A g_L [(r_A - 1\ d\Omega)/r_A 4\pi] [C_A \mu_A(\lambda_{pri})\csc\phi/(\mu_m(\lambda_{pri})\csc\phi + \mu_m(\lambda_L)\csc\psi)] \quad (1)$$

where all symbols are as defined by Matsumoto and Fuwa [1]. All terms in Eqn. 1 with the exception of ω_A and μ_A were assumed to be essentially independent of the energy of the detected line (e.g., atomic number). It was stated "Although ω_A varies slightly from element to element, the variation is

[a]Present address: Link Systems, High Wycombe, Great Britain.

0003-2670/86/$03.50

negligible, compared with the value of μ's" [1]. However, inspection of data presented by Giauque et al. [4] shows that the fluorescence yield varies almost linearly with the absorption edge energy (E_A) for photoejection of K electrons in the range of atomic numbers 16 (sulfur) to 33 (arsenic). This is in agreement with the expression

$$\omega = Z^4/(A + Z^4) \tag{2}$$

where the constant A has a value of 10^6 for K lines [5]. When $Z \propto 30, Z^4 \propto A$ and non-linearity is significant. Because the difference between the absorption-edge energy and emission-line energy is small compared to the magnitude, a similar approximately linear relationship is expected, and observed, between ω_A and K_α line energy.

Matsumoto and Fuwa assumed that all terms in Eqn. 1 are constant with the exception of the μ values. Using the Bragg-Pierce law ($\mu = KZ^4\lambda^3$) and the Moseley law ($\lambda = KZ^{-2}$), the authors developed the expression

$$I_L/C_A \propto Z_A^4/\lambda_L^3 \propto Z_A^{10} \propto E_A^5 \tag{3}$$

in which I_L/C_A is the sensitivity for element A. However, if one restores to the original expression the assumption that $\omega_A \propto E_A$ over a narrow energy range, then Eqn. 3 becomes

$$I_L/C_A \propto E_A^5 \omega_A \propto E_A^6 \tag{4}$$

and

$$\log (I_L/C_A) = 6 \log E_A + \log K' \tag{5}$$

Thus, the limiting slope in the case of an infinitely thick sample should be 6 and not 5 as predicted by Matsumoto and Fuwa [1].

One can also consider a limiting value of an analogous slope for infinitely thin samples. By considering that absorption effects are negligible and constant in a thin film sample, Eqn. 1 can be expressed as

$$I_L/C_A \propto \mu_A(\lambda_{pri})\omega_A \tag{6}$$

Again using substitutions from the Bragg-Pierce and Moseley laws, Eqn. 6 becomes

$$I_L/C_A \propto Z_A^4 \lambda_L^3 \omega_A \propto Z_A^{-2} \omega_A \propto E_A^2 \tag{7}$$

Because absorption effects are neglected, the sample is assumed to be two-dimensional and sensitivity is expressed relative to mass per unit area, M_A. An analogous expression to Eqn. 5 for thin samples is given by

$$\log (I_L/M_A) = 2 \log E_A + \log K'' \tag{8}$$

If the infinitely thin specimen is prepared from a constant volume or mass of sample, such as a filtered precipitate, then $M_A \propto C_A$, and Eqn. 8 has the same form as Eqn. 5 with the difference that the limiting value of the slope is now 2. Samples with thicknesses between these limiting cases should exhibit slopes between 2 and 6.

Matsumoto and Fuwa noted that the results obtained by them indicated a linear relationship between log (I_L/C_A) vs. log E_A only when the absorption edge of the analyte element was at an energy below that of the useful characteristic line of the anode element of the x-ray tube. This involves the implicit assumption that the voltage at which the tube is operated is sufficient to excite the characteristic lines of the target, and sufficiently high to move the majority of continuum intensity to an energy higher than these lines. Wavelength-dispersive x-ray spectrometers as used by Matsumoto and Fuwa do not routinely utilize primary filters between the x-ray tube and sample, although these authors did use filters. Energy-dispersive x-ray spectrometers do routinely include such filters and can be used to reduce the intensity of continuum radiation at energies below the characteristic lines of the target element. This provides a primary radiation source which is effectively more "monochromatic" at the energy of the characteristic line of the target element. Therefore, the proposals of Matsumoto and Fuwa are perhaps even more appropriate for energy-dispersive x-ray spectrometry.

In the case of trace element determinations, after application of preconcentration methods [6, 7], the relative recovery of individual elements can be estimated by using these relationships. Poor recovery of any one element as a result of chemical effects will be indicated by sensitivity values not fitting the log—log relationship. The retention of elements during fusion methods may be confirmed, or the interpolation of sensitivities for multi-element samples using only a few elements in standards or standard additions [1] can be employed. Coetzee and Lieser [8] have recently described the use of this concept as a calibration procedure to reduce the required number of standards. Examples of both applications are presented in this report. Criteria for the use of filtered x-ray tube excitation are discussed.

EXPERIMENTAL

Apparatus

All spectra were taken using a Tracor Xray (Mountain View, CA) Spectrace 440 energy-dispersive x-ray spectrometer equipped with a Ag-anode, side-window x-ray tube. A 0.025-mm thick silver filter or a Whatman W-41 filter paper were used as primary filters. Tube voltage and current were varied and are given for each case. Spectral intensity data were extracted with a Tracor Northern Corporation (Middleton, WI) TN-2000 analyzer and software. Because this software extracts the $K_\alpha - K_\beta$ sum, there is no need to correct by using the g_L factor in Eqn. 1 [1].

Samples

All samples were prepared in conjunction with other work and were taken for use in this investigation without further modification. The fusion samples had been prepared as multi-element standards [9]. Concentrations in the fused pellets were confirmed by dissolution of a portion of the residual glass

from the casting process and quantitation by atomic absorption spectrometry. The pellets were prepared by the fusion of a flux mixture consisting of nine parts of lithium tetraborate, one part of silica gel, a small amount of an oxidant (1.5% lithium nitrate), and measured amounts of the elements of interest. Elemental components were added by either the addition of weighed solid compounds (oxides or nitrates) or by micropipetting aqueous standard solutions (30—1000 μl per element) directly into the flux mixture. It was necessary to dry the flux for several hours at 80°C before fusion if aqueous solutions were used. In some cases, serial dilutions of previously fused standard glass were performed to obtain the final concentration. Fusions were done in a 95% platinum/5% gold crucible (Matthey-Bishop, Malvern, PA) over a compressed air/natural gas flame until the melt was clear (30—60 min). The fused product was then poured into a round graphite mold (31-mm diameter) maintained at 450°C on a hot plate. After allowing the discs to anneal at this temperature for 20—30 min, the mold and discs were removed from the hot plate and allowed to cool to room temperature. This procedure produced 31-mm diameter discs weighing 8—10 g. Before quantitation, the discs were polished by wet grinding on a 120-mesh belt grinder, polishing with alumina paste, and rinsing in sequence with tap water, dilute nitric acid, deionized water, and methanol.

Trace elements in water were preconcentrated by using procedures previously reported [6, 7]. The specimen presented to the x-ray spectrometer contains, in principle, the mass of analyte present in the original water sample converted to a thin film precipitate on a membrane filter. The procedure used for preparation of the precipitates with dibenzyldithiocarbamate (DBDTC) is to adjust the pH of 100 ml of sample to 2.5 ± 0.03 with 0.1 M HCl or 0.1 M NaOH as required and then buffer with 2 ml of 0.1 M potassium hydrogenphthalate solution. To this 1.0 ml of 1.2% (w/v) of the sodium salt of DBDTC in methanol was added followed by 15 min stirring and then 15 min quiescent aging. The precipitate was then filtered under vacuum through a 25-mm diameter, 0.45-μm pore diameter Gelman Metricel (GA-6) filter. The filter was air-dried for 5 min and mounted between two 0.25 mil mylar sheets using a Chemplex x-ray sample cup.

RESULTS AND DISCUSSION

Equation 1 involves the assumption that excitation is done with monochromatic radiation of wavelength λ_{pri}. This can be approximated by highly filtered radiation from an x-ray tube [10]. In general, a filter of the same material as the anode can be used to attenuate significantly the intensity of energies below those of the tube characteristic lines. By careful selection of voltage, continuum intensity below the energy of these lines can be minimized. Figure 1 shows the dependence of the relationship between sensitivity (total $K_\alpha - K_\beta$) and E_A for the elements shown in the atomic number range 24 (chromium) to 33 (arsenic) for tube voltages of 12, 25, 30, and 45 kV,

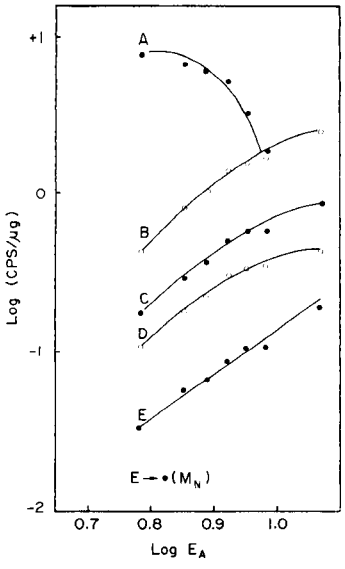

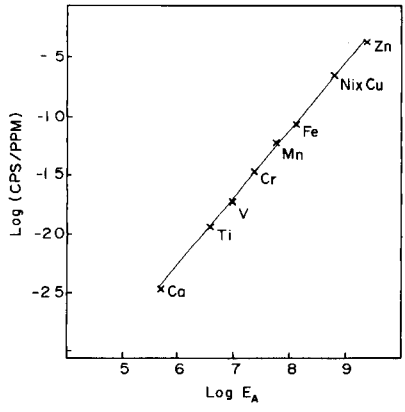

Fig. 1. Log sensitivity vs. log E_A for elements precipitated on a membrane filter: (A) 12 kV, 0.20 mA, W-41 filter; (B) 25 kV, 0.02 mA, 0.025 mm Ag filter; (C) 30 kV, 0.02 mA, 0.025 mm Ag filter; (D) 45 kV, 0.02 mA, 0.025 mm Ag filter; (E) 45 kV, 0.05 mA, 0.127-mm Ag filter.

Fig. 2. Log sensitivity vs. log E_A for elements in a fused pellet: 45 kV, 0.02 mA, 0.025-mm Ag filter.

using a Whatman 41 paper filter, a 0.025-mm Ag, or a 0.127-mm Ag filter with a silver x-ray tube. These data are for elements collected as a DBDTC precipitate on a membrane filter. At 12 kV, neither is the continuum located at sufficiently high energy to assume $\mu_M(\lambda_{pri}) \gg \mu_M(\lambda_A)$ even at the lower energies, nor are the characteristic lines of the anode excited. At 25 kV, the filtered continuum has sufficient intensity above approximately 10 keV that first approximations of a monochromatic source from the filtered continuum are evident for the low energy lines. At 30 kV, the characteristic K-lines of silver are excited, and even at the higher x-ray energies, the approximations are better as shown by slightly improved linearity. Finally, at 45 kV, the characteristic lines of the silver anode provide most of the excitation, and the continuum has substantial intensity at energies higher than the K-lines of silver. Inspection of the tube output as scatter from a polyester plug shows that there is substantial radiation below the Ag K-lines. Therefore, the degree of linearity is further increased by a thicker silver filter, although there is a decrease in absolute sensitivity resulting from attenuation of the x-ray beam. It is readily seen that a highly filtered x-ray tube operated at sufficiently high kV can approximate a monochromatic source of sufficiently high energy to meet the required approximations for Eqns. 5 and 8 over a useful energy range. Absolute sensitivity is sacrificed to achieve this goal.

The results are consistently low for manganese in all cases, as illustrated by the Mn point for curve E. This is an example of the use of the proposed relationship to ascertain whether good recovery is achieved in the sample preparation. In this case, it is well known that the recovery for manganese is low for DBDTC precipitation. Thus, the observed sensitivity is below the predicted value. For the case of 45 kV, 0.05 mA and a 0.127-mm silver filter, the relationship $\log (\text{cps}/\mu\text{g}) = 2.52\,(\pm 0.15) \log E_A - 3.40\,(\pm 0.14)$ is obtained with a correlation coefficient of 0.991 if manganese is not included in the fit. The deviation from the predicted limiting slope may be in part an indication that the samples are not infinitely thin.

In the examples presented here, thick samples are represented by fused pellets of lithium tetraborate containing either standardized amounts of elements of interest, or prepared using soil or sediment samples. Table 1 shows the parameters taken from a log-sensitivity versus log-energy plot under several conditions. Figure 2 shows a plot for calcium/zinc data at 45 kV. The least-squares fit of the data gives $\log (\text{cps/ppm}) = 5.44\,(\pm 0.23) \log E_A - 5.67\,(\pm 0.19)$ with a correlation coefficient of 0.999. The elements used in these studies were Ca, Ti, V, Cr, Mn, Fe, Ni, Cu, and Zn. One of the uses of these plots is immediately noted in that copper is in all cases below the least-squares line and is found to be outside the 95% confidence interval. Poor retention of copper in fusions has been verified by atomic absorption spectrometry [9]. By making a log sensitivity vs. $\log E_A$ plot, points significantly below the line are suspect in retention or recovery. The slope values in Table 1 range from 5.20 to 5.74, all near but significantly below the predicted limiting value of 6.

The preparation of multi-element standards for fused samples is a tedious and time-consuming process. The use of these plots to interpolate sensitivity factors can save considerable effort as indicated by Coetzee and Lieser [8]. To illustrate this point, a fused standard was prepared containing Ti, Fe, and Zn. Specimens prepared from river sediment samples, and by addition of known amounts of elements of interest to the flux, were analyzed. A plot of

TABLE 1

Parameters obtained from log sensitivity vs. $\log E_A$ for samples fused with lithium tetraborate[a]

Tube voltage (kV)	25	30	45	45
Filter	0.025-mm Ag	0.025-mm Ag	0.025-mm Ag	0.127-mm Ag
Element range	Ca—Zr	K—Zr	Ca—Zn	Ca—Zn
Slope	5.52	5.20	5.74	5.69
Intercept	−6.07	−5.45	−5.64	−6.37
Correlation	0.994	0.998	0.999	0.994

[a]Copper not included.

TABLE 2

Results for sediment AR-2 obtained by using log sensitivity vs. log E_A for calibration[a]

Element	This work (mean ± s.d.)	Working curve method
K (%)	2.03 ± 0.05	1.92 ± 0.04
Ca (%)	1.60 ± 0.09	1.94 ± 0.1
Ti ($\mu g\ g^{-1}$)	1520 ± 41	1624 ± 40
Mn ($\mu g\ g^{-1}$)	321 ± 25	272 ± 21
Fe (%)	1.52 ± 0.08	1.46 ± 0.07
Co ($\mu g\ g^{-1}$)	<LLD	36 ± 31
Zn ($\mu g\ g^{-1}$)	97 ± 3	101 ± 3

[a]Results are given as concentration in sediment.

log-sensitivity (cps/μg/g) versus log E_A (keV) for the three standard elements Ti, Fe, and Zn, gave log sensitivity = 5.17 log E_A − 5.42 with R = 0.99999. These data were obtained at 30 kV, 0.03 mA, 1000-s counting time (live) by using a 0.025-mm Ag filter with a silver target tube. The results were used to determine K, Ca, Ti, Mn, Fe, Co and Zn in a sediment sample taken from the Arkansas River near Pueblo, Colorado, in which these elements had previously been determined. Three replicate specimens were independently prepared and the results are shown in Table 2. It is interesting that the precision obtained by the proposed method is similar to that obtained for the more careful and time-consuming method requiring a working curve for each element. Except for manganese and calcium which show errors of about 18%, the other errors are 6% or less (relative). Considering that a single standard with only three elements was used, the mean difference between the two methods of less than 10% is quite impressive. It is also important to note that given a background reading of a specimen near the energy of an element to be determined, good estimate of the lower limit of detection can be calculated from the background values and the predicted sensitivity.

Finally, a further empirical relationship was found for the fused-sample data. By multiple regressions of all data under identical x-ray conditions, except for variation in tube voltage, the relationship

$$\log(\text{sensitivity}) = 5.688 \log E_A + 2.343 \log \text{kV} - 9.449 \quad (9)$$

was obtained. By means of this relationship, Ca, Fe and Zn were determined at 25, 30, 35, 40 and 45 kV with an average error of 12% for Ca, 2.7% for Fe and 16% for Zn. The relationship in Eqn. 9 is empirical, but the dependence on tube voltage is not out of line with that expected from intensity/voltage relationships. The advantage of this method is that at least semi-quantitative estimates can be obtained under different tube voltages with only two known elements in the matrix.

The authors acknowledge contributions to this paper in the form of computations done by S. Caravajal (Denver University) and P. Theussl and B. Platzer (T. U. Graz). One of us (W. W.) acknowledges the instrument support from grant number P5200 from the "Fonds fur Forderung der wissenschaftlichen Forschung, Vienna". This work was supported in part by NSF Research Grant CHE 78-23123, EPA Cooperative Agreement No. R806520-03, the Henry and Camille Dreyfus Fund and the AMAX Foundation.

REFERENCES

1 K. Matsumoto and K. Fuwa, Anal. Chem., 51 (1979) 2355.
2 T. Takamatsu, Bunseki Kagaku, 27 (1978) 193.
3 E. P. Bertin, Principles and Practice of X-Ray Spectrometric Analysis, 2nd edn., Plenum Press, New York, 1975.
4 R. D. Giauque, F. S. Goulding, J. M. Jaklevic and R. H. Pehl, Anal. Chem., 45 (1973) 671.
5 E. P. Bertin, Principles and Practice of X-Ray Spectrometrometric Analysis, 2nd edn., Plenum Press, New York, 1975, p. 83.
6 A. T. Ellis, D. E. Leyden, W. Wegscheider, B. B. Jablonski and W. B. Bodnar, Anal. Chim. Acta, 142 (1982) 73.
7 A. T. Ellis, D. E. Leyden, W. Wegscheider, B. B. Jablonski and W. B. Bodnar, Anal. Chim. Acta, 142 (1982) 89.
8 P. P. Coetzee and K. H. Lieser, Fresenius Z. Anal. Chem., 322 (1985) 386.
9 K. I. Mahan and D. E. Leyden, Adv. X-Ray Anal., 25 (1982) 95.
10 R. A. Vane and W. D. Stewart, Adv. X-Ray Anal., 23 (1980) 231.

Analytica Chimica Acta, 188 (1986) 67—72
Elsevier Science Publishers B.V., Amsterdam — Printed in The Netherlands

DETERMINATION OF TRACE METALS IN NUCLEAR-GRADE URANIUM DIOXIDE BY X-RAY FLUORESCENCE SPECTROMETRY

VERA LUCIA RIBEIRO SALVADOR and KENGO IMAKUMA*

Comissão Nacional de Energia Nuclear, Instituto de Pesquisas Energéticas e Nucleares, Caixa Postal 11049, São Paulo, SP (Brasil)

(Received 12th September 1985)

SUMMARY

A method is described for the simultaneous determination of low concentrations of Ca, Cr, Cu, Fe, Mn and Ni in nuclear-grade uranium dioxide by x-ray fluroescence spectrometry, without the use of chemical treatment. The lower limtis of detection range from 2 $\mu g\ g^{-1}$ for nickel and manganese to 5 $\mu g\ g^{-1}$ for copper. Samples are prepared in the form of double-layer pellets with boric acid as a binding agent. Standards are prepared in a U_3O_8 matrix, which is more chemically stable than UO_2 and has similar matrix behaviour. The correlation coefficients for calibration curves are better than 0.999. Errors range from 2.4% for chromium to 6.8% for nickel.

Many thermonuclear reactors utilize uranium dioxide as fuel, which must have a high grade of purity in order to guarantee safe operation. Several techniques have been developed for the determination of trace elements in nuclear materials. Trace concentrations are usually determined by neutron activation, optical emission spectrometry, atomic absorption spectrometry and spark-source mass spectrometry. These techniques are very sensitive but can show some limitations depending on the elements to be determined.

In this work, x-ray fluorescence spectrometry was investigated for the determination of some impurities in nuclear fuel, namely Ca, Cr, Cu, Fe, Mn and Ni. The concentration range studied was 0.001—0.015% [1].

EXPERIMENTAL

Preparation of standards and sample

Standards were prepared by adding known amounts of Ca, Cr, Cu, Fe, Mn and Ni to 1.0 g of Specpure U_3O_8 and adding boric acid to give a total mass of 2.0 g. These mixtures were ground in a mortar and pressed at 1.6 ton cm^{-2} for 1 min into a circular mold (40-mm diameter) to form a double-layer pellet. Samples were mixed with boric acid in a 1:1 ratio and pressed into pellets as described for standards.

A commercial standard disk of aluminium metal was prepared for detection of fluctuations of x-ray intensities.

0003-2670/86/$03.50

Study of characteristic first-order reflection K_α *line*

The high mass-absorption coefficient of uranium in the matrix causes a considerable absorption effect on the characteristic lines of the elements of interest. An approximately constant amount of uranium was utilized in the standards and samples in order to compensate for this effect.

The K_α lines of the elements, detected with a tungsten target tube, LiF (200) analyzer crystal, and scintillation counter, are shown in Fig. 1. The positions of lines and possible interferences from other elements were examined for each spectrum.

Instrumentation

The commercial, semi-automatic x-ray spectrometer used was coupled with a stabilized 3-kW generator. A tungsten target x-ray tube was used for

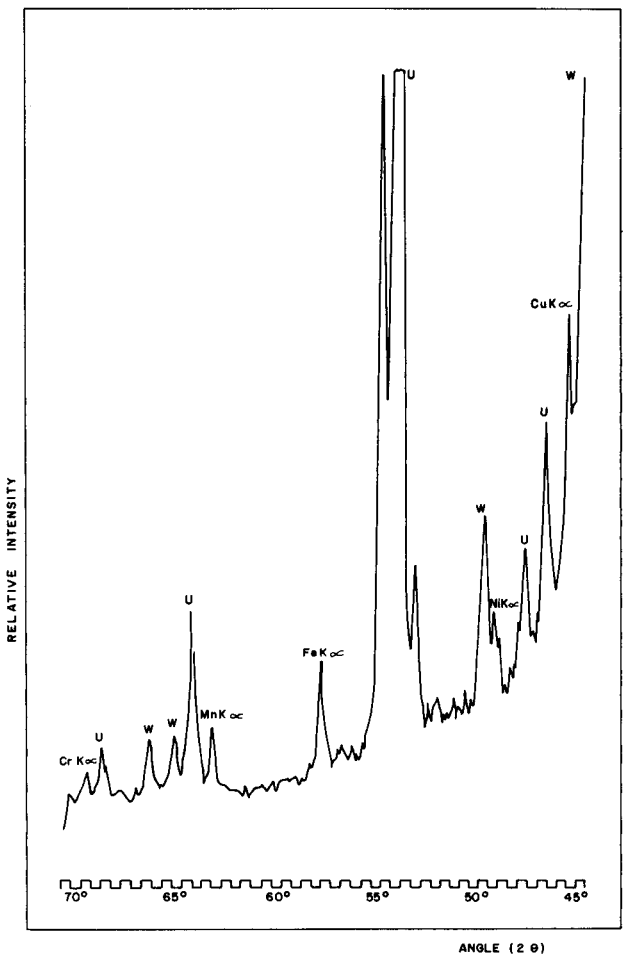

Fig. 1. The K_α spectra of Cr, Mn, Fe, Ni and Cu, and the L spectrum of uranium recorded with a LiF(200) analyzer, scintillation counter and tungsten x-ray tube.

Cr, Cu, Fe, Mn and Ni; a chromium tube and a flow proportional counter were used for calcium. The analyzer crystal was LiF(200) for all elements except calcium for which a EDDT(020) crystal was used. Tube voltages and currents were 50 kV and 50 mA, respectively, for all elements except calcium, for which the current was 35 mA.

A six-position specimen chamber permitted sequential measurements of fluorescence intensities of six pellets. For each set of measurements, the spectrometer was loaded with five standards or samples; the remaining position was occupied permanently by the aluminium standard.

The Siemens relation [2] for several pairs of currents and voltage, i.e., $(I_b)^{1/2}/I_f$ = the minimum value, and the Díaz-Guerra relation [3], i.e., $[(I_f + I_b)^{1/2} - (I_b)^{1/2}]$ = the maximum value, were used, where I_b is the background intensity and I_f is the net fluorescent intensity. For these conditions, the sensitivities and lower limits of detection are expected to be maximal and minimal, respectively. Conditions established in this manner are summarized in Table 1.

RESULTS AND DISCUSSION

Calibration graphs

The standards were processed in triplicate and, for each standard, the average net intensity was plotted vs. concentration (Fig. 2). Background intensity was subtracted from each sample spectrum and the fluctuation of the counts was corrected, when necessary, by means of a standard pellet. Least-squares statistics for the calibration graphs are listed in Table 2.

TABLE 1

Optimized conditions for the proposed method

Characteristic line ($n = 1$)		Ca K_α	Cr K_α	Cu K_α	Fe K_α	Mn K_α	Ni K_α
Wavelength (Å)		3.360	2.291	1.542	1.937	2.103	1.659
Bragg angle	*Line*	44.85°	69.38°	45.03°	57.53°	63.00°	48.68°
	Background	43.35°	66.90°	44.70°	57.00°	62.65°	48.30°
		45.52°	69.86°	45.50°	58.06°	63.40°	49.06°
Fixed time (s)		100	200	100	100	400	100
Collimator (μm)		450	150	150	150	150	150
Pulse height analyzer	*Base-line* (V)	0.80	0.55	0.65	0.60	0.60	0.65
	Channel window (V)	0.85	0.85	1.05	0.95	0.95	0.90

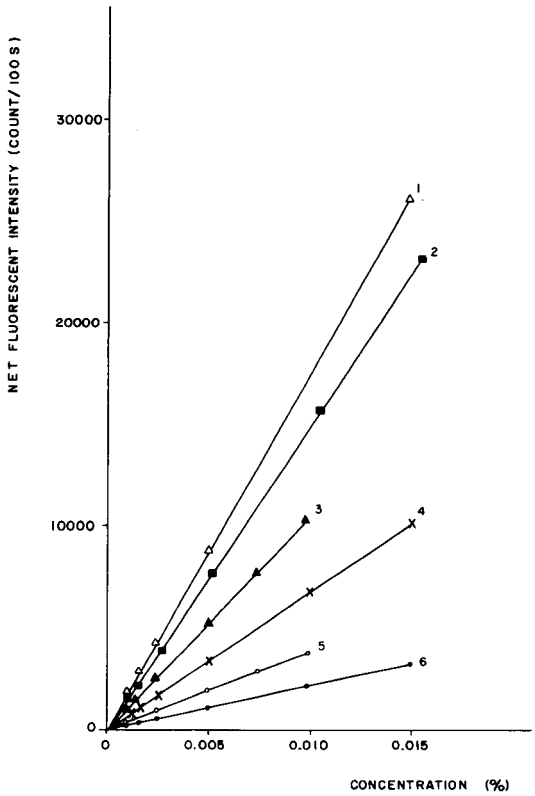

Fig. 2. Calibration graphs: (1) calcium; (2) nickel; (3) copper; (4) iron; (5) manganese; (6) chromium.

The error caused by the use of a U_3O_8 matrix instead of UO_2 was neglected because the absorption coefficients of U_3O_8 and UO_2, for the wavelengths considered, are nearly the same [4].

TABLE 2

Least-squares statistics for calibration graphs

Element	Intercept (a)	Slope (b)	Standard errors			Correlation coefficient
			s_{xy}	s_b	s_b	
Ca	−66	174	137	85	1	0.9999
Cr	76	41.2	75	46	0.6	0.9996
Cu	−65	105	159	112	2	0.9993
Fe	27	67.7	65	40	0.5	0.9998
Mn	−56	152	125	87	2	0.9998
Ni	37	149	109	67	0.8	0.9999

Imprecision, inaccuracy, sensitivity and lower limit of detection

The imprecision and inaccuracy of the methods were tested on samples containing 1.0 g of standard no. 95-2 U_3O_8 from New Brunswick Laboratory. The results, based on a minimum of five replicates for each sample, are listed in Table 3. The values obtained for imprecision and inaccuracy are less than 5% for all elements except copper and nickel. The larger errors for these two elements are probably caused by interfering lines from other elements.

The sensitivities and estimated detection limits (3σ criterion) are given in Table 4.

The use of double-layer pressed pellets has contributed to improve detection limits, because of the low degree of dilution. When fused pellets are used, the detection limits for calcium, copper and iron are usually about 400—500 $\mu g\ g^{-1}$ [5]. The imprecision and inaccuracy of the method are similar to those achieved with emission spectrometry [6].

TABLE 3

Imprecision and inaccuracy for the method

Element	Cr	Cu	Fe	Mn	Ni
Nominal concentration ($\mu g\ g^{-1}$)	42	21	220	22	44
Concentration found ($\mu g\ g^{-1}$)	41 ± 2	22 ± 2	218 ± 6	22 ± 6	47 ± 2
Imprecision (%)	4.9	9.1	2.8	4.5	4.3
Inaccuracy (%)	2.4	4.8	4.5	0.0	6.8

TABLE 4

Sensitivity and lower limit of detection

Element	Sensitivity (10^3 counts s^{-1}/%)	Lower limit of detection ($\mu g\ g^{-1}$)
Ca	17.0	4
Cr	2.2	4
Cu	10.1	5
Fe	6.9	3
Mn	3.7	2
Ni	15.0	2

REFERENCES

1 Standard Specification for Sintered Uranium Dioxide Pellets ASTM-C 776-79.
2 H. Siemens, Z. Erzbergbau Metallhuettenwes., 15 (1962) 153.
3 J. P. Díaz-Guerra, Jen., 468 (1981).
4 R. Muller, Spectrochim. Acta, 20 (1964) 143.
5 CEA-CETAMA-ACCU 1978 (1978).
6 R. P. Gomes, A. R. Lordello and A. Abrão, IEA-476 (1977)

Analytica Chimica Acta, 188 (1986) 73—84
Elsevier Science Publishers B.V., Amsterdam — Printed in The Netherlands

ISOTOPE RATIO DETERMINATIONS BY INDUCTIVELY COUPLED PLASMA/MASS SPECTROMETRY FOR ZINC BIOAVAILABILITY STUDIES

ROBERT E. SERFASS*

Department of Food and Nutrition, Iowa State University, Ames, Iowa 50011 (U.S.A.)

JOSEPH J. THOMPSON and R. S. HOUK

Ames Laboratory-USDOE and Department of Chemistry, Iowa State University, Ames, Iowa 50011 (U.S.A.)

(Received 15th April 1986)

SUMMARY

A method is described for the measurement of $^{67}Zn/^{68}Zn$ and $^{70}Zn/^{68}Zn$ ratios by inductively coupled plasma/mass spectrometry with ultrasonic nebulization. The method provides sufficient accuracy and precision for zinc bioavailability studies that use samples of human feces or blood plasma. Extraction of zinc from ashed samples yields aqueous solutions sufficiently devoid of matrix ions that could affect count rates and isotope ratios. Effects of sodium matrix, zinc concentration, and instrumental parameters on the precision of isotope ratio determinations are documented. Additions of spikes enriched in ^{67}Zn and ^{70}Zn to natural-abundance fecal samples verify that ratios can be determined on solutions 30 μM in zinc (<300 nmol of zinc per sample) with relative accuracies of $<1\%$ and relative standard deviations (r.s.d.) of $\leqslant 1\%$ over the range from natural abundance to 370 atom% excess of ^{70}Zn and to 84 atom% excess of ^{67}Zn.

Absorption of zinc depends upon the physiological status of the individual and on the presence of potentiating or inhibiting food components in the intestine. For example, there is some concern over the inhibitory effects of phytic acid, found in many foods, on zinc absorption [1]. Diverse methods have been used to assess absorption of zinc [2, 3]. Radioisotopic techniques have been most widely used. Aside from the ethical questions concerning radioisotopic administration to human subjects for research purposes, the existence of only one radioisotope of zinc with a convenient radioactive half-life precludes the direct comparison of absorption of zinc from different food sources in the same meal.

The existence of five stable isotopes of zinc facilitates the organization of zinc bioavailability studies with human subjects in complete safety. A barrier to this application of stable isotopic methods has been the necessity to use neutron activation analysis or thermal ionization mass spectrometry (t.i.m.s.) to determine the isotopic ratios. Procedures for sample preparation and quantitation by these two methods are exacting and time-consuming, and equipment is not widely available. Isotopic ratios by neutron activation

0003-2670/86/$03.50

techniques are not sufficiently precise for many biological applications. A further disadvantage of these techniques is that isotopic ratios of only three of the five stable zinc isotopes can be determined, and only one of these three is sufficiently rare to be considered a tracer for most applications. All five stable isotopes of zinc can be measured by mass spectrometry; an added advantage of t.i.m.s. is the greater precision attainable, as exemplified for biological samples by the results of Turnlund and co-workers [1, 4].

New instrumentation has been developed for use in nutritional tracer studies. A quadrupole mass spectrometer with a thermal ionization source has been described [5] and is commercially available [6]. This instrument is less expensive than t.i.m.s. instruments, provides greater sample throughput, and exhibits good precision (0.1—1.0%) for the measurement of isotope ratios. The techniques of sample preparation are derived from t.i.m.s. and possess the drawbacks characteristic thereof, namely, lengthy preparation procedures and lack of simultaneous multielement capabilities.

Conventional organic mass spectrometers can be adapted for use in inorganic isotopic studies. Volatile metal chelates can be formed and introduced into a mass spectrometer either by gas chromatography (g.c./m.s.) [7, 8] or by direct insertion probe with ionization by electron impact (e.i.m.s.) [9]. Although more rapid than t.i.m.s. (15 min per sample [9]), these techniques generally have not shown the precision and accuracy required for nutritional research, and additional sample preparation is required to form the volatile chelates. Fast atom bombardment (f.a.b.) mass spectrometry has been employed to quantify calcium isotopes rapidly, precisely (0.3% r.s.d.), and directly on small volumes of blood plasma [10]. But the mass spectrometer must be operated at high resolution if isobaric ions are not separated from the analyte during sample preparation. An application of f.a.b. to quantifying iron isotopes [11] required a liquid—liquid extraction, and precision was not as good as reported for calcium [10]. It remains to be seen whether f.a.b. is useful for other elements and in different matrices.

Inductively coupled plasma/mass spectrometry (i.c.p./m.s.) has several advantages over other methods. Isotopic information can be obtained for several elements concomitantly. The instrument need not be dedicated to the nutritional project inasmuch as more than 100 samples can be processed easily in one day (about 13 per hour). Sample homogeneity is assured more readily because samples are handled as dilute solutions.

In this paper, i.c.p./m.s. is applied for rapid measurement of zinc isotope ratios of ashed human blood plasma and fecal samples. Only a simple complexation and extraction of zinc followed by re-extraction into aqueous 1.2 M hydrochloric acid is required prior to i.c.p./m.s. The attained precision clearly is sufficient for nutritional research, the measurements are of acceptable accuracy for the systems studied, and the time and expense per sample are less than for thermal ionization procedures. This work is unusual in that a commercially available instrument is used with an ultrasonic nebulizer, as

opposed to the pneumatic nebulizer provided with the instrument. The increased sensitivity afforded by ultrasonic nebulization should improve precision at a given concentration, permit attainment of the same precision at shorter integration times, and permit determination of ratios with similar precision at a lower concentration than is possible with pneumatic nebulization.

EXPERIMENTAL

Materials and reagents

Enriched ^{67}ZnO (93.11 atom%) and ^{70}ZnO (85.03 atom%) were obtained from Oak Ridge National Laboratory. Nitric and hydrochloric acids used for preparing solutions were reagent grade, subjected to sub-boiling redistillation in silica [12]. Aqueous ammonia used for pH adjustment was reagent grade, subjected to isopiestic distillation [12]. Deionized water with a resistivity greater than 10 megohm-cm was used to prepare all solutions. Diethylammonium diethyldithiocarbamate (DDDC) was prepared from reagent-grade starting materials [13] and was dissolved fresh daily in reagent-grade tetrachloromethane for extractions [14]. The concentration of zinc impurity in DDDC and tetrachloromethane was found to be insignificant by using electrothermal atomic absorption spectrometry.

Sample preparation

A normal fasting male human subject was given 50.3 μmol (3.49 mg) of enriched ^{70}Zn orally as the aqueous chloride and was not permitted to eat for the next 4 h. Antecubital blood was drawn into heparinized, trace metal-free, evacuated blood collection tubes and was centrifuged (30 min at 600 g) to separate plasma from cells and platelets. Samples of blood plasma (8 ml each) containing approximately 120 nmol of zinc were lyophilized and ashed at 480°C for 48 h in porcelain crucibles. The ash was dissolved in a minimal volume of 6 M hydrochloric acid, and pH was adjusted to 2.5—3.0 with 1.2 M HCl or aqueous ammonia added dropwise as required.

Feces (10.4588 g) from a formula-fed human infant and containing zinc at natural abundance was lyophilized and ground to a fine powder inside a sealed polyethylene bag. Ashing, dissolution, and pH adjustment were as described for plasma. One 50-ml aliquot of this fecal solution of zinc concentration (mean ± s.d.) 59.2 ± 0.3 μM was taken directly for extraction (sample 0-0). Spiked fecal solution was prepared by adding 2 ml of an aqueous 278 ± 1 μM solution (pH 3) of enriched ^{67}Zn as chloride to 250 ml of the unspiked fecal solution. One 50-ml aliquot of the ^{67}Zn-spiked fecal solution was taken for extraction without addition of ^{70}Zn (sample 67-0). Four doubly-spiked fecal solutions (samples 67-1, 67-2, 67-4, 67-8) were prepared by adding 1, 2, 4, or 8 ml of enriched ^{70}Zn solution (zinc concentration 10.08 ± 0.07 μM) to 50-ml aliquots of the ^{67}Zn-spiked fecal solution before extraction.

Zinc was extracted [14] at pH 2.5—3.0 from five volumes of each aqueous

solution of ashed feces or blood plasma by two successive aliquots of DDDC (0.04% w/v) in one volume of tetrachloromethane, and re-extracted from the two volumes of tetrachloromethane phase into two successive aliquots of one-half volume of 1.2 M HCl. Samples were then ready for i.c.p./m.s.

Instrumentation

A Sciex Model 250 i.c.p./m.s. was used to measure all isotope ratios. Detailed descriptions of the instrument and its analytical performance have been reported [15—17]. The only modifications were the replacement of the standard Sciex i.c.p. torch with one designed by Ames Laboratory [18] and the substitution of an ultrasonic nebulizer [19] (with aerosol desolvation) for the standard concentric, pneumatic nebulizer supplied by Sciex. No mass flow controller for the aerosol gas flow was found necessary. The quadrupole was operated in a multiple-pass "peak hopping" mode as described previously [17]. Three *m/z* positions spaced 0.1 dalton apart about the peak top were monitored for each isotope. The mass spectrometer collected data at each *m/z* position for a period called the dwell time (typically 100 ms), after which it was quickly stepped to the next *m/z* position. The cycle was repeated for all the isotopes of interest until the total accumulated dwell time at each *m/z* position exceeded some preset value called the measurement time (typically 1.0 s). The total count or count rate for each isotope was then evaluated by averaging the signals accumulated at the three *m/z* positions for each peak. Thus the total time spent on each isotope was (measurement time) × 3. The effect of dwell time and total measurement time on zinc isotope precision will be discussed.

The "multiple elements" software package was used to quantify isotope ratios rather than the "isotope ratio" program. Approximately one-fifth the instrument time is required for a set of measurements using the former software package because extensive statistical calculations are not performed between measurements by the computer in this mode. The latter software has the advantage of variable dwell times for the different zinc isotopes. Precision was excellent even though an equal portion of the total measurement time was allotted to each of the three isotopes.

Optimization of the i.c.p./m.s. for precise measurement of zinc isotope ratios was similar in many respects to methods described elsewhere for accurate quantitation of trace elements with internal standardization [17]. The mass spectrometer was operated in low resolution to provide maximal sensitivity. The instrument was allowed at least a 30-min warm-up time. Zinc ratios of a 2 mg l^{-1} solution were then monitored for several minutes. Changes were made mostly in the aerosol gas flow rate and in the ion lens settings (lens B and ring lens) until maximal short-term precision was attained. This usually corresponded to obtaining good count rates at a modest flow rate of aerosol gas. Typical conditions were 1.2 kW forward power, 1.0 l min^{-1} auxiliary flow rate, 13 l min^{-1} outer argon flow rate, and 1.2 l min^{-1} aerosol flow rate. The ion lens settings normally were 60, 75, 50, and 12 for

A, B, C, and the ring lens, respectively [17]. The actual voltages corresponding to these potentiometer settings can be obtained from the authors or from the instrument manufacturer. After the above procedures, long-term precision was monitored until the ratios stopped drifting (normally less than 1 h). Thereafter, the absolute ratios did not change by more than 2% over a 7-h period.

The extracted zinc samples, at concentrations of 20 μM (plasma samples) to 30 μM (fecal samples) in 1.2 M HCl were pumped at 2.5 ml min^{-1} into the ultrasonic nebulizer. The sample tube was rinsed in deionized water, and 1% (v/v) nitric acid was pumped into the nebulizer briefly between samples. Appropriate blanks were put through all procedures. Isotope ratios were also determined on standard solutions containing zinc at natural abundance (30 μM in 1.2 M HCl) so that ratios of the extracted samples could be normalized to the natural abundance standard. Natural zinc standard solutions in 1% (v/v) nitric acid were used to evaluate effects of zinc concentration (i.e., Zn^+ count rate) and of instrumental parameters on precision of isotope ratios. Various amounts of sodium chloride were added to zinc standard solutions to study effects of sodium matrix on isotope ratios.

RESULTS AND DISCUSSION

Extraction procedures

The procedures used here provide some advantages for i.c.p./m.s. compared to the ion-exchange separations required for zinc isotope ratio measurements on biological samples by thermal ionization methods. Samples containing comparatively small (μg) amounts of zinc can be prepared and concentrated for ratio determinations rapidly without appreciable zinc loss or zinc contamination. Zinc recoveries (assessed by atomic absorption spectrometry before and after extraction) from these plasma and fecal samples ranged from 90 to 98%. Higher recoveries can be achieved at the risk of carrying over into the extractant some of the extracted phase that contains large amounts of cations (Na^+, Ca^{2+}) that can suppress Zn^+ count rates and alter isotope ratios. Other elements that can be extracted with Zn (Fe, Co, Ni, Ga) [14] do not constitute spectral interferences at m/z = 67, 68, and 70. Sodium is almost completely excluded from the extract, as evidenced by the observation that no sodium emission was seen either in the flame of the atomic absorption spectrometer or in the i.c.p. while extracted solutions were being examined.

Diethylammonium diethyldithiocarbamate was selected for this procedure over other more commonly available carbamates primarily because it will extract zinc into tetrachloromethane at pH $<$ 3 [14]. The low pH optimum is extremely important for separation of zinc from matrices that contain large amounts of calcium and phosphates, such as milks, infant formulas, and fecal samples. At pH $>$ 3, calcium phosphates precipitate from solutions of ash of such samples, and zinc coprecipitates with them. This precludes the use of

common zinc-complexing reagents (dithizone, for example) that can extract zinc at pH > 6.5. The extraction procedure described here was used successfully to extract zinc for i.c.p./m.s. from bovine milk, infant formulas, and human urine, as well as from feces and blood plasma.

Factors affecting precision and accuracy

Spectral scans of blanks taken through the extraction procedure showed small amounts of S, N, C, and Cl peaks, from hydrochloric acid and residual DDDC, in addition to normal background peaks [15]. Background count rates at m/z = 67, 68, and 70 were usually very low (50—100 counts s^{-1}), showing no indication of any interfering molecular species, trace zinc, or isobaric ^{70}Ge. Background at 70 dalton approached 200 counts s^{-1} on one day, possibly caused by a chlorine molecular species (such as $^{35}Cl_2^+$) or $(NO^+)Ar$. Because of the small natural abundance of ^{70}Zn, best results were then obtained by subtracting the blank.

Tables 1—4 contain data concerning the various factors that affect precision of isotope ratio measurements by i.c.p./m.s. Precision of such measurements is presumably a composite of the two uncertainties present in the count rate of each isotope: one is due to the total number of ions counted (counting statistics) and the other to small fluctuations in the rate at which

TABLE 1

Effect of dwell time and total measurement time on zinc isotope precision (% r.s.d. of 10 consecutive measurements of the indicated measurement time is in parentheses)[a]

Meas. time[b] (s)	Ratios at different dwell times					
	50 ms		100 ms		200 ms	
	$^{67}Zn/^{68}Zn$	$^{70}Zn/^{68}Zn$	$^{67}Zn/^{68}Zn$	$^{70}Zn/^{68}Zn$	$^{67}Zn/^{68}Zn$	$^{70}Zn/^{68}Zn$
0.2	0.2147 (1.1)	0.0335 (1.2)	0.2114 (2.1)	0.0343 (2.3)	0.2148 (2.9)	0.0336 (3.5)
0.4	0.2152 (1.5)	0.0337 (1.4)	0.2114 (1.3)	0.0340 (1.6)	0.2157 (2.0)	0.0336 (2.9)
0.8	0.2147 (0.8)	0.0333 (1.1)	0.2123 (0.7)	0.0343 (1.3)	0.2153 (1.4)	0.0334 (1.8)
1.0	0.2151 (0.5)	0.0335 (1.3)	0.2130 (0.6)	0.0341 (1.0)	0.2163 (1.7)	0.0336 (1.3)
2.0	0.2147 (0.3)	0.0333 (0.7)	0.2132 (0.4)	0.0339 (0.3)	0.2161 (1.6)	0.0334 (1.3)
5.0	— —	— —	0.2140 (0.4)	0.0338 (0.4)	0.2154 (0.7)	0.0333 (0.6)

[a]Conditions: 1.2 kW forward power, 1.0 l min^{-1} aerosol flow rate (ultrasonic nebulization), 1.0 l min^{-1} auxiliary flow rate; 2 mg l^{-1} total Zn (200 000 counts s^{-1} at ^{68}Zn); background < 50 counts s^{-1} at all three masses. [b]At each of three measurements per peak.

TABLE 2

Effect of zinc concentration and count rate on isotope precision[a]

[Zn] (mg l^{-1})	^{68}Zn count rate (counts s^{-1})	$^{67}Zn/^{68}Zn$[b]	$^{70}Zn/^{68}Zn$[b]
0.1	10090	0.2175 (2.3)	0.0325 (3.0)
0.5	54990	0.2204 (1.2)	0.0316 (2.3)
1.0	107700	0.2204 (1.2)	0.0321 (2.1)
2.0	224300	0.2176 (0.9)	0.0319 (0.7)
5.0	564700	0.2183 (0.9)	0.0319 (1.4)
10.0	1030000	0.2179 (0.9)	0.0317 (1.0)

[a]Conditions: 1.25 kW, 1.4 l min^{-1} aerosol flow rate; 10 determinations of 1 s each (100 ms dwell time). [b]With % r.s.d. in parentheses.

TABLE 3

Effect of aerosol gas flow rate and forward power on zinc isotope ratios[a]

Flow rate (l min^{-1})	Ratios at different forward power					
	1.0 kW		1.2 kW		1.4 kW	
	$^{67}Zn/^{68}Zn$	$^{70}Zn/^{68}Zn$	$^{67}Zn/^{68}Zn$	$^{70}Zn/^{68}Zn$	$^{67}Zn/^{68}Zn$	$^{70}Zn/^{68}Zn$
1.8	—	—	—	—	0.2176 (1.6) [160,000]	0.0273 (4.5)
1.6	—	—	0.2051 (1.1) [150,000]	0.0282 (2.6)	0.2164 (0.4) [260,000]	0.0330 (0.8)
1.4	0.2210 (4.4) [30,000]	0.0236 (4.2)	0.2025 (0.8) [155,000]	0.0354 (0.7)	0.2230 (2.7) [40,000]	0.0352 (3.4)
1.2	0.2004 (1.1) [105,000]	0.0381 (1.5)	0.2173 (0.3) [230,000]	0.0329 (0.8)	—	—
1.0	0.2124 (0.7) [140,000]	0.0346 (1.5)	0.2226 (1.7) [110,000]	0.0313 (1.4)	—	—
0.9	0.2227 (1.6) [70,000]	0.0317 (1.3)	0.2204 (0.8) [45,000]	0.0327 (2.9)	—	—

[a]R.s.d. (% r.s.d. given in parentheses) is for 10 consecutive measurements of 1.0 s each, 100 ms dwell time, 3 measurements per peak. Numbers in square brackets are the ^{68}Zn count rate (per second).

TABLE 4

Effect of sodium matrix on zinc isotope ratios (5 mg l^{-1} total zinc)[a]

[Na] (M)	^{68}Zn (counts s^{-1})	$^{67}Zn/^{68}Zn$[b]	$^{70}Zn/^{68}Zn$[b]
0	565 000	0.2183 (0.9)	0.0319 (1.4)
1×10^{-4}	530 000	0.2184 (1.4)	0.0319 (1.0)
5×10^{-4}	446 000	0.2195 (1.2)	0.0315 (0.8)
1×10^{-3}	372 200	0.2198 (0.5)	0.0316 (1.3)
5×10^{-3}	145 000	0.2232 (0.7)	0.0307 (0.7)
1×10^{-2}	76 450	0.2264 (0.6)	0.0310 (1.4)

[a]Conditions as for Table 2. [b]With % r.s.d. in parentheses.

each ion arrives at the detector. The former uncertainty is inherent in pulse counting with an electron multiplier. Assuming random errors in counting, this error amounts to $N^{1/2}/N$, where N is the total number of counts made during the measurement period. Count-rate fluctuations can be caused by various phenomena including nebulizer instability, fluctuations in ion optical voltages, m/z calibrations, or discriminator threshold, etc. If the latter fluctuations predominate, precision cannot be improved beyond a certain level, unless the stability of the i.c.p./m.s. is actually improved. If errors arising from counting statistics predominate, then precision can be improved simply by changing the zinc count rate or by increasing the integration time of each measurement.

From Table 1, it can be seen that increasing the total measurement (integration) time of each determination can improve the precision, up to a point. For example, the precision did not improve at all going from 2- to 5-s measurement time with a 100-ms dwell time. The data in Table 1 were obtained for 2 mg l^{-1} zinc, which gave a ^{68}Zn count rate of 2×10^5 counts s^{-1}. Therefore, the total counts for measurement times of 2 and 5 s would be approximately 4×10^5 and 1×10^6, respectively, for ^{68}Zn. The counting precision should thereby improve from about 0.4% to 0.2% for the $^{67}Zn/^{68}Zn$ ratio, or even somewhat better if one considers the averaging of three measurements per peak. The observation that it did not improve probably indicates that i.c.p./m.s. parameters, rather than counting statistics, limited precision at measurement times greater than 2 s.

Table 1 also shows the effect of dwell time on precision. If the dwell time was too short, the quadrupole switched from peak to peak very rapidly. About 50 ms was as low a dwell time as was normally found useful. The precision and accuracy at 100 ms dwell time were as good as at 50 ms, and the longer dwell time speeded up measurement time slightly by avoiding the software overhead time expended in too many "hops". A yet longer dwell time (200 ms) did not perform as well, probably because it did not permit effective averaging of low-frequency noise. As the number of cycles (measurement time/dwell time) per measurement became similar, precision

approached that of shorter dwell times. For example, precision at 5.0-s measurement time and 200-ms dwell time (25 cycles) was similar to that at 2.0-s measurement time and 100-ms dwell time (20 cycles), albeit at the expense of increased overall time. A "sequential" (single-pass peak hopping) scanning mode was also tried under identical conditions, with use of a 1.0-s measurement time. This effectively meant a 1000 ms dwell time, and results were not very precise, showing a 3—4% short-term variation. Therefore, the multichannel (i.e., multiple-pass) mode is recommended for isotope ratio determinations with this device. The i.c.p./m.s. used here does not have a fast, repetitive, continuous scanning and averaging mode as used by Gray and Date [20, 21], so the above comparison does not include this sort of data-acquisition method.

Data in Table 2 seem to indicate that increasing total counts (N) by increasing the concentration (count rate) of zinc did not improve the precision to the same extent as increasing the measurement time. Yet these data were acquired by using a higher aerosol gas flow rate than in Table 1 (1.4 vs. 1.0 l min^{-1}). Different operating conditions for the i.c.p./m.s. changed the attainable precision. This is verified in Table 3, where it is seen that the lower aerosol flow rate usually gave better precision for sets of conditions yielding similar count rates. Our experience is that instrumental operating conditions should be selected to optimize the most important figure of merit (in this case, precision of isotope ratio determinations) for the particular determination being done. Simply maximizing the signal for analyte ions may lead to disappointing performance in terms of stability or interferences.

Changes in the background matrix can influence the accuracy of isotope ratios determined under constant i.c.p./m.s. parameters of operation. Table 4 shows the effects of various concentrations of sodium chloride in a 5 mg l^{-1} zinc solution. The instrument had been warmed up and was giving very reproducible ratios before this experiment. Measurements on a blank solution of sodium chloride showed no detectable zinc in the reagents. It should be noted that both ratios changed systematically even at (moderate) sodium chloride concentrations for which the absolute suppression of the zinc signal was not excessive. At 0.01 M Na^+, the change in both ratios amounted to approximately 4%. The relative standard deviations, which are listed, illustrate that these changes represented real, detectable differences in the isotope ratios. One possible explanation for the observed difference in ratios could be loss of linearity of the electron multiplier at high count rates. But the multiplier was linear to at least 10^6 counts s^{-1}, as shown in Table 2. It is also doubtful that interfering molecular chlorine species were being formed at increased sodium chloride concentrations, because none were observed from the hydrochloric acid matrix. A more likely explanation is that the i.c.p. and/or nebulizer underwent real changes at higher salt concentrations, which affected the isotope ratios. For this reason, the accuracies of the ratios in the fecal matrix were studied.

Verification of accuracy in fecal matrix

For planned clinical studies, the linear range required for $^{70}Zn/^{68}Zn$ measurements is from about 50 to 400 atom% excess of ^{70}Zn. If one wishes to compare bioavailability of zinc from two separate dietary sources in the same meal, using ^{70}Zn and ^{67}Zn simultaneously as tracers, for example, both the relative precision and accuracy should be 1% or better over this range. The linearity, precision, and accuracy of response were tested by spiking four aliquots of fecal solution with 46—371 atom% excess of ^{70}Zn. Fecal aliquots were also spiked with ^{67}Zn to compare the precision and accuracy of ^{67}Zn and ^{70}Zn as tracers, to serve as an internal check on the stability of instrumentation, and to verify the atomic absorption determination of the zinc concentration of the unspiked fecal solution. The zinc isotope ratio results by i.c.p./m.s. are shown in Table 5. The precision of the $^{70}Zn/^{68}Zn$ determinations was near 1% r.s.d. (mean 1.1%). The precision of the $^{67}Zn/^{68}Zn$ determinations was 1% r.s.d. or less (mean 0.5%). The $^{70}Zn/^{68}Zn$ and $^{67}Zn/^{68}Zn$ ratios of the unspiked fecal sample (0-0) are within experimental uncertainty of those of natural-abundance zinc standard in 1.2 M HCl.

The $^{70}Zn/^{68}Zn$ and $^{67}Zn/^{68}Zn$ ratios of the fecal solutions are shown in Table 6 normalized to the ratios for the natural-abundance zinc standard. The expected values were calculated from atomic absorption determinations of the molar zinc concentrations of the unspiked and spiking solutions, taking into account the relative amounts of ^{67}Zn, ^{68}Zn, and ^{70}Zn that are added when spiking with enriched ^{67}Zn (93.11 atom%) and with multiple volumes of enriched ^{70}Zn (85.03 atom%). The linear regression line through the $^{70}Zn/^{68}Zn$ values of Table 6 is $y = 0.9984x + 0.0023$. The correlation coefficient is $r = 0.99988$. The slope and intercept do not differ significantly from the ideals of 1.0 and 0, respectively. For the ^{70}Zn-spiked solutions (67-1, 67-2, 67-4, 67-8), the observed $^{70}Zn/^{68}Zn$ values were 100.0 ± 1.0

TABLE 5

Observed zinc isotope ratios of fecal solutions[a]

Sample[b]	$^{70}Zn/^{68}Zn$		$^{67}Zn/^{68}Zn$	
	Ratio	% r.s.d.	Ratio	% r.s.d.
STD	0.03155	0.98	0.2262	0.43
0-0	0.03159	1.4	0.2275	0.60
67-0	0.03127	1.1	0.4148	0.42
67-1	0.04610	0.85	0.4141	0.20
67-2	0.06036	1.3	0.4119	0.84
67-4	0.09151	1.3	0.4113	0.28
67-8	0.1479	1.0	0.4109	1.00

[a]I.c.p./m.s. conditions: 1.0 l min^{-1} aerosol gas flow rate, 1.25 kW, 0.8 l min^{-1} auxiliary flow rate, 2 s measurement time, 100 ms dwell time, 10—12 determinations per sample.
[b]STD, natural abundance Zn standard; 0-0, unspiked feces; 67-*n*, feces spiked with constant amount of ^{67}Zn and variable amount of ^{70}Zn.

TABLE 6

Label recovery[a]

Sample[b]	$^{70}Zn/^{68}Zn$		$^{67}Zn/^{68}Zn$	
	Observed	Expected	Observed	Expected
0-0	1.001	1.000	1.006	1.000
67-0	0.991	0.997	1.834	1.841
67-1	1.461	1.464	1.831	1.840
67-2	1.913	1.930	1.821	1.839
67-4	2.900	2.860	1.819	1.837
67-8	4.688	4.710	1.817	1.833

[a]Ratios normalized to ratios from natural-abundance standard in 1.2 M HCl. Conditions as for Table 5. [b]Same sample designations as for Table 5.

(mean ± s.d.)% of the expected values. The observed $^{67}Zn/^{68}Zn$ values of the ^{70}Zn-spiked solutions were in a decreasing series compared with the ^{67}Zn-spiked solution that was not spiked with enriched ^{70}Zn (solution 67-0). This observation corresponds to the increasing amounts of ^{68}Zn relative to ^{67}Zn that were added when spiking with multiple volumes of ^{70}Zn. For the ^{67}Zn-spiked solutions (67-0, 67-1, 67-2, 67-4, 67-8), the observed $^{67}Zn/^{68}Zn$ values were 99.3 ± 0.3 (mean ± s.d.)% of the expected values. The observed $^{67}Zn/^{68}Zn$ values all differed from the expected values by less than 1%. When one considers that the expected values are based on zinc concentration determinations by atomic absorption spectrometry, the precision and accuracy of which are not better than 0.4—0.5% relative, it is evident that the observed and expected values agree within the overall experimental error.

In vivo enrichment of blood plasma zinc

The $^{70}Zn/^{68}Zn$ ratios (normalized to natural-abundance zinc standards) of zinc extracts of samples of ashed blood plasma are shown in Table 7. Simul-

TABLE 7

In vivo enrichment of blood plasma zinc with ^{70}Zn

Time[a] (h)	Normalized ratio[b]	R.s.d. (%)	Time[a] (h)	Normalized ratio[b]	R.s.d. (%)
−48	1.014	1.4	2	3.160	1.2
−24	0.986	1.5	4	2.529	1.5
0.5	1.709	1.5	24	1.931	2.4
1	4.656	1.2	168	1.494	2.7

[a]Blood samples drawn at indicated times. ^{70}Zn spike administered at time = 0. [b]$^{70}Zn/^{68}Zn$ ratios normalized to a natural-abundance standard in 1.2 M HCl. Conditions as for Table 5, except 5—8 determinations per sample.

taneous determinations of $^{67}Zn/^{68}Zn$ ratios at natural abundance (not shown) served to confirm instrumental stability. The times listed are those at which blood was drawn from the subject, relative to time zero, at which 50.3 μmol of enriched ^{70}Zn was administered as the chloride in 250 ml of water. This amount of zinc is representative of the zinc content of a typical meal. Plasma zinc enrichment peaked (366 atom% excess) approximately 1 h after ingestion, decreased gradually thereafter, and remained substantial 7 days later. Interpretable results could have been achieved with half as much ^{70}Zn, bringing the enriched stable isotope cost per subject under $90 at current prices. The precision of these plasma ratios was not as good as for the fecal samples because the zinc concentrations of the plasma solutions were less than those of the fecal solutions, but precision was acceptable for the intended purpose.

This is Journal Paper No. J-12257 of the Iowa Agriculture and Home Economics Experiment Station, Ames (Project No. 2730). This work is supported in part by the Director of Energy Research, Office of Basic Energy Sciences, U.S. Department of Energy. The Ames Laboratory is operated by Iowa State University for the U.S. Department of Energy under contract No. W-7405-Eng-82.

REFERENCES

1 J. R. Turnlund, J. C. King, W. R. Keyes, B. Gong and M. C. Michel, Am. J. Clin. Nutr., 40 (1984) 1071.
2 G. E. Inglett (Ed.), Nutritional Bioavailability of Zinc, American Chemical Society, Washington, DC, 1983.
3 N. W. Solomons, Am. J. Clin. Nutr., 35 (1982) 1048.
4 L. Wada, J. R. Turnlund and J. C. King, J. Nutr., 115 (1985) 1345.
5 A. L. Yergey, N. E. Vieira and J. W. Hansen, Anal. Chem., 52 (1980) 1811.
6 M. Schmidt and M. A. Northup, Am. Lab., 18 (1986) 125.
7 C. Veillon, in J. R. Turnlund and P. E. Johnson (Eds.), Stable Isotopes in Nutrition, American Chemical Society, Washington, DC, 1984, Ch. 7.
8 D. L. Hachey, J. C. Blais and P. D. Klein, Anal. Chem., 52 (1980) 1131.
9 N. S. Shaw, D. D. Millen, M. Gilbert, D. A. Roe and D. R. Campen, in J. R. Turnlund and P. E. Johnson (Eds.), Stable Isotopes in Nutrition, American Chemical Society, Washington, DC, 1984, Ch. 8.
10 D. L. Smith, Anal. Chem., 55 (1983) 2391.
11 J. Eagles, S. J. Fairweather-Tait and R. Self, Anal. Chem., 57 (1985) 469.
12 M. Zief and J. W. Mitchell, Contamination Control in Trace Elemental Analysis, Wiley, New York, 1976, pp. 102–106.
13 H. Bode and F. Neumann, Z. Anal. Chem., 169 (1959) 410.
14 H. Bode and F. Neumann, Z. Anal. Chem., 172 (1960) 1.
15 D. J. Douglas and R. S. Houk, Prog. Anal. At. Spectrosc., 8 (1985) 1.
16 G. Horlick, S. H. Tan, M. A. Vaughan and C. A. Rose, Spectrochim. Acta, Part B, 40 (1985) 1555.
17 M. D. Palmieri, J. S. Fritz, J. J. Thompson and R. S. Houk, Anal. Chim. Acta, 184 (1986) 187.
18 R. H. Scott, V. A. Fassel, R. N. Kniseley and D. E. Nixon, Anal. Chem., 46 (1974) 75.
19 K. W. Olson, W. J. Haas, Jr. and V. A. Fassel, Anal. Chem., 49 (1977) 632.
20 A. R. Date and A. L. Gray, Spectrochim. Acta, Part B, 40 (1985) 115.
21 A. L. Gray, Spectrochim. Acta, Part B, 40 (1985) 1525.

Analytica Chimica Acta, 188 (1986) 85—94
Elsevier Science Publishers B.V., Amsterdam – Printed in The Netherlands

DETERMINATION OF TRACE ELEMENTS IN BIOLOGICAL MATERIALS BY INSTRUMENTAL EPITHERMAL NEUTRON ACTIVATION ANALYSIS

F. CHISELA* and P. BRÄTTER

Spurenelementforschung in der Biomedizin, Hahn-Meitner Institut GmbH, Glienickerstr. 100, D-1000 Berlin 39 (Federal Republic of Germany)

(Received 6th June 1986)

SUMMARY

The use of reactor epithermal neutrons in instrumental activation analysis is described for the determination of trace elements via long-lived isotopes. A boron carbide filter is used. Results of analyses of human erythrocytes, plasma, urine and some biological reference materials are given to demonstrate the applicability of the method to biological samples. Bromine, iron, cesium, rubidium, selenium and zinc and cobalt are determined. The method provides accuracy and reliability similar to conventional thermal neutron activation but is faster. Limits of detection attainable with the two techniques are compared.

The value of instrumental neutron activation analysis (i.n.a.a.) for the determination of trace elements is widely recognized [1, 2]. This technique has many desirable features including high sensitivity, multi-element capability and the flexibility to allow either short-lived or long-lived isotopes to be utilized for the determination of elements [1]. Most importantly, a minimum of sample treatment is needed, which makes the procedure less prone to errors and contamination [3] and also amenable to automation for the analysis of large numbers of samples.

In materials of complex chemical composition, however, the many constituent elements characteristically present in high concentration induce high activities which impose a serious practical limitation on the usefulness of i.n.a.a. in many applications. In biological materials, for instance, the observed γ-ray spectrum of the sample irradiated with the total reactor spectrum of neutrons is very often dominated by high-energy γ-ray, Compton and bremsstrahlumg background activities from such radionuclides as ^{24}Na, ^{38}Cl, ^{42}K, ^{32}P and ^{82}Br. These activities usually obscure the required peaks from radionuclides of trace elements and generally worsen the detection conditions, leading to poor precision and accuracy. The possibility of waiting for long periods of time, sometimes up to 3 months [4], to let the activities of such radionuclides decay to a level where instrumental measurement is possible has been widely practised. For many applications, however, especially

0003-2670/86/$03.50

in clinical and environmental trace element research, this time lapse in obtaining results is a serious drawback. Moreover, long decay periods mean that rapid instrumental detection of other radionuclides with half-lives shorter than or comparable to those of the interfering activities are impossible. In general, the speed of i.n.a.a. can be increased by using short irradiation and counting times but this is not suitable for long-lived isotopes requiring long irradiation times to produce accurately measurable activities. In practice, experimental conditions must be optimized appropriately for each particular problem. Behne and Jürgensen [4], for instance, have shown that irradiation for 5 days at a thermal neutron flux of 10^{13} cm^{-2} s^{-1} followed by decay for 3 months is optimal for the instrumental determination of selenium and other elements in biological materials via their long-lived radionuclides.

Epithermal activation has been used frequently in the determination of trace elements by i.n.a.a. in different materials [5–8]. This technique enhances the detection conditions for trace elements with nuclides having high ratios of resonance integral to thermal neutron cross-section (RI/σ_0), in the presence of interfering nuclides which are activated by thermal neutrons but have no resonance peaks in the epithermal region. The basic principles are well established [9—11]. The outstanding practical feature is the substantial decrease of interfering matrix activities so that considerable time can be saved by measuring the activity of the sample after minimal waiting time. For the determination of elements for which epithermal activation is sensitive, reasonably short irradiation times and decay times can be used and i.n.a.a. becomes more cost-effective.

A neutron activation scheme based on conventional "thermal" and epiboron neutron irradiation has been adopted in this Institute for the determination of trace elements in biological materials. In this paper, some results are presented for the analysis of selected biological materials by instrumental epithermal neutron activation methods. Particular emphasis is given to the optimization of conditions for the determination of elements via the assay of long-lived isotopes.

EXPERIMENTAL

Samples of human blood and urine were collected daily for 7 days from different adults in this Institute. Samples to be analyzed by epithermal neutron activation were taken from three different individuals for three consecutive days in the case of blood and for one day in the case of urine. The blood was separated into plasma and erythrocytes immediately after collection; aliquots (200 μl) were pipetted into clean quartz ampoules and evaporated in the oven at 50°C before heat-sealing. For the standard reference materials, several samples of NBS SRM-1566 (oyster tissue) and NBS SRM-1577 (bovine liver) and Bowen's kale were accurately weighed into quartz ampoules (20–50 mg) and dried in an oven to a constant weight before heat-sealing.

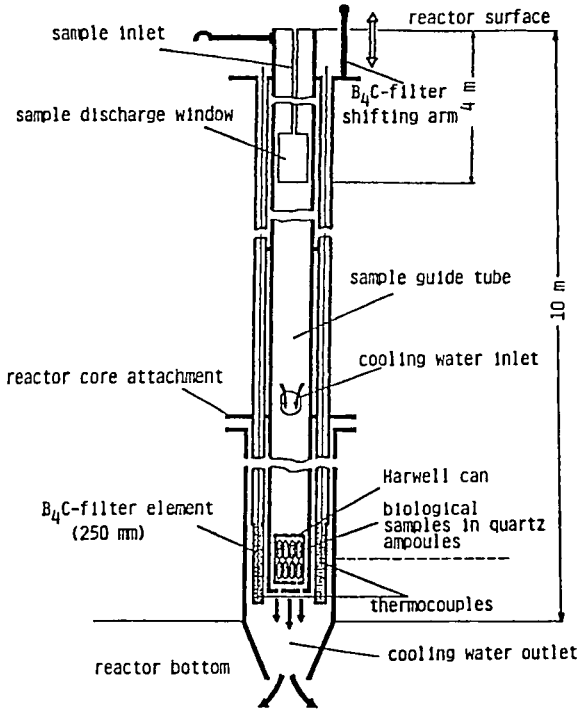

Fig. 1. Schematic diagram of the design of a B_4C-filtered epithermal irradiation facility for the BER-II reactor.

The irradiation facilities of the BER-II 5-MW swimming pool-type reactor were used for sample irradiation. Epithermal activation was done with a boron-carbide filtered irradiation facility, shown schematically in Fig. 1, for which the thermal neutron flux was 3×10^{13} cm^{-2} s^{-1} (Φ_{epi}/Φ_{th} = 1.8%). Details of the design and construction of the shield have been reported elsewhere [12]. The use of boron compounds as filters in neutron activation has been recommended [13–15] and the advantages offered by these filters relative to cadmium filters were recently evaluated [16]. Irradiation times of about 24 h were used in all sample irradiations. Waiting and counting times were chosen with the aim of optimizing the measurement of long-lived radionuclides. In initial experiments, the best irradiation and counting conditions consistent with acceptable accuracy and precision were established. The spectra were measured with an intrinsic well-type germanium detector (Detector Systems, Wiesbaden) and associated electronics.

RESULTS AND DISCUSSION

A useful index characterizing the sensitivity of determinations by epithermal n.a.a. is the ratio of resonance integral to thermal neutron cross-

TABLE 1

Some nuclear data for the radionuclides used [17]

Element	Radionuclide	Half-life	γ-Peak used (keV)	RI/σ_0
Ag	^{110m}Ag	250 d	658.0	297.8
Br	^{82}Br	35.34 h	776.6	16.67
Co	^{60}Co	5.27 y	1332.5	2.0
Cr	^{51}Cr	27.0 d	320.1	0.53
Cs	^{134}Cs	2.06 y	796.3	15.50
Fe	^{59}Fe	44.60 d	1291.3	1.05
Mo	^{99}Mo/^{99}Tc	66.7 h	141.0	53.57
Ni	^{58}Co	70.8 d	811.0	(n, p) reaction
Rb	^{86}Rb	18.66 d	1076.6	14.0
Sc	^{46}Sc	84.0 d	889.3	0.44
Se	^{75}Se	120.0 d	264.5	9.1
Zn	^{65}Zn	245.0 d	1115.5	1.95

section (RI/σ_0). Table 1 contains these values along with essential nuclear constants for the nuclides used in this work. Generally, epithermal n.a.a. is favourable for those elements with high RI/σ_0 values.

In order to establish the best conditions for epithermal n.a.a., NBS SRM-1566 (oyster tissue) and Bowen's kale were measured after irradiation for 37.5 h with epithermal neutrons. The γ-spectra of the samples were measured for 1 h after decay periods of 10, 16 and 21 days. Table 2 gives the results obtained for Se, Rb, Fe, Zn and Co along with precision and accuracy and the detection limits obtained for these waiting periods. The standard deviations given are due to counting statistics only. The errors given are the difference between the mean content found and the certified value, expressed as a percentage, i.e., relative error.

If the 5% level of precision generally recognized as acceptable in n.a.a. is applied to the results in Table 2, it is evident that better precision (<10% RSD) under these conditions is achieved for most elements after 21 days of decay time. Exceptions arise for elements for which epithermal neutron activation is not the most favourable method, i.e., those with low RI/σ_0 values (here, iron in oyster tissue). Better accuracy and lower detection limits are also obtained after a 21-d decay period. With the exception of iron, all the elements determined in these materials have reasonably high RI/σ_0 values and therefore epithermal neutron activation should be favourable for their instrumental determination at $\mu g\ g^{-1}$ levels using similar analytical conditions. In Bowen's kale, the concentration of selenium ($0.012\ \mu g\ g^{-1}$) is near the detection limit for epithermal n.a.a. under the conditions applied and therefore its determination is difficult even after 21 days of decay.

For the analysis of biological materials by means of long-lived isotopes, the major interfering activity comes from the ^{32}P bremsstrahlung which

TABLE 2

Precision, accuracy and detection limit (DL) for trace elements in standard reference materials as a function of decay time (10—21 days) after epithermal neutron activation

Element	10 d			16 d			21 d			Certified value ($\mu g\ g^{-1}$)
	$x \pm s$[a]	Error (%)	DL[b]	$x \pm s$[a]	Error (%)	DL	$x \pm s$[a]	Error (%)	DL[b]	
Oyster tissue (SRM 1566)										
Se	2.02 ± 2 (9)	3.8	0.5	2.19 ± 0.1 (4)	4.2	0.3	2.21 ± 0.1 (2.2)	5.2	0.2	2.1 ± 0.5
Rb	4.29 ± 1.4 (33)	3.6	1.7	4.34 ± 0.6 (13)	2.5	0.3	4.49 ± 0.2 (3.3)	0.9	0.6	4.45 ± 0.09
Fe	234 ± 34 (15)	20	23	173 ± 27 (15)	11	10	201 ± 26 (13)	3	5.8	195.0 ± 34
Zn	861 ± 20 (2)	1.1	11	876 ± 7 (0.8)	2.8	6.5	854 ± 3 (0.35)	0.23	4.1	852.0 ± 14
Co	0.6 ± 0.08 (12)	>50	0.15	0.4 ± 0.04 (9)	3	0.1	0.4 ± 0.03 (7)	3	0.04	(0.4)
Bowen's kale										
Se	ND[c]			0.15 ± 0.02 (13)	15	0.1	0.11 ± 0.01 (9)	15	0.06	0.12
Rb	49.3 ± 2 (4.3)	5.2	1.2	50 ± 1.7 (3.4)	3.8	0.7	54 ± 0.6 (1)	3.8	0.5	52.2
Fe	142 ± 16 (12)	18	33	135 ± 10 (7)	12	26	127 ± 4 (3)	5	12	118.0
Zn	30.4 ± 4 (14)	7.3	7	32.9 ± 1 (3.3)	0.07	3.3	32.2 ± 0.5 (1.5)	1.6	1.8	33.2
Co	0.08 ± 0.01 (12)	36	0.08	0.06 ± 0.01 (16)	2.5	0.01	0.06 ± 0.01 (5.2)	4.3	0.009	0.058

[a]Mean ($\mu g\ g^{-1}$, dry weight) and standard deviation, with relative standard deviation (%) in parentheses. Means are based on 3—5 separate analyses. [b]In $\mu g\ g^{-1}$ (dry weight). [c]Not determined.

smears the spectrum and raises the background count rate. Consequently, the half-life of phosphorus-32 ($T_{0.5}$ = 14.3 d) determines the ultimate time scale of the analysis. However, epithermal neutron irradiation should depress the activity of ^{32}P, because the value of RI/σ_0 for this nuclide is very low (0.44). To compare the benefits of epithermal n.a.a. relative to thermal n.a.a., SRM-1566 (oyster tissue) was analyzed after irradiation for 48 h and 60 h, respectively. The results of the determination along with the limits of detection and precision by both techniques are compared in Table 3. The counting times given in the table were the optimum consistent with a maximum analyzer dead-time of 10%. Typical γ-spectra of the oyster tissue material measured under these conditions are given in Fig. 2 for both irradiation procedures. Although precision and accuracy are generally similar, lower detection limits are obtained with thermal n.a.a. for many elements; rubidium is an exception because the prolonged waiting period of more than 2 months is inappropriate for the rather short half-life ($t_{0.5}$ = 18.6 d). The total time required in epithermal n.a.a. is shortened by a factor of 3—4 as a result of the substantial reduction of the ^{32}P background activity.

The applicability of the epithermal activation technique to "real" biological samples was tested by analyzing selected body fluids. Tables 4 and 5 give the results obtained for erythrocytes, plasma and urine, respectively,

TABLE 3

Comparison of precision, detection limits and time of analysis for SRM-1566 by epithermal and thermal n.a.a.

Element	Epithermal		Thermal		Certified value ($\mu g\ g^{-1}$)
	$x \pm s$[a]	DL[b]	$x \pm s$[a]	DL[b]	
Ag	0.86 ± 0.09 (10.5)	0.024	0.93 ± 0.06 (6.5)	0.016	0.89 ± 0.09
Br	52.90 ± 3.3 (6.2)	1.6	—	—	(55)
Co	0.42 ± 0.07 (16.7)	0.01	0.34 ± 0.01 (2.9)	0.001	(0.4)
Cr	—	—	0.75 ± 0.10 (13.3)	0.036	0.69 ± 0.27
Fe	212.5 ± 37.0 (17.4)	6.2	218.9 ± 9.0 (4.1)	2.8	195.0 ± 34
Mo/Tc	0.16 ± 0.04 (25.0)	0.016	—	—	(<0.2)
Ni(Co)	0.98 ± 0.10 (10.2)	0.01	—	—	1.03 ± 0.19
Rb	5.04 ± 0.10 (1.9)	0.07	4.27 ± 0.19 (4.5)	1.2	4.45 ± 0.09
Sc	—	—	0.015 ± 0.002 (13.3)	0.0004	—
Se	2.04 ± 0.04 (1.9)	0.04	2.21 ± 0.08 (3.6)	0.02	2.10 ± 0.5
Zn	887.60 ± 10.0 (1.1)	0.56	884.6 ± 17.0 (1.9)	0.18	852.0 ± 14.0
Irradiation time	48 h		60 h		
Cooling time	15—21 d		50—70 d		
Counting time	7200 s		7200 s		

[a]Values are arithmetic means ($\mu g\ g^{-1}$, dry weight) with standard deviation and relative standard deviation (%) in parentheses, from 10 parallel determinations. [b]In $\mu g\ g^{-1}$ (dry weight).

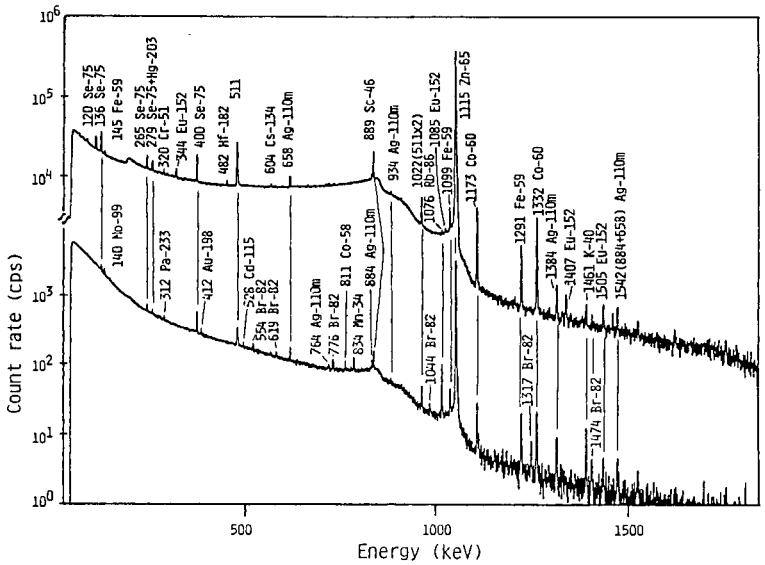

Fig. 2. γ-Spectrum of NBS SRM-1566 (oyster tissue) measured after irradiation (for 48 h) with epithermal neutrons and total reactor spectrum of neutrons. Upper spectrum: without boron carbide filter (decay time 50 d, counting time 7200 s). Lower spectrum: with boron carbide filter (decay time 15 d, counting time 7200 s).

compared with those obtained in a separate analysis by the thermal neutron activation procedure. The decay period used in the thermal neutron procedure is more than the maximum normally used in this laboratory for instrumental n.a.a. For epithermal n.a.a., the irradiation time of 24 h and the cooling period of 21—30 days were chosen on the basis of the results obtained from the analysis of the reference materials described above. In erythrocytes (Table 4), the precision for Br, Fe, Rb, Se and Zn by the epithermal procedure falls within the range generally accepted for instrumental n.a.a. (~5%) [1]. Comparison with the results obtained by the thermal procedure shows that Co and Cs are definitely below the detection limits for the epithermal technique under these conditions. A longer irradiation time might increase the sensitivity for these two elements, because their RI/σ_0 ratios are reasonably high. The results obtained for plasma (Table 4) show the same detection capability for the epithermal technique with precision similar to that for erythrocytes. As in erythrocytes, Co and Cs are below the detection limits of the epithermal procedure. The situation is similar in the results obtained for urine (Table 5) by the epithermal procedure, although here higher levels of cesium are apparent in all samples except one. The waiting time used in the thermal procedure is too long and leads to poor precision because of low count rates, particularly for selenium determinations. All the values obtained in these analyses were compared with those reported in the literature [18] and found to be within the accepted ranges.

TABLE 4

Results obtained for human blood by instrumental epithermal and thermal n.a.a.

Element	Epithermal[a]			Thermal[b]		
	Subject 1	Subject 2		Subject 1	Subject 2	
	$x \pm s$[c]	$x \pm s$[c]	DL[d]	$x \pm s$[c]	$x \pm s$[c]	DL[d]
Erythrocytes						
Br	6.5 ± 0.4 (6)	5.5 (4)	1.0	ND		
Co	ND			0.003 ± 0.001 (33)	0.006 ± 0.002 (24)	0.0004
Cs	ND			0.025 ± 0.002 (8)	0.023 ± 0.002 (8)	0.004
Fe	2803 ± 105 (3)	2317 ± 47 (6)	1.6	2892 ± 101 (4)	2912 ± 179 (6)	10
Rb	9.9 ± 0.5 (5)	10.6 ± 0.3 (3)	0.4	ND		
Se	0.36 ± 0.03 (8)	0.44 ± 0.01 (2)	0.10	0.39 ± 0.07 (17)	0.42 ± 0.06 (14)	0.002
Zn	32.8 ± 0.8 (2)	30.9 ± 0.2 (0.6)	0.6	ND	29.2 ± 2 (6)	0.05
Blood plasma						
Co	ND			0.009 ± 0.001 (14)	0.01 ± 0.002 (20)	0.0005
Cs	ND			0.016 ± 0.002 (12)	0.015 ± 0.002 (13)	0.003
Fe	10.85 ± 0.6 (5)	11.3 ± 0.7 (6)	1.5	11.2 ± 0.9 (6)	11.5 ± 1.1 (9)	8.1
Rb	2.0 ± 0.1 (6)	2.1 ± 0.3 (14)	0.3	ND		
Se	0.86 ± 0.10 (10)	0.79 ± 0.15 (18)	0.10	0.82 ± 0.11 (13)	0.88 ± 0.14 (15)	0.02
Zn	7.1 ± 0.6 (9)	8.3 ± 1.3 (15)	0.4	6.7 ± 0.9 (14)	7.1 ± 0.8 (12)	0.03

[a]Irradiation time 24 h, decay time 21 d, counting time 7200 s. [b]Irradiation time 5 d, decay time 7 months, counting time 7200 s. [c]Mean values ($\mu g\ g^{-1}$) are given with standard deviation (and relative standard deviation, %). $n = 3$ for epithermal n.a.a. and $n = 2$ for thermal n.a.a. [d]In $\mu g\ g^{-1}$.

TABLE 5

Results obtained for human urine collected from 5 adults on one day, by epithermal[a] and thermal[b] n.a.a.[c]

Element	1	2	3	4	5	DL
Co[d]	(0.009 ± 0.001)	(0.02 ± 0.002)	(0.02 ± 0.001)	(0.012 ± 0.001)	(0.004 ± 0.001)	(0.0007)
Cs	0.23 ± 0.001 (0.21 ± 0.007)	0.25 ± 0.002) (0.27 ± 0.01)	0.27 ± 0.006 (0.28 ± 0.01)	ND (0.08 ± 0.003)	0.31 ± 0.005 (0.26 ± 0.01)	0.02 (0.002)
Fe	ND ND	20.5 ± 1.2 (23.3 ± 1.4)	25.1 ± 1.8 (24.6 ± 1.4)	6.3 ± 0.3 (4.4 ± 0.8)	ND ND	5.5 (6.4)
Rb[e]	34.4 ± 0.8	31.4 ± 0.7	54.0 ± 1.2	15.9 ± 0.7	49.7 ± 1.0	1.0
Se	0.24 ± 0.003 (0.23 ± 0.009)	0.50 ± 0.07 (0.42 ± 0.02)	0.46 ± 0.01 (0.44 ± 0.02)	0.11 ± 0.01 (0.13 ± 0.009)	0.28 ± 0.02 (0.29 ± 0.001)	0.7 (0.05)
Zn	10.6 ± 0.2 (9.9 ± 0.1)	8.3 ± 0.6 (7.7 ± 0.1)	7.8 ± 0.3 (8.2 ± 0.1)	9.9 ± 0.4 (7.7 ± 0.1)	6.1 ± 0.8 (6.1 ± 0.7)	2.0 (0.04)

[a]Irradiation time 24 h, decay time 30 d, counting time 7200 s. [b]Irradiation time 5 d, decay time 7 months, counting time 7200 s. [c]The results (all in $\mu g\ g^{-1}$) by the thermal neutron method are given in parentheses. Standard deviations relate to counting statistics. [d]Not determined by the epithermal method. [e]Not determined by the thermal method.

In epithermal n.a.a., nuclear interferences arising especially from threshold (n, p) reactions are a significant source of errors. This is simply because the intensities of these reactions become comparable to those induced by the (n, γ) thermal neutron reactions, when the thermal neutron energy spectrum is removed. Davies et al. [14] discussed this problem and estimated the severity of the interferences after both short and long irradiations, when the concentration of the interfering element was 10 mg kg^{-1}. In general, interfering nuclear reactions are more serious for short-lived analysis where threshold nuclear reactions are more prevalent. During lengthy irradiations, however, cobalt may interfere with the determination of iron through the $^{59}Co(n, p)\ ^{59}Fe$ reaction, but for the biological materials analyzed in this work this interference can be considered negligible because the cobalt concentration is very much lower than that of iron.

Conclusions

Epithermal neutron activation yields comparable quality in the results of the instrumental determination of selenium, rubidium and zinc in these biological samples at upper and lower $\mu g\ g^{-1}$ levels. The total analysis time required is approximately three weeks to achieve results with acceptable precision and accuracy. Much lower detection limits for most elements, however, are usually provided by thermal neutron activation analysis, as is evident from the above results. This finding is consistent with the fact that the epithermal neutron flux is usually one or two orders of magnitude lower than the thermal neutron flux in many irradiation facilities. Accordingly, unless the relative change in the activation cross-section of an isotope when

epithermal neutrons are used (i.e., RI/σ_0: Φ_{th}/Φ_{epi}) compensates this reduction in neutron flux significantly, the sensitivity of epithermal neutron activation is likely to be lower than that of the thermal neutron activation method.

The authors thank Dr. W. Frenzel for his comments during the preparation of this paper. F. Chisela is grateful to DAAD for financial support provided through a Fellowship.

REFERENCES

1 V. P. Guinn and J. Hoste, Neutron Activation Analysis, in Elemental Analysis of Biological Materials, Technical Report Series No. 197, International Atomic Energy Agency, Vienna, 1980, Chap. 7 pp. 105—140.
2 W. Michaelis, H. U. Fanger, R. Niedergesäss and H. Schwenke, Paper presented at the Symposium on Instrumental Multi-Element Analysis, April, 1984, Jülich, F.R.G.
3 S. Amiel, Non-destructive Activation Analysis with Nuclear Reactors and Radioactive Neutron Sources, Elsevier, Amsterdam, 1981.
4 D. Behne and H. Jürgensen, J. Radioanal. Chem., 42 (1978) 447.
5 E. Steinnes and J. J. Rowe, J. Radioanal. Chem., 37 (1977) 849.
6 Z. Randa, Radioanal. Lett., 24 (1976) 157.
7 P. A. Baedecker, J. Radioanal. Chem., 40 (1977) 115.
8 A. G. Hanna and H. Al-Shahristani, J. Radioanal. Chem., 37 (1977) 581.
9 Z. Prouza and M. Rakovic, Isotopenpraxis, 3 (1967) 389.
10 D. C. Borg, R. E. Segel, P. Kienle and L. Campbell, Int. J. App. Radiation Isotopes, 11 (1960) 10.
11 T. Bereznai, D. Bodizs and G. Keömley, J. Radioanal. Chem., 36 (1977) 509.
12 F. Chisela, D. Gawlik and P. Brätter, paper presented at the 7th International Conference on Modern Trends in Activation Analysis, June, 1986, Copenhagen, Denmark, J. Radioanal. Chem., in press.
13 H. Bem and D. E. Ryan, Anal. Chim. Acta, 124 (1981) 373.
14 J. A. Davies, P. A. Hart and A. C. Jefferies, J. Radioanal. Chem., 98 (1986) 275.
15 F. Chisela, D. Gawlik and P. Brätter, Analyst, 111 (1986) 405.
16 F. Chisela, Ph.D. Thesis, Technische Universität Berlin, 1986.
17 Handbook of Nuclear Activation Cross-Sections, Technical Report Series, No. 156, International Atomic Energy Agency, Vienna, 1974.
18 G. V. Iyengar, W. E. Kollmer and H. J. M. Bowen, The Elemental Composition of Human Tissues and Body Fluids, Verlag Chemie, Weinheim, 1978.

Analytica Chimica Acta, 188 (1986) 95—100
Elsevier Science Publishers B.V., Amsterdam — Printed in The Netherlands

DETERMINATION OF CHOLESTEROL WITH A LABORATORY-BUILT CHEMILUMINESCENCE SYSTEM

AKIYOSHI TANIGUCHI, YUZURU HAYASHI*[a] and HIDETAKA YUKI

Faculty of Pharmaceutical Sciences, Toho University, 2-2-1, Miyama, Funabashi-shi, Chiba (Japan)

(Received 14th May 1986)

SUMMARY

Chemiluminescence measurement by a laboratory-built computer system equipped with an automated injection device is applied to a cholesterol enzymatic assay. The hydrogen peroxide produced by cholesterol esterase and oxidase is mixed rapidly with horseradish peroxidase-luminol solution (pH 10.5) and the light emission data are processed by a Fourier-transform digital filter to produce peak-height measurements. A blood serum volume of 0.2 μl and an observation time of 0.5 s are required.

Assays of cholesterol in blood serum, which may be present in micellar association with phospholipids, proteins and triglycerides, play a significant role in the diagnosis of a number of diseases. Several non-enzymatic methods have been used widely for routine tests [1, 2], but most current assays utilize enzyme-catalyzed reactions [3—5]. The assays for total cholesterol are based on the reactions:

$$\text{cholesterol ester} + H_2O \xrightarrow[\text{esterase}]{\text{cholesterol}} \text{cholesterol} + \text{fatty acid}$$

$$\text{cholesterol} + O_2 \xrightarrow[\text{oxidase}]{\text{cholesterol}} \text{cholest-4-en-3-one} + H_2O_2$$

The hydrogen peroxide produced can be quantified spectrophotometrically [5, 6], fluorimetrically [7, 8], amperometrically [3, 4] or by chemiluminescence [2, 9—12].

Chemiluminescence assays have been extensively investigated because of their promising properties such as high sensitivity, extended dynamic range and inexpensive instrumentation [13—15]. Recently, a computer system for such measurements, equipped with an automated rapid injection device, was developed in this laboratory [16]. With this system, luminol participating in

[a]Present address: National Institute of Hygienic Sciences, 1-18-1 Kamiyoga, Setagaya-ku, Tokyo 158 (Japan)

0003-2670/86/$03.50

a slow chemiluminescence reaction continuing for more than 40 s was determined in just 0.5 s by Fourier-transform peak-height measurements [17]. Taniguchi et al. [18] indicated that the reproducibility was improved by an appropriate choice of mixing modes. Such simple peak-height measurements, providing satisfactory rapidity and precision, would be useful in routine clinical analysis. This paper describes the application of the technique to the determination of cholesterol.

EXPERIMENTAL

Reagents

The reagents used were luminol and hemin (Tokyo Kasei), microperoxidase (M-6756; Sigma), 30% hydrogen peroxide solution (Santoku), horseradish peroxidase (HRP, E.C. 1.11.1.7; Toyobo), cholesterol standard solution (Precimat Cholesterol; Boehringer), cholesterol kit (Monotest Cholesterol; Boehringer), firefly luciferin (Sigma), cholesterol oxidase from *Streptomyces* (E.C. 1.1.3.6; Toyobo), cholesterol esterase from *Pseudomonas* (E.C. 3.1.1.13; Toyobo), standard human serum (Q-PAK-I, Q-PAK-II; Hyland), tetra(4-carboxyphenyl)porphine (TCPP; Tokyo Kasei) and tetraphenylporphine tetrasulfonate (TPPS; Tokyo Kasei). Tetra(4-*N*-methylpyridyl)porphine iron(III) (TMPyP–Fe) was a gift from Prof. M. Sato and Dr. A. Tohara (Teikyo University). All other reagents (analytical grade) were used as received.

Stock solutions of luminol, hemin and microperoxidase were prepared as described by Hayashi et al. [16, 17]. Stock solutions of HRP (200 μM) and luciferin (2 mM) were made in 10 mM phosphate buffer, pH 7.4, and stored at 4°C. Other enzyme solutions were prepared by dissolving 2 mg of cholesterol oxidase (17.5 U mg^{-1}) in 10 ml of 5 mM phosphate buffer in 0.1 M NaCl (PBS) at pH 7.0, and 2 mg of cholesterol esterase (100 U mg^{-1}) in 10 ml of 5 mM PBS at pH 7.0.

Methods

The computer system used was described previously in detail [17]. The pneumatically-driven automated injection device rapidly adds the reagents to the analyte solution in a cuvette. The light emitted is recorded by a transient memory with 12-bit resolution and 2-μs conversion time (TMR-120, Kawasaki Electronica), to which a personal computer (Sharp MZ-2000) is interfaced by a GP–IB unit. A mixing mode was chosen because of the superior reproducibility of the chemiluminescence measurements in this system. A round-bottomed glass test tube (8 mm i.d., 5 mm high) was used for the measurement; 300 μl of sample was placed in the test tube and 60 μl of the reagent (see below) injected [18]. The temperature was maintained at 23–25°C. The corrected data (total intensity minus blank for each of the 2048 sampling points) were manipulated by the Fourier-transform digital filter for smoothing the noisy data and for peak-height measurements.

The pH dependence of the luminol chemiluminescence was examined by rapidly injecting 60 μl of 0.9 μM hydrogen peroxide in degassed double-distilled water into 300 μl (sample solution) of 300 μM luminol and 2 μM catalyst (HRP, microperoxidase or water-soluble porphyrins) in 0.1M carbonate buffer, pH 8.8—12.3. For the study of luciferin dependence, the reagent compositions were the same as those for the pH dependence except that 13 μM luciferin was included in the sample solution. The light emission was monitored by the computer-controlled system. The HRP dependence was studied by injecting the solution as above into a sample solution of 100 μM luminol and 0.1—5 μM HRP in 0.1 M carbonate buffer, pH 10.5. The luminol dependence was also studied in this way; the sample solution was 5 μM HRP and 1—300 μM luminol in 0.1 M carbonate buffer, pH 10.5.

For the study of hydrogen peroxide dependence, the injection solution was 600 μM luminol and 30 μM HRP in 0.2 M carbonate buffer, pH 10.8; the sample solution was 2–810 nM hydrogen peroxide in 5 mM PBS, pH 7.0. The dependence on cholesterol oxidase was investigated by adding 200 μl of cholesterol standard solution, 1000-fold diluted with 5 mM PBS at pH 7.0, to 100 μl of 11.7–350 U l^{-1} cholesterol oxidase solution in the buffer, and incubating for various times at 37°C. The measurement was made by injection of 60 μl of a peroxidase mixture consisting of 600 μM luminol and 30 μM HRP in 0.2 M carbonate buffer, pH 10.8 (see Fig. 2). Dependence on cholesterol esterase concentration was studied similarly by adding the standard human serum (200 μl), 1000-fold diluted with 5 mM PBS at pH 7.0, to a solution (100 μl) of cholesterol esterase (100–3000 U l^{-1}) containing 117 U l^{-1} cholesterol oxidase, 9 mM sodium cholate and 0.51 mM Carbowax-6000 [19] and incubating at 37°C for various times for both hydrolysis and oxidation; the mixture was then injected.

For the determination of free cholesterol, a portion of cholesterol standard solution, diluted with 5 mM PBS at pH 7.0 (200 μl), was added to a cholesterol oxidase solution (117 U l^{-1}), incubated for 5 min at 37°C and measured by the injection of the chemiluminescent mixture.

RESULTS AND DISCUSSION

Figure 1 compares the luminol chemiluminescence when catalyzed by HRP (pH 10.5) and microperoxidase (pH 12.3). The latter has been reported by Schroeder and Yeager [20] to be superior for analytical purposes. Light production by HRP is much faster than by microperoxidase, the latter reaching a maximum ca. 4 s after hydrogen peroxide injection and decaying to the background level in 80 s. Microperoxidase has been shown to be an excellent catalyst for a flow system [12], but was not suitable for the rapid peak-height determination by the Fourier-transform digital filter, which requires a sharp peak [17]. Thus, HRP was used as a catalyst in all subsequent experiments.

The pH dependence of the emission rate and the peak height was examined

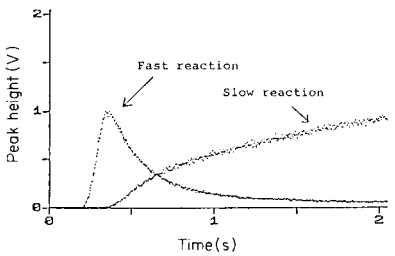

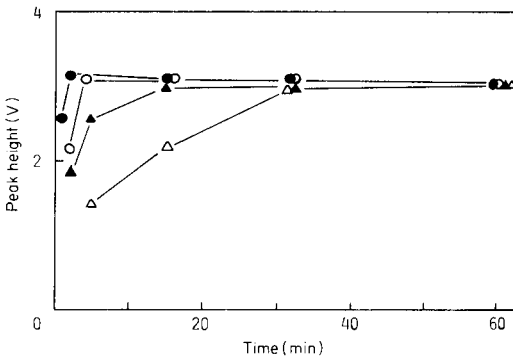

Fig. 1. Printer output data of chemiluminescence production catalyzed by HRP (fast reaction, pH 10.5) and microperoxidase (slow reaction, pH 12.3).

Fig. 2. Effect of cholesterol oxidase concentration: (•) 350; (○) 117; (▲) 35; (△) 11.7 U l^{-1}.

in the range 8.8—12.3. The rate referred to is the first-order decay portion following the peak [16, 17]. The rate in the presence of HRP was at least 100-fold greater than with microperoxidase, but the peak of the latter was at most only 50 times higher. The peak height of HRP-catalyzed chemiluminescence increased with increasing pH until it levelled off above pH 10.5. The effects of HRP and luminol concentrations were studied at pH 10.5; the peak height was approximately proportional to the HRP concentration over the range 10^{-7}—10^{-5} M and increased with increasing luminol concentration (10^{-6}—10^{-4} M). Because the more concentrated HRP solutions are viscous and therefore mixing with the hydrogen peroxide solution would be hampered, the reagent mixture finally adopted was 5 μM HRP and 100 μM luminol at pH 10.5. This allowed hydrogen peroxide to be determined in just 0.5 s by use of the digital filter.

The log—log calibration graph for hydrogen peroxide was linear over the range 0.8—100 pmol per tube with a slope of 1.30. The lowest determinable amount is comparable to that given by the method of Olsson [12]. This limit is defined here as the minimum analyte concentration at which the log—log calibration line remains linear. In the more concentrated hydrogen peroxide region where the cholesterol in serum was to be determined (see below), the relative standard deviation (RSD) of the peak-height data was satisfactory (<3%), but at the detection limit, the RSD was ca. 8%. The normal range of total cholesterol in sera from adults is 100—400 mg dl^{-1} [2], thus the results indicate that the present method can be applied to 0.2 μl of serum.

Hara et al. [21, 22] showed that some water-soluble synthetic porphyrins such as TCPP—Fe and TCPP—Pd could catalyze luminol chemiluminescence effectively, and applied them in a flow-cell system. The chemiluminescent activity was examined, therefore, for the similar catalysts, TCPP—Fe,

TPPS—Fe and TMPyP—Fe, synthesized by the methods of Harris and Toppen [23] and Adler et al. [24]. The total light emissions and the peak heights were comparable to the results obtained with microperoxidase except that TPPS—Fe showed very little emission. However, the emissions were too slow to be useful: for HRP, the emission rate constant was 0.88 s^{-1} (pH 12.3); for microperoxidase, 0.027 s^{-1}; for TCPP—Fe, 0.024 s^{-1}; for TMPyP—Fe, 0.034 s^{-1}; and for TPPS—Fe, 0.0027 s^{-1}. The enhancement of chemiluminescence by luciferin reported by Whitehead et al. [25] was also studied, but it had only a small effect on the emission when the catalysts described above were used: for HRP, the rate constant was slightly changed to 1.27 s^{-1} (pH 12.3); for microperoxidase, 0.037 s^{-1}; for TCPP—Fe, 0.020 s^{-1}; for TMPyP—Fe, 0.031 s^{-1}; and for TPPS—Fe, 0.0019 s^{-1}.

Sera were diluted 1000-fold for easy manipulation. The appropriate conditions for the enzyme reactions were studied. The optimal pH for cholesterol oxidase is 6.5—7.0 and for cholesterol esterase is 7.0—9.0, therefore, pH 7.0 was adopted for the enzyme reaction sequence. Figure 2 shows that the rate increases with the concentration of cholesterol oxidase and that the reaction is almost complete in 4 min at 117 U l^{-1}. The log—log calibration graph for free cholesterol was linear over the range 0.01—3 nmol per tube (slope = 1.25) when 117 U l^{-1} cholesterol oxidase was used with a 5-min incubation time. The optimal concentration of cholesterol esterase was found in the same way to be 3000 U l^{-1} and the incubation time 15 min. However, a single incubation period was adopted for both hydrolysis and oxidation. Triton X-100 [26] had no effect on the reaction rate, but 9 mM sodium cholate enhanced the rate effectively. The enzyme mixture chosen consisted of 117 U l^{-1} cholesterol oxidase, 3000 U l^{-1} cholesterol esterase, 9 mM sodium cholate and 0.51 mM Carbowax-6000 in 5 mM PBS, pH 7.0; the incubation time was 15 min at 37°C.

A correlation study was made with a commercially available kit, Monotest Cholesterol (enzymatic and spectrophotometric), for 20 serum samples ranging from 100 to 350 mg dl^{-1} total cholesterol; the correlation coefficient was 0.932 (slope = 0.83). Within-run and between-run reproducibilities were satisfactory, the RSD being 2.41 and 2.24%, respectively. Seitz [27] stated that uric acid may consume hydrogen peroxide and that it may be necessary to separate uric acid by precipitation with zinc hydroxide/barium sulfate before the chemiluminescent reaction. Bostick and Hercules [28] and Malavolti et al. [2] have discussed this subject. The need for elimination of uric acid must be considered, but the present serum dilution method did not seem to be greatly affected by the presence of uric acid in serum. The commercial kit needs 20 μl of blood serum, whereas the present method requires only 0.2 μl. The results suggest that 1 μl of serum can suffice for several assays based on hydrogen peroxide-producing enzymes for substrates such as glucose [28], creatine [29] and uric acid [30]. The present method should be especially effective for clinical tests on newborn children.

We thank Prof. M. Sato and Dr. A. Tohara (Teikyo University) for their kind gift of TMPyP—Fe. We also thank Dr. M. Uchiyama and Dr. T. Shibazaki for their useful suggestions.

REFERENCES

1 B. Zak, Clin. Chem., 23 (1977) 1201.
2 N. L. Malavolti, D. Pilosof and T. A. Nieman, Anal. Chim. Acta, 170 (1985) 199.
3 M. Masoom and A. Townshend, Anal. Chim. Acta, 174 (1985) 293.
4 T. Yao, M. Sato, Y. Kobayashi and T. Wasa, Anal. Biochem., 149 (1985) 387.
5 R. Deeg and J. Ziegenhorn, Clin. Chem., 29 (1983) 1798.
6 C. Matsubara, K. Kudo, T. Kawashita and K. Takamura, Anal. Chem., 57 (1985) 1107.
7 H. Hwang and P. K. Dasgupta, Anal. Chim. Acta, 170 (1985) 347.
8 A. L. Lazrus, G. L. Kok, S. N. Gitlin, J. A. Lind and S. E. McLaren, Anal. Chem., 57 (1985) 917.
9 N. L. Malavolti, D. Pilosof and T. A. Nieman, Anal. Chem., 56 (1984) 2191.
10 D. Pilosof and T. A. Nieman, Anal. Chem., 54 (1982) 1698.
11 P. van Zoonen, D. A. Kamminga, C. Gooijer, N. H. Velthorst and R. W. Frei, Anal. Chim. Acta, 167 (1985) 249.
12 B. Olsson, Anal. Chim. Acta, 136 (1982) 113.
13 L. J. Kricka and H. G. Thorpe, Analyst, 108 (1983) 1274.
14 W. R. Seitz, CRC Crit. Rev. Anal. Chem., 13 (1981) 1.
15 F. R. Leach, J. Appl. Biochem., 3 (1981) 473.
16 Y. Hayashi and H. Yuki, Chem. Pharm. Bull., 32 (1984) 3079.
17 Y. Hayashi, M. Ikeda and H. Yuki, Anal. Chim. Acta, 167 (1985) 81.
18 A. Taniguchi, Y. Hayashi and H. Yuki, Chem. Pharm. Bull., 34 (1986) 3475.
19 C. C. Allain, L. S. Poon, C. S. G. Chan, W. Richmond and P. C. Fu, Clin. Chem., 20 (1974) 470.
20 H. R. Schroeder and F. M. Yeager, Anal. Chem., 50 (1978) 1114.
21 T. Hara, M. Toriyama, H. Miyoshi and S. Syogase, Bull. Chem. Soc. Jpn., 57 (1984) 3009.
22 T. Hara, M. Toriyama and K. Tsukagoshi, Bull. Chem. Soc. Jpn., 57 (1984) 587.
23 F. L. Harris and D. L. Toppen, Inorg. Chem., 17 (1978) 71.
24 A. D. Adler, F. R. Longo, F. Kampas and J. B. Kim, J. Inorg. Nucl. Chem., 32 (1970) 2443.
25 T. P. Whitehead, G. H. Thorpe, T. J. N. Carter, C. Groucutt and L. J. Kricka, Nature, 305 (1983) 158.
26 P. N. Tarbutton and C. R. Gunter, Clin. Chem., 20 (1974) 724.
27 W. R. Seitz, Methods Enzymol., 57 (1978) 445.
28 D. T. Bostick and D. M. Hercules, Anal. Chem., 47 (1975) 447.
29 P. Fossatil, L. Precipe and G. Berti, Clin. Chem., 29 (1983) 1494.
30 J. D. Artiss and W. M. Entwistle, Clin. Chim. Acta, 116 (1981) 301.

Analytica Chimica Acta, 188 (1986) 101—109
Elsevier Science Publishers B.V., Amsterdam — Printed in The Netherlands

FLUORESCENCE STUDIES OF THE KINETICS OF BINDING AND REMOVAL OF METAL IONS IN PROTEINS

JOSEPH J. PESEK* and GWEN L. ROSSER
Department of Chemistry, San Jose State University, San Jose, CA 95192-0101 (U.S.A.)
ROBERT J. DOWE and JOHN F. SCHNEIDER
Department of Chemistry, Northern Illinois University, Dekalb, IL 60115 (U.S.A.)
(Received 8th April 1986)

SUMMARY

Fluorescence-quenching studies involving native protein fluorescence are used to monitor the rates of binding and removal of Hg(II), Cu(II), Ag(I), methylmercury(I), and *p*-chloro-mercuribenzoate in various protein systems (ovalbumin, bovine serum albumin, myoglobin, lysozyme, and insulin). In some cases, the fluorescence quenching as a function of time can be used to evaluate the rate constants for the binding of a particular metal ion to a protein. In many cases, multiple binding sites with different rate constants can be differentiated. The restoration of fluorescence vs. time on addition of various chelating agents (BAL, EDTA, cysteine and penicillamine) to the metal/protein system can be used to monitor metal ion removal. Multiple binding sites also can be differentiated kinetically in the removal experiments. In some cases, the appearance of multiple steps in the binding or removal or a metal or ion could be explained by small conformational changes. The rates of removal can help in estimating the effectiveness of various reagents as models for drugs in the treatment of heavy-metal poisoning.

Although the symptoms and physiological effects of many forms of acute metal poisoning are known [1, 2], much remains to be learned about the biochemical mechanisms. One significant mechanism may be the binding and consequent inactivation of enzyme sulfhydryl groups [3]. In general, it has been proposed [4] that metals can affect body functions through the inhibition of critical enzymes, the disruption of protein synthesis by binding with RNA, and the disruption of other syntheses by metal ion antagonism. Treatments for heavy-metal poisoning are not adequate because they are not specific and are sufficiently dangerous that they are used only in acute cases. The commonest drugs now in use are disodium calcium (ethylenedinitrilo)-tetraacetate (CaEDTA) and 2,3-dimercapto-1-propanol (BAL) [5]. The first, CaEDTA, is very inselective and chelates most di- and tri-valent metals. Important trace metals are removed along with the poisonous metal which could disrupt other processes if the treatments were not halted periodically. The other, BAL, itself causes very serious side-effects and the mercury/BAL complex is even more toxic than mercury alone.

There is a great need for drugs which are more selective, free from harmful

0003-2670/86/$03.50

side-effects, and applicable to use in treatment of chronic heavy-metal poisoning. Current methods of testing potential drugs involve in vivo experiments. While these tests are useful in clinical evaluations, they provide little information on the mechanism of removal and have produced conflicting results such as the reports [6, 7] regarding the effectiveness of CaEDTA in removing mercury. Well-controlled in vitro experiments could be the answer to rapid evaluation of the effectiveness of chelating agents and resolution of the removal mechanism. By studying rates of removal from metal/protein complexes, it may be possible to determine the best attacking groups and the proper stereochemical relationships in the chelating agent.

An early study [8] showed that halide-ion nuclear magnetic resonance spectroscopy (n.m.r.) can be useful in evaluating the binding and removal of metal ions from proteins. A more recent study [9] has shown that a combination of halide-ion n.m.r. and fluorescence spectrometry provides even more detail about the metal/protein complex. Early attempts [10] to study the removal of metal ions from proteins by chelating agents utilizing halide-ion n.m.r. proved difficult and required the use of stopped-flow techniques. In many cases, the rates for the removal of metal ions from proteins by chelating agents are too fast to be monitored even with stopped-flow mixing. The concentrations required in the n.m.r. method generally lead to half-lives of less than 1 s, the lower limit of measurement by this technique. Because these are second-order reactions, a technique which allows measurement at lower concentrations should yield half-lives which can be more easily measured. It has been shown [9] that fluorescence spectrometry utilizing native protein fluorescence has a limit of detection for metal/protein complexes of about 10^{-7} M, a factor of 10^2 or 10^3 lower in concentration than can be achieved with halide-ion n.m.r. Therefore, fluorescence spectrometry could be a useful technique for measuring the rates of removal of metal ions from proteins by various chelating agents. Such a method could be used to evaluate the structural effects of various chelating agents and aid in the design of more efficient and selective drugs as well as provide a means of in vitro screening of these new drugs.

EXPERIMENTAL

Materials and apparatus

Bovine serum albumin (BSA), fraction V, was obtained from General Biochemical. Ovalbumin (Grade V), lysozyme (Grade I), insulin, and myoglobin (type I) were all obtained from Sigma Chemical Co. Protein concentrations were quantified spectrophotometrically and all solutions were buffered (0.01 M) to maintain constant pH. Metal ion solutions were prepared from reagent-grade nitrate or chloride salts. Sodium *p*-chloromercuribenzoate (PMB) was obtained from Aldrich. The chelating agents were obtained from the following sources: EDTA (Baker), BAL (Aldrich), L-cysteine (Nutritional Biochemical Corp.) and D,L-pencillamine (Aldrich).

Relative fluorescence intensities and spectra were measured with either an

Aminco-Bowman spectrofluorimeter equipped with a ratio photometer attachment or a Baird Atomic SF-5 spectrofluorimeter. The excitation wavelength was 280 nm and the emission was monitored at 355 nm. The excitation and emission slit widths were 1 mm and 2 mm, respectively. A Corning Model 7 pH meter equipped with either a Fisher combination electrode or combination microelectrode was used for pH measurements.

Procedures

Fluorescence was measured for 5 μM protein solutions. The amount of quenching was measured by adding varying amounts of metal ion with a Gilmont microburet such that the volume increase was small. Kinetic measurements were made by adding chelating agents to the metal/protein solution with a Gilmont microburet so that the total volume increase was less than 5%. The solutions were thoroughly mixed, placed in a cuvette, and the fluorescence intensities vs. time were recorded. It is assumed that the metal ion, when complexed with a ligand, causes no quenching of the native protein fluorescence.

RESULTS AND DISCUSSION

The binding and removal of metal ions from metal/protein complexes can be quantified by observing the decrease or increase, respectively, in the relative fluorescence. In all cases, when the rate can be measured, a second-order rate for removal is defined [11] by

$$[1/(a-b)] \ln [b(a-x)/a(b-x)] = k_2 t \tag{1}$$

where a is the initial concentration of chelating agent, b is the initial concentration of metal/protein complex, and x is the concentration of uncomplexed protein. A similar equation can be written for the binding reaction. If a ratio of metal-to-protein greater than 1:1 is used, then the relative amount of quenching caused by each equivalent of metal ion must be evaluated.

The concentration of the uncomplexed protein is proportional to the increase in the relative fluorescence and can be calculated as:

$$[P]_u = (RF) \times [P]_c/(RF)_{tot} \tag{2}$$

where $(RF)_{tot}$ is the total decrease in the relative fluorescence after addition of metal ion; (RF) is the increase in relative fluorescence after addition of chelating agent; $[P]_c$ is the initial concentration of metal/protein complex; and $[P]_u$ is the concentration of protein from which metal ions have been removed. In the case for which the initial concentrations of both metal/protein complex and chelating agent are equal, the second-order rate equation simplifies to

$$(1/[P]_c) - (1/[P]_u) = k_2 t \tag{3}$$

or

$$(1/F) - (1/F^0) = k_2 t \tag{4}$$

where F^0 is the initial value of the fluorescence and F the relative fluorescence after addition of the chelating agent. The rate of binding of metals to proteins can be evaluated by using Eqn. 4 where the decrease in relative fluorescence is proportional to the formation of the metal/protein complex.

Figure 1 shows the experimental results of relative fluorescence vs. time for the reaction of ovalbumin with mercury(II), (PMB), and methylmercury. The binding reactions follow the expected second-order kinetics described by Eqn. 1. Kinetic results for the binding of two equivalents of mercury(II) are summarized in Table 1. The slow rate of binding correlates with the results obtained in the ^{35}Cl-n.m.r. line-broadening experiments [9]. The absence of broadening indicates that the potential binding sites are relatively inaccessible. The 2:1 ratio of metal to protein was chosen because ovalbumin has at least two free sulfhydryl groups and exhibits significant quenching. The mole—ratio studies [9] for mercury(II), PMB, and methylmercury indicate that each equivalent contributes approximately 50% to the total quenching.

The present study indicates that the binding of Hg(II) to ovalbumin involves three steps. The first step results in a 50% decrease of the total fluorescence quenching upon the addition of Hg(II). The initial rapid reaction probably corresponds to the binding of Hg(II) to a free sulfhydryl group in ovalbumin. The subsequent steps, each accounting for 25% of the total quenching, could be due to the binding of a second equivalent to another sulfhydryl group but would not explain why the third step is faster than the second. The last two steps could be interpreted as a process in which a P—S—Hg(II) group comes in closer proximity with one or more tryptophan residues, or the binding of P—S—Hg(II) to the nitrogen of the indole ring of

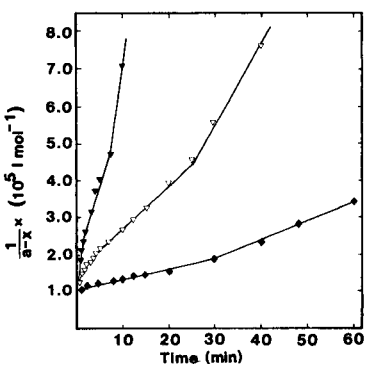

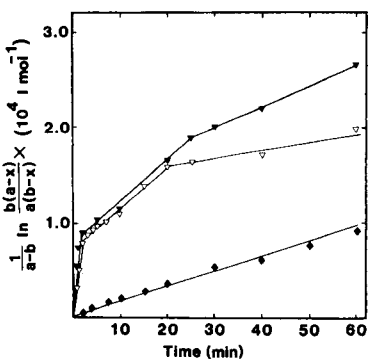

Fig. 1. Kinetic plots for reaction of ovalbumin with: (▽) Hg(II); (▼) methylmercury; (♦) PMB. a is the initial concentration of ovalbumin and x the concentration at time t. Protein concentration, 5 μM.

Fig. 2. Kinetic plots for reaction of BAL with: (▽) 2:1 Hg(II)/ovalbumin; (▼) 2:1 methylmercury/ovalbumin; (♦) 2:1 PMB/ovalbumin. a is the initial concentration of the 2:1 ovalbumin complex, b the initial concentration of BAL, and x the concentration at time t. Protein concentration, 5 μM.

TABLE 1

Rate constants (l mol^{-1} s^{-1}) for binding of metal and other ions (M) in ovalbumin and their removal with ligand L

M[a]	Binding[b]			L	Removal[b]		
	k_1	k_2	k_3		k_1	k_2	k_3
Hg(II)	603 ± 47	195 ± 5	378 ± 10	BAL	65.3 ± 7.5	6.9 ± 0.9	1.7 ± 0.3
PMB(I)	86 ± 3	195 ± 21		BAL	2.77 ± 0.33	2.47 ± 0.73	
				Pen[c]	0.56 ± 0.08		
MeHg(I)	4100 ± 200	1360 ± 120	2350 ± 690	BAL	119 ± 37	7.3 ± 2.2	3.50 ± 0.90
				EDTA	144 ± 17	6.23 ± 0.52	
				Cys[d]	119 ± 23	16.8 ± 4.0	
				Pen	48.7 ± 4.0	22.7 ± 3.5	
Ag(I)	83000	11100 ± 2900		BAL	185 ± 28	380 ± 40	711 ± 100
				Cys	1060 ± 100	480 ± 110	840 ± 110
				Pen	570 ± 90		

[a]2:1 M/protein ratio in all cases; protein concentration, 5 μM. [b]Errors are ±1 standard deviation. [c]Penicillamine. [d]Cysteine.

tryptophan. This would involve a conformational change. If such a process does occur, the conformational change must be small and must not significantly alter the secondary structure because no effect is observed in the optical rotatory dispersion (ORD) spectrum of ovalbumin on the addition of up to ten equivalents of mercury. Another possible explanation would be that the binding of the second equivalent of mercury involves two different sites on the protein.

A similar phenomenon has been reported by Boyer [12] for the reaction of PMB with ovalbumin under certain conditions. An increased reaction rate was observed after one-third of the sulfhydryl groups had reacted. It was suggested that the formation of the first mercaptide initiated a conformational change which facilitated the reaction of the other sulfhydryl groups [13].

The kinetics of fluorescence quenching by methylmercury are very similar to that of Hg(II) and are summarized in Table 1. However, the binding of PMB occurs in only two steps as shown in the table. Chen [14] obtained difference spectra with PMB which showed no perturbation of the tryptophan absorption. Thus the two-step process could be the binding of PMB ions to two accessible sulfhydryl groups with steric factors prohibiting further interactions with tryptophan.

There are other possible interactions between mercury(II) ion or methylmercury with thiol groups of proteins which might contribute to a multistep binding process. Hughes [15] observed the formation of dimers, $(PS)_2$—Hg(II), when mercaptoalbumin reacted with mercury(II) chloride. Mercury(II) could react with two sulfhydryl groups on the same protein depending on the spatial arrangement of the thiols. For organomercurials, intramolecular transfer, transmercaptidation, from one sulfhydryl group to another has been reported [16, 17].

Figure 2 shows the experimental results of relative fluorescence vs. time

for the reaction of metal/ovalbumin complexes with BAL. The removal reactions also follow the second-order kinetics described by Eqn. 1. The increase in fluorescence for the 2:1 Hg(II)/ovalbumin complex upon addition of BAL occurred in three successively slower steps until 100% of the fluorescence was restored. The results are given in Table 1. These results could be explained by either an initial breaking of a P—S—Hg(II)—tryptophan bridge and subsequent removal of two equivalents of Hg(II) or possibly removal of one equivalent of Hg(II) rapidly followed by removal of the second equivalent in two steps from two different binding sites.

As shown in Table 1, the destruction of the 1:2 ovalbumin/methylmercury complex by BAL occurs in three distinct steps for the complete restoration of fluorescence. The addition of large excesses of EDTA, cysteine, or penicillamine produces only a 50% return of the relative fluorescence and occurs in two steps. This can be interpreted as either the removal of one equivalent of methylmercury from two different sites or the disruption of the interaction between the bound metal and nearby tryptophans and the removal of one equivalent of metal from one site.

The results for the 2:1 PMB/ovalbumin system are also shown in Table 1. Of the chelating reagents tested, BAL is effective in removing PMB from the complex, and penicillamine is partly effective. As in the binding of two equivalents, a two-step process with differing rates is observed.

Silver(I) also produces significant quenching in ovalbumin and binding of two equivalents occurs in two steps. The rate constants are given in Table 1. In the binding process, the addition of the first equivalent accounts for approximately 60% of the quenching while the second equivalent accounts for about 40% of the fluorescence decrease. Table 1 also shows the results of various chelation studies. When a 1:1 ligand/silver ratio is used, BAL and cysteine are completely effective, EDTA is ineffective, and penicillamine is about 40% effective. Therefore, penicillamine probably removes the weaker of the two silver ions held in the complex. The removal by BAL and cysteine involves three steps; this is identical to the behavior of the mercury(II) complex. When a ten-fold excess of the chelating agents is added, EDTA removes one equivalent of silver(I) while BAL, cysteine, and penicillamine remove two equivalents. It is interesting to note that when an excess of chelating agent is used, the removal of two equivalents occurs in only two steps. The first step probably involves the removal of the less strongly bound Ag(I) and reduces the interaction with nearby tryptophan. This would explain the restoration of 70% of the relative fluorescence. The more strongly bound silver is removed in a second step that accounts for the restoration of the remaining 30% of fluorescence. Rogers [18] suggested that the quenching by silver was a result of conformational changes. In another study by Chen [19], ovalbumin showed less quenching upon addition of Ag(I) in 8 M urea solution than did the native protein. Therefore, conformational changes which result in the tryptophans being further removed from the binding sites decrease the fluorescence quenching of the metal.

In addition to ovalbumin, the kinetics of binding and removal of various metal ions in several other common proteins were studied. Table 2 summarizes some of these results. The binding of four equivalents of Hg(II) to lysozyme occurs in two relatively fast steps as does the removal by EDTA and cysteine while removal by penicillamine occurs in three steps. This appears to be an unusual case because in all other proteins, pencillamine behaved like cysteine. It should be noted that the rate of removal in the first two steps is slower for pencillamine than EDTA. This also is unusual because in all other examples, pencillamine was always faster than EDTA. This may be due to a steric effect of the two methyl groups and the fact that formation of a 2:1 complex is necessary for removal. The rate for the removal of Hg(II) by BAL is too fast to measure without use of rapid mixing techniques. The results for the Hg(II)/bovine serum albumin system are very similar to those of Hg(II)/lysozyme except that removal by all chelating agents with measurable rates occurs in three steps. These results confirm the relative rates measured by ^{35}Cl-n.m.r. [10] which showed that BAL > cysteine > pencillamine > EDTA. The observation that the same three steps occur for the formation of both 2:1 and 1:1 complexes supports the mechanism proposed in this earlier study that the removal occurs after formation of a ternary metal/protein/ligand species with subsequent formation away from the protein of the 2:1 species for certain ligands.

Titration of a 10^{-5} M solution of myoglobin with Hg(II) indicates the formation of a 3:1 or 4:1 complex. Table 3 shows the results of rate constant determinations at various metal/protein ratios. When the ratio is 3:1 or greater, three separate rates are observed. The values for each of the individual steps remain constant within experimental error for all ratios except

TABLE 2

Rate constants (l mol^{-1} s^{-1}) for binding of metal ions in various proteins and their removal with ligand L[a]

Complex	Binding		L	Removal		
	k_1	k_2		k_1	k_2	k_3
Hg(II)/lysozyme[b]	9500 ± 500	1900 ± 200	EDTA	1500 ± 200	330 ± 30	—
			Cys	2500 ± 500	440 ± 20	
			Pen	1400 ± 200	210 ± 40	93 ± 5
Hg(II)/BSA[b]	6500 ± 700	2700 ± 600	EDTA	420 ± 10	170 ± 60	85 ± 7
			Cys	2800 ± 200	1400 ± 200	400 ± 50
			Pen	1000 ± 100	110 ± 10	65 ± 4
Cu(II)/BSA[b]	—	—	EDTA	1600 ± 300	210 ± 20	—
Cu(II)/insulin[c]	—	—	EDTA	270 ± 30	—	—
			Cys	250 ± 40	—	—
			BAL	900 ± 50	—	—

[a]In all cases, the protein concentration was 5 μM. Errors are ± standard deviation. [b]4:1 complex. [c]2:1 complex.

TABLE 3

Rate constant (l mol^{-1} s^{-1}) for myoglobin/mercury complex[a]

Hg(II)/myoglobin ratio	k_1	k_2	k_3
3	1.83 ± 0.41	0.42 ± 0.06	0.014 ± 0.004
4	2.35 ± 0.52	0.36 ± 0.05	0.067 ± 0.020
5	2.51 ± 0.53	0.45 ± 0.06	0.080 ± 0.023
6	2.63 ± 0.58	0.46 ± 0.06	0.072 ± 0.022
7	2.22 ± 0.43	0.41 ± 0.05	0.089 ± 0.024
8	2.43 ± 0.47	0.34 ± 0.05	0.059 ± 0.020
9	2.18 ± 0.42	0.48 ± 0.06	0.079 ± 0.023
15	2.00 ± 0.41	0.33 ± 0.05	0.058 ± 0.020

[a]Errors are ±1 standard deviation. Myoglobin concentration was 5 μM in all cases.

3:1. At this ratio, the rate constant for the slowest step is considerably less than the values found at higher ratios. This could be accounted for by the binding of four equivalents of mercury(II) per myoglobin with the last two metal ions being bound at slightly different rates.

In addition to Hg(II) and Ag(I), copper(II) is also a very effective quencher of protein fluorescence. Binding of Cu(II) to BSA as well as removal was too fast to measure in all cases except EDTA. The removal of the metal ion from the 1:4 BSA/Cu(II) complex occurred in two steps with each step accounting for the restoration of 50% of the quenched fluorescence. Binding of Cu(II) to insulin was also too fast to measure. However, removal by EDTA, cysteine, and BAL occurred in a single step. These results are summarized in Table 2.

In conclusion, fluorescence spectrometry appears to be a useful method for monitoring the kinetics of the binding and removal of metal ions in protein systems. In many cases, even when the kinetics of binding are too fast to measure, the removal of the metal ion by chelating agents can be monitored.

REFERENCES

1 D. H. K. Lee (Ed.), Metallic Contaminants and Human Health, Academic Press, New York, 1972.
2 B. L. Vallee and D. D. Ulmer, Ann. Rev. Biochem., 41 (1972) 91.
3 A. Shulman and F. P. Dwyer, in F. P. Dwyer and D. P. Mellor (Eds.), Chelating agents and Metal Chelates, Academic Press, New York, 1964. Ch. 9.
4 D. D. Ulmer and B. L. Vallee, Second Annual Conference on Trace Substances in Environmental Health, Columbia, MO, 1968.
5 A. Soffer and M. Chenoueth, Chelation Therapy, C. C. Thomas, Springfield, IL, 1964, Chap. 2.
6 J. Glomme and K. H. Gustafson, Acta Med. Scand., 164 (1959) 175.
7 S. Bionde and A. Guarino, Folia Med. (Naples), 39 (1956) 1065.
8 J. L. Sudmeier and J. J. Pesek, Anal. Biochem., 41 (1971) 39.
9 J. J. Pesek, R. L. Dowe and J. F. Schneider, Anal. Chim. Acta, 170 (1985) 187.
10 J. L. Sudmeier and J. J. Pesek, Inorg. Chem., 10 (1971) 860.
11 G. W. Castellan, Physical Chemistry, Addison-Wesley, Reading, MA, 1971, p. 737.

12 P. D. Boyer, J. Am. Chem. Soc., 76 (1954) 4331.
13 N. B. Madsen, Metabolic Inhibitions, 2 (1963) 119.
14 R. F. Chen, Arch. Biochem. Biophys., 142 (1971) 552.
15 W. L. Hughes, Cold Springs Harbor Symp. Quant. Biol., 17 (1950) 79.
16 G. Szabolski, E. Biszku and M. Stojgo, Acta Physiol. Acad. Sci. Hung., 17 (1960) 183.
17 G. D. Smith and H. K. Schochman, Biochemistry, 10 (1971) 4576.
18 K. S. Rogers, Enzymolygia, 36 (1969) 153; 37 (1969) 174.
19 R. F. Chen, Arch. Biochem. Biophys., 158 (1973) 605.

Analytica Chimica Acta, 188 (1986) 111—118
Elsevier Science Publishers B.V., Amsterdam — Printed in The Netherlands

DETERMINATION OF TOTAL TIN IN GEOLOGICAL MATERIALS BY ELECTROTHERMAL ATOMIC ABSORPTION SPECTROMETRY

ERIK LUNDBERG* and BJÖRN BERGMARK
Department of Analytical Chemistry, University of Umeå, S-901 87 Umeå (Sweden)
(Received 26th March 1986)

SUMMARY

A graphite-furnace atomic-absorption spectrometric method is described for the determination of total tin in geological materials. Samples are decomposed by fusion with lithium metaborate and the melt is dissolved in diluted (1 + 9) nitric acid. Spectral and non-spectral interferences are minimized by a combination of platform volatilization, "normal" heating rate, addition of ammonia as chemical modifier, use of integrated absorbance values and Zeeman background correction. Results are reported for six reference materials showing good accuracy and a precision of 12% at the 3 $\mu g\ g^{-1}$ level. The detection limit for tin in the original materials is 0.7 $\mu g\ g^{-1}$.

Traces of tin are commonly found in many silicate rocks, soils and sediments, partly as a constituent of the silicate lattice [1—3], and partly in the form of cassiterite, tin(IV) oxide [1, 2]. Knowledge of the relative distribution of tin in these two forms is important in studies related to the geochemistry of tin, and in geochemical prospecting [1, 3, 4].

Whereas cassiterite in geological samples can be converted into tin(IV) iodide and separated by volatilization from the bulk of interfering elements by heating with ammonium iodide [2, 5—7], total tin can only be released by fusion with an alkaline flux such as lithium metaborate [8—10]. Methods that have been used for determining tin in geological materials include spectrophotometry [2], flame atomic absorption spectrometry (a.a.s.) [4], polarography [11], X-ray fluorescence spectrometry [12] and neutron activation analysis [13]. Considering tin concentrations of 1—10 $\mu g\ g^{-1}$, all of these methods, with the possible exception of neutron activation, are subject to considerable error because they are insufficiently sensitive or selective. However, low levels of tin can be determined by a.a.s., as the hydride [7—10], through aspiration of an organic tin extract into a flame [5] or by dispensing the extract into a graphite furnace [14], or by inductively-coupled plasma atomic emission spectrometry following hydride generation [6]. Most of these methods, including hydride-generation a.a.s. [8, 10], require a multistage process to complete the analysis with minimal interference effects. Hence, there is a need for a reasonably simple and rapid method for determining low levels of tin in geological samples. The difference between

0003-2670/86/$03.50

the total tin determined by fusion with lithium metaborate and the cassiterite tin would give an estimate of the tin held in the lattice of silicates.

This paper describes a method involving fusion of the sample with lithium metaborate to release the total tin, dissolution of the melt in nitric acid and subsequent, direct determination of tin by graphite-furnace a.a.s. Optimization of the analytical parameters to minimize interference effects are discussed, and six geological reference materials are used to demonstrate the accuracy and precision attainable with the method.

EXPERIMENTAL

Instrumentation and reagents

All experiments were done with a Perkin-Elmer Zeeman-3030 atomic absorption spectrometer, equipped with an HGA-600 graphite furnace, an AS-60 autosampler and a PR-100 printer. The instrumental parameters are summarized in Table 1.

A 1000 μg ml^{-1} stock solution of tin was prepared by dissolving 0.1000 g of tin (99.9%; AnalaR, BDH) in 10 ml of concentrated hydrochloric acid and 1 ml of 90% formic acid (gentle heating), followed by dilution to 100 ml with distilled water. Standard solutions were prepared by dilution with (1 + 9) nitric acid, and were stored in acid-washed polyethylene bottles. Lithium metaborate (purum; Merck) was purified before use as described by Suhr and Ingamells [15].

The chemical modifier, ammonia solution, was prepared by (1 + 4) dilu-

TABLE 1

Instrumental parameters

Stage	Temp. (°C)	Ramp (s)	Hold (s)	Gas flow (ml min^{-1})
1	160	20	20	300
2	200	10	10	300
3	1000	30	20	300
4	300	1	15	300
5	2500	1[a]	5	0
6	2650	1	3	300
Wavelength (nm)		286.3[b]		
Spectral bandwidth (nm)		0.7		
Lamp source (power)		EDL (12.5 W)[c]		
Sample volume (μl)		20		
Modifier volume (μl)		20		
Integration time (s)		4.5—5.0		

[a]Ramp = 0 for experiments with maximum heating rate; absorbance readings are taken at this stage. [b]This line is about 20% more sensitive than the 224.6-nm line in Zeeman a.a.s. [c]A Varian power supply was used for the Perkin-Elmer electrodeless discharge lamp (EDL).

tion of ammonia liquor (p.a., Merck). The diammonium hydrogenphosphate magnesium nitrate modifier (referred to as the $(NH_4)_2HPO_4$ modifier) was prepared by dissolving 1.0 g of $(NH_4)_2$ HPO_4 (p.a. Baker) and 0.10 g magnesium nitrate (p.a., Merck) in 100 ml of 0.05 M nitric acid. The ascorbic acid/iron modifier (referred to as the ascorbic acid modifier) was prepared by dissolving 5 g of ascorbic acid (p.a., Merck) and 0.02 g of iron(III) nitrate nonahydrate (p.a., Merck) in 100 ml of 0.05 M nitric acid. All other chemicals used were of analytical-reagent grade, and the argon was SR-grade.

Materials

Reference materials MRG-1 (gabbro), SY-2 and SY-3 (syenite), and SO-4 (chernozemic A horizon soil) were obtained from CANMET (Canada Center for Mineral and Energy Technology) and materials AN-G (anorthosite) and BE-N (basalt) from CRPG (Centre de Recherches Pétrographiques et Géochimiques, France).

Pyrolytically-coated graphite tubes with pyrolytic graphite platforms were used in the Perkin-Elmer HGA-600. Preliminary experiments were done with home-made, tungsten-impregnated [16], standard graphite platforms, which had performance characteristics similar to those of pyrolytic graphite platforms. Before use, pyrolytically-coated tubes were conditioned by heating four times to 2650°C with a ramp time of 60 s and a hold time of 0 s, followed by twice heating to 2650°C with a ramp time of 1 s and a hold time of 5 s.

Procedure

The sample (0.250 g) was carefully mixed with 0.250 g of lithium metaborate in an agate mortar and transferred to a 15-ml platinum crucible. The mixture was fused in a muffle furnace (type 1300, Thermolyne Corp.) at 950°C for 15 min. After cooling, the bead formed was transferred to a 100-ml teflon vessel equipped with a magnetic stirring bar, and 30.0 g of (1 + 9) nitric acid was added. The vessel was heated to 50°C on a hot-plate (fitted with a magnetic stirrer motor) for 20—30 min to dissolve the bead completely. The clear solution thus obtained was further diluted three times with diluted (1 + 19) nitric acid directly in an autosampler vial.

The tin content of the dissolved lithium metaborate blank as well as that in each of the dissolved reference materials was determined by means of the standard additions technique. The blank value was subtracted prior to calculation of the tin concentrations in the solid reference materials. All results given in Table 2 and in the figures are based on peak-area values and represent the means of at least three determinations.

RESULTS AND DISCUSSION

Sample decomposition

Fusion with lithium metaborate as a flux has been shown to decompose geological materials, bringing both lattice-bound and cassiterite tin into solu-

TABLE 2

Determination of tin in six geological reference materials

Reference material	Tin concentration ($\mu g\ g^{-1}$)	
	This work	Recommended or reported values
MRG-1	3.2 ± 0.42[a]	3.2B[b], 3.28[c]
SY-2	4.6 ± 0.87	4B[b], 4.80[c]
SY-3	5.5 ± 0.99	6?[b], 5.50[c]
SO-4	1.1 ± 0.28	1.13[c], 3[d]
BE-N	3.0 ± 0.34	1.9[e], 2.4[e]
AN-G	<0.7	0.26[e], 1.5[e], 8[e]

[a]Five independent dissolutions. The results of the other materials are based on 3—4 dissolutions. The precision is expressed as ±1 s.d. [b]See Abbey [22]; values are classified as "A", "B", or "?", where "A" means the greatest reliability. [c]See [23]. [d]See [24]. [e]See [25].

tion [8—10, 14]. Exceptions were found to be materials with a high sulphur content (>10%), which did not form a bead but rather a nonhomogeneous "gel" when fused with this flux. The flux/sample ratio used in the previous work referred to was 3:1. Because it was found here that lithium metaborate contributed to the non-specific absorbance signal during atomization, tests were made in which the fraction of lithium metaborate was decreased; it was found that ratios of 3:1 and 1:1 gave the same tin signal for the reference material MRG-1, whilst the non-specific signal was decreased by 40%. A ratio of 1:1 is thus sufficient for the graphite-furnace a.a.s. determinations.

Spectral interferences

Even though the geological samples were diluted about 360 times, many sample constituents were still present in sufficient concentrations to cause high background signals. The nature of the background seems to be complex; even the Zeeman background corrector could not compensate accurately for it. This can be seen in Fig. 1, where "normal" and maximum heating rates during atomization are compared with respect to spectral interferences. When the maximum heating rate was utilized for tin in SY-2 (Fig. 1b), the resulting background absorbance was as high as 0.84 and partly overlapped the tin signal, causing the latter to cross the baseline and continue below it. The resulting tin peak-height or peak-area signal will produce erroneous results, even if an "integration window" around the peak is set by means of the Zeeman 3030 software. However, by applying a lower heating rate (RAMP = 1), the tin and background peaks could be separated in time to a greater extent (Fig. 1a). Because the tin signal then returns properly to the baseline, correct peak-area values can be obtained by selecting an integration time of 5 s. It should be observed that the lower heating rate did not result in decreased sensitivity.

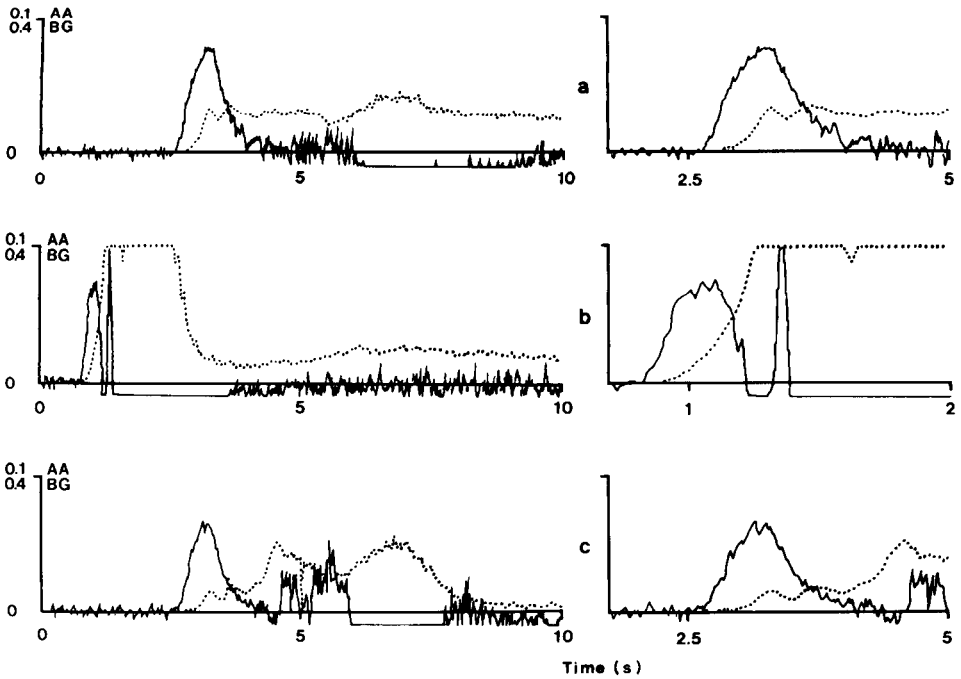

Fig. 1. Specific (AA; —) and non-specific (BG; · · ·) absorbance traces obtained for reference material SY-2 under different conditions: (a) normal heating rate (RAMP = 1) and gas stop; (b) maximum heating rate and gas stop; (c) normal heating rate and a 10 ml min^{-1} mini-flow during atomization. Scale expansion was done by means of the Z3030 software (right-hand traces).

The influence of a mini-flow of inert gas (10 ml min^{-1}) during atomization on the specific and non-specific signals is shown in Fig. 1(c). The tin signal decreases slightly whereas, unexpectedly, the non-specific signal increases. Fewer spectral interferences were thus obtained when gas stop was used during atomization.

Non-spectral interferences

It is well known that the determination of tin in many materials is difficult because of matrix interferences, especially by chloride and sulphate [17, 18]. In order to decrease these interferences, platform vaporization/atomization in combination with a chemical modifier was applied to the geological samples. Vaporization from a platform not only decreased spectral and non-spectral interferences but also increased the peak-area sensitivity for tin by 40%, which is in line with findings reported elsewhere [18, 19].

Several modifiers have been proposed for tin [18, 20, 21]. Figure 2 shows the specific and non-specific signals obtained for 1 ng of tin by using the modifiers ammonia, $(NH_4)_2HPO_4$ and ascorbic acid at optimum ashing temperatures. Ammonia has, by means of radioactive measurements, been shown

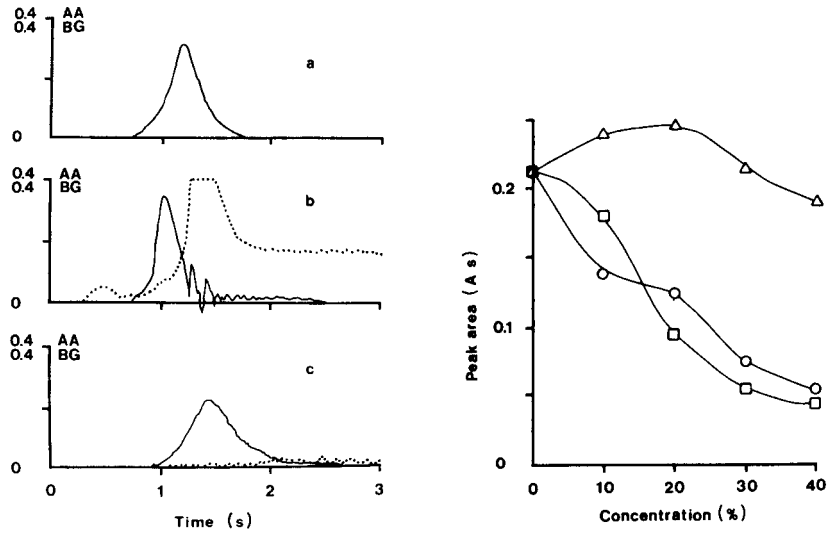

Fig. 2. Specific (AA; —) and non-specific (BG; · · ·) absorbance traces obtained for 1 ng of tin with different modifiers: (a) ammonia; (b) $(NH_4)_2HPO_4$; (c) ascorbic acid. Ashing temperatures were 1000, 1200 and 1300°C, respectively.

Fig. 3. Influence of different concentrations of elements on the integrated signal for 1 ng of tin: (△) aluminium; (○) silicon; (□) iron. Appropriate amounts of the interfering elements (e.g., 0, 25, 50, 75 and 100 mg of iron powder) were mixed with lithium metaborate and fused as described in the Experimental section. To the dissolved bead, tin was then added to give a final concentration of 50 ng g^{-1}.

to stabilize tin up to 800°C [18]. From ashing curves examined for all the modifiers, it was concluded that effective stabilization was also achieved with the $(NH_4)_2HPO_4$ modifier, whereas the tin peak-area signal was about 10% lower when the ascorbic acid modifier was used. The large non-specific signal introduced by the $(NH_4)_2HPO_4$ modifier (background absorbance = 0.74; area = 0.68) excluded its application as a modifier for tin. The performance of the modifiers ammonia and ascorbic acid, when the reference material MRG-1 was vaporized at optimized conditions, was investigated. The tin peak-area values obtained were very similar for the two modifiers, but the ascorbic acid modifier suffered from the serious disadvantage that a large carbon residue accumulated on the platform causing irreproducible results. Hence, ammonia was found to be the most suitable modifier for dissolved geological samples; it not only stabilizes tin, but also removes chloride as ammonium chloride during ashing, and leaves no residue on the platform.

Figure 3 shows interference effects on tin from three main constituents of geological materials, silicon, iron and aluminium. These interferences are probably the reason why the slopes of the standard addition curves, based on peak areas, differ for each of the six reference materials. As a consequence of the different slopes, quantitation against aqueous tin standards was impos-

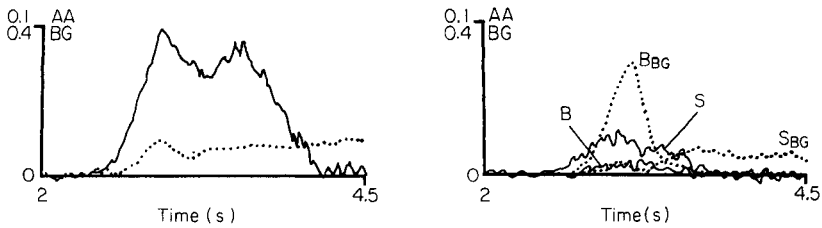

Fig. 4. Specific (AA; —) and non-specific (BG; · · ·) absorbance traces obtained for reference material SY-2 with 0.2 ng of tin added. Comparison with Fig. 1(a) shows that the addition contributes mainly to the second peak.

Fig. 5. Specific (AA; —) and non-specific (BG; · · ·) absorbance traces obtained for a lithium metaborate blank (B; area = 0.005 A s) and the reference material SO-4 (S; area = 0.020 A s).

sible. When the standard addition technique was used, it was observed that the signal traces obtained for the additions often consisted of two peaks (Fig. 4). Evaluation by means of peak-height values would thus give erroneous tin concentrations, and therefore all analytical results reported are based on peak-area values.

Application to geological samples

The values obtained for tin in some reference materials (five rocks and one soil) are compared with recommended or reported values in Table 2. Although the testing is by no means exhaustive, the data show that the method is capable of yielding accurate results. That the determination of tin is troublesome is reflected in the individual results obtained by different laboratories and techniques for the reference material SY-2, on which the derivation of the recommended value was based [22]; the data reported were 2.5, <10, 2, 5.5, 4.1, <4, <7, 3, 10, 5.7, 3.1 4 and 4.4 $\mu g\ g^{-1}$ tin [22]. For the proposed method, the relative standard deviation at the 3 $\mu g\ g^{-1}$ level was about 12% (Table 2), which can be regarded as acceptable, considering the low concentration and the interferences discussed above.

The detection limit, defined as the concentration in the diluted sample that corresponds to an integrated absorbance value twice that obtained for the lithium metaborate blank, is estimated to be 0.7 $\mu g\ g^{-1}$ tin in a geological material. To demonstrate the overall performance of the method close to the detection limit, Fig. 5 shows signal traces for a blank and the reference material SO-4, which has been found to have a tin concentration close to 0.7 $\mu g\ g^{-1}$.

The fairly rapid method described here for the determination of tin in geological materials should also be applicable to materials of diverse chemical composition such as sediments.

The authors are indebted to Dr. Bernhard Welz, Perkin-Elmer, FRG, for providing the Zeeman 3030 spectrometer, to Mr. Hans Östling, Perkin Elmer,

Sweden, for the loan of a tin electrodeless discharge lamp, and to Dr. Wolfgang Frech for fruitful discussions. They also thank Mrs. Karin Olsson for skillful technical assistance and Mr. Douglas Baxter for revising the manuscript. This work was supported by the Swedish Natural Science Research Council.

REFERENCES

1 L. H. Ahrens and W. R. Liebenberg, Am. Mineral., 35 (1970) 571.
2 J. Agterdenbos and J. Vlogtman, Talanta, 19 (1972) 1295.
3 A. M. R. Neiva, Min. Mag., 40 (1976) 453.
4 B. Moldan, I. Rubeška, M. Mikšovský and M. Huka, Anal. Chim. Acta, 52 (1970) 91.
5 E. P. Welsch and T. T. Chao, Anal. Chim. Acta, 82 (1976) 337.
6 B. Pahlavanpour, M. Thompson and S. J. Walton, J. Geochem. Explor., 12 (1979) 45.
7 D. Gladwell, M. Thompson and S. J. Wood, J. Geochem. Explor., 16 (1981) 41.
8 K. S. Subramanian and V. S. Sastri, Talanta, 27 (1980) 469.
9 A. Hall, Chem. Geol., 30 (1980) 135.
10 C. Y. Chan and M. W. A. Baig, Anal. Chim. Acta, 136 (1982) 413.
11 A. M. Bond, T. A. O'Donnell, A. B. Waugh and R. J. W. McLaughlin, Anal. Chem., 42 (1970) 1168.
12 D. P. Schweinsberg and B. J. Hefferman, Talanta, 17 (1970) 332.
13 O. Johansen and J. Richardson, Analyst (London), 94 (1969) 976.
14 L. Zhou, T. T. Chao and A. L. Meier, Talanta, 31 (1984) 73.
15 N. H. Suhr and C. O. Ingamells, Anal. Chem., 38 (1966) 730.
16 H. Fritzsche, W. Wegscheider, G. Knapp and H. Ortner, Talanta, 26 (1979) 219.
17 M. Tominaga and Y. Umezaki, Anal. Chim. Acta, 110 (1979) 55.
18 E. Lundberg, B. Bermark and W. Frech, Anal. Chim. Acta, 142 (1982) 129.
19 W. Slavin and D. C. Manning, Spectrochim. Acta, Part B, 35 (1980) 701; Part B, 37 (1982) 955.
20 E. Pruszkowska, D. C. Manning, G. R. Carnrick and W. Slavin, At. Spectrosc., 4 (1983) 87.
21 J. Long-zhu, At. Spectrosc., 5 (1984) 91.
22 S. Abbey, Reference Materials — Rock Samples SY-2, SY-3, MRG-1, Canada Centre for Mineral and Energy Technology, Report 79-35, 1979.
23 S. Terashima, Geostand. Newsl., 6 (1982) 77.
24 W. S. Bowman, G. H. Faye, R. Sutarno, J. A. Mckeague and H. Kodama, Geostand. Newsl., 3 (1979) 109.
25 K. Govindaraju, Geostand. Newsl., 4 (1980) 49.

Analytica Chimica Acta, 188 (1986) 119—126
Elsevier Science Publishers B.V., Amsterdam — Printed in The Netherlands

DETERMINATION OF SILICONE IN FATS AND OILS BY ELECTROTHERMAL ATOMIC ABSORPTION SPECTROMETRY WITH IN-FURNACE AIR OXIDATION

D. A. McCAMEY*[a], D. P. IANNELLI, L. J. BRYSON and T. M. THORPE
Procter and Gamble Company, 6071 Center Hill Road, Cincinnati, OH 45224 (U.S.A.)
(Received 7th March 1986)

SUMMARY

A graphite-furnace atomic absorption spectrometric method is reported for determination of dimethylpolysiloxane (silicone) in edible fats and oils. It incorporates an air-oxidation step in the furnace program to reduce matrix interferences. The detection limit is 0.3 mg kg^{-1} in soils, and short-term precision is about 6% at silicone concentrations of 1.7—2.0 mg kg^{-1}. The procedure was successfully applied to a variety of commercial frying fats and oils, to quantify silicone loss during polish filtration during oil manufacture, to quantify sorption of antifoam onto fried food, and to detect fugitive sources of silicone encountered in deep-fat frying operations.

Dimethylpolysiloxanes, or silicones, have been added to commercial frying fats and oils since the early 1950's. These compounds act as antioxidants [1—3], stabilizers to reduce thermal deterioration of fats [4—8], and anti-foam agents [1, 9]. Their precise functions depend, among other properties, on the concentration of silicone in the fat or oil. Typically 0.03—0.05 mg kg^{-1} is sufficient to reduce oxidative deterioration, presumably by formation of a protective film at the surface of the oil [9]. At concentrations from 0.5 to about 30 mg kg^{-1}, silicone prevents foaming and protects against thermal deterioration. However, the amount of silicone actually permitted in food is limited by the FDA to 10 mg kg^{-1} [10]. Because of this regulatory constraint and because of the highly concentration-dependent performance of silicone, an accurate and precise procedure is needed to quantify these compounds at trace levels in fats and oils.

Historically, most of the methods used to determine silicone were tedious, time-consuming, insufficiently sensitive, or too costly for routine application [11]. Atomic absorption spectrometry (a.a.s.) offered the most promise for quantifying trace levels of silicone. Paralusz [11], Neal [12], and Neal et al. [13] determined silicone at concentrations in the 1—10 mg kg^{-1} range in cottonseed oil, cake mixes, paper products, and polymers after extraction

---

[a]Present address: Procter & Gamble Co., Miami Valley Laboratories, P.O. Box 39175, Cincinnati, OH 45247, U.S.A.

0003-2670/86/$03.50

with methyl isobutyl ketone or petroleum ether. Nitrous oxide/acetylene flame a.a.s. was used to detect extracted silicone as silicon. Freeman et al. [14] applied a.a.s. with direct aspiration of a 50% (v/v) solution of cooking oil in hexane into a nitrous oxide/acetylene flame to determine as little as 0.3 mg kg^{-1} silicone in oils. However, for oils actually used to fry potato chips, the limit of determination was 1 mg kg^{-1}. The physical properties of each oil altered aspiration and nebulization characteristics of samples and led to unpredictable amounts of background noise. A similar approach was used by Doeden et al. [15] to measure silicone in hydrogenated and nonhydrogenated fats and oils down to 1 mg kg^{-1}. Non-flame a.a.s. was used by Kundu [16] to quantify silicone which had been extracted from saponified vegetable oils. This procedure was time-consuming and had a detection limit of only 3 mg kg^{-1}.

This paper describes a graphite-furnace a.a.s. procedure to determine silicone in commercial fats and oils which overcomes the limitations of earlier methods. The procedure is simple, rapid, and allows detection (S/N = 3) down to 0.3 mg kg^{-1} silicone. In addition, it is demonstrated that "in-furnace" air oxidation of the oil improves reproducibility by reduction of matrix interferences.

EXPERIMENTAL

Apparatus

The instrument used was a Perkin-Elmer (PE) Model 4000 atomic absorption spectrometer equipped with a PE HGA-500 graphite furnace, AS-40 autosampler, and a Model 056 dual-pen recorder. A PE Intensitron silicon hollow-cathode lamp was operated at 30 mA. The silicon line at 251.6 nm was used with a monochromator slit of 0.2 nm (Low Height setting). Absorbance signals were measured as peak heights with a 4.0-s sampling period. Pyrolytic graphite tubes were used in the furnace, and the autosampler was programmed to deliver 20-μl aliquots. Furnace conditions are summarized in Table 1.

Millipore 0.5-μm Millex (Part No. SLSR025NB) disposable filter units were used to filter all samples and standards. These filters separate all of the

TABLE 1

Graphite furnace conditions for determination of silicone

Step	Temp. (°C)	Ramp (s)	Hold (s)	Gas	Flow (ml min^{-1})
1 Dry	110	10	10	Ar	300
2 Oxidize	250	10	15	Air	300
3 Ar purge	250	1	24	Ar	300
4 Char	800	10	15	Ar	300
5 Atomize	2600	0	6	Ar	0
6 Cool	20	2	3	Ar	300

interfering iso-octane-insoluble forms of silicon (e.g., inorganic silicates) from the iso-octane-soluble silicone.

Samples and chemicals

Dow Corning 200 dimethylpolysiloxane (500 centistokes; silicone; Dow Corning Corp., Midland, MI) was used to prepare standard silicone solutions. The solvents were petroleum ether (30—60°C) and iso-octane (Burdick and Jackson, Muskegon, MI). Partially hydrogenated soybean oils of various iodine value (Procter & Gamble Co., Cincinnati, OH) were used in standard solutions and for recovery studies. Solvents and oils were checked in advance for silicone contamination.

All other chemicals were reagent grade or better. Specific chemicals used in the interference studies were: sodium chloride (Diamond Crystal Salt Co., St. Clair, MI), Cabosil silicon dioxide (Cabot Corp., Tuscola, IL), soybean lecithin (Central Soya Co., Decatur, IN), diglycerides (Aldrich), and iron-4-cyclohexanebutyrate and nickel 4-cyclohexylbutyrate (Spex Industries).

Procedures

Contamination control. Because silicones are so widely encountered within and outside the laboratory, special procedures are needed to avoid contamination of the instrument, glassware, samples, standards, and reagents. The largest source of contamination can be from the analyst's hands (e.g., from silicone-containing hand lotions and hair-care products). All glassware and sample cups for the autosampler must be thoroughly rinsed to remove silicone. This is done by carefully washing each item with three portions of petroleum ether.

Preparation of standards. Calibration standards are made by pipetting 5 and 10 ml of a 5 mg l^{-1} solution of silicone (Dow Corning 200) in iso-octane into separate 100-ml volumetric flasks, each containing 5 g of a silicone-free fat or oil. A blank containing fat without added silicone is also prepared. The flasks are heated gently on a steam bath to melt the fat (diluted with about 50 ml of iso-octane to effect dissolution), mixed well, cooled to room temperature, and finally diluted to volume with iso-octane. These solutions contain 0, 5 and 10 mg of silicone per kg of fat.

During early work it was observed that the instrumental response to silicone depended on the iodine value of the fat and its concentration in iso-octane (Fig. 1). To account for this effect, three hardened soybean oils with iodine values of 90, 100, and 120 were identified as representative of most of the fats and oils examined and encompassed the usual range of responses. These fats were individually added to calibration standards at the 5% (w/v) level in order to match the matrices encountered with unknowns. As shown in Fig. 1, 5% fat in solution yields a higher response than a 2.5% solution or any lower fat concentration. A concentration higher than 5% was not used because of solubility problems.

Unfamiliar samples were initially tested to establish which calibration plot

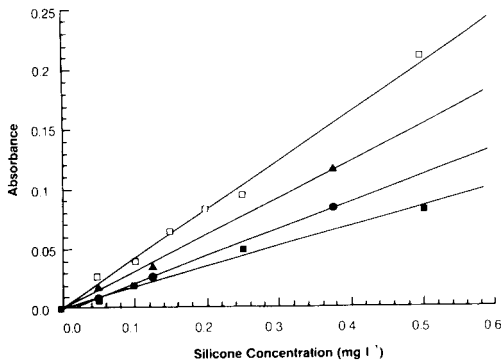

Fig. 1. Effects of iodine value (IV) and fat concentration on the response to silicone: (□) 5% IV-120 oil; (▲) 2.5% IV-120 oil; (●) 2.5% IV-100 oil; (■) iso-octane without oil.

best matched the instrument response for the sample. This was done by processing the sample and the sample spiked with 0.25 mg l^{-1} silicone. The difference between these absorbance readings was compared to the response to a 0.25 mg l^{-1} standard on each calibration line for the three reference fats. The sample was matched to the calibration line for which the spike recovery and the 0.25 mg l^{-1} standard agreed within 10%. If a sample yielded results which did not agree with any of the three calibration curves within 10%, then a similar fat or oil stock containing no silicone was obtained for use in preparing calibration solution. To date, the three model fats selected have proved satisfactory for determination of silicone in 28 edible fats and oils found in food services.

In subsequent determinations, quantification was made using only the calibration line obtained with the matrix fat which gave best recovery.

Preparation of samples. Samples are prepared by accurately weighing 5.00 g of sample into a pre-rinsed 100-ml volumetric flask. Liquid oils are weighed directly after thorough mixing. Solid fats are completely melted on a steam bath, mixed well, and then weighed rapidly. The sample is diluted in the same manner as the calibration standards.

Standards and samples. All standards and samples are filtered through a 0.5-μm Millex filter attached to a pre-rinsed and dried glass syringe. The first 7—8 ml of sample is used to rinse the filter and is discarded. The remaining solution is filtered directly into a clean autosampler cup.

With the instrumental conditions given in Table 1, standard solutions are run at the beginning and end of each batch of samples in order to account for any changes in instrument response. For the most precise work, blank solvent (iso-octane) is injected between each sample or standard to eliminate graphite-furnace memory effects [17].

RESULTS AND DISCUSSION

Optimization of furnace temperatures

The oxidation, char, and atomization temperatures were chosen at 250°C, 800°C, and 2600°C, respectively (Table 1). These were selected to maximize linearity, sensitivity, and tube lifetime. The use of argon in the third step of the furnace program removes the air before the temperature is raised to the higher char-value. Tube lifetime does not appear to be affected by use of air oxidation.

In initial optimization experiments, the atomization temperature was held constant at 2750°C and the char temperature was varied from 100 to 1000°C (Fig. 2A). At 250°C, response to silicone in oils was highest. Furthermore, addition of air in this temperature region produced a more linear response to silicone, and less dependence on fat matrix (Fig. 3). The discontinuity observed near 400°C (Fig. 2A) and the two-humped charring curve were reproducible and indicate the possibility of two consecutive and different silicone or fat matrix oxidation or charring mechanisms. For this reason, an 800°C char step was inserted after the 250°C oxidation to assure that the matrix and silicone polymer were completely decomposed. In a second experiment (Fig. 2B), the oxidation and char temperatures were held constant at their previously selected values (250°C and 800°C) while the atomization temperature was varied from 2100 to 2700°C. An atomization temperature of 2600°C was selected because maximum sensitivity was achieved and higher temperatures shortened tube life.

Quantification by peak height vs. peak area and linearity of response

Responses were measured as peak height rather than peak area. Reports that peak-area measurements could correct for some matrix-dependent responses [17] were not substantiated for edible fats and oils. Peak areas were

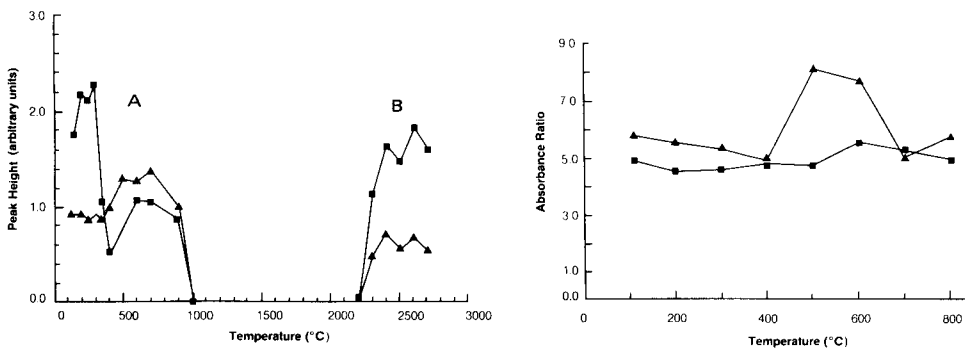

Fig. 2. Effects of char (A) and atomization (B) temperature on the response to silicone (0.5 mg l^{-1}): (■) 5% IV-100 oil; (▲) iso-octane without oil.

Fig. 3. Linearity of response versus char temperature in air: (■) IV-100 oil; (▲) IV-120 oil. Linearity was measured as the ratio of absorbance for 0.5 mg l^{-1} silicone to the absorbance for 0.1 mg l^{-1} silicone.

found to be just as prone to variation with matrix as peak heights.

The air-oxidation step was added to the furnace program because it reduced the nonlinearity experienced in early determinations of silicone with graphite-furnace a.a.s. using only argon charring (Fig. 4). This resulted in low recoveries of silicone as shown in Fig. 5. This problem was especially severe at low silicone concentrations. Between 0.05 and 0.80 mg l^{-1}, only 44—88% of the silicone added to oils was recovered when an argon char was used. Addition of the air oxidation stage improved the recoveries to 95—98% for 0.15 mg l^{-1} silicone and they were still at 80% for 0.1 mg l^{-1} silicone. This procedure, including air oxidation, has linear range up to 1.25 mg l^{-1} in solution or 25 mg kg^{-1} in fat samples.

Accuracy, precision and reproducibility

The accuracy of the procedure was evaluated with two sets of recovery experiments. In the first, known concentrations of silicone were added to a "silicone-free" fat with an iodine value of 100. This was accomplished in two ways: (1) silicone was added at concentrations of 0, 3.2, 6.4, and 19.0 mg kg^{-1} to the fat with high shear mixing; (2) silicone (in iso-octane solution) was added to fat contained in volumetric flasks. The second recovery study was based on spiking fourteen commercial fats with known amounts of silicone. For both experiments, recoveries averaged 95.2%, with a relative standard deviation of 6.1%, supporting the accuracy of the method. Recoveries were not influenced by the levels of silicone added in the spiking experiments.

Short-term relative standard deviations were typically in the range of 5.8—6.4% for silicone concentrations of 1.7—2.0 mg kg^{-1}. In order to assess the continued, long-term performance of the method, a secondary standard, or working reference material (WRM), was prepared. The WRM was prepared from a brand-name frying oil which was readily available. Over a six-month period, this sample was processed repeatedly and found to contain 2.6 ± 0.2 mg kg^{-1} silicone. The long-term relative standard deviation was 7.7%.

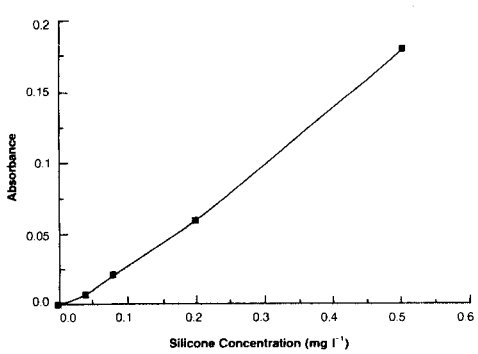

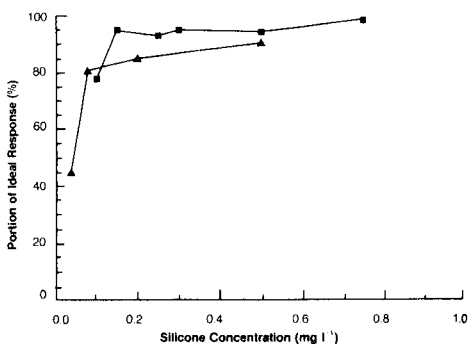

Fig. 4. Nonlinear response to silicone with an argon char for a 5% solution of IV-100 oil.

Fig. 5. Comparison of the effect of air char and argon char on linearity of response to silicone from a 5% solution of IV-100 oil: (■) air char; (▲) argon char.

Interference studies

Previous a.a.s. methods for silicon report chloride as a major interferent [17]. Therefore, the proposed procedure was checked for possible interferences from common additives and components of fats. These materials, the concentrations added, and typical concentrations in frying oils are presented in Table 2. Results are reported as the percentage recovery of a known 3 or 5 mg kg^{-1} silicone standard in the presence of each interferent. Only the high level of iron (10 mg kg^{-1} in fat) produced a significant effect. Silicon dioxide did not interfere with the determination because it is effectively filtered from solution during sample preparation. Lecithin and diglycerides might have altered the ability of sample solutions to spread over the surface of the graphite tubes, resulting in different behavior of silicone during the flameless sampling, but only minor effects were noted with either of these materials.

Applications

Analyses of a variety of commercial oils, fats, and shortenings with iodine values from 48 to 108 showed that the materials contained 0.7—6.6 mg kg^{-1} silicone; only one of the twelve samples tested contained no silicone.

The method was also used to show that silicone contained in an edible oil (initially 3.7 mg kg^{-1}) is removed relatively rapidly (in less than 1 day) through sorption onto the cooked food during deep fat frying until it reaches a steady state of about 1 mg kg^{-1}. It was also shown that new filters used to remove particulate material from used frying oil can be a source of fugitive silicone in the cooking operations. Lastly, the final polish, filtration of an edible-oil process stream was found to remove a significant proportion of any silicone added prior to the cartridge filter. In some cases, losses as high as 80% were observed, although they were typically in the 40—50% range. These applications demonstrate the utility of this graphite-furnace a.a.s. procedure in the study of the behavior of dimethylpolysiloxane in commercial uses of edible fats and oils.

TABLE 2

Effects of interferences on recovery of silicone

Interferent	Typical concentration in fat or oil (mg kg^{-1})	Concentration of interferent added (mg kg^{-1})	Average recovery of silicone (%)[a]
Nickel	0.1—0.2	2.0, 10.0	105
Iron	0.1—0.3	2.0	105
		10.0	126
Silicon dioxide	600—2400	5000	94
Lecithin	30—150	10, 100	98
Diglycerides	1.0—5.0%	0.05—4%	105
Sodium chloride	Trace—2%	2%	95

[a]In all tests, 3 mg kg^{-1} silicone in fat or oil was used except for diglycerides where the silicone content was 5 mg kg^{-1}.

The authors recognize the contributions of Jo Ann Ferris and Linda McKinley to the understanding of the behavior of silicone in graphite-furnace a.a.s. and to the development of early versions of this method. The contribution of Mary Jo Bast in verifying the validity of peak-height quantification is also acknowledged.

REFERENCES

1 J. B. Martin, U.S. Patent 2.634.213, 1953.
2 H. Kusaka, J. Kakizaki, T. Shinozaki and S. Ohta, Yukagaku, 29 (1980) 341.
3 F. Drawert and B. Schraufstetter, Z. Lebensm.-Unters. Forsch., 179 (1984) 237.
4 V. K. Babayan, U.S. Patent 2.998.319, 1961.
5 R. D. Dobson, L. H. Going and E. R. Hair, U.S. Patent 3.449.113, 1969.
6 H. Kusaka, A. T. Katsumasa and S. Ohta, Yukagaku, 33 (1984) 349.
7 A. S. Huang, O. A. Hsieh, C. L. Huang and S. S. Chang, J. Am. Oil Chem. Soc., 58 (1981) 997.
8 E. Yuki and K. Morimoto, Yukagaku, 31 (1982) 915.
9 K. D. Fisher, Evaluation of the Health Aspects of Methylpolysilicones as Food Ingredients, Federation of American Societies for Experimental Biology, Bethesda, MD, 1981.
10 Code of Federal Regulations, Vol. 21, Section 173.340, 1981.
11 C. M. Paralusz, Appl. Spectrosc., 22 (1968) 520.
12 P. Neal, J. Assoc. Off. Anal. Chem., 52 (1969) 875.
13 P. Neal, A. D. Campbell, D. Firestone and M. H. Aldridge, J. Am. Oil Chem. Soc., 46 (1969) 561.
14 I. P. Freeman, F. B. Padley and W. L. Sheppard, J. Am. Oil Chem. Soc., 50 (1973) 101.
15 W. G. Doeden, E. M. Kushibab and A. C. Ingala, J. Am. Oil Chem. Soc., 57 (1980) 73.
16 M. K. Kundu, Fette. Seifen. Anstrichm., 79 (1977) 170.
17 W. Slavin, Graphite Furnace AAS: A Source Book, Perkin-Elmer Corp., Norwalk, CT, 1984.

Analytica Chimica Acta, 188 (1986) 127—135
Elsevier Science Publishers B.V., Amsterdam — Printed in The Netherlands

A STUDY ON THE GENERATION OF HYDROGEN SELENIDE AND DECOMPOSITION OF TETRAHYDROBORATE IN HYDRIDE-GENERATION ATOMIC ABSORPTION SPECTROMETRY

J. AGTERDENBOS and D. BAX

Analytisch Chemisch Laboratorium der Rijksuniversiteit Croesestraat 77a, 3522 AD Utrecht (The Netherlands)

(Received 20th March 1986)

SUMMARY

Literature data on the decomposition of sodium tetrahydroborate predict that the reagent is decomposed within 1 ms of being mixed with an acidic sample. This is confirmed experimentally. Hydrogen selenide and other hydrides must therefore be formed even more quickly. The reaction coil often used in continuous flow systems is not necessary for completion of the reaction, but in its absence low results are obtained because the coil contributes to the separation of the hydride from the liquid phase. A study of the effects of Co^{2+}, Ni^{2+} and Cu^{2+} indicates that their interference arises at least partly from enhanced decomposition of tetrahydroborate, thus allowing less hydride formation.

Hydride-generation atomic absorption spectrometry (a.a.s.) has found wide application in the determination of elements giving volatile hydrides. The analyte in the acidic sample is converted to its hydride which is swept to a heated quartz cuvette and decomposed there. The atoms formed are measured by a.a.s. The main advantage of the technique, when compared to flame a.a.s. is that in the latter the dilution factor for the analyte on conversion from solution to atoms in the gas phase is 10^5—10^6, while in the hydride technique this factor is only ca. 500 [1]. The sensitivity is therefore improved by about 10^3. The technique, including interferences by transition metals, has been reviewed by Nakahara [2].

Several studies have been made on the mechanism of the reactions in the heated cuvette [1, 3—7], but the processes in the preceding steps have received much less attention. For selenium (used as an example in the present paper), these steps are: (i) the conversion of selenium(IV) to hydrogen selenide, usually with sodium tetrahydroborate; (ii) the separation of the volatile hydride from the liquid phase; and (iii) the transport of the hydride to the heated absorption cuvette.

Separation and transport are achieved with a carrier gas (stripping gas). The excess of reagent is decomposed (oxidized) by water. In an acidic medium this process is represented by:

$$BH_4^- + H^+ + 3H_2O \rightarrow H_3BO_3 + 4H_2(g) \quad (1)$$

0003-2670/86/$03.50

Studies [8, 9] on the rate of this reaction and on the catalytic action of transition metals have been summarized [10, 11]. Until now this work has not been considered in studies of hydride-generation a.a.s., yet there are many results that are of relevance to the present study. The rate of reaction 1 between pH 3.8 and 14 is given by [9, 11]:

$$-\mathrm{d}[BH_4^-]/\mathrm{d}t = k_1[H^+][BH_4^-] + k_2[BH_4^-] \quad (2)$$

where $k_1 = 2.18 \times 10^{11}\ T \exp(-4000/T)$ mol min^{-1} and $k_2 = 1.72 \times 10^7\ T \exp(-10380/T)$ min^{-1}. At pH < 3.8 the reaction seems too fast to be measured. The decomposition is catalyzed by Mn^{2+}, Fe^{2+}, Co^{2+}, Ni^{2+}, Ru^{3+}, Rh^{3+}, Pd^{2+}, Ir^{4+} and Pt^{4+}, OsO_4, colloidal platinum, active carbon and some metals or alloys [8, 11]. Sometimes metal/boron compounds (Mn, Ni, Co, Ag, Au and possibly Cu, Bi and Pd) or metals are formed, and these compounds or metals also may catalyze reaction 1. The quantitative information given on the catalytic effect is not useful for the present work as the conditions (high pH, high metal concentration) are too different from those of interest here. Some of the data may be useful for studies on analytes requiring high pH values for their conversion to hydrides, however.

In the present work, the rate of reaction 1 and the catalytic effect of some ions were studied under the conditions usual for hydride-generation a.a.s. of selenium and several other elements. The a.a.s. measurements were made only for selenium. As the results suggested that the stripping of the gaseous hydrogen selenide from the liquid phase was a limiting factor in the overall process, some work on this point was also done. Some data on hydrogen selenide of relevance are as follows: solubility in water, 0.096 mol l^{-1} (15°C), 0.084 mol l^{-1} (25°C), 0.073 mol l^{-1} (35°C); solubility in hydriodic acid solution (25°C), 0.085 mol l^{-1} (in 0.2 mol l^{-1} HI) and 0.110 mol l^{-1} (in 2.73 mol l^{-1} HI) [12]; acidity constants, $pK_1 = 3.6$, $pK_2 = 15$ [13]. The pH of a sodium tetrahydroborate solution (0.1 mol l^{-1}) is ca. 10.0 [10].

No studies on the rate of hydride formation seem to have been reported for the conditions usual in the present technique, but it has been suggested [14] that the peak width of the absorbance signal (about 20 s in the cited experiments) corresponds to the time required for hydride formation. The interference of transition metals in the analytical applications of the technique has been discussed by many authors, and some of them (e.g., refs. 15—17) give suggestions as to the mechanism of such interferences. In none of these studies, however, was the catalytic effect of the metals on tetrahydroborate decomposition considered as a possible cause of interference.

EXPERIMENTAL

The apparatus for hydride-generation a.a.s. was as described previously [1]. The acidic sample solution (A) and the alkaline sodium tetrahydroborate solution (B) were transported (4 ml min^{-1} each) by a peristaltic pump to intersecting channels at right angles (reaction cross C, Fig. 1). The channels

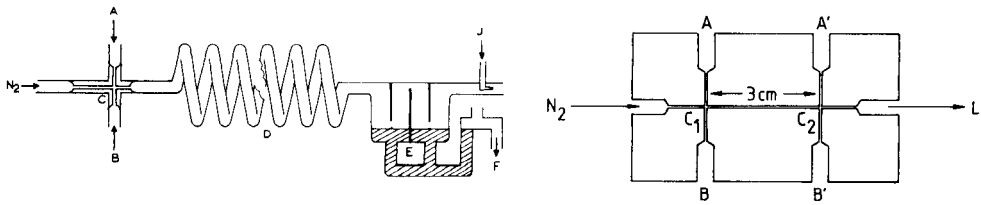

Fig. 1. Apparatus used for generation, separation and transport of the volatile hydride. On the right-hand side, the gas mixture enters the heated quartz cuvette (not drawn). A, Sample solution; B, $NaBH_4$ solution (both coming from the peristaltic pump); C, reaction cross; D, reaction coil; E, gas/liquid separator; F, waste; J, extra gas inlet (not used in the present work).

Fig. 2. Double reaction cross made of perspex (polymethylmethacrylate): A, B, see Fig. 1; L is connected either to a titration vessel or to D (Fig. 1), depending on the type of experiment (see text); A', B' are inlets for NaOH during the reaction-rate studies and for interferent or acid during the interference studies.

in the cross had an i.d. of 0.5 mm and so the two liquid streams collided at ca. 30 cm s^{-1} each, and mixed thoroughly and rapidly. The carrier gas (nitrogen at 500 ml min^{-1}) swept the reaction products through a reaction coil D (i.d. 3 mm, length 1.5 m, made into a spiral with a diameter of 3 cm and a pitch of 1 cm) and over a gas/liquid separator E, to the electrically heated quartz cuvette. For some a.a.s. measurements, reaction coil D was removed and a direct connection made between C and E. In others, coil D was replaced by a straight tube T (15 cm long, 3 mm i.d.).

For measurements of the rate of reaction 1, a double reaction cross (Fig. 2) was used. No analyte was present in these measurements. An acidic solution, 2 mol l^{-1} hydrochloric acid or 1 mol l^{-1} sulphuric acid (in some experiments also containing Ni^{2+}, Co^{2+} or Cu^{2+}), was pumped through channel A, and an alkaline tetrahydroborate solution (1% w/v) was pumped through channel B (4 ml min^{-1} each). The solutions were mixed in the first cross C_1 and the reaction products were swept to the second cross C_2 with a carrier gas flow of 500 ml min^{-1}. The diameter of the channels was 0.5 mm and the distance C_1—C_2 was 3 cm. If the rates of transport of the liquid and the gas are assumed to be equal, then the time required for the reactants to pass from C_1 to C_2 is about 1 ms. At the second cross C_2, a sodium hydroxide solution (2 mol l^{-1}, 2 × 4 ml min^{-1}) was pumped through channels A' and B' in order to stop the decomposition reaction.

The double reaction cross was also used in interference studies with a.a.s. Here in all cases a 0.16% tetrahydroborate solution was added through B (4 ml min^{-1}). The solution added through A (4 ml min^{-1}) contained selenium(IV) alone or with interferent. No sodium hydroxide solution was used here. In those cases for which the solution added through A contained no interferent, the interferent was added through A' and B'. When the solution added through A did contain interferent, the solution added through A' and B' contained acid only. Thus in all cases the interferent was present in

the solution during the passage of hydrogen selenide through reaction coil D. A much slower flow through A′ and B′ (both 0.14 ml min^{-1}) than through A and B was applied in order to add as little solution as possible to the usual total flow rate of 8 ml min^{-1}. Therefore the interferent concentrations added through A′ and B′ had to be increased appropriately.

All sodium tetrahydroborate solutions were 0.2% (w/v) in sodium hydroxide to increase their stability. Selenium(IV) solutions were prepared from sodium selenite pentahydrate. The nitrogen contained $\leqslant$1000 ppm of oxygen. For the measurements of the rate of reaction 1, the sodium tetrahydroborate that was not decomposed was measured by iodimetric titration [18, 19]: the alkaline solution was mixed with an excess of potassium iodate solution and stirred for 3 min; the solution was then acidified, an excess of iodide was added, and the iodine formed from the remaining iodate was titrated with thiosulphate. Reaction 1 suggests that in a sufficiently alkaline medium tetrahydroborate does not decompose. This was confirmed by experiments. Even the addition of 25 mg l^{-1} cobalt(II) to a solution of 1% tetrahydroborate/0.2% sodium hydroxide, though giving a black precipitate (probably CoB_2 [8, 11]), resulted in only slight decomposition of the tetrahydroborate (ca. 6.5% in 20 min). It was concluded that in alkaline solutions the degree of decomposition is not affected by the presence of cobalt(II) at the levels of interest.

RESULTS AND DISCUSSION

The decomposition rate of sodium tetrahydroborate

At 25°C the constants in Eqn. 2 are $k_1 = 0.96 \times 10^8$ min^{-1} mol and $k_2 = 3.8 \times 10^{-6}$ min^{-1}. Therefore under all conditions of interest, k_2 can be neglected, and

$$t_f = -\ln(1-f)/k_1[H^+] \qquad (3)$$

where t_f is the time (min) required to decompose a fraction f of the tetrahydroborate. Table 1 shows results of calculations based on Eqn. 3 (for pH = 0 and 2, it is assumed that Eqns. 2 and 3 still hold). From the Table, it is clear that the addition of some alkali to the reagent solution (pH ca. 10) improves the stability considerably. Table 1 also shows that at low pH values, as used in most analytical applications, the decomposition is very rapid. This was confirmed by experiments with the double reaction cross, the results of which are given in Table 2. The difference between the measured values in Table 2 and the values calculated from Eqn. 3 may be due to the time required for mixing of the reactants or to deviations from Eqn. 3 at pH < 3.8. No effort was made to investigate this point further as the difference is not of practical interest.

The rate of formation of hydrogen selenide cannot be measured in this way, but it is certainly greater than the decomposition rate of sodium tetra-

TABLE 1

Time required for the decomposition of various fractions, f, of the sodium tetrahydroborate initially present at various pH values, calculated from Eqn. 3

f	Time needed at different pH in range 0–12						
	0	2	4	6	8	10	12
0.05	0.032 μs	3.2 μs	0.32 ms	0.032 s	3.2 s	5.3 min	0.37 day
0.50	0.43 μs	43 μs	4.3 ms	0.43 s	43 s	72 min	5 day
0.95	1.9 μs	190 μs	19 ms	1.9 s	190 s	320 min	22 day
0.9999	5.8 μs	580 μs	58 ms	5.8 s	580 s	980 min	68 day

TABLE 2

The measured degree of decomposition of 0.2% (w/v) sodium tetrahydroborate during its transport from C_1 to C_2 (Fig. 2) after mixing with sulphuric acid solutions without and with metal ion (M^{2+}) present

Acidic solution	Degree of decomposition (%)		
	Co^{2+}	Cu^{2+}	Ni^{2+}
H_2SO_4 (1 mol l^{-1})	80	80	80
+2.5 mg l^{-1} M^{2+}	81	81	80
+7.5 mg l^{-1} M^{2+}	88	84	100
+25 mg l^{-1} M^{2+}	100	95	100

hydroborate and so the reported width of the peak signal (20 s) cannot be due to the slow formation of hydrogen selenide. Table 2 also shows that the decomposition is enhanced by traces of the three metal ions considered in this paper under the usual analytical conditions. This confirms the evidence that the interference of the metals is caused by their catalytic action on tetrahydroborate decomposition. As it is known that the formation of hydrogen selenide is promoted by halide ions [20] and that the presence of iodide decreases the influence on the selenium signal of many interferents, some experiments were done, similar to those reported in Table 2, but with replacement of sulphuric acid (1 mol l^{-1}) by hydrochloric acid (2 mol l^{-1}) and addition of iodide (1 mol l^{-1}) to the tetrahydroborate solution. The decomposition rate was not influenced by these changes. This shows that the decomposition of tetrahydroborate is not retarded by halides.

The function of the reaction coil

From the experiments described above, it seems clear that the formation of hydrogen selenide is complete before the liquid reaches coil D, so this coil is not necessary for hydride formation. Atomic absorption measurements

TABLE 3

The influence of the type of connection between the reaction cross C and the gas/liquid separator E

Se conc. (ng l^{-1})	Absorbance[a]		
	D	T	DC
25	0.187	0.124 (66%)	0.101 (54%)
50	0.345	0.218 (63%)	0.194 (56%)

[a]D, coil (1.50 m); T, tube (15 cm); DC, direct connection; the selenium was dissolved in 1 mol l^{-1} H_2SO_4. Values in parentheses give the fraction of the values found with the reaction coil.

made when the coil was replaced by tube T or where a direct connection between C and E was made are listed in Table 3. These data show that the shorter the tube length between C and E, the lower the results. It seems justified to conclude that coil D is necessary for more complete stripping of the hydride from the liquid.

Mechanism of the metal ion interference

The experiments described above suggest that the interference on the determination of selenium caused by transition metal ions may be due to the effect of the transition metal ions on the decomposition of sodium tetrahydroborate, so that the reagent has decomposed before its reaction with the analyte is complete. To clarify this point, a series of a.a.s. measurements was made with the transition metal added with or after the selenium, as described in the experimental section.

The results in Table 4 show that the presence of a transition metal ion during the formation of hydrogen selenide and decomposition of sodium tetrahydroborate in C_1, causes a considerable decrease of the signal. If the interferent is added after the reactions have taken place, the signal is hardly changed. It is concluded, therefore, that no reaction occurs between hydrogen selenide and the transition metal ion during their passage through the coil. This is in contrast to the mechanism proposed by Meyer et al. [15] where the formation of insoluble selenides was considered as the prime cause of interference. The suggestion that the interference is caused by competition of the interferent with selenium(IV) for the tetrahydroborate [16] seems not to be realistic, as the tetrahydroborate is present in large excess [17]. The theory that the interference is caused by capture and decomposition of the evolved hydride by the finely dispersed metal precipitate, resulting from the reduction of the interferent ions by tetrahydroborate [17] should be modified in two ways. One is that the reaction between metal ions and tetrahydroborate in several cases results in the formation of metal borides [11]. The second is that all data on the hydride-generation technique suggest

TABLE 4

Influence of the place of addition (Fig. 2) of interfering transition metal ions (M^{2+}) on the absorbance of 50 $\mu g\ l^{-1}$ selenium added at C_1 ([M^{2+}] in mg l^{-1})

Acid in C_1	[M^{2+}]			Absorbance
	Added in C_1	Added in C_2	Present in D	
2 M HCl	0	0	0	0.317
	250 Co^{2+}	0	120 Co^{2+}	0.111
	0	7140 Co^{2+}	120 Co^{2+}	0.311
1 M H_2SO_4	0	0	0	0.207
	250 Co^{2+}	0	120 Co^{2+}	0.111
	0	7140 Co^{2+}	120 Co^{2+}	0.203
1 M H_2SO_4[a]	0	0	0	0.438
	250 Co^{2+}	0	120 Co^{2+}	0.155
	0	7140 Co^{2+}	120 Co^{2+}	0.438
1 M H_2SO_4	250 Ni	0	120 Ni^{2+}	0.098
	0	7140 Ni^{2+}	120 Ni^{2+}	0.187
1 M H_2SO_4	250 Cu	0	120 Cu	0[b]
	25 Cu	0	12 Cu	0[b]
	0	7140 Cu^{2+}	120 Cu	0.208

[a] 100 μg Se l^{-1}. [b] A black precipitate (copper boride?) was formed in the first reaction cross.

that at least 700°C is required for the decomposition of metal selenides. Therefore if a mechanism similar to the one proposed by Welz and Melcher [17] is a cause of interference, this should be described more cautiously as an interference caused by the elimination of the gaseous hydride by products of the reaction between interfering metal ions and reagent.

In our opinion, however, the effect of the transition metal ions on the decomposition of tetrahydroborate also contributes to the interference. This argument is mainly based on the influence of the addition of potassium iodide to the tetrahydroborate solution. In the determination of selenium(IV), such an addition results in a considerable decrease of the interference caused by metal ions [20, 21] but there is no such beneficial effect in the determination of arsenic(III). It has been shown [5] that the addition of iodide to a sodium tetrahydroborate solution also has a considerable effect on the efficiency of the conversion of selenium(IV) to hydrogen selenide. In the absence of iodide, at least 0.1% tetrahydroborate is required for maximum conversion; a concentration of 0.04% [3] results in a considerably lower conversion. In the presence of iodide, however, 0.001% tetrahydroborate gives a similar maximum conversion. In the conversion of arsenic(III) to arsine, the presence of iodide has no effect on the required concentration of tetrahydroborate. These results strongly suggest that iodide catalyzes the reaction between selenium(IV) and tetrahydroborate, and that this effect contributes to the decrease of the interferences caused by transition metal ions.

CONCLUSIONS

The formation of hydrogen selenide and the decomposition of tetrahydroborate are fast reactions. The conditions used analytically are such that the hydride is formed before a considerable proportion of the reagent has decomposed. If transition metal ions are present in excessive concentrations, however, the decomposition rate of the reagent is increased, so that hydrogen selenide formation is incomplete. Iodide catalyzes the formation of hydrogen selenide. Therefore, even in the presence of much higher concentrations of interfering metal ions, the hydride formation reaction is rapid enough to result in complete conversion to the hydride. Other interference mechanisms may also be possible, such as that proposed by Welz and Melcher [17], as modified in the present paper.

Studies of the type reported here and elsewhere [1, 3–7, 22] may lead to improved apparatus and procedures. One has to be aware, however, that the choice of the design of the apparatus and the procedure is partly governed by the aim of the analysis. For procedures where peak signals are obtained, an increase in the rate of the stripping process, for instance, will result in faster response (less peak broadening). This is important when hydride-generation a.a.s. is coupled to liquid chromatography. In batch processes, the increased stripping rate will result in higher and narrower peaks, provided that the flow of the carrier gas is not increased. For continuous flow systems of the type used in the present work, the sensitivity may be increased, at first sight, if complete stripping of the hydride from the liquid is achieved with a slower gas flow. Unfortunately, however, a slow flow results in a longer residence time of the gas mixture in the absorption cuvette, and this may result in disappearance of analyte atoms by dimerization or condensation in the absorption cuvette [1, 5]. This disadvantage of low gas flows cannot be expected in hydride-generation inductively-coupled plasma spectrometry.

The type of analyte considered can influence the choice of the procedure. For instance, the solubility of the hydride in the liquid phase will influence the effectiveness of the stripping process. The solubility of arsine (0.008 mol l^{-1} at 20°C [23]) is less than that of hydrogen selenide (0.096 mol l^{-1}). The acid properties of the hydride may also be of importance. In aqueous solutions of pH > 3, a considerable proportion of the hydrogen selenide is present as HSe^- ions and therefore cannot be stripped. As arsine has essentially no acidic properties, such a restriction cannot be expected in the determination of arsenic. This has already been shown for arsenic(III). Conversion to arsine and stripping of arsine from the solution were achieved in solutions of pH up to 5.5 [24].

The authors thank C. L. de Ligny for reading the manuscript carefully and making many useful suggestions for improvements, and M. C. Schoondermark for his contribution to the experimental work and to discussions on this work.

REFERENCES

1 J. Agterdenbos, J. P. M. van Noort, F. F. Peters, D. Bax and J. P. ter Heege, Spectrochim. Acta, Part B, 40 (1985) 501.
2 T. Nakahara, Prog. Analyt. Atom. Spectrosc., 6 (1983) 163.
3 D. Bax, F. F. Peters, J. P. M. van Noort and J. Agterdenbos, Spectrochim. Acta, Part B, 41 (1986) 275.
4 J. Agterdenbos, J. P. M. van Noort, F. F. Peters and D. Bax, Spectrochim. Acta, Part B, 41 (1986) 283.
5 J. Agterdenbos and D. Bax, Fresenius Z. Anal. Chem., 323 (1986) 783.
6 B. Welz and M. Melcher, Analyst, 108 (1983) 213.
7 J. Dedina and I. Rubeska, Spectrochim. Acta, Part B, 35 (1980) 119.
8 H. I. Schlesinger, H. C. Brown, A. E. Finholt, J. R. Gilbreath, H. R. Hoekstra and E. K. Hyde, J. Am. Chem. Soc., 75 (1953), 215.
9 R. E. Mesmer and W. L. Jolly, Inorg. Chem., 1 (1962) 608.
10 Gmelin's Handbuch der Anorganischen Chemie, 8. Aufl., System Nr. 21 Erg. Bd 3, Verlag Chemie, Weinheim, 1966, pp. 1212–1230.
11 Gmelin's Handbuch der Anorganischen Chemie, 8. Aufl. Band 33 Borverbindungen Teil 8, Erg. Werk der 8. Aufl., Springer, Heidelberg, 1976, pp. 19—26.
12 A. J. McAmis and W. A. Felsing, J. Am. Chem. Soc., 47 (1925) 2633.
13 R. H. Wood, J. Am. Chem. Soc., 80 (1958) 1559.
14 B. Welz and M. Melcher, Anal. Chim. Acta, 131 (1981) 17.
15 A. Meyer, Ch. Hofer, G. Tölg, S. Raptis and G. Knapp, Fresenius Z. Anal. Chem., 296 (1979) 337.
16 F. D. Pierce, T. C. Lamoreaux, H. R. Brown and R. S. Fraser, Appl. Spectrosc., 30 (1976) 38.
17 B. Welz and M. Melcher, Analyst, 109 (1984) 569.
18 D. A. Lyttle, E. H. Jensen and W. A. Struck, Anal. Chem., 24 (1952) 1843.
19 I. M. Kolthoff, R. Belcher, V. A. Stenger and G. Matsuyama, Volumetric Analysis, Vol. III, Interscience, New York, 1957, p. 374.
20 J. Agterdenbos, J. T. van Elteren, D. Bax and J. P. ter Heege, Spectrochim. Acta, Part B, 41 (1986) 303.
21 M. Ikeda, Anal. Chim. Acta, 167 (1985) 289.
22 J. Dedina, Anal. Chem., 54 (1982) 2097.
23 P. Corriez and A. Berton, Bull. Soc. Chim. Fr., (1950) 43.
24 J. Aggett and A. C. Aspell, Analyst, 101 (1976) 341.

Analytica Chimica Acta, 188 (1986) 137—150
Elsevier Science Publishers B.V., Amsterdam – Printed in The Netherlands

COMPUTER SYSTEM AND FLOW CELL FOR AUTOMATED POTENTIOMETRIC AND CONSTANT-CURRENT STRIPPING ANALYSIS

LARS RENMAN, DANIEL JAGNER* and RICKARD BERGLUND

Department of Technical Analytical Chemistry, Chemical Centre, University of Lund, P.O. Box 124, S-221 00 Lund (Sweden)

(Received 11th June 1986)

SUMMARY

A flow cell and a personal computer-based system for potentiometric and constant-current stripping analysis are described. The thin-layer cell is designed for teflon-embedded glassy carbon electrodes in a spring-regulated holder, allowing simple instalment and leak-free behaviour. The personal computer is interfaced to hardware components such as potentiostat, amplifier, peristaltic pump, six inlet valves for different solutions, auto-sampler and strip-chart recorder. User-accessible commands allow electrolysis, stripping current, pump flow rates, valves, stripping transient recording, derivation, filtration and integration to be controlled, and through a number of user-defined programs, to be performed in unattended operation. This is described by an example. Through a software interface to a high-level language (BASIC), results from any number of analytical runs can be further evaluated by standard addition, or from calibration curves, or by statistical methods.

Potentiometric stripping analysis is based on the potentiostatic reduction and simultaneous amalgamation of the metal analytes on a mercury film-coated glassy carbon electrode and the subsequent chemical re-oxidation of these elements [1]. During oxidation (stripping) the working electrode potential is monitored. If the mass transport during reduction and oxidation is diffusion-controlled, the time needed for reoxidation of an element is proportional to the sample concentration of the element and the time of electrolysis and inversely proportional to the concentration of oxidants in the stripping medium [2]. A key difference between potentiometric stripping analysis and the anodic-stripping voltammetric techniques is that the only effect caused by the presence of oxidants in the stripping solution is an increase in the stripping rate. Consequently, potentiometric stripping analysis can be done in solutions without deoxygenation and this is the main reason for the wide acceptance of the technique. The rapid oxidation rate in solutions containing dissolved oxygen decreases the detection limit, however, if a normal strip-chart recorder is used for recording of the stripping transient. For this reason, computerized data acquisition was introduced early in the development of potentiometric stripping analysis [3–5]. Computerization has the further advantage that it considerably simplifies the use of flow

0003-2670/86/$03.50

systems in potentiometric stripping analysis [6]. This facilitates automated performance and stripping medium exchange, whereby increased resolution between overlapping stripping peaks can be obtained. It has been shown recently that this flow approach permits analysis analogous to cathodic stripping analysis. In this approach, concentrated electrolytes, e.g. 5 M calcium chloride, containing low concentrations of dissolved oxygen are used as stripping media. Reduction is done by means of constant current and the potential vs. time transient is monitored as in potentiometric stripping analysis. So far, this principle has been exploited only for the determination of nickel(II) and cobalt(II) as their dimethylglyoxime complexes [7]. Preliminary results do, however, indicate that this principle can be used also for the determination of, for example, selenium and molybdenum and organic compounds such as riboflavine.

In the present paper a computerized system is described for flow potentiometric and constant-current stripping analysis. The purpose is to show, by means of a simple application, that these techniques can be fully automated, i.e., the results can be obtained during unattended operation. Because the computer program controlling operation of the system and evaluation of the data is comprised of over 3500 assembler instructions, only those parts of the program which are vital for the operation of the system will be described. Further details can be obtained through correspondence with the authors.

FLOW SYSTEM

The flow system consists of a thin-layer cell into which six different solutions can be sucked in any required order by means of a peristaltic pump. All inlet tubings are made of teflon with an inner diameter of 0.8 mm. The dead volume between the entry point of the six solutions and the flow cell is approximately 50 μl, i.e., the delay time is 3 s for a flow rate of 1 ml min^{-1}.

Flow cell

From a practical point of view, the flow cell is the single most important part of the automated system. It has to fulfil several requirements. First, it must be simple to disassemble and reassemble for polishing of the glassy carbon electrode. Secondly, it must not leak even when highly viscous solutions such as concentrated calcium chloride are sucked through the cell. Thirdly, the internal potential drop (iR drop) must be kept at a minimum. In potentiometric stripping analysis, the iR drop is of importance only in the electrolysis phase, because no current passes through the cell during stripping. However, sample electrolysis is done in solutions without deoxygenation. Thus the electrolysis current is normally of order of magnitude of 10 μA, i.e., the internal cell resistance must be less than 1 kΩ in order to allow control of the electrolysis potential with an accuracy of 10 mV. Fourthly, because the electrolyte-containing tubings of the flow system act as antennae, the flow cell must be isolated from the noise, mostly of line frequency, picked up by these electrolytes.

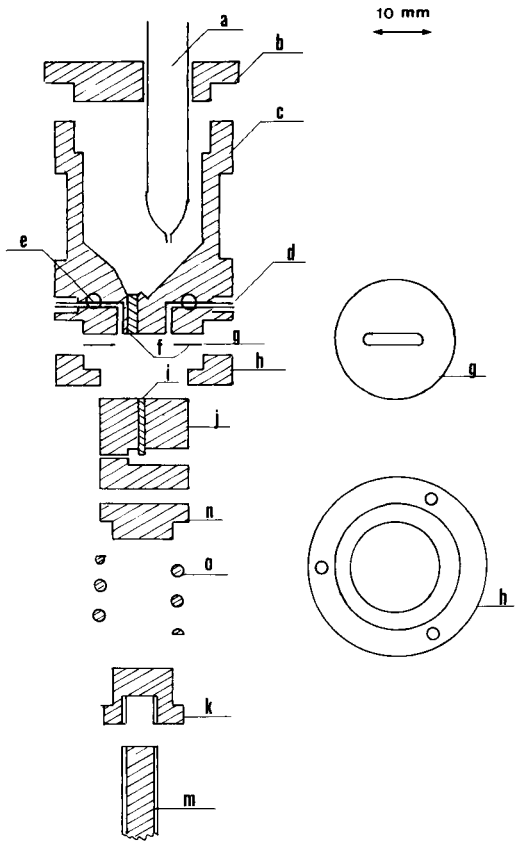

Fig. 1. Flow cell assembly: (a) calomel reference, (b) reference compartment lid, (c) reference compartment, (d, e) platinum tube flow inlet and outlet, (f) ceramic plug, (g) polyethylene spacer, (h) spacer holder, (i) glassy carbon rod, (j) teflon body, (k, m) titanium holder, (o) spring, and (n) holder top.

The thin-layer flow cell shown schematically in Fig. 1 is a modification of a flow cell used previously for potentiometric stripping analysis [6]. When disassembled, it consists of three parts. The first part is the perspex calomel reference (a) compartment (c), onto which the polyethylene spacer (g) is fixed by means of three titanium screws through the spacer holder (h). The reference compartment is separated from the flow channel of the spacer by means of a 1-mm diameter ceramic plug (f) mounted 3 mm downstream from the centre of the glassy carbon electrode. The inlet and outlet channels of the reference compartment (d, e) are platinum tubes with an inner diameter of 0.4 mm. During electrolysis, the downstream tube acts as counter electrode, and during stripping both tubes are connected to earth in order to protect working and reference electrodes from electrolyte noise. The diameter of the spacer (g) is 10 mm and the length of the flow channel 7 mm. Normally the thickness of the spacer is 0.2 mm and the width of the flow

channel is equal to the diameter of the glassy carbon electrode, i.e., 1, 2 or 3 mm.

The second part of the flow cell is the glassy carbon rod (i), pressure-fitted into a teflon body (j) with a diameter of 10 mm and a height of 15 mm. Electrical connection to the glassy carbon rod (length 10 mm, diameter 1, 2 or 3 mm, Ringsdorff, F.R.G.) is obtained by silver epoxy glue (Allied Products Corp., New Haven, Conn.). The third part of the flow cell is the titanium holder (n, o, k, m). When the teflon-embedded glassy carbon electrode is being fitted onto the spacer through the electrode holder, the 200N spring (o) of the holder makes it possible to adjust for minor geometric imperfections in the teflon body caused by electrode polishing, thus considerably improving non-leakage behaviour.

The flow cell in Fig. 1 can be disassembled and reassembled in less than thirty seconds. The pressure drop when water at 20°C is sucked through the cell at a flow rate of 1 ml min^{-1} is approximately 1.8 kPa for a spacer thickness of 0.2 mm and a flow channel width of 2 mm. When concentrated calcium chloride is sucked through the cell under the same conditions, the pressure drop is approximately 16.2 kPa. The internal potential drop in 0.1 M hydrochloric acid ($i \cong 10\ \mu A$) is approximately 3 mV.

COMPUTER-CONTROLLED EXPERIMENTAL PARAMETERS

Figure 2 shows a block scheme of the flow-system components which are under computer control during operation of the system.

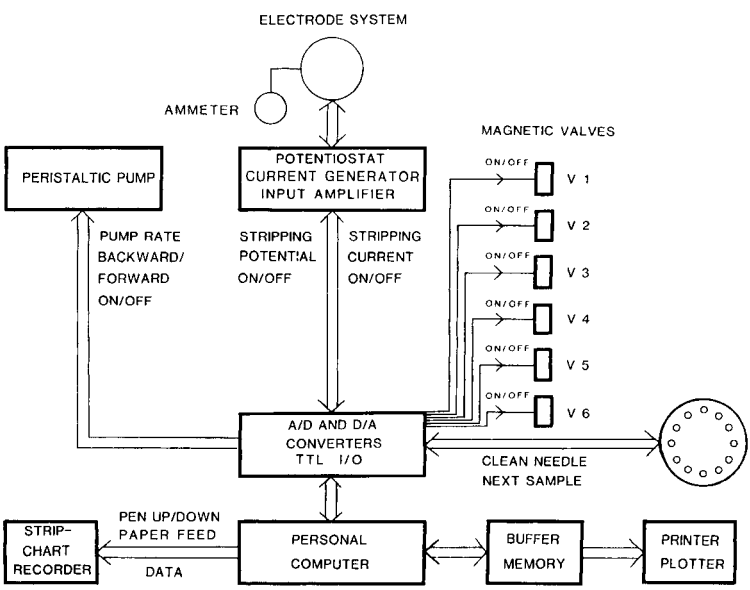

Fig. 2. Computerized system components.

The personal computer (ABC806, Luxor, Motala, Sweden) has a 3-MHz Z80 processor capable of addressing 64 kbyte primary memory, and through software control, a further 512 kbyte by memory bank switching. Programs and data are stored on a double 640-kbyte floppy disc station. The computer is equipped with two 12-bit D/A converters, one 12-bit A/D converter and 16/32 TTL input/output channels (Databoard, Dataindustrier, Stockholm, Sweden). One of the D/A converters is used to control, via the potentiostat, the electrolysis potential in the region −2.047 to +2.048 V with a resolution of 1 mV. The other D/A converter is used for graphical display of experimental results on the strip-chart recorder (Servogor Model 310, BBC Goertz, Vienna, Austria) and for generation of constant reductive or oxidative currents between 0.01 and 20.47 μA with a resolution of 0.01 μA. The TTL output channels are used to control these D/A functions by affecting relays in the potentiostat circuitry.

The TTL output channels also control the rate of the peristaltic pump (Minipuls 2, Gilson) at seven equidistant levels as well as pump on/off and pump direction. By varying the inner diameter of the peristaltic pump tube, flow rates in the region 0.01—4 ml min^{-1} can be achieved. The TTL channels are also used for opening and closing of the six inlet valves (Angar Scientific Model 190, Cedar Knolls, N.J.) in random choice order and for controlling the autosampler (Hook and Tucker Model A40, New Addington, England) which can accommodate 40 or 20 samples with maximum volumes of 7 or 20 ml, respectively.

Stripping curves can be illustrated graphically either on the strip-chart recorder or on a printer/plotter (ThinkJet, Hewlett-Packard). The latter is also used for digital presentation of results. All data for the printer/plotter are transferred via a 128-kbyte buffer memory (Spriinter, Mutek, Quarry Hill, England), making it possible to display the digital and graphical results of one electrolysis/stripping cycle while the computer is in command of the next cycle.

The ammeter shown in Fig. 2, which has a user-selectable range of ±10 or ±100 μA, is used solely for diagnostic purposes, and is not interfaced with the computer.

PROGRAMMING

The most important parts of the computer program for automated potentiometric stripping analysis are those which are concerned with real-time data acquisition, digital filtration and peak searching and peak integration. Other important aspects are editing of the user-defined programs, displays of the status of the computer-controlled instrumental parameters during execution, and finally evaluation of the results by means of standard additions or calibration curves.

Example of programming

A normal cycle in flow potentiometric stripping analysis consists of mercury pre-plating of the working electrode, electrolysis in the sample, recording of the stripping and background curves in a suitable medium and finally cleaning of the electrodes and simultaneous evaluation of results. Thus, in order to simplify programming of the automated system, the control program is divided into 10 subprograms numbered 0—9. These programs may be used individually, in "subroutine calls" or chained with "jump" commands. An example is given in Table 1, the composition of the six different solutions used in inlet valves V1—V6 being specified in Table 2. In this example, program no. 0 is used as main program, program no. 1 controls mercury pre-plating, program no. 2 sample introduction and electrolysis, program no. 4 recording of stripping and background curves and graphical display on printer/plotter and strip-chart recorder, and program no. 5 integration of the stripping peaks.

Figure 3A shows dt/dE vs. E representations of the sample curve and the background-corrected curve as obtained on the strip-chart recorder; Fig. 3B shows the same results as obtained on the printer/plotter. Because the results were obtained after electrolysis for 30 s in a sample containing 10 $\mu g\ l^{-1}$ each of Cd(II) and Pb(II), they can be directly compared with the corresponding results obtained by square-wave voltammetry in non-deoxygenated solutions [8].

Real-time data acquisition

Figure 4 illustrates the importance of the data-acquisition rate in potentiometric stripping analysis. Figure 4(a) shows the sample and background-

TABLE 1

User-defined program used in the example given

Instruction	Time	Comment
Program no. 0		
H 25600	0	Set measurement frequency to 25600 Hz.
F 15, 15	0	Set averaging filter to 15 mV and Savitzky-Golay filter to 15 mV.
T −100	0	Stop registration of stripping transient at $E = -100$ mV.
R −150	0	Reset electrolysis potential at −150 mV immediately after potential T (−100 mV) is reached.
U −520	0	Upper potential limit for graphical display set to −520 mV.
L −900	0	Lower potential limit for graphical display set to −900 mV.
C 1, 1	0	Call program no. 1 (mercury pre-plating) once.
C 2, 1	30	Call program no. 2 (sample introduction) once. Wait 30 s.
C 4, 1	0	Call program no. 4 (measurements and result display) once.
V 4	0	Open valve 4 (rinsing solution), close previously opened valves.
P +1	0	Set pump rate at 1 in forward direction.
Program no. 1		
V 1	0	Open valve 1 (acidic ethanol), close previously opened valves.

TABLE 1 (continued)

Instruction	Time	Comment
P +3	5	Set pump rate at 3 in forward direction. Wait 5 s.
V 3	5	Open valve 3 (plating solution), close previous valve. Wait 5 s.
E -600	2	Apply electrolysis potential of −600 mV for 2 s.
E off	4	Disconnect potential for 4 s.
E −800	2	Apply a potential of −800 mV for 2 s.
E off	4	Disconnect potential for 4 s.
E −1000	30	Apply a potential of −1000 mV for 30 s.
E −50	2	Apply a potential of −50 mV for 2 s.
Program no. 2		
P +5	1	Set pump rate at 5 in forward direction. Wait 1 s.
V 2	0	Open valve 2 ("sample" solution), close previous valve.
E −1000	0	Apply a potential of −1000 mV (wait 30 s according to C 2, 1 in program no. 0).
Program no. 4		
P +1	5	Set pump rate at 1 in forward direction. Wait 5 s.
V 5	30	Open valve 5 (stripping solution), close previous valve. Wait 30 s.
M sample	2	Measure sample stripping curve. Wait 2 s at reset potential −150 mV (c.f. R −150 in program no. 0).
E −1000	2	Set potential at −1000 mV. Wait 2 s.
M backgr	0	Measure background stripping curve.
E −200	0	As above.
P +3	0	As above.
V 4	0	As above.
G +2	0	Set graphical output gain to +2 (arbitrary scale).
d sample	0	Display dt/dE vs. E result for sample data on printer/plotter.
d corr	0	Display dt/dE vs. E result for sample-background data on printer/plotter.
D sample	0	Display dt/dE vs. E result for sample data on strip-chart recorder.
D corr	0	Display dt/dE vs. E result for sample-background data on strip-chart recorder.
J 5	0	Jump to program no. 5.
Program no. 5		
l Cd	0	Label to be used in digital display.
s 0	0	Set standard/standard addition concentration to 0.
v 0	0	Set volume correction value to 0%.
S 60	0	Set integration peak-search width to 60 mV.
B 120	0	Set baseline width for baseline-fit algorithm to 120 mV.
W 120	0	Set peak width for integration to 120 mV.
X yes	0	Activate baseline-fit algorithm.
Y yes	0	Activate background subtraction before integration.
I −760	0	Integrate peak at −760 mV (±search width of 60 mV).
Y no	0	Deactivate background subtraction before integration.
I −760	0	As above.
X no	0	Deactivate baseline-fit algorithm.
Y yes	0	As above.
I −760	0	As above.
N	0	Perform form feed on printer/plotter.

TABLE 2

Composition of solutions used in the example given

Valve	Solution composition	Comment
1	Ethanol, 95% (v/v) in 0.1 M HCl	Rinsing solution for removal of microbubbles
2	10 $\mu g\ l^{-1}$ Cd(II) and Pb(II)	"Sample" in 0.25 M $CaCl_2$/0.1 M HCl
3	50 mg l^{-1} Hg(II) in 3.5 M $CaCl_2$	Mercury pre-plating solution
4	0.5 M HCl	Rinsing solution
5	10 mg l^{-1} Hg(II) in 5 M $CaCl_2$	Stripping solution
6	Not used	Normally used for sample with standard additions

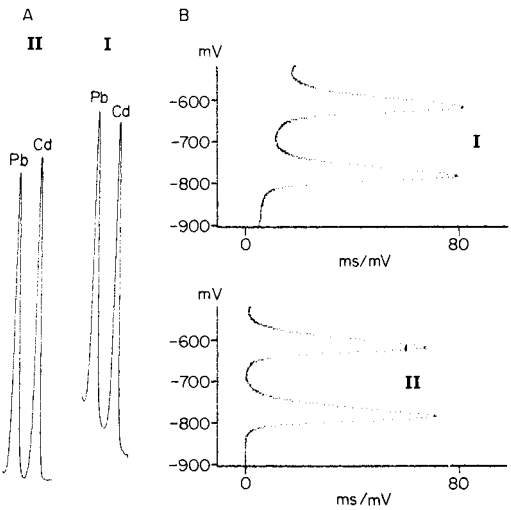

Fig. 3. Displays of the potential region −900 to −520 mV vs. SCE for 10 $\mu g\ l^{-1}$ each of Cd(II) and Pb(II) with a sample electrolysis time of 30 s: (I) sample data; (II) background-corrected data. (A) Strip-chart recorder; (B) printer/plotter display. Experimental parameters as in Tables 1 and 2.

corrected dt/dE vs. E curves obtained on the strip-chart recorder with the same experimental conditions as in Table 1, except that the curves are displayed with the output gain equal to −2, i.e. one fourth of that in Fig. 3. Figure 4(b) shows the result of the same experiment when the measurement frequency was decreased from 25.6 kHz to 0.1 kHz and the output gain increased accordingly from −2 to 128. The increase in the "digital noise" level produced by the decrease in sampling rate is very obvious.

The conversion time of the A/D converter used is approximately 30 μs, i.e., the maximum sampling rate is equal to 33 kHz. During data acquisition the program must, however, also check if the threshold potential value (T in Table 1) has been reached, and also allocate the measured potential value to

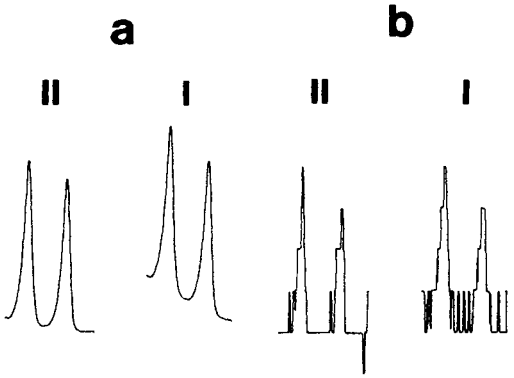

Fig. 4. Effects of data-acquisition rate on experimental results: (a) 25.6 kHz and (b) 0.1 kHz, under same conditions as in Fig. 3. (I) Sample data; (II) background-corrected data.

a relevant memory address. Although most of this is done during the conversion phase of the A/D converter, the maximum sampling rate attained is 25.6 kHz. With the memory space available for primary data, 512 kbyte, this sampling rate allows continuous data acquisition for 5.12 s for each of the sample and background curves. By decreasing the sampling rate, the programmable rates being 50—25600 Hz, the sampling time can be increased proportionally. This sampling method, with no real-time data reduction, allows the primary stripping curve to be "replayed" on a strip-chart recorder after sampling, and furthermore allows a detailed evaluation of primary data and the use of different data reduction and digital filtering methods on the same data set. With an alternative sampling algorithm, including real-time data reduction producing a dt/dE vs. E projection of the stripping curve [4], the same sampling rates can be used for an almost infinite time. This alternative procedure does, however, set obvious limitations on post-sampling manipulations of data.

Data reduction and digital filtering

A simple "multichannel" algorithm is used to produce a dt/dE vs. E representation of the primary stripping curve (E vs. time) data, which can be comprised of up to 256 kwords with the memory space available. As the A/D converter input is dimensioned to potentials in the −2.047 to +2.048 V range, and a 12-bit resolution is used, this results in a set of 4096 counters, one for each 1-mV level. Optional background subtraction is also included in this step. Though not implemented, this algorithm could also include a digital filter reducing, e.g., line noise frequencies, which, because of the relatively time-consuming calculations required, is not suitable for implementation in real-time data acquisition in this system.

The dt/dE representation of the stripping curve may be filtered in two ways. First, a non-weighted averaging filter can be used. Secondly, a quadratic/

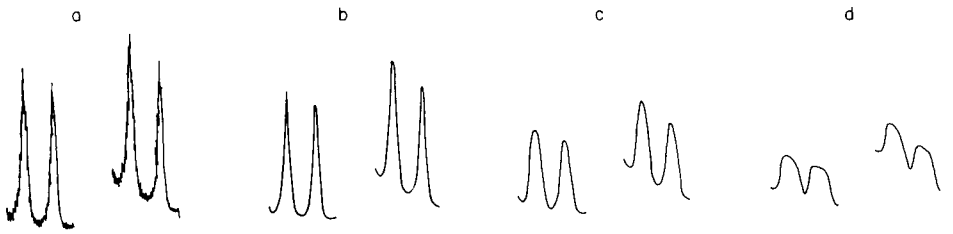

Fig. 5. Effects of averaging filter: (a) unfiltered data; (b) 15-mV filter; (c) 60-mV filter; (d) 120-mV filter. Data were the same as in Fig. 4(a). No Savitzky-Golay filter was used.

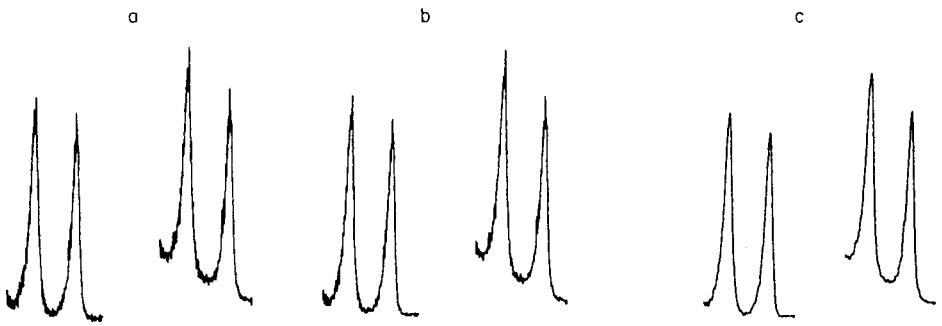

Fig. 6. Effects of Savitzky-Golay filter: (a) unfiltered data; (b) 5-mV filter width; (c) 15-mV filter width. Data were the same as in Figs. 4(a) and 5. No averaging filter was used.

cubic Savitzky-Golay filter [9] can be applied. The two filters, which both can be of random-choice width, can be combined (cf. F in Table 1). Figures 5 and 6 show the effects of these filters on the same set of experimental data. With the 1-mV resolution used, Savitzky-Golay filters in the 5—25 mV range do not cause adverse effects on data, provided that a sufficient amount of primary data are treated. For low-density data, the averaging filter must be used to produce a data set with acceptable digital noise levels. As is obvious in Fig. 5, large averaging filters cause excessive broadening and distortions, in the extreme leading to overlap of elemental peaks or annihilation of useful data. This further stresses the need of high data acquisition rates, as is demonstrated in Fig. 4.

Peak searching and integration

Integration can be applied directly to the sample data or after background correction. After parameters defining the peak-searching and integration algorithms have been set, a command stating the approximate peak potential prompts integration (cf. Table 1).

First, the primary data are derived and filtered as described above. Secondly, the peak is sought in the proximity of the stated potential. Two different algorithms can be used in the peak-searching step. Most simply, the maximum dt/dE value is sought around the stated potential within the

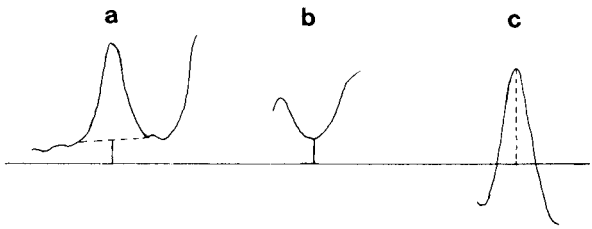

Fig. 7. Schematic description of calculated baseline-fit algorithm: (a) primary dt/dE data, (b) baseline values calculated from (a), and (c) result of subtraction of (b) from (a), which is used for peak maximum detection.

stated search width (S in Table 1), and the position of this value defines the peak potential. The alternative algorithm involves the subtraction of a linear baseline calculated from the dt/dE data prior to the determination of the highest dt/dE value, as described in Fig. 7. This mode of subtracting a calculated baseline allows peak maxima on steep background slopes to be identified correctly. The width of the calculated baseline is user-defined (B in Table 1).

Thirdly, the peak area is calculated for the peak at the potential determined as above, using a user-defined peak width (W in Table 1). The area counts calculated are then corrected by subtracting baseline offset values as defined by the dt/dE values at the peak end-points, i.e., at potentials corresponding to the peak potential $\pm W/2$ (see Table 1). Each integration report gives the individual values for both peak halves, as well as the summed peak-area count, allowing a check on peak symmetry, or the use of only one peak half value in further calculations. For each integration done, a graphical display of dt/dE vs. E and peak limits accompanied by numerical data and pertinent system parameters is given on the printer/plotter. Figure 8 shows the result of different peak-searching and integration algorithms on the same set of primary data.

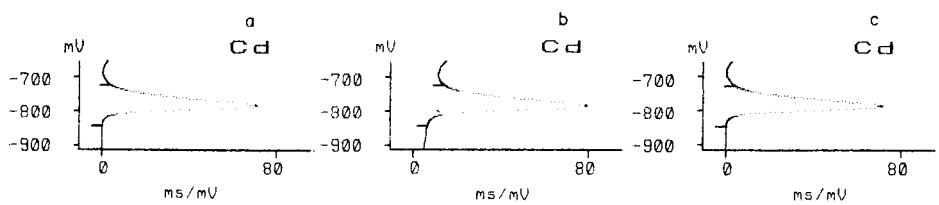

Fig. 8. Results from peak-search and integration algorithms on the Cd(II) peak from the same data as in Fig. 4(a): (a) with background correction and baseline fit; (b) with baseline fit only; (c) with background correction only. Peak areas: (a) 2.348 s; (b) 2.325 s; (c) 2.328 s.

Procedures for standard additions and calibration curves

The numerical data generated by the integration routines are stored internally in the computer memory, together with peak potentials, sample identity number, labels, standard concentration and volume-correction data. Values of standard concentrations, as well as sample volume errors to correct for standard additions made, can be included in the user-defined programs. A command prompting the execution of any of a number of BASIC programs loaded from the floppy-disc station transfers these data to a set of arrays allowing random use. As any BASIC program may be implemented, calculations for standard addition and calibration curve can be performed after each sample analysis, or batchwise after the completion of a number of analysis cycles, or both. BASIC programs can also be used to implement other evaluation methods, as well as system routines, such as statistics, result filing and network communication.

Program commands and parameters not illustrated in Table 1

All commands and system parameters may be performed or set, respectively, either in a direct command mode, or in user-defined programs. Apart from the commands and parameters illustrated in the example in Table 1, various other functions are implemented in the system. These include commands to output the primary data signal, i.e., E vs. time, on the strip-chart recorder, oxidative or reductive constant-current generation during stripping, and subdivision of computer memory to allow multiple scans to be performed. Commands for the simultaneous opening and closing of more than one valve in the flow system, for autosampler control, as well as for printer/plotter and strip-chart recorder control, e.g., form feeds and paper feed and pen control, are also included.

Program control and editing

The user-defined programs, as exemplified in Table 1, consist of ten individual programs of up to 24 lines each. For each line, one command or parameter definition can be entered, as well as a time-delay value in the range 0 s to 10 h, to be performed after the command execution (cf. Table 1).

Each program can be run or repeated a number of times at random choice. As each program can jump to or call any other program, all programs can be accessed in random-choice order. During the run of an analytical cycle, the computer CRT displays the program currently being executed with a cursor tracer on current line. Time delays under execution are also traced with a count-up clock. The computer CRT is also used to give a real-time trace of pertinent system parameters, such as electrolysis potential, valves currently open, and pump flow rate, as these are being altered during execution.

User programs are easily entered and altered from the computer keyboard by using a screen-oriented editor which includes commands for insertion, deletion and copying. For each entry made, an automatic syntax check is performed, ensuring that non-allowed commands are excluded. User programs

can be saved to and loaded from the floppy-disc station and listed on the printer/plotter.

DISCUSSION

Deoxygenation of solutions is time-consuming, vulnerable to contamination and difficult to automate. Thus the possibility inherent in potentiometric and constant-current stripping analysis of operating in oxygen-containing solutions is the basis for the successful automation of these techniques. Although not yet fully proven, preliminary experiments strongly suggest that all analytical techniques based on anodic or cathodic stripping voltammetry can also be implemented on the automated system for flow potentiometric and constant-current stripping analysis. Normally, this results in a considerable decrease in the time needed for the analysis and simultaneous improvement in detection limits. Moreover, potentiometric stripping analysis is capable of analyzing complicated matrices such as acid-diluted whole blood [10], so that it seems justified to claim that the automated system not only simplifies, but also widens, the applicability of electrochemical stripping techniques. Automated generation of pseudo-polarograms, i.e., plots of analytical signal vs. electrolysis potential, and the determination of the complexing capacity of natural water are easily implemented with the system.

So far, the automated system for stripping analysis has been used only in a university research environment. Thus its possible use in routine analysis still has to be evaluated. In laboratories specializing in clinical, food or environmental analysis, for example, several trace element determinations can be done by means of stripping analysis. Frequently, the only sample pretreatment needed is dilution with a suitable matrix modifier. Under such circumstances, the only manual (or separately automated) operation necessary would be the dilution of a sample aliquot with the matrix modifier and another sample aliquot with the matrix modifier containing a standard addition of suitable magnitude. After these solutions have been placed in two different flow inlets of the analyzer and the relevant analytical procedure has been entered from floppy discs, the rest of the analysis is performed automatically. This includes suction of samples and reagents to the solution entry point, formation of the mercury film, electrolysis/stripping cycles in the two samples any pre-chosen number of times, and generation of the results report. If more than two electrolysis/stripping cycles have been performed for the two samples, the relevant standard deviations can also be reported. Finally, the analytical procedure includes closing down of the system by back-flushing (e.g., with water through the inlet valves) to avoid formation of salt deposits if the analyzer is not to be used for some days. Thus, the analyzer is likely to save time not only when several samples are to be processed using an autosampler, but also, and probably even to a greater extent, when only very few samples are to be analyzed.

REFERENCES

1 D. Jagner and K. Årén, Anal. Chim. Acta, 100 (1978) 375.
2 D. Jagner, Analyst, 107 (1982) 593.
3 T. Anfält and M. Strandberg, Anal. Chim. Acta, 103 (1978) 379.
4 A. Granéli, D. Jagner and M. Josefsson, Anal. Chem., 52 (1980) 2220.
5 J. Mortensson, E. Quizel, H. J. Skov and L. Kryger, Anal. Chim. Acta, 112 (1979) 297.
6 L. Andersson, D. Jagner and M. Josefsson, Anal. Chem., 54 (1982) 1371.
7 H. Eskilsson, D. Jagner and C. Haraldsson, Anal. Chim. Acta, 175 (1985) 79.
8 M. Wojciechowski, W. Go and J. Osteryoung, Anal. Chem., 57 (1985) 155.
9 A. Savitzky and M. J. E. Golay, Anal. Chem., 36 (1964) 1627.
10 D. Jagner, M. Josefsson, S. Westerlund and K. Årén, Anal. Chem., 53 (1981) 1406.

Analytica Chimica Acta, 188 (1986) 151—164
Elsevier Science Publishers B.V., Amsterdam — Printed in The Netherlands

THE FLUORIDE ION-SELECTIVE ELECTRODE IN FLOW INJECTION ANALYSIS
Part 3. Applications

WOLFGANG FRENZEL* and PETER BRÄTTER

Spurenelemente in Gesundheit und Ernährung, Hahn-Meitner-Institut für Kernforschung, Glienickerstr. 100, D-1000 Berlin 39 (F.R.G.)

(Received 2nd June 1986)

SUMMARY

Flow-injection potentiometry with a combination fluoride-selective electrode is used to determine fluoride in tap water, beverages and urine. Excellent sensitivity (down to 1 $\mu g\ l^{-1}$) and long-term stability are obtained, with a sample throughput of 30—40 h^{-1}, based on triplicate injections at 120 h^{-1}. The commonly used buffer TISAB-III is unsuitable for the analysis of undiluted tea and urine samples. The application of a modified citrate-containing TISAB overcomes interferences caused by high natural ionic strength and avoids complexation of fluoride. Recoveries after spiking tap water, tea and urine with fluoride concentrations ranging from 0.01 to 1 mg l^{-1} are in the range 91—106%. The equipment used provides a flexible system allowing fast changes between different buffers and carrier streams depending on the samples presented.

The importance of fluoride determinations can be realized by considering the various materials which contain fluorine compounds and the processes in which fluoride or fluorine plays a role. There are abundant applications in environmental and industrial monitoring and in the fields of geological and biomedical research [1—3]. Studies of the biomedical aspects of fluoride require analyses of water and foodstuffs as well as body fluids (urine and blood) and tissues (e.g., bone, teeth) to provide information about the ingestion and excretion of fluoride. Thus, many materials with substantially different composition have to be analyzed; the most commonly applied methods of determination are titrimetry, spectrophotometry, neutron activation, and potentiometry with the fluoride-selective electrode [4—7].

Direct potentiometry with the lanthanum fluoride single-crystal electrode is one of the most suitable approaches for determinations of fluoride in biological and environmental samples because it offers excellent selectivity and sensitivity, and is cheap and simple to use [8—13]. The method is also suitable for automation and high sample throughput when used in batch or flow analyzers [14—18]. Of course, the fluoride-selective electrode is sensitive only to free fluoride, so that determinations of total fluorine require previous treatment (e.g., digestion, extraction, decomplexation) [9, 13, 19—22]. For samples in which soluble inorganic fluoride is the only form of fluorine

0003-2670/86/$03.50

present, the addition of a TISAB solution is sufficient to release fluoride completely [8, 10, 23–25]; the activity measured in such samples can be related directly to the fluoride content.

In two previous papers [26] the incorporation of the fluoride electrode in a flow-injection system was reported. Procedural aspects were discussed and interference problems were investigated in detail. Flow-injection methods based on the fluoride electrode have been described earlier [27–30] but few of these papers were concerned with the analysis of real samples. In the present paper, the optimal conditions for the determination of fluoride in tap water, beverages and urine are outlined. Emphasis is laid on the requirement for particular TISAB solutions to obtain accurate results at low fluoride levels. General aspects concerning sample frequency, carry-over, and long-term stability of the flow-injection method are discussed.

EXPERIMENTAL

Apparatus and equipment

The instrumentation used was described in the previous parts of this series [26]. In the present work, the wall-jet flow cell was always used with a distance of 0.5 mm between the inlet nozzle and sensing membrane. The injection volume was set to approximately 125 μl by choosing a suitable loop. Flow rates in the 0.5–1.5 ml min^{-1} range were adjusted by varying the height of the carrier bottle and were calibrated volumetrically. The switching valve (see Part 2) was retained to allow variation of the carrier solution without changing the carrier reservoir. Thus, different procedures can be run after renewed calibration with minimal delay. Polyethylene containers were used throughout for sampling and storage. Samples were handled by using pipettes with disposable tips (Eppendorf, Finnpipet). All plasticware was precleaned with nitric acid (1 + 1) and rinsed with high-purity water (deionized and twice-distilled).

Chemicals and solutions

Fluoride standards were prepared daily by serial dilution of a 1 g l^{-1} stock (Merck Titrisol) with twice-distilled water. TISAB-III (Cat. 94-09-11, Orion Research) was used as recommended by the maker. Two modified TISAB solutions were prepared as previously described [26] and as recommended by Tušl [31], respectively. The latter contained 1 mol of trisodium citrate and 28 ml of concentrated perchloric acid (67%) per litre. The TISAB solutions were mixed with standard and sample solutions at various ratios between 1:1 and 1:10 before injection. The salts used were of highest available purity. Sodium hydroxide was of analytical-grade quality; the nitric and hydrochloric acids were of high purity (Merck, Suprapur).

Sample collection, storage and preparation

The tap-water samples were collected at various private Berlin houses after the 50-ml polyethylene bottles had been flushed thoroughly with the water.

Up to 10 ml of the fruit juices, soft drinks and wines were transferred directly from the bottles or cans by means of a pipette into 10-ml polyethylene containers. The tea samples were prepared as follows: 5 g of loose tea or one tea bag (1.5—3 g of tea) was placed into a 100-ml Eppendorf flask and infused with 50 ml of boiled tap water; the flasks were shaken occasionally during the first 1—2 min, the tea leaves were then allowed to settle and, after exactly 5 min, 10 ml was transferred by pipette to a polyethylene bottle. Urine samples were collected at random from male adults in 100-ml polyethylene bottles. In some instances, morning and evening urine from the same person was taken and analyzed separately.

The water and beverage samples were measured within 6 h after collection. Urine samples were usually measured within 24 h after collection. Meanwhile they were kept in the refrigerator.

Generally, 1-ml portions of the fluoride standards and sample solutions were pipetted into 2-ml polyethylene tubes fitted with caps, 100 μl of the selected TISAB was added and the mixture was vigorously shaken. To account for the slow reaction between interfering elements such as calcium and aluminium and the masking agent [24, 32, 33], samples were injected not less than 10 min after mixing. When the citrate-containing TISAB was used, up to 1 ml was sometimes added to the samples. Diluted samples were prepared by pipetting appropriate portions of the sample and twice-distilled water into the tube to obtain a final volume of 1 ml. In the recovery and standard-addition experiments, the samples were spiked with various volumes of fluoride standards. If necessary, volume corrections were considered in calculating the fluoride content of the samples.

Procedure

The carrier solution was prepared by mixing the desired TISAB with twice-distilled water. Fluoride was added to give a final concentration between 50—500 $\mu g\ l^{-1}$ depending on the measuring range [26]. After thorough deaeration, this solution was propelled through the system until a stable baseline (±0.05 mV) was obtained. Standards and samples were prepared for particular measurements by using the same TISAB composition and concentration as that of the carrier, to prevent liquid-junction potential problems [34] and ionic strength effects [26]. At the beginning of a measuring period, a test run was made by successive injections of some standard solutions to ensure proper functioning of the system. Subsequently, calibration standards covering the required working range were injected threefold followed by the injection of the particular samples. Frequent recalibration was done to check the stability of the system. The recorder sensitivity was set between 20 and 200 mV full-scale, depending on the maximum height of the signal expected and the precision required.

RESULTS AND DISCUSSION

Carry-over studies and sampling frequency

In continuous flow systems (AutoAnalyzer principle), interaction between successive samples (carry-over) is a serious problem and has to be studied for each particular procedure. In flow injection analysis, the entire residence time of a sample in the system is usually of the order of a few seconds so that a further injection is not made before the preceding sample has been completely washed out. Consequently, carry-over effects are not normally observed in flow-injection methods. However, precautions are necessary not to contaminate the samples within the injection port. Therefore, the sample loop of the injection valve must be carefully rinsed with twice-distilled water or sample solution prior to injections. Figure 1 shows the recorder trace obtained for alternate injections of two standards containing 10 μg l^{-1} and 1 mg l^{-1} fluoride, respectively; the carrier fluoride concentration was 100 μg l^{-1}. Carry-over and contamination problems are not evident.

The sampling frequency in flow systems is often evaluated theoretically on the basis of half-wash times, dispersion and other characteristics of the signal [35, 36]. A more practical approach which considers that only one sample is processed in the flow system at a time, yields a sampling frequency

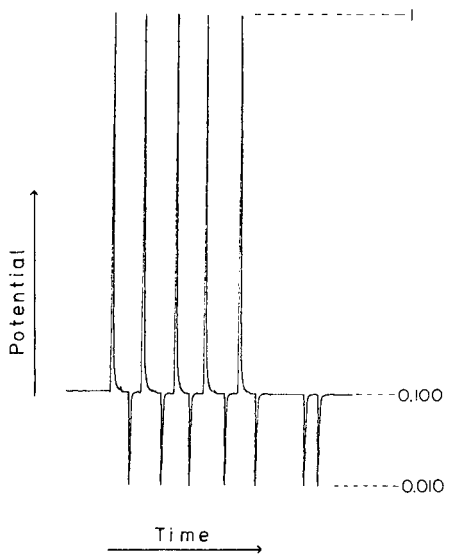

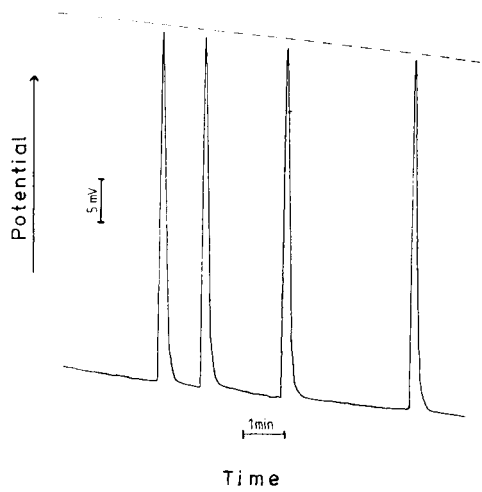

Fig. 1. Carry-over experiment. Standards containing 1 mg l^{-1} and 10 μg l^{-1} fluoride were injected alternately into a carrier containing 100 μg l^{-1} fluoride. Flow rate 0.75 ml min^{-1}, injection volume 125 μl. The numbers are the fluoride levels in mg l^{-1}.

Fig. 2. Electrode drift and potential reading in flow-injection potentiometry. Fluoride standards (500 μg l^{-1}) were injected over about 15 min. Carrier fluoride level, 100 μg l^{-1}. For emphasis, a line is drawn parallel to the sloping baseline.

which is governed by the overall residence time of the sample. This time depends mainly on the flow rate, the injection volume and the response time of the particular electrode. Given that two injections of each sample seem adequate and that some time is needed for calibration and recalibration, a distinction has to be made between injection frequency and sample throughput. The experimental set-up used here allows an injection frequency of about 120 h^{-1} which corresponds to a sample throughput of 30—40 h^{-1}.

Long-term stability

Electrode drift and changes of the response time of the ion-selective electrode are difficulties often encountered in potentiometric flow-through measurements. Drift can usually be attributed to slow changes in liquid-junction potential and alteration of the reference electrode system as a result of temperature gradients [34]. In flow-injection potentiometry such problems, though they exist, are negligible. The fast intermittent reading of the signal and the baseline easily allows for correction of parallel drift as is demonstrated in Fig. 2. The absolute peak potential is changed by about 3 mV in 15 min whereas the deviation of the potential difference (peak height) is less than ±0.05 mV. Variations of response time over a period of time, however, would be serious in flow-injection potentiometry because the potential differences (i.e., the slope of the calibration plot) are changed.

Recalibration after several hours and even after an overnight shut-down usually gave reproducible results within 2% standard deviation. Nevertheless, frequent recalibration was made to guarantee reliability; given the high injection frequency, this is entirely acceptable. Over time spans of several days or weeks, the slope of the calibration plot decreased. This is obviously due to slowly changed surface conditions at the electrode membrane. After repolishing of the electrode [26, 29], the initial slope was retained.

Analysis of tap water

In view of the public legislation for surveillance of tap water and the fluoridation of potable water in several countries, the monitoring of fluoride is of considerable importance. The potentiometric approach is well accepted and applied in batch and flow-through systems [8, 37—39]. In applying the flow-injection method, a TISAB-III solution (1:10 dilution) containing 100 $\mu g\ l^{-1}$ fluoride was used as the carrier. Samples and standards were also mixed with TISAB-III (see above). Figure 3(a) shows the recorder trace for the calibration followed by a set of 15 samples and recalibration. The last of the samples (15) was freshly collected snow after snow had fallen for 5 days; the level was below 100 $\mu g\ l^{-1}$ and so was not estimated. The calibration plot which was used for graphical evaluation is presented in Fig. 3(b). The corresponding fluoride contents of the samples are given in Fig. 3(a) above the signals.

The reproducibility of the method was tested by tenfold injection of two samples of tap water (Nos. 7 and 11). The average peak heights measured

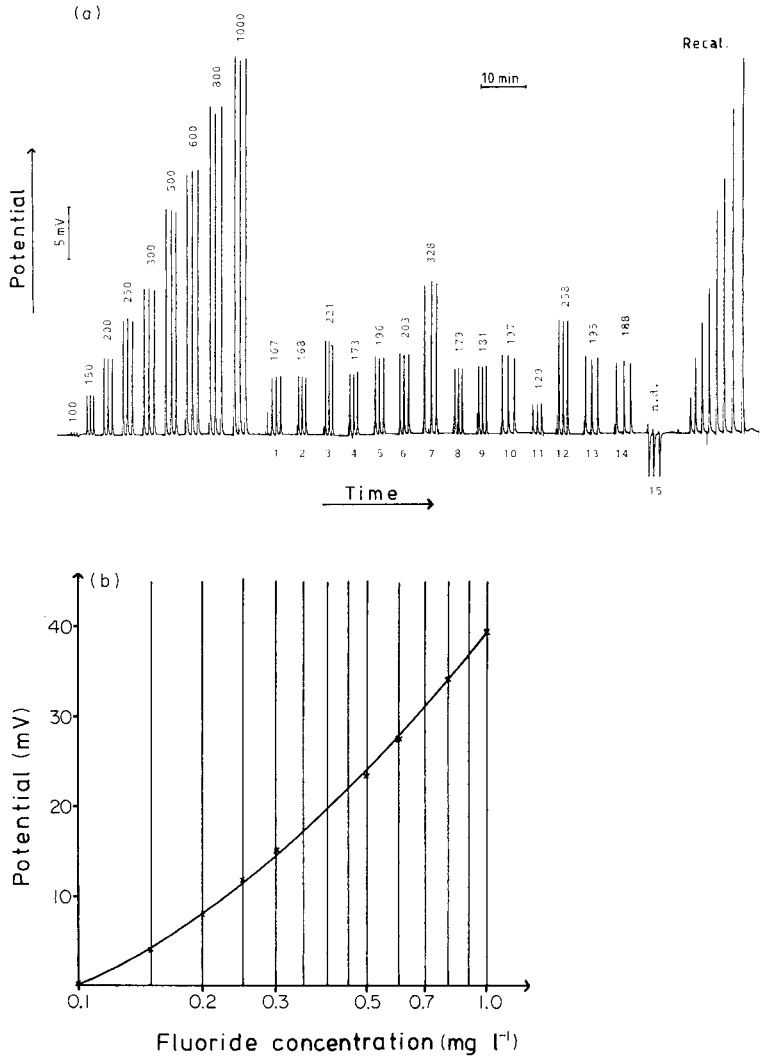

Fig. 3. (a) Recording obtained in the calibration and determination of fluoride in tap water; carrier fluoride level 100 μg l^{-1}. (b) Calibration plot based on the data of Fig. 3(a).

were 15.72 mV and 3.10 mV with a standard deviation of 0.19 (1.2%) and 0.08 (2.6%), respectively. As graphical curve-fitting such as was done in this work is to some extent subjective, calculation of the corresponding concentrations could be prone to relatively large errors. For the two samples, the fluoride contents were found to be 328 μg l^{-1} and 129 μg l^{-1} with relative errors of 3.5% and 4.6%, respectively. Better precision would, of course, be obtained by standardization in narrower steps and by using better resolution on the chart recorder. Computer calculation would eliminate the problem of subjective judgement but might not improve the precision of the method.

TABLE 1

Recovery experiment with spiked tap-water. (Samples were mixed with TISAB-III in a 10:1 ratio. For experimental conditions, see text)

Sample	Fluoride ($\mu g\ l^{-1}$)		Recovery (%)	Sample	Fluoride ($\mu g\ l^{-1}$)		Recovery (%)
	Added	Found			Added	Found	
1	—	168	—	8	—	180	—
	50	208	95.4		50	232	100.8
	100	263	98.9		100	275	98.2
	200	352	95.6		500	711	104.6
	500	680	101.8		1000	1196	101.4
	1000	1180	101.0				
2	—	170	—	11	—	129	—
	20	195	102.6		10	141	101.4
	40	212	100.2		20	148	99.3
	60	228	99.1		50	176	98.3
	100	265	98.2				
	200	378	102.2				
6	—	203	—	16	—	161	—
	10	217	101.9		50	206	97.6
	20	225	100.9		100	260	99.6
	50	249	98.4		200	357	98.9

To investigate the reliability of the method, a series of recovery experiments was made. Spiked tap-water samples were analyzed, with the results presented in Table 1. The recovery is in the range 95—105% which makes the method suitable for the fast sequential monitoring of tap water and municipal water supplies.

Determination of fluoride in beverages

The same experimental conditions as used for tap waters were tested and found inappropriate because transient phenomena [26] were sometimes observed. Therefore, the modified TISAB-III containing additional sodium nitrate was used. After the samples had been mixed with TISAB, carbon dioxide was occasionally generated because of the acidification to pH 5.2. Such samples could not be measured within the first 15 min after mixing because of poor reproducibility; this was probably due to irregular hydrodynamic conditions which appear when gas bubbles stick to the sensing membrane. A typical recorder trace for the analysis of soft drinks, fruit juices and wines and the corresponding calibration plot are shown in Fig. 4. The calibration is extended to fluoride concentrations below that of the carrier. The reliability was established as was done for the tap waters by recovery experiments and was found to be in the 91—106% range.

Test runs with tea samples gave very high signals indicating fluoride levels above 1 mg l^{-1}. Extended calibration up to 5 mg l^{-1} and the signals obtained

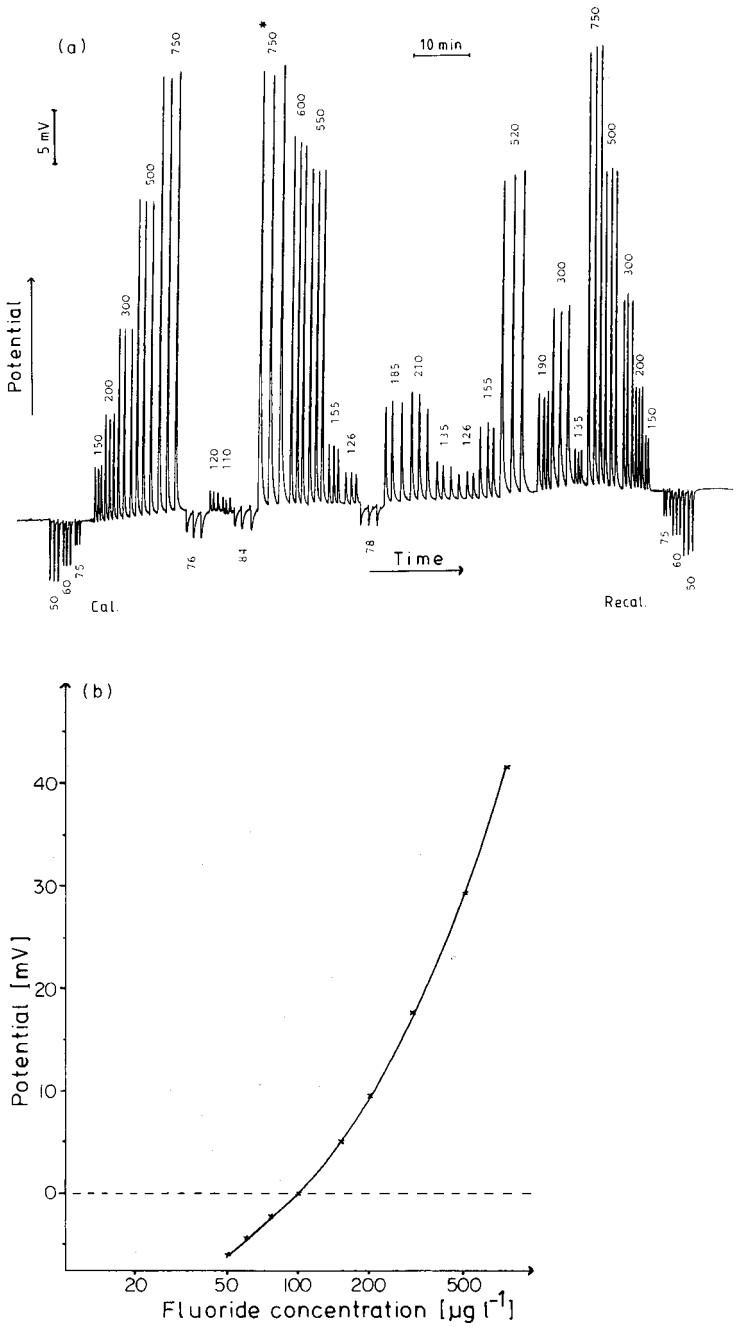

Fig. 4. (a) Recorder trace in the analysis of beverages; carrier fluoride level 100 $\mu g\ l^{-1}$, injection volume 125 μl, flow rate 0.7 ml min^{-1}; calculated fluoride contents ($\mu g\ l^{-1}$) are given above the signals. After the calibration (50—750 $\mu g\ l^{-1}$ fluoride), 4 samples of red wines, 4 samples of white wines, 4 soft drinks, and 6 fruit juices were injected in triplicate; the asterisk indicates a repeat injection of the 750 $\mu g\ l^{-1}$ standard. (b) Calibration plot based on the data of Fig. 4(a).

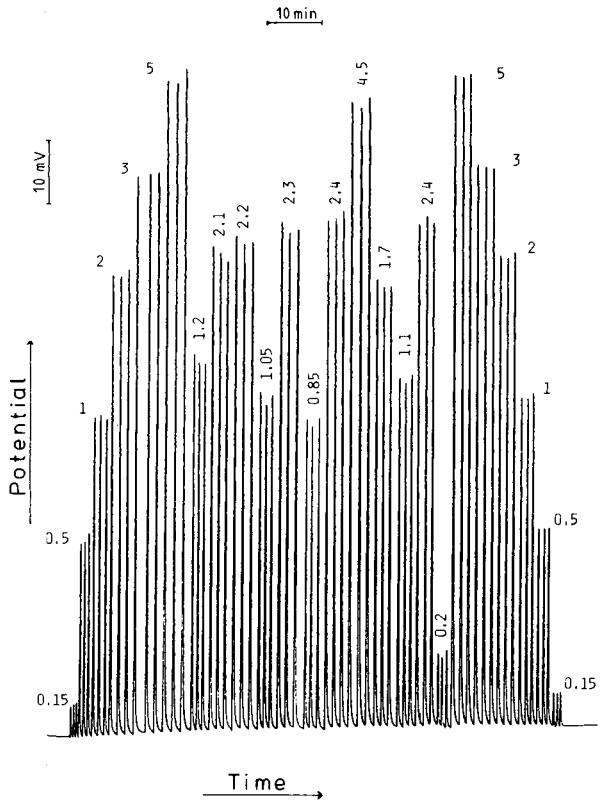

Fig. 5. Extended calibration and analysis of 11 undiluted tea samples using TISAB-III. Calculated concentrations in mg l^{-1} are given above the signals. The last sample (0.2 mg l^{-1}) is the boiled tap water which was used for preparation of the teas.

for the tea samples are shown in Fig. 5. The effect of interferents was evaluated by defined dilution of the samples because it is assumed that possible interferences become negligible when the absolute amount of the interferent decreases. Recovery experiments were done by adding fluoride to the diluted tea samples. The results are summarized in Tables 2 and 3; the values given are corrected for the respective dilutions. Significantly lower fluoride contents were found in some of the undiluted samples when TISAB-III was used; this is presumably caused by incomplete masking of complex-forming elements (e.g., Al) or ionic strength effects [26]. This assumption was sustained by measurements done with the modified TISAB or the citrate buffer; the latter offers both increased ionic strength and better masking ability [31]. In Table 3, the results obtained for the direct injection of the undiluted and diluted tea samples are compared for the three TISAB solutions.

Analysis of urine

The application of direct potentiometry to estimate urinary fluoride concentrations has been investigated by many authors and is considered as a

TABLE 2

Recovery of fluoride added to 1:10 diluted tea samples using TISAB-III and the modified TISAB-III

Sample	F^- added ($\mu g\ l^{-1}$)	TISAB-III		Modified TISAB-III	
		F^- found ($\mu g\ l^{-1}$)	Recovery (%)	F^- found ($\mu g\ l^{-1}$)	Recovery (%)
T_4	—	185	—	192	—
	50	230	97.9	239	98.8
	100	271	95.1	281	96.2
	200	396	102.9	389	99.2
	500	700	102.2	703	101.6
T_7	—	120	—	144	—
	50	175	102.9	189	97.4
	100	219	99.6	251	114.1
	200	320	100.0	348	101.2
	500	648	104.5	629	97.7
T_{17}	—	65	—	70	—
	10	73	97.3	78	97.5
	20	80	94.1	88	97.8
	50	120	104.4	125	104.2
	100	176	106.7	163	95.9
	200	258	97.4	282	104.4

TABLE 3

Comparison of results obtained in the analysis of diluted and undiluted tea samples using TISAB-III, modified TISAB-III and citrate TISAB, respectively

Sample	Dilution factor	Fluoride content found ($mg\ l^{-1}$)		
		TISAB-III	Modified TISAB-III	Citrate TISAB
T_2	1	1.01	1.25	1.23
	2.5	1.12	1.25	1.28
	5	1.43	1.22	1.25
	10	1.37	1.31	1.18
	20	1.51	1.16	1.26
T_4	1	1.65	1.91	1.89
	2.5	1.79	1.86	1.90
	5	1.86	1.93	1.83
	10	1.94	1.91	1.87
	20	1.87	1.97	1.92
T_7	1	1.04	1.46	1.49
	1.5	1.18	1.51	1.42
	2.5	1.29	1.48	1.51
	5	1.38	1.43	1.46
	10	1.50	1.50	1.46
	20	1.45	1.44	1.48

standard method [11, 12, 18, 39, 40]. However, careful examination of the particular procedures and the TISAB compositions used in these papers raises doubts about the suitability of some of these procedures. The composition of urine depends very much on factors such as biological variables (e.g., age and sex), nutrition habits, state of health of the subject and on the time and frequency of collection [41, 42]. Urine is a hypertonic fluid with medium osmolality in the 500—1500 mosmol l^{-1} range [41]. Calculating the ionic strength on the assumption that only monovalent ions are present gives a value of at least 0.25 mol l^{-1}. Given the ionic strength effects previously reported [26], this high inherent ionic strength of urine requires either sample dilution or the use of an optimized TISAB. The use of the citrate TISAB at various concentration was investigated for the determination of natural and diluted urine. A 1:1 mixture of the citrate TISAB and urine was appropriate to eliminate any ionic strength effects and was therefore preferred.

Figure 6 shows the recording obtained during a 1-h run. The peak heights of the calibration standards at the beginning and those of the recalibration in the end are essentially identical. The urinary fluoride contents of 8 males are given in Table 4. The values found in diluted and undiluted samples given in Table 5 show excellent agreement which indicates the reliability of the procedure.

Conclusions

The flow-injection method with the fluoride-selective electrode is easily applicable to the determination of traces of fluoride in water, beverages and urine. However, for the analysis of samples with high inherent ionic strength

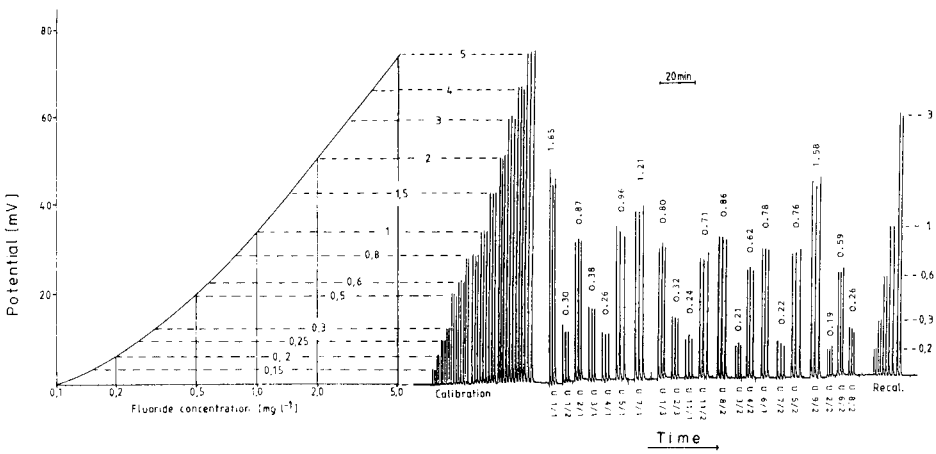

Fig. 6. A typical recording obtained during a 2-h run of urine analysis. Samples and standards were mixed with citrate TISAB in a 1:1 ratio (injection volume 125 μl, flow rate 0.6 ml min^{-1}). Fluoride concentrations (mg l^{-1}) are given above the signals. The corresponding calibration plot for 0.15—5 mg l^{-1} fluoride is given at the left.

TABLE 4

Urinary fluoride levels of 8 subjects determined by flow injection potentiometry[a]

Sample	Mean F^- content ($\mu g\ l^{-1}$)	S.d. ($\mu g\ l^{-1}$)	R.s.d. (%)	Sample	Mean F^- content ($\mu g\ l^{-1}$)	S.d. ($\mu g\ l^{-1}$)	R.s.d. (%)
U_4	346	11.4	3.3	U_{10}	1636	57.7	3.5
U_5	1604	59.0	3.7	U_{12}	796	35.1	4.4
U_6	558	30.3	5.4	U_{13}	2250	92.7	4.1
U_8	402	14.8	3.7	U_{15}	1408	57.6	4.1

[a]Urine samples were mixed 1:1 with citrate TISAB. Results given were obtained from five measurements made within one week after sampling.

TABLE 5

Comparison of results obtained in the analysis of diluted and undiluted urine samples. All samples were mixed 1:1 with citrate TISAB

Sample	Dilution factor	Fluoride measured ($\mu g\ l^{-1}$)	Fluoride calculated ($mg\ l^{-1}$)	Mean ($mg\ l^{-1}$)	S.d. ($mg\ l^{-1}$)	R.s.d. (%)
U_5	2	803	1.61			
	4	410	1.64			
	8	210	1.68	1.64	0.07	4.2
	10	165	1.65			
	20	76	1.52			
	40	43	1.72			
U_{12}	2	395	0.79			
	3	263	0.79			
	4	188	0.75	0.78	0.02	2.5
	8	100	0.80			
	16	48	0.77			
U_{13}	2	1075	2.15			
	4	545	2.18			
	6	341	2.05			
	10	193	1.93	2.07	0.115	5.5
	14	157	2.20			
	20	103	2.06			
	40	48	1.92			

and fairly large amounts of interfering elements, the composition of the particular TISAB used must be optimized. The citrate TISAB used in the present work overcomes the interferences observed in the analysis of undiluted tea and urine samples but it reduces the sensitivity and causes peak broadening when compared to the commonly used TISAB-III.

Recoveries of added fluoride were found to be excellent even at concen-

trations in the low $\mu g\ l^{-1}$ range. Exciting features of the flow-injection method are its ease of operation, cheap equipment, short start-up time, long-term stability, and high sample throughput which meet the requirements for a routine method in clinical laboratories and in environmental monitoring. The experimental set-up presented in this series of papers allows for fast changes from one analytical procedure to another so that the method is very flexible. Determinations of fluoride in liquid samples with substantially different compositions can be done with minimum delay. Application to the analysis of other kinds of samples (e.g., plasma, surface and waste water) and to the determination of total fluorine in bone, food, airborne particles, etc., after suitable digestion is obvious and will be the subject of future work.

The technical assistance of Frank Nowak is greatly appreciated. We also thank Frank Chisela for his continuous interest and Philip Gardiner for valuable support.

REFERENCES

1 R. A. Durst, in Ion-Selective Electrodes, NBS Spec. Publ. 314, Washington, 1969, p. 375.
2 P. L. Bailey, Ion-Sel. Electrode Rev., 1 (1979) 116.
3 J. Koryta, Anal. Chim. Acta, 139 (1982) 1; 159 (1984) 1; 183 (1986) 1.
4 T. S. Ma, in I. M. Kolthoff and P. J. Elving (Eds.), Treatise on Analytical Chemistry, Part II, Vol. 12, Wiley, New York, 1965, p. 117.
5 Commission on Microchemical Techniques and Trace Analysis, Pure Appl. Chem., 45 (1976) 33.
6 R. J. Hall, Analyst, 93 (1968) 461.
7 P. Brätter, D. Gawlik, P. Jost, J. Möller and P. Reimers, Fresenius Z. Anal. Chem., 283 (1977) 121.
8 H. Ballczo and M. Sager, Fresenius Z. Anal. Chem., 296 (1979) 382.
9 P. N. Vijan and B. Alder, Am. Lab., 12 (1984) 16.
10 C. Fuchs, D. Dorn, C. A. Fuchs, H.-V. Hennig, C. McIntosh, F. Scheler and M. Stennert, Clin. Chim. Acta, 60 (1975) 157.
11 D. C. Cowell, Med. Lab. Technol., 32 (1975) 73.
12 M. Vandeputte, L. Dryon, A. Vercruysse and D. L. Massart, Fresenius Z. Anal. Chem., 279 (1976) 149.
13 K. Irlweck and H. Sorantin, Mikrochim. Acta, II (1977) 25.
14 I. Sekerka and J. F. Lechner, Talanta, 20 (1973) 1167.
15 W. L. Chek, R. W. Cattrall and I. C. Hamilton, Anal. Chim. Acta, 177 (1985) 235.
16 J. Mertens, P. Van den Winkel, A. Henrion-Boeckstijns and D. L. Massart, J. Pharm. Belg., 29 (1974) 181.
17 D. E. Erdmann, Environ. Sci. Technol., 9 (1975) 252.
18 D. C. Cowell, Anal. Chim. Biochem., 14 (1977) 269, 275.
19 L. Singer and W. D. Armstrong, Arch. Oral Biol., 14 (1969) 1343.
20 P. J. Ke, L. W. Regier and H. E. Power, Anal. Chem., 41 (1969) 1081.
21 P. Venkateswarlu, Anal. Chem., 46 (1974) 878; Anal. Biochem., 68 (1975) 512.
22 N. R. Quaker and M. Gurney, Anal. Chem., 49 (1977) 53.
23 M. S. Frant and J. W. Ross, Anal. Chem., 40 (1968) 1169.
24 B. Vickery and M. L. Vickery, Analyst, 101 (1976) 445.
25 P. A. Evans, G. J. Moody and J. D. R. Thomas, Lab. Pract., 20 (1971) 644.
26 W. Frenzel and P. Brätter, Anal. Chim. Acta, 185 (1986) 127; 187 (1986) 1.

27 J. Slanina, W. A. Lingerak and F. Bakker, Anal. Chim. Acta, 117 (1980) 91.
28 P. Van den Winkel, G. de Backer, M. Vandeputte, N. Mertens, L. Dryon and D. L. Massart, Anal. Chim. Acta, 145 (1983) 207.
29 W. J. van Oort and E. J. J. M. van Eerd, Anal. Chim. Acta, 155 (1983) 21.
30 T. Greatorex and P. B. Smith, J. Inst. Water Eng. Sci., 39 (1985) 81.
31 J. Tuśl, J. Assoc. Off. Agric. Chem., 53 (1970) 267.
32 D. C. Cowell, Med. Lab. Sci., 35 (1978) 265.
33 R. Bock and S. Strecker, Fresenius Z. Anal. Chem., 235 (1968) 322.
34 R. A. Durst, in H. Freiser (Ed.), Ion-Selective Electrode in Analytical Chemistry, Vol. 1, Plenum Press, New York, 1978, p. 311.
35 P. M. G. Broughton, A. H. Gowenlock, J. J. McCormack and D. W. Neill, Ann. Chim. Biochem., 227 (1974) 1260.
36 J. Růžička and E. H. Hansen, Anal. Chim. Acta, 99 (1978) 64.
37 D. Weil and K. E. Quentin, Z. Wasser Abwasser Forsch., 11 (1978) 133.
38 W. Manley, Proc. Ann. Conf. B. C. Water Waste Assoc., 1976, p. 200.
39 L. Singer, W. D. Armstrong and J. J. Vogel, J. Lab. Clin. Med., 74 (1969) 354.
40 J. Tuśl, Anal. Chem., 44 (1972) 1693.
41 C. Lentner, (Ed.), Geigy Scientific Tables, Vol. 1, Ciba-Geigy, 1981, p. 53 ff.
42 M. Bradley, G. B. Schumann, P. C. J. Ward, in J. B. Henry (Ed.), Clinical Diagnosis and Management, Vol. 1, W. B. Saunders, Philadelphia, 1979, p. 559.

Analytica Chimica Acta, 188 (1986) 165—175
Elsevier Science Publishers B.V., Amsterdam — Printed in The Netherlands

FLOW-INJECTION CATALYTIC DETERMINATION OF MOLYBDENUM WITH BIAMPEROMETRIC DETECTION IN A MICROPROCESSOR-CONTROLLED SYSTEM

M. TROJANOWICZ*, A. HULANICKI, W. MATUSZEWSKI and M. PAŁYS
Department of Chemistry, University of Warsaw, Pasteura 1, 02-093 Warsaw (Poland)
A. FUKSIEWICZ, T. HULANICKA-MICHALAK, S. RASZEWSKI and J. SZYLLER
Computer Centre, University of Warsaw, Warsaw (Poland)
W. AUGUSTYNIAK
Department of Physics, University of Warsaw, Warsaw (Poland)
(Received 9th May 1986)

SUMMARY

The flow-injection determination of molybdenum(VI) is based on its catalytic effect on the oxidation of iodide by hydrogen peroxide. The triiodide ion formed in this reaction is detected amperometrically in a flow-through cell containing two platinum wire electrodes polarized at 100 mV. After optimization of the measuring conditions, the detection limit is 1.2 $\mu g\ l^{-1}$ Mo(VI) and the linear range extends to 1 $mg\ l^{-1}$. Interference of various metal ions and their removal is described. The procedure was tested on the determination of molybdenum(VI) in soil extracts.

Flow-injection determinations of traces of molybdenum(VI) have been based on spectrophotometry of the molybdenum(V) thiocyanate complex [1, 2] and on the molybdenum(VI)-catalyzed oxidation of iodide by hydrogen peroxide [3, 4]. In the catalytic method, potentiometric detection can be achieved with an iodide-selective electrode [3], but lower detection limits were obtained for spectrophotometric detection of triiodide [4]. The same spectrophotometric mode of detection was used earlier in continuous-flow measurements [5, 6].

Platinum wire electrodes have been used in flow-injection measurements with potentiometric detection [7] and in amperometric detection in three-electrode flow cells with auxiliary and reference electrode [8—12]. The flow cells based on wire electrodes are simple in design, usually have very small dead volumes, and allow for easy exchange of the wire working electrodes. Further simplification in cell construction can be achieved by using amperometric detection with two polarized platinum-wire electrodes. Such measurements in the detection of one component of a reversible redox system require the application of only small polarizing voltages (usually <100 mV). Biamperometric detection is widely used for end-point determination in

0003-2670/86/$03.50

coulometric titrations of reducing substances with electrolytically generated iodine. In amperometric flow-injection measurements, it has been used for the determination of nitrite based on its reaction with iodide [13] and for the determination of sulfur(II) compounds which induce the iodine/azide reaction [14].

The aim of the present work was to optimize the experimental parameters for application of biamperometric detection in the flow-injection determination of molybdenum(VI), based on its catalytic effect on the oxidation of iodide. The determination of molybdenum under optimized conditions was then applied in the home-made microprocessor-controlled system described below.

EXPERIMENTAL

Apparatus

The measuring system used consisted of a multichannel peristaltic pump (model MP13GJ-4; Ismatec, Zurich), a home-made rotary injection valve shifted manually or with an electromagnetic switch, a flow cell connected to an a.c./d.c. polarograph (model PLP 225C; Cobrabid, Warszawa), a strip-chart recorder (model TZ 4100; Laboratorni Pristroje, Praha) and a microprocessor control/processing system.

The design of the flow-through cell with two platinum wire electrodes (0.5-mm diameter) is shown in Fig. 1. A constant polarizing voltage (usually 100 mV) was applied from the potentiostat circuit of the polarograph. The output from the polarograph, which is proportional to the magnitude of current flowing between the working electrodes in the flow cell, was recorded on the strip-chart recorder and/or applied to the analog input of the microprocessor system.

The manifold of the flow system (Fig. 2) was made from polypropylene tubing (0.9 mm i.d.) with home-made perspex connectors. Pump tubing was from Elkay.

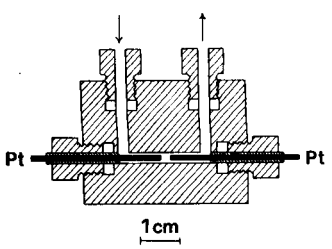

Fig. 1. Schematic diagram of the flow cell with two platinum wire electrodes. The internal diameter of the channel is 1.5 mm.

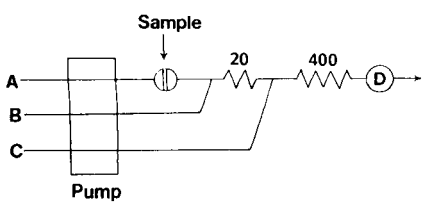

Fig. 2. Manifold of the flow system used: A, distilled water; B, H_2O_2 in 0.1 M H_2SO_4; C, 0.2 M KI. Coil lengths given in cm; flow rates are described separately.

Microprocessor control/processing system

The main units of the control system are a digital voltmeter (model V-541; Meratronik, Warszawa), a microprocessor with central processing unit (see below), memory and interface boards, a hexadecimal keyboard (KDHEX-79; Impol, Warszawa) and a 16-column printer (model UJD-1316; Mera-Elwro, Wrocław).

The digital voltmeter is used to convert the output from the polarograph, or from the pH meter for potentiometric detection. Three ports of the parallel interface are used for transmission of digital data (5 digits) from the measurement and for additional information about that result and the status of voltmeter. In the configuration used, the voltmeter provides 18 data points per second.

The modular construction of the microprocessor unit is based on boards (Impol, Warszawa) that can be installed in a 19-in. SR-1 cassette. Slots for exchangeable printed circuit boards are wired according to multibus architecture. The central processing board (CPU-80/79) used is based on an Intel 8080 microprocessor with 16 kbyte EPROM and 16 kbyte RAM and a power supply (SPS-1). A universal PB-1 board is used to interface the V-541 voltmeter and a parallel DIO-55-1 interface is used with certain alterations to connect the printer and electromagnetic valve switch to the control unit.

The central processing unit supervises the functioning of all the other boards and interfaces. With the 8080 microprocessor, it has a 8224 clock generator and 8228 bus, with another 10 kbyte EPROM addressed with the help of 8205 decoders. A further 8279 circuit controls the keyboard and display. Codes of characters typed on the keyboard are stored in RAM. Address, data and control buses are buffered with 8216 circuits. The system is equipped with a separate hexadecimal keyboard with 16 alphanumeric keys and 17 function keys (Fig. 3), the operational meaning of which is summarized in Table 1. A display window for information output is built from a 7-digit CQYP-71 LED display.

Software

The EPROM contains a Monitor program, floating-point package and utility routines to run flow-injection measurements.

The Monitor program controls the system after switching the power on. For user interaction, via keyboard and display, the system is divided into three sections X, Y and Z. In the X section, the symbol of the currently performed command is displayed, whereas the Y and Z sections display the parameters of a given command or appropriate information for the operator. In order to call any given Monitor command, the appropriate function key must be pressed; this is followed by typing in the required values of the parameters and pressing the ACCEPT key.

The floating-point package performs basic arithmetic operations and some other functions with integer, floating-point and binary-coded decimal numbers. Calculations with seven-digit precision can be done within the range from -2^{128} to 2^{128}.

TABLE 1

List of function keys on the hexadecimal keyboard used in the microprocessor control system

Key	Meaning or activity
F1	Start phase 1
F3	Start phase 3
KAL	Input the concentrations of standard solutions
QKAL	Check typed-in concentrations of standard solutions
PR	Input number of sample injections
UST	Write a constant value into memory cell of given address
SPR	Check (and modify) the content of memory cell of given address
KON	Continue measurement interrupted with pressed key INT
TIM	Input time interval (s) between measurements, of which results are compared with EPS value (TIM1) and time of delay (s) between injection and start of reading a signal (TIM2)
EPS	Input the maximum value of signal deviation in time interval TIM1 during phase 1 of experiment (mV)
TMAX	Input the maximum time interval (min) for baseline stabilization
STMIM	Input limiting values of concentrations of standard solutions
ACC	Input of typed values of parameters
CLR	Clear last typed value
INT	Interrupt the program execution without changing the content of microprocessor registers and RAM memory
RST	Initialize system; the same action turns the power supply off and on

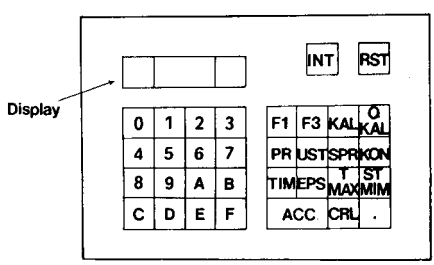

Fig. 3. Schematic diagram of the keyboard used.

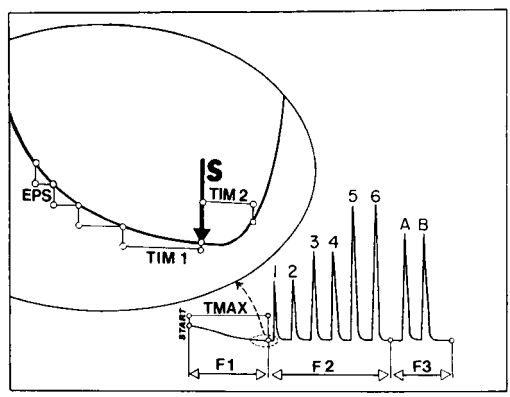

Fig. 4. Schematic diagram of a microprocessor-controlled flow-injection measurement (see text for further details).

Three routines are available corresponding to the three phases of flow-injection measurements: base-line stabilization, calibration with standard solutions, and measurement of unknown samples followed by calculation of

results. The routines can be used for detectors exhibiting a linear relationship between signal and concentration (amperometry, spectrophotometry) or for detectors with logarithmic dependence on concentration (potentiometry). Although the whole experiment is controlled by the microprocessor system, it must be supervised by the operator. The control system informs the operator via the display about the present status, confirms accepted commands and indicates detected errors. The operator types in the required data and parameters related to the experiment and after each phase is complete, decides about further action.

For the calculation of concentration C_x in an unknown sample providing signal S_x (peak value), the mean S_x is first calculated from several injections; then the standard signals S_1 and S_2 closest to S_x and such that $S_1 < S_x < S_2$ are selected. If none of the injected standards gives a smaller or larger signal than S_x, then calculation of C_x is based on two standards nearest to S_x. Concentration C_x is calculated from the following formulae for linear or logarithmic dependence of signal vs. concentration, respectively:

$$C_x = [(C_2 - C_1)(S_1 - S_x)/(S_1 - S_2)] + C_1$$

$$\log C_x = [(\log C_2 - \log C_1)(S_1 - S_x)/(S_1 - S_2)] + \log C_1$$

This procedure [15] requires less RAM in the system than linear regression. Moreover, it can also be used in cases of non-linear calibration relationships.

Procedure for measurements

After the system has been initialized by pressing keys RST and KAL, the concentration values of all the standard solutions are typed in; the values are printed out simultaneously on the printer. Values of all parameters of the measurement are input, preceded by pressing keys TMAX, TIM, STMIM, EPS and PR (Table 1). Pressing key F1 then prints out all typed values; the system requires information about the detector (1 for linear, 0 for logarithmic).

In phase 1 of the experiment, baseline stability is tested. The meanings of particular parameters and phases are illustrated schematically in Fig. 4. TMAX fixes the maximum time interval (up to 99 min), during which the system monitors stabilization of the baseline. Within that period, at time intervals (s) set by parameter TIM1, the system checks if changes in the baseline signal are within the range (mV) set by parameter EPS. If a change greater than EPS occurs in a time shorter than TIM1, the system counts the time TIM1 from the moment when the EPS value was exceeded. When changes in the baseline signal in time interval TIM1 are smaller than EPS, the value of the baseline signal is shown on the LED display and printed out. The system is then ready to start phase 2 (calibration). Standard solutions are injected in previously programmed sequence, the present status being displayed. The rotary valve is turned to the injection position after the ACCEPT key has been pressed by the operator, and returns to the filling position after the peak top has been recognized by the system. In the algorithm used, an

important role in obtaining satisfactory measurements is played by the value of parameter TIM2, which sets the time interval during which the control system does not react to the detector response. This interval is counted from the injection time to a point on the ascending part of the peak and must be estimated experimentally for a given manifold. Inclusion of this procedure in the software enables any effect of accidental signal changes, that might be recognized as peaks from injected species, to be neglected. After the injection of all standard solutions has been completed, the system signals the beginning of phase 3 (measurements of unknown samples). When the number of injected samples equals the value initially programmed, the result of measurements is displayed and printed out. This completes one measurement cycle. Using keys F1 or F3, one can return to different points of the whole run.

Solutions

A stock standard solution containing 100 mg l^{-1} molybdenum(VI) was prepared by dissolution of analytical-grade ammonium heptamolybdate (POCh, Gliwice, Poland) in triple-distilled water. Less concentrated standard solutions of molybdenum(VI) were obtained by consecutive dilution. Standard molybdenum(VI) solutions below 1 mg l^{-1} and the carrier solutions of potassium iodide and hydrogen peroxide in sulphuric acid were prepared daily. All reagents used were of analytical-grade purity.

Aqueous soil extracts were prepared by vigorous shaking of 50 g of freshly sampled greenhouse soil for 45 min with 150 ml of distilled water, followed by filtering twice under suction.

RESULTS AND DISCUSSION

Optimization of experimental conditions

The magnitude of the flow-injection signal in a given catalytic determination with biamperometric detection depends on the polarizing voltage, the geometry of the whole flow system including the detector, the flow rate, injected sample volume and concentration of reagents in the carrier solutions. Under given hydrodynamic conditions, the current intensity between the electrodes in d.c. amperometric measurement depends on the applied voltage, reaching a plateau. In the system used here (flow rate 2.4 ml min^{-1} in each channel, 6.0 mM hydrogen peroxide in 0.1 M sulphuric acid in channel B), the current increased quickly as the applied voltage was increased from 10 to 100 mV, at which a near plateau was observed; 100 mV was therefore applied in subsequent work.

Some parameters of the catalytic determination of molybdenum(VI) are not affected by the detection technique used, hence parameters such as the concentrations of strong acid in the hydrogen peroxide solution and of potassium iodide optimized earlier by Fang and Xu [4] for spectrophotometric triiode measurements were used similarly here. An increase in the iodide concentration causes an increase in the free iodine blank, which

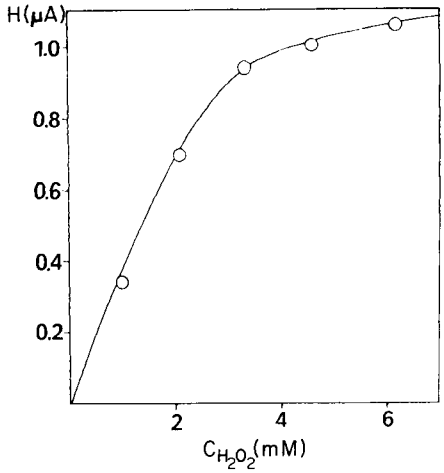

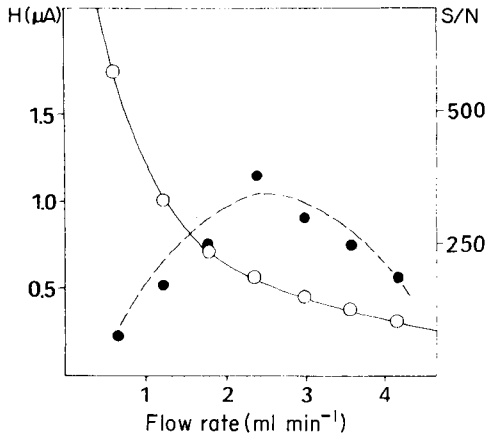

Fig. 5. Effect of hydrogen peroxide concentration in 0.1 M H_2SO_4 used in line B on peak height for injection of 0.8 mg l^{-1} Mo(VI) solutions. Sample volume 140 μl, flow rate 2.4 ml min^{-1} in each channel.

Fig. 6. Effect of total flow rate on the peak height (○) and signal/noise ratio (●) for injections of 0.8 mg l^{-1} Mo(VI) solutions. Sample volume 140 μl; 6.0 mM H_2O_2 in 0.1 M H_2SO_4 in line B.

increases the baseline noise. The effect of hydrogen peroxide concentration is shown in Fig. 5. Up to about 3 mM concentration, the peak height increases linearly with peroxide concentration, but above 6 mM no significant increase was observed. That value (0.023%) was used for further measurements; it is very similar to the concentration used in spectrophotometric measurements.

The effect of flow rate is more complicated here than in spectrophotometric measurements. An increase in the flow rate diminishes the residence time of injected samples and so also decreases the degree of reaction between hydrogen peroxide and iodide, but it also facilitates transport of the depolarizer to the electrode surface. The resultant signal increases monotonously with decrease in flow rate, but baseline oscillations increase simultaneously leading to a decrease in the *S/N* ratio (Fig. 6). Consideration of Fig. 6 indicates that a flow rate of 2.4 ml min^{-1} in each channel gives best results.

In flow-injection measurements, the signal magnitude can generally be increased by enlarging the injected sample volume, the limiting factor being the degree of attainment of equilibrium. For the manifold used and two different flow rates, such relationships are shown in Fig. 7. Above 250 μl, there is only a slight increase in the peak height, therefore that sample volume can be considered as optimal.

Typical peaks for injections of 20—200 μg l^{-1} molybdenum(VI) solutions, obtained under optimized conditions, are shown in Fig. 8. The linear plot of

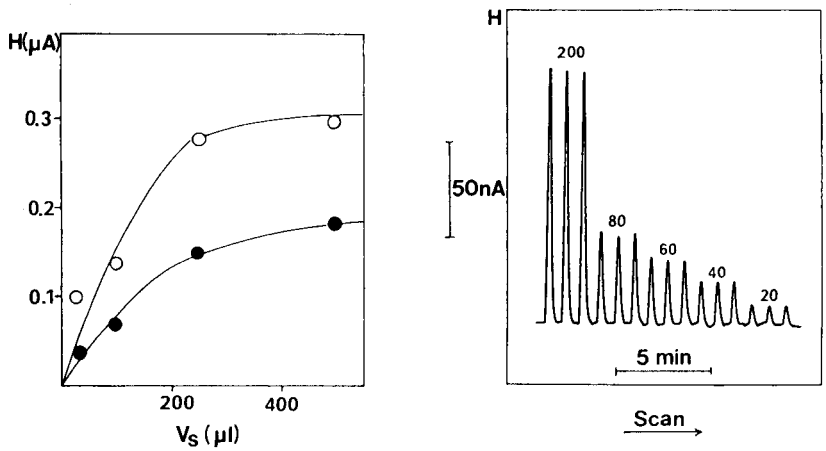

Fig. 7. Effect of sample volume on peak height for injection of 0.1 mg l^{-1} Mo(VI) solution at flow rates of 1.2 (○) and 2.4 (●) ml min^{-1} (6.0 mM H_2O_2 in 0.1 M H_2SO_4 in line B).

Fig. 8. A typical output for the flow-injection determination of molybdenum(VI). Concentrations of injected solutions are given in μg l^{-1}. Sample volume 250 μl: flow rate 2.4 ml min^{-1}; 6.0 mM H_2O_2 in 0.1 M H_2SO_4 in line B.

peak height vs. concentration had a correlation coefficient of 0.9989. A linear plot was also obtained over the whole investigated range of molybdenum(VI) concentrations up to 1 mg l^{-1}. The detection limit was estimated from a comparison of the signal magnitude for 10 μg l^{-1} Mo(VI) with the noise level, caused mainly by peristaltic pump pulsation. For S/N = 2, the detection limit was 1.2 μg l^{-1} Mo(VI).

Interferences

The interfering effects of heavy metal ions on molybdenum(VI) have been considered in most papers reporting catalytic determinations of molybdenum. The results obtained with biamperometric detection are shown in the third column of Table 2. Tungsten(VI) interferes because of its catalytic effect and chromium(VI) by oxidation of iodide in acidic medium. An equimolar amount of iron(III) does not affect the signal, but at higher concentrations it causes significant decrease of the signal probably as result of catalytic decomposition of hydrogen peroxide in the presence of iron(III). Adding citrate to the iodide solution decreases the tungsten(VI) interference [3], but fluoride is more effective. Both masking agents, however, significantly decrease the sensitivity of the molybdenum(VI) determination (Table 2).

The use of masking agents to eliminate iron(III) interference, either added to the iodide solution or pumped instead of distilled water in line A, was not effective. This is shown for sulphosalicylic acid, as an example, in Table 3.

TABLE 2

Error (%) in the determination of 0.1 mg l^{-1} Mo(VI) in the presence of interfering species with and without masking agents added to iodide solution in line C

Interferent	Conc. added (mg l^{-1})	Error (%)			
		Without masking agent	With masking agent		
			0.001 M EDTA	0.02 M Citrate	0.01 M Fluoride
W(VI)	0.1	24	29	12	−1.3
V(V)	0.1	1.9	0.6	1.5	−2.6
Cr(VI)	0.1	25	24	51	46
Mn(II)	1.0	0	−2.5	0	0
Cu(II)	1.0	−2.5	−2.1	−6.0	−2.6
Fe(III)	0.1	1.9	0	0	1.3
	1.0	−50	−45	−39	−36
	5.0	−63	−74	−51	−61
Signal[a]		121	123	50	60

[a]For 0.1 mg l^{-1} Mo (nA).

TABLE 3

Error (%) in the determination of 0.1 mg l^{-1} Mo(VI) in the presence of iron(III) masked with sulphosalicylic acid

Fe(III) conc. (mg l^{-1})	Error (%)[a]		
	A	C	S
1.0	−46	−52	0
5.0	−70	−73	−1.2

[a]A, 0.02 M sulphosalicylic acid used in line A (Fig. 2). C, 0.1 M sulphosalicylic acid added to iodide solution in line C. S, 0.02 M sulphosalicylic acid added to sample solution before injection.

Iron(III) interference can be avoided by adding the masking agent to the sample before injection, which supports the explanation about the catalytic role of iron(III) ions in hydrogen peroxide decomposition. The decomposition process is much faster than the slow formation of iron(III) complexes in the flow stream. A similar effect to that shown in Table 3 for sulphosalicylate was observed for oxalate, but its presence in the sample substantially decreased the sensitivity of the molybdenum(VI) determination. As was mentioned earlier [4, 5], the chromium(VI) interference can be eliminated by reducing chromium with hydrogen peroxide and evaporating to dryness.

TABLE 4

Results (mg l^{-1}) for molybdenum(VI) in soil extracts[a]

Sample	Peak height (μA)	Manual interpretation		Microprocessor result	
		Sample	Sample +0.1 mg l^{-1} Mo	Sample	Sample +0.1 mg l^{-1} Mo
1	0.62	0.31	0.39	0.31	0.40
2	0.68	0.34	0.44	0.35	0.44
3	0.56	0.28	0.39	0.28	0.40
4	0.58	0.29	0.40	0.29	0.40
5	0.64	0.32	0.43	0.32	0.43
6	0.72	0.36	0.48	0.36	0.48

[a]Conditions: 6.0 mM hydrogen peroxide; flow rate 1.9 ml min^{-1} in each line; sample volume 100 μl. Parameters of microprocessor-controlled measurement: 10 injections of standard solutions TIM1 = 10, TIM2 = 40, EPS = 1, PR = 2.

Determination of molybdenum(VI) in soil extracts

As an example of application of the method, molybdenum(VI) was determined in greenhouse soil extracts. It was assumed that extraction with distilled water would not remove iron(III) from the soil. The possible presence of chromium(VI) in the extracts was examined by using a spectrophotometric diphenylcarbazide method. Only trace contents below 3 μg l^{-1} chromium(VI) were found. The conditions for the determination of molybdenum(VI) by the flow-injection method are shown in the legend to Table 4. In this table, results obtained manually are compared to those obtained with the microprocessor-controlled system. These results show good agreement for both interpretations as well as satisfactory accuracy in recovery measurements.

Conclusions

The biamperometric method of detection in the flow-injection catalytic determination of molybdenum(VI) is an alternative to spectrophotometric methods reported earlier. It offers similar sensitivity and selectivity, but has the advantage of insensitivity to the colour of injected solutions, which can be important for the slightly yellowish soil extracts. Flow-cell design is simple and can be reproduced in any analytical laboratory. The method developed illustrates the analytical advantages of flow-injection procedures; the difficult and usually time-consuming catalytic determination can be performed at a sampling rate of 100 h^{-1}.

REFERENCES

1 H. Bergamin, J. X. Medeiros, B. F. Reis and E. A. G. Zagatto, Anal. Chim. Acta, 101 (1978) 9.
2 F. J. Krug, O. Balia F^{o} and E. A. G. Zagatto, Anal. Chim. Acta, 161 (1984) 245.

3 H. Müller, in E. Pungor and I. Buzás (Eds.), Modern Trends in Analytical Chemistry, Akademiai Kiado, Budapest, 1984, p. 353.
4 Z. Fang and S. Xu, Anal. Chim. Acta, 145 (1983) 143.
5 R. Fuge, Analyst, 95 (1970) 171.
6 E. G. Bradfield and J. F. Stickland, Analyst, 100 (1975) 1.
7 B. Karlberg and S. Thelander, Analyst, 103 (1978) 1154.
8 J. A. Lown, R. Koile and D. C. Johnson, Anal. Chim. Acta, 116 (1980) 33.
9 J. A. Lown and D. C. Johnson, Anal. Chim. Acta, 116 (1980) 41.
10 K. W. Pratt Jr. and D. C. Johnson, Anal. Chim. Acta, 148 (1983) 87.
11 S. Hughes and D. C. Johnson, Anal. Chim. Acta, 149 (1983) 1.
12 D. MacKoul, D. C. Johnson and K. G. Schick, Anal. Chem., 56 (1984) 436.
13 A. Hulanicki, W. Matuszewski and M. Trojanowicz, Paper presented at Euroanalysis V Conference, Kraków, Poland, 1984.
14 J. Kurzawa, Anal. Chim. Acta, 173 (1985) 343.
15 R. Caulcutt and R. Boddy, Statistics for Analytical Chemists, Chapman and Hall, London, 1983, Chap. 8.

Analytica Chimica Acta, 188 (1986) 177—185
Elsevier Science Publishers B.V., Amsterdam — Printed in The Netherlands

THE DETERMINATION OF ALUMINIUM IN SEAWATER AND FRESHWATER BY CATHODIC STRIPPING VOLTAMMETRY

CONSTANT M. G. VAN DEN BERG*, KEVIN MURPHY and JOHN P. RILEY
Department of Oceanography, University of Liverpool, Liverpool L69 3BX (Great Britain)
(Received 20th May 1986)

SUMMARY

Dissolved aluminium in seawater and freshwater is determined by cathodic stripping voltammetry (c.s.v.) preceded by adsorptive collection of complex ions with 1,2-dihydroxyanthraquinone-3-sulphonic acid (DASA) on the hanging mercury drop electrode. Complexation of aluminium by DASA is rapid and no waiting period or heating of the sample is required. Optimal conditions are a DASA concentration of 10^{-5} M, a solution pH of 7.1—7.3 and an adsorption potential of −0.9 V; the c.s.v. scan is done in the differential-pulse mode. The limit of detection is 1 nM aluminium for an adsorption time of 45 s. The total time needed, including 5-min deaeration and a standard addition, is 10—15 min per sample. No serious interferences were found; u.v. irradiation is recommended for samples containing high levels of organic materials.

The concentration of dissolved aluminium in seawater generally lies between about 5 nM (in arctic waters [1]) and 40 nM (deep-sea Northwest Atlantic [2]). Aluminium occurs in seawater of pH 8 predominantly in the form of the hydroxy complexes $Al(OH)_4^-$ and $Al(OH)_3^0$ [3]. Its concentration in seawater is usually determined fluorimetrically with Lumogallion [4]. Although this is a sensitive technique with a detection limit of around 2 nM aluminium, it has the drawback that a long waiting time (12—24 h) is required for development of the fluorescence.

It is difficult to determine aluminium directly by electrochemical techniques because the reduction potential of Al(III) is very negative at −1.75 V vs. SCE, in a 0.05 M barium chloride electrolyte [5]. This is very close to the reduction potentials of sodium, barium and potassium, so that high concentrations of these ions interfere with the determination of aluminium. The reduction wave of hydrogen precedes that of aluminium, but is well separated from it when the hydrogen ion concentration does not exceed that of aluminium [5]. In an electrolyte solution of 0.007 M KNO_3 at pH 4, it is possible to determine aluminium at levels between 2×10^{-7} and 2×10^{-5} M by differential pulse polarography [6]. More conveniently, aluminium can be determined polarographically after complexation with di-*o*-hydroxyazo dyes [7]; in presence of excess of dye, two peaks are obtained. The first (more positive) peak is due to the unreacted dye, and the second one is related to reduction of the dye complexed by aluminium. The half-wave potentials associated

0003-2670/86/$03.50

with these reductions are more positive than those of hydrogen or aluminium itself (at −0.5 V at pH 4.5), but the limit of detection is more than 10^{-7} M. A voltammetric method has been described which depends on the oxidation of the aluminium complex of the dye solochrome violet RS (SVRS) (at +0.7 V) after adsorption onto a carbon paste electrode [8], but the sensitivity is similar to that of the direct polarographic technique. This dye has also been used recently to determine aluminium in a cathodic stripping voltammetric (c.s.v.) procedure in which the aluminium complex is first adsorbed onto a hanging mercury drop electrode (HMDE) [9]. The limit of detection by this technique is claimed to be 5.5 nM for a 10-min adsorption time; however, the method has the drawback that the slow reaction rate of SVRS with the aluminium ion necessitates a preliminary heating of the sample for 10 min at 90°C.

In this report, a procedure is described for determining aluminium in natural waters, including seawater, by c.s.v. of its complex with 1,2-dihydroxyanthraquinone-3-sulphonic acid (DASA). Advantages of the new procedure are the fast reaction kinetics which obviate the need to heat the sample after addition of this reagent, and a lower limit of detection of 1 nM (27 ng l^{-1}) aluminium after an adsorption time of 45 s. The reduction current of the ligand, DASA, in the adsorbed complex is indicative of the dissolved aluminium concentration. In this aspect, the method differs from the determination by c.s.v. of other metals such as copper [10] or nickel [11] in which the current arises from the reduction of the metal in the adsorbed complex. This technique has recently been reviewed [12].

Several different compounds were tested for their suitability to produce a reduction wave with aluminium; they were selected either because they had been used before in c.s.v., or because of their known chelating properties. The following compounds did not produce a peak with aluminium: salicylhydroxamic acid, diphenylcarbazide, 1-nitroso-2-naphthol, 2-(2-bipyridyl)-benzimidazole, dithizone, 8-quinolinol, ammonium pyrrolidinedithiocarbamate (APDC), chromotropic acid, pyridylazoresorcinol, pyridylazonaphthol, and diethylenetriaminepenta-acetic acid. An aluminium peak was obtained with DASA and only the experiments with this compound are presented here.

EXPERIMENTAL

Equipment and reagents

A PAR 174A polarograph was used with a 303 static mercury drop electrode (SMDE) and a Metrohm E649 magnetic stirrer. The surface area of the HMDE was 2.8 mm^2. Potentials are quoted relative to the Ag/AgCl, saturated KCl reference electrode. Experiments involving pH measurements were done with a manual Kemula HMDE (Metrohm) and a 20-ml polarographic cell; pH was measured with a Metrohm 605 pH meter and a combination glass/reference electrode, calibrated against NBS pH buffers. All experiments were

done in a laminar flow hood to prevent contamination of equipment and solutions with traces of aluminium.

Standard aluminium solutions were prepared by dilution of commercial atomic absorption spectrometric standard solutions with 0.1 M hydrochloric acid. An aqueous stock solution of 10^{-3} M DASA was prepared in double distilled water (from quartz). The aqueous stock pH buffer solution prepared was a 1 M solution of BES(*N,N'*-bis-(2-hydroxyethyl)-2-amino-ethane sulphonic acid) in 0.4 M sodium hydroxide (AristaR, BDH). Addition of this buffer to give a concentration of 0.01 M in seawater produced a pH of 7.1. Traces of metal ions present in the pH buffer were removed by treatment with 10^{-4} M manganese dioxide followed by filtration [10]. A stock solution of 0.1 M EDTA was prepared in distilled water and adjusted to pH 7.1 by addition of sodium hydroxide.

Seawater used to optimize the experimental conditions was collected from the Menai Straits and had a salinity of 32°/$_{oo}$; it was stored in 50-l polyethylene containers and batches were u.v.-irradiated for 3 h with a 1-kW mercury vapour lamp to destroy organic matter and then stored in quartz containers.

Procedure for the determination of aluminium in seawater

The sample (10 ml) is pipetted into the polarographic cell; 10 μl of the BES pH buffer is added (giving pH 7.1) followed by 100 μl of 10^{-3} M DASA stock solution, giving a working concentration of 10^{-5} M DASA. After deaeration of the solution with inert gas (argon or nitrogen) for 5 min, the stirrer is started, and the potentiostat is set to −0.9 V. A new mercury drop is then extruded which signifies the beginning of the adsorption time. The stirrer is stopped after 60 s and 10 s is allowed for the solution to become quiescent. The differential-pulse cathodic-stripping scan is then started, at a rate of 20 mV s^{-1}, with a pulse height of 25 mV and a pulse time of 0.1 s. The aluminium peak appears at −1.12 V in seawater, and −1.07 V in freshwater. The aluminium concentration in the sample is evaluated from a repeated measurement after a standard addition.

The peak current/aluminium concentration relationship is linear up to 100 nM Al under the stated conditions with a stirred adsorption time of 1 min. The linear range can be extended by reducing the adsorption time, or by adsorbing from unstirred solution; in the latter case, the linear range extends up to 600 nM with a 15-s adsorption time.

Interference by high concentrations of zinc in polluted seawater (greater than 50 nM) can be overcome by using an adsorption potential of −1.0 V (the zinc peak is at −1.08 V in seawater), and scanning from −0.9 V. Zinc in freshwater or seawater can also be masked by adding 10^{-4} M EDTA to the sample prior to the measurement. Interference caused by high concentrations of organic surface-active material is eliminated by u.v.-irradiation of the acidified (pH 2.8 ± 0.2) sample followed by neutralisation and buffer addition.

RESULTS AND DISCUSSION

Cyclic voltammetry

Cyclic voltammetric scans of 10^{-5} M DASA in seawater of pH 7.1 show reversible reduction of free DASA (not complexed by aluminium) (Fig. 1A). The main reduction peak appeared at −0.63 V in agreement with half-wave potentials quoted for substituted anthraquinones [5]. The oxidation peak potential of the reversing scan is displaced slightly (by 5 mV) from that of the reduction peak as a result of diffusion of the reduced DASA away from the surface of the HMDE. The peaks increase in height when the scans are repeated because of adsorption of DASA onto the electrode. The oxidation peak can be brought back to its original magnitude by holding the scan at −0.8 V before scanning back. A second oxidation peak is apparent at −0.53 V and its reduction counterpart at −0.535 V becomes apparent only on the second scan; this second peak is presumably due to different stabilisation of the two quinone groups of the DASA.

In the presence of 600 nM aluminium and after stirred adsorption at −0.9 V for 30 s, a peak related to DASA stabilised by aluminium complexation appears at −1.17 V (Fig. 1B). This reduction step is irreversible; the returning scan reveals only a poorly defined and broad peak. This irreversibility may be due to the slow formation of the DASA/Al complex, as the reduction of DASA itself is reversible. The reduction peak does not shift in a negative direction when the scan rate is increased to 200 or 500 mV s^{-1}, confirming that the reduction step itself is fast, and that irreversibility is due to relatively slow complexation kinetics. Upon repeating the scan, the reduction peak is smaller because of diffusion of the ligand and the metal away from the electrode.

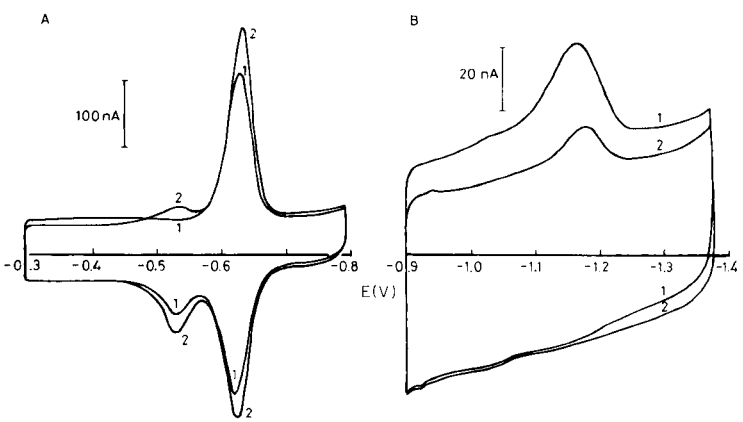

Fig. 1. A. Cyclic voltammetry of 10^{-5} M DASA: (A) in seawater at pH 7.1 (scan rate 50 mV s^{-1}); (B) in seawater containing 500 nM Al, preceded by 30-s stirred adsorption at −0.9 V. In (A), scan 1 was done immediately after extrusion of a new mercury drop; scan 2 was a repeat scan on the same drop. In (B), scan 2 was a repeat scan on the same drop.

The peak height of the DASA/Al complex in the presence of 600 nM aluminium does not increase when the stirred adsorption time is lengthened from 30 s to 60 s, apparently because of saturation of the drop surface with adsorbed free DASA and DASA/Al complex ions. The charge involved in the reduction of the adsorbed DASA/Al complex is only about 5 nC under these conditions, equivalent to an adsorbed layer of 9×10^{13} molecules/cm^2; this was calculated by dividing the current by nFA, where A is the surface area of the drop, F the Faraday constant, and n the number of electrons involved in the reduction of DASA (n = 2 [5]). The amount of DASA/Al complex adsorbed onto the HMDE at maximum surface coverage is much less (100×) than that of metal complexes with catechol, APDC, or dimethylglyoxime [12] as a result of the competitive adsorption of free DASA. This competitive adsorption diminishes the collection efficiency for aluminium.

Effects of the adsorption potential and solution pH

The effect of the solution pH on the peak height obtained for the aluminium in seawater was investigated by using c.s.v., without the addition of buffer. It was found that the peak height was constant at pH values between 5.7 and 8.5, whereas at lower pH values the peak rapidly diminished and disappeared at pH 5.4. However, the slope of the baseline was best at neutral

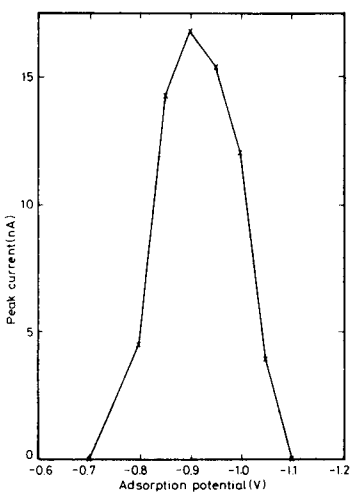

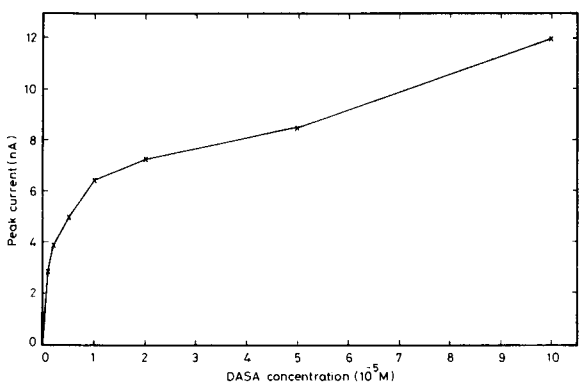

Fig. 2. The effect of varying the adsorption potential on the c.s.v. peak height for 40 nM aluminium in seawater containing 10^{-5} M DASA and 0.01 M BES. Conditions: scan rate 20 mV s^{-1}, pulse rate 10 s^{-1}, pulse amplitude 25 mV, 1-min stirred adsorption; each scan started from −0.9 V.

Fig. 3. The effect of varying the DASA concentration on the c.s.v. peak height obtained for 35 nM aluminium in seawater containing 0.01 M BES buffer (pH 7.1). Each measurement was preceded by 30-s stirred adsorption at −1.0 V, and each scan was started from −0.9 V (scan rate 20 mV s^{-1}, pulse rate 10 s^{-1}).

pH, and BES pH buffer, giving a pH of 7.1, was selected as it gave good separation of the DASA/Al peak from the hydrogen wave.

The potential applied to the electrode during the period of adsorption strongly affects the peak height obtained as shown in Fig. 2. No peak for aluminium is visible when adsorption potentials near to or more positive than the reduction peak for free DASA are selected (positive of −0.7 V); under these conditions the DASA/Al peak is masked because of saturation of the drop surface by free DASA. Greatest peak height is obtained at −0.9 V, whereas the peak height diminishes when adsorption potentials nearer to the DASA/Al peak (at −1.16 V) are selected.

The effects of varying the DASA concentration and the adsorption time

The peak height of the DASA/Al complex was measured by c.s.v. as a function of the DASA concentration. It was found (Fig. 3) that the peak height increases strongly with the DASA concentration up to about 2×10^{-5} M DASA. This increase reflects the increased formation of the DASA/Al complex in solution at higher DASA concentrations. Adsorption of the DASA/Al complex is favoured over the adsorption of free DASA by applying an adsorption potential of −0.9 V, negative of the reduction potential of free DASA (at −0.7 V). At DASA concentrations above 2×10^{-5} M, the background current caused by dissolved free DASA increases, which produces a sloping baseline. The optimal DASA concentration for the determination of aluminium in seawater is therefore $1-2 \times 10^{-5}$ M DASA.

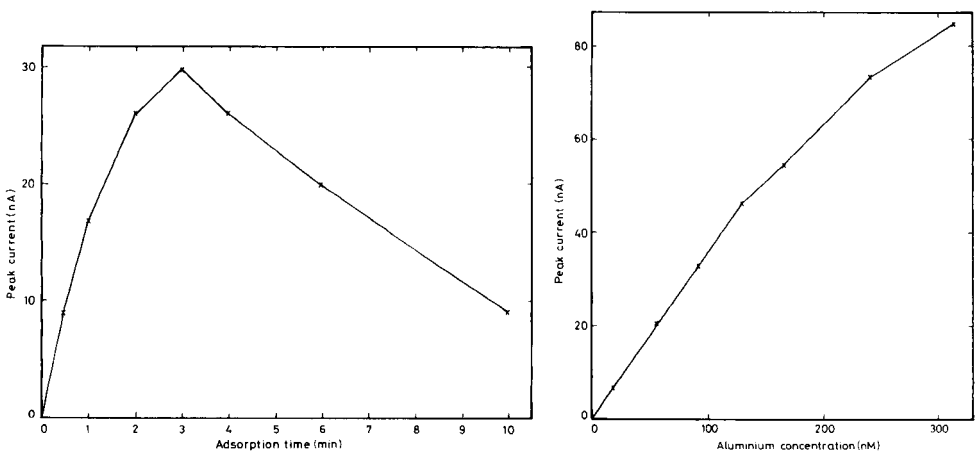

Fig. 4. Effect of varying the adsorption time on the c.s.v. peak height for 40 nM aluminium in seawater containing 10^{-5} M DASA and 0.01 M BES.

Fig. 5. The c.s.v. peak height for the DASA/Al complex as a function of the aluminium concentration in u.v.-irradiated seawater containing 10^{-5} M DASA and 0.01 M BES. Each measurement was preceded by 30-s stirred adsorption at −0.9 V; instrumental conditions as for Fig. 2.

With increasing collection time (at 10^{-5} M DASA in seawater containing 40 nM aluminium and from stirred solution) the adsorption of the DASA/Al complex onto the HMDE is enhanced (Fig. 4). This increased adsorption is non-linear as a function of collection time, as the mercury drop quickly becomes saturated with free and complexed DASA. At adsorption times longer than 3 min, the peak height related to aluminium decreases as a result of an increase (and an apparent shift in the positive direction) of the hydrogen wave, caused by the adsorption of free DASA.

Determination of aluminium in seawater and freshwater

The optimal conditions for the determination of aluminium in water are a neutral pH, a DASA concentration of 10^{-5} M and an adsorption potential of −0.9 V. The relationship of peak current to aluminium concentration is linear up to ca. 130 nM when a stirred adsorption time of 30 s is used, as shown in Fig. 5. (The seawater used in this experiment had been u.v.-irradiated to remove organic material and treated with manganese dioxide to remove trace metal contamination.) The plot is curved at higher aluminium levels because of saturation of the drop surface. The sensitivity for low aluminium levels is improved by increasing the adsorption time (see Fig. 4) but the linear range is then diminished. Thus the peak height increases linearly with the aluminium concentration up to 60 nM when stirred adsorption is continued up to 2 min, but it is linear to 600 nM when unstirred adsorption for 15 s is used.

Figure 6 shows the scan obtained for 15 nM aluminium in seawater in the presence of 10^{-5} M DASA, 0.01 M BES buffer (pH 7.1) after a stirred adsorption time of 45 s; in order to mask a small peak attributed to zinc on the shoulder of the aluminium peak, the adsorption potential was −1.0 V, whereas the scan was started at −0.9 V. Scans 2 and 3 (Fig. 6) represent standard additions of 7 and 14 nM aluminium, respectively. The relative

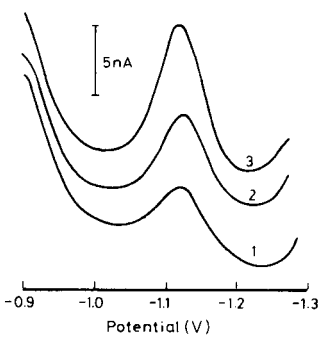

Fig. 6. Stripping scans for aluminium in seawater containing 10^{-5} M DASA and 0.01 M BES buffer, showing the reduction peak obtained for adsorbed DASA/Al complex. Aluminium concentration: (1) 15 nM; (2) 22 nM; (3) 29 nM. Conditions: scan rate 20 mV s^{-1}, pulse rate 10 s^{-1}, pulse amplitude 25 mV, adsorption potential −1.0 V, stirred adsorption time 45 s; each scan was started at −0.9 V.

standard deviation for the measurement of 15 nM aluminium was 2% (n = 8); from 3 times the standard deviation, a detection limit of 1 nM aluminium was calculated. This limit is lower than that (5.5 nM Al) obtained with solochrome violet RS as chelating agent after a 10-min adsorption period [9]. The limit of detection with DASA can be decreased to about 0.4 nM by increasing the adsorption time to 3 min.

Aluminium was determined repeatedly in two freshwater samples by using the recommended c.s.v. procedure. A sample from the River Test, Hampshire, was found to contain 35.3 ± 0.6 nM aluminium (n = 8), whereas a sample of Liverpool tapwater contained 271 ± 3 nM aluminium (n = 6). The relative standard deviations of these determinations were 1.7 and 1.1%, respectively. The river sample had to be irradiated prior to the determination in order to remove interfering organic material, whereas the tapwater could be analysed without prior treatment.

Interferences

Trace metals can interfere if, under the conditions used, they form complexes with DASA which adsorb onto the HMDE and produce a peak close to that of aluminium. The major cations, magnesium, calcium and sodium, did not interfere, and aluminium can be determined successfully in freshwater and seawater. No interference in the determination of 15 nM aluminium was observed when the recommended procedure was applied after the additions of 10^{-7} M Cu, Fe(III), As, In, Se(IV), V, Cr(III) and Cr(VI), 10^{-8} M Cd, Pb, Ti, Sn, Sb and Mn, and 10^{-9} M Se(VI), Tl, Ge and Ga. At concentrations several orders of magnitude higher than those occurring in seawater, peaks near that of aluminium were produced by gallium, antimony and zinc. Of these, only zinc was found to interfere as it may be present at enhanced levels because of sample contamination. Interfering levels (>50 nM) of zinc in seawater can be masked by adsorbing at −1.0 V and initiating the scan from −0.9 V. It was also found that addition of 10^{-4} M EDTA to freshwater completely masked 100 nM zinc without affecting the aluminium response.

Dissolved organic matter in samples can interfere by competitive complexation and masking of aluminium, or by surface-active effects which can diminish the surface area of the HMDE available for DASA/Al adsorption. The possible interfering effects of natural chelating substances were tested by adding EDTA to seawater and measuring aluminium by c.s.v. The DASA/Al peak was not suppressed by up to 10^{-4} M EDTA. Possible interference by natural organic surface-active material was tested by adding the non-ionic surfactant Triton X-100 to the sample; the DASA/Al peak was diminished by 12% by 0.1 mg l^{-1} and by 21% by 0.2 mg l^{-1}, and was completely masked by 1 mg l^{-1} Triton X-100. Ultraviolet irradiation of samples containing high levels of organics (estuarine samples) is therefore recommended in order to eliminate this interference (no such interference was observed in untreated seawater, salinity 34.5%, collected in the English Channel). This u.v.-irradiation should be applied after acidification of the sample to pH 2.8 ± 0.2, as a loss

of aluminium (of variable magnitude), presumably by adsorption onto the quartz container walls, was observed when irradiation was done at the natural sample pH (pH 8).

This investigation was supported in part by a grant of the Department of the Environment to K. M. We are grateful to Mr. J. Murphy for preparation of the drawings and to Ms. S. Perry for typing of the manuscript.

REFERENCES

1 R. M. Moore, Geochim. Cosmochim. Acta., 45 (1981) 2475.
2 D. J. Hydes, Science, 205 (1979) 1260.
3 C. F. Baes, Jr. and R. E. Mesmer, The Hydrolysis of Cations, John Wiley, New York, 1976, p. 122.
4 D. J. Hydes and P. S. Liss, Analyst, 101 (1976) 922.
5 I. M. Kolthoff and J. J. Lingane, Polarography, Vol. II, Interscience, New York, 1952, pp. 513, 703.
6 G. S. P. Ritchie, A. M. Posner and I. M. Ritchie, Anal. Chim. Acta, 117 (1980) 233.
7 H. H. Willard and J. A. Dean, Anal. Chem., 22 (1950) 1264.
8 H. Specker, H. Monien and B. Lendermann, Chem. Anal. (Warsaw), 17 (1971) 1003.
9 J. Wang, P. A. M. Farias and J. A. Mahmoud, Anal. Chim. Acta, 172 (1985), 57.
10 C. M. G. van den Berg, Anal. Chim. Acta, 164 (1984) 195.
11 B. Pihlar, P. Valenta and H. W. Nürnberg, Fresenius Z. Anal. Chem., 307 (1981) 337.
12 C. M. G. van den Berg, Sci. Total Environ., 49 (1986) 89.

Analytica Chimica Acta, 188 (1986) 187—194
Elsevier Science Publishers B.V., Amsterdam — Printed in The Netherlands

STRIPPING VOLTAMMETRY OF THORIUM BASED ON ADSORPTIVE ACCUMULATION

JOSEPH WANG* and JAVAD M. ZADEII

Department of Chemistry, New Mexico State University, Las Cruces, New Mexico 88003 (U.S.A.)

(Received 30th May 1986)

SUMMARY

A sensitive stripping voltammetric procedure for quantifying thorium is described. The chelate of thorium with the azo dye Mordant Blue 9 is adsorbed on the hanging mercury drop electrode, and the reduction current of the accumulated chelate is measured during a negative-going potential scan. Cyclic voltammetry is used to characterize the interfacial and redox behaviors. The effects of pH, dye concentration and accumulation potential are discussed. The detection limit is 4×10^{-10} M (4-min accumulation), a linear current-concentration relationship is observed up to 1.3×10^{-7} M, and the relative standard deviation (at the 6×10^{-8} M level) is 3.1%. Possible interferences by trace metals and organic surfactants are investigated. Simultaneous quantitation of thorium and nickel is illustrated.

Because of the importance of thorium, highly sensitive methods are required for its determination in various matrices. Neutron activation methods [1], mass spectrometry [2], and x-ray fluorescence spectrometry [3] have been used recently, but these techniques require costly instrumentation. Because of the extremely negative reduction potential of thorium, its polarographic wave is masked by the large hydrogen evolution background current [4]. As a result, no attempts have been made to measure thorium by direct polarography, or by the more sensitive method of stripping voltammetry [5]. Early studies indicated, however, that thorium forms a polarographically-active chelate with the dihydroxyazo dye solochrome violet RS [6, 7]. A distinct reduction wave was obtained when thorium ions were added to the dye-containing solution. The height of this wave was proportional to the thorium concentration; a limit of detection of 6×10^{-4} M thorium was reported.

This paper describes a very sensitive stripping voltammetric procedure for trace determination of thorium. Low levels of certain metal ions can be quantified by using accumulation of their appropriate complexes at an electrode and stripping voltammetry of the surface species [8]. Chelating agents such as dimethylglyoxime [9, 10], catechol [11—13], and dihydroxyazo dyes [14, 15], have been used for trace quantitation of nickel [9], cobalt [10], vanadium [11], uranium [12], iron [13], aluminum [14] and titanium [15]. As a result of these efforts, the scope of stripping voltammetry has

0003-2670/86/$03.50

been extended. The current work demonstrates that a similar approach based on the formation of a thorium chelate with the dihydroxyazo dye Mordant Blue 9 (Color Index 14855) can be exploited for trace quantitation of thorium. The results of an investigation into the adsorptive stripping behavior of the thorium/Mordant Blue 9 chelate, are described in the following sections.

EXPERIMENTAL

The equipment used to obtain the voltammograms, a PAR 264A voltammetric analyzer with a PAR 303 static mercury drop electrode, was described in detail earlier [14, 15]. All solutions were prepared from double-distilled water. A 1000 mg l^{-1} thorium stock solution (atomic absorption standard Aldrich) was diluted as required for calibration and standard additions. Dihydroxyazo dyes were purchased from Aldrich; a 10^{-4} M stock solution of Mordant Blue 9 [C.I. 14855; 6-(5-chloro-2-hydroxy-4-sulfophenylazo)-5-hydroxy-1-naphthalenesulfonic acid, disodium salt] was prepared daily. Supporting electrolyte was 0.05 M acetate buffer (pH 6.5).

The procedure used was similar to that reported previously [14], except for the use of a 2×10^{-6} M Mordant Blue 9 solution and a preconcentration potential of −0.36 V. The chelate was formed at room temperature, with the solution stirred for 2 min.

RESULTS AND DISCUSSION

Interfacial and redox behaviors

Figure 1 shows voltammograms for acetate buffer solution (pH 6.5) containing 2×10^{-6} M Mordant Blue 9 before (A) and after (B) adding 50 $\mu g\ l^{-1}$ of thorium. Stirring the dye-containing solution for 60 s, while holding the electrode at −0.18 V, prior to the scan (A, scan 1) results in two cathodic peaks (at −0.33 V and −0.44 V) associated with the reduction of the adsorbed dye. No peaks are observed upon scanning in the positive direction. Subsequent scans result in disappearance of the first peak and sharp decrease of the second peak, indicating rapid desorption of the dye from the surface. When the same experiment is repeated in the presence of 50 $\mu g\ l^{-1}$ thorium (B), an additional peak, associated with the reduction of the adsorbed metal chelate, is observed at −0.51 V (on the tail of the free-dye peak). Also observed is a slight decrease of the free-dye peaks. When a potential of −0.36 V was applied during the stirring period, only a single cathodic peak from reduction of the adsorbed chelate is observed (C). This peak is larger than the chelate peak obtained following accumulation at −0.18 V, presumably because of reduced competition by the free dye for surface sites. The reduction of metal chelates of azo dyes is known to proceed at the azo linkage [16, 17]; the shift in peak potential, compared to the free dye, is attributed to the involvement of the azo group in the coordination. When

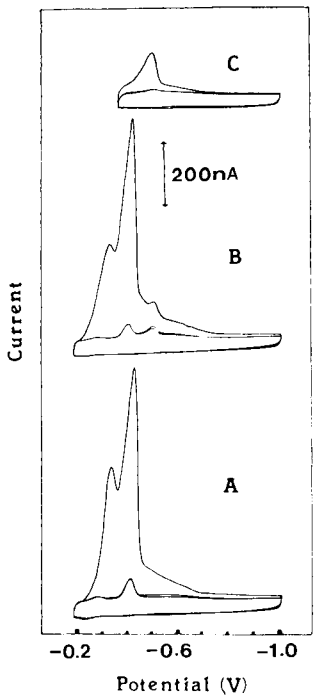

Fig. 1. Repetitive cyclic voltammograms obtained after 60-s stirring: (A, B) at −0.18 V; (C) at −0.36 V. (A) 2×10^{-6} M Mordant Blue 9; (B, C) as (A) after addition of 50 μg l^{-1} thorium. Electrolyte, acetate buffer (pH 6.5); scan rate, 50 mV s^{-1}.

50 μg l^{-1} thorium, 2×10^{-6} M Mordant Blue 9 were stirred at −0.36 V, maximum surface coverage was observed after 60 s. The maximum charge calculated by integration of the area under the chelate peak ("cut and weigh" method), was found to be 0.161 μC. This value corresponds to an adsorbed layer of 2.0×10^{-11} mol cm^{-2}. Because of the mixed adsorbed layer, the area occupied by a single chelate molecule cannot be estimated. The effect of potential scan rate on the chelate peak current and potential was evaluated at maximum adsorption density. A plot of log (peak current) vs. log (scan rate) was linear, with a slope of 0.89, over the 10—200 mV s^{-1} range. A slope of 1.00 is expected for an ideal reaction of surface species. The peak potential shifted 170 mV in the negative direction when the scan rate was increased from 10 to 500 mV s^{-1}. A plot of peak potential vs. log scan rate was linear with a slope of 10, over the 20—200 mV s^{-1} range (correlation coefficient, 1.000).

The interfacial behavior of the thorium/Mordant Blue 9 chelate can be utilized for effective preconcentration, prior to the voltammetric measurement. As a result, trace levels of thorium can be quantified by means of adsorptive stripping voltammetry. For example, Fig. 2 shows linear scan voltammograms for 8 μg l^{-1} (3.4×10^{-8} M) thorium, in the presence of

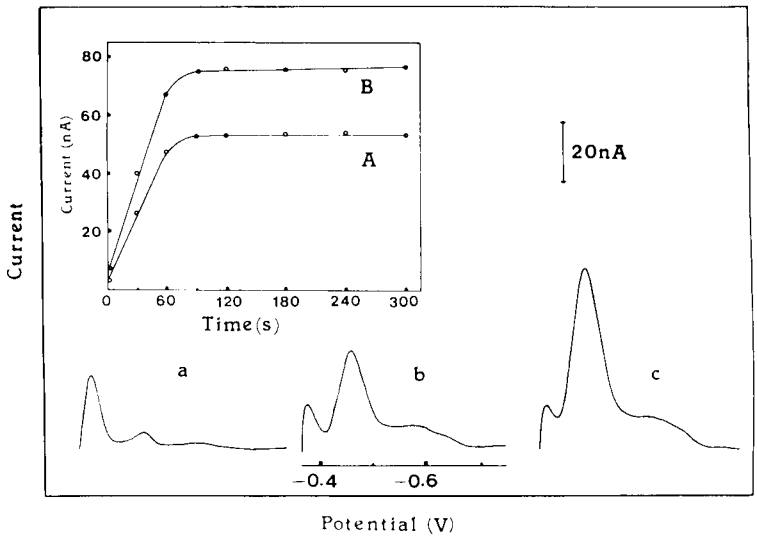

Fig. 2. Linear scan voltammograms for 8 $\mu g\ l^{-1}$ thorium after different preconcentration times: (a) 0; (b) 30; (c) 60 s. Preconcentration at −0.36 V with 400 rpm stirring. Inset are current vs. preconcentration time plots: (A) 8 $\mu g\ l^{-1}$ Th; (B) 14 $\mu g\ l^{-1}$ Th. Conditions: 2×10^{-6} M Mordant Blue 9; otherwise as for Fig. 1.

2×10^{-6} M Mordant Blue 9, after different preconcentration times. The chelate stripping peaks are well defined, with peak potential at −0.48 V and peak half-width of 59 mV. A rapid increase of the chelate peak is observed with increasing preconcentration time, indicating an enhancement of the chelate concentration on the mercury surface. For example, a 60-s preconcentration period resulted in an 18-fold enhancement of the peak, compared to the response without preconcentration (compare curves a and c). At thorium concentrations of 8 and 14 $\mu g\ l^{-1}$, plots of current vs. preconcentration time (Fig. 2) show that the current is independent of preconcentration time at times longer than 90 s (upon achieving adsorption equilibrium). As in conventional stripping voltammetry, a trade-off between sensitivity and speed is required to optimize the preconcentration time. Times of 30 s and 300 s suffice for convenient quantitation of thorium at the 10 and 1 $\mu g\ l^{-1}$ levels respectively.

Preliminary experiments were done with various complexing ligands and supporting electrolytes in order to examine their utility for the quantitation of thorium by adsorptive stripping voltammetry. The azo dyes eriochrome black T (Mordant Black 11) and solochrome violet RS did not yield the desired response in solutions such as acetate buffer, sodium hydroxide sodium tartrate, PIPES, ammonium chloride, potassium nitrate, or ammonium acetate. No response was observed in acidic or basic PIPES solutions containing catechol. In contrast, Mordant Blue 9 yielded a well defined stripping response in thorium-containing acetate buffer solutions, but not in

sodium tartrate, PIPES or ammonium chloride. Accordingly, the following experiments were done with acetate buffer solutions containing Mordant Blue 9.

Figure 3 shows the effect of various conditions on the thorium-chelate stripping response. The solution pH strongly affects the chelate peak (Fig. 3A); the peak was larger over the pH 6.0–7.5 range, with maximum adsorption at about pH 6.5. A 90-mV negative shift of the peak potential was observed on increasing the pH from 5.5 to 8.0 (not shown). The peak increased with the Mordant Blue 9 concentration to about 1×10^{-6} M (Fig. 3B). According to Turnham [6], the azo dye/thorium ratio in such chelates is 2:1. To assure thorium chelation over the entire submicromolar level of interest, a Mordant Blue 9 concentration of 2×10^{-6} M was used in all subsequent work. When the preconcentration potential was changed (Fig. 3C), the peak height increased slowly on changing the potential over the 0.0 to −0.25 V range; under these conditions the chelate peak appeared as a small shoulder of the free dye peak. The highest chelate peak was observed after accumulation at −0.35 V, but a preconcentration potential of −0.36 V offered improved signal/background characteristics (particularly with respect to the preceding free dye peak) and was used throughout. The potential dependence of adsorption was also evaluated from electrocapillary studies. Both the dye and subsequent thorium additions decreased the surface tension (drop time) of the DME, particularly over the 0.1 to −0.4 V range, with the largest decrease around the potential of zero charge (ca. −0.25 V).

Other parameters affecting the response include the mass transport during the preconcentration step and stripping mode during the measurement step. For example, a stirring rate of 400 rpm resulted in a 2.8-fold enhancement of the response, compared to that obtained in a quiescent solution (15 $\mu g\ l^{-1}$ thorium, 1-min preconcentration). Such mass-transport control indicates a fast rate of chelate adsorption. The linear-scan stripping mode offered improved signal/background characteristics relative to the differential pulse waveform. The latter yielded a broad peak (half-width of 71 mV) at a potential of −0.47 V. As a result of its response characteristics and speed advantage, the linear scan mode was preferred.

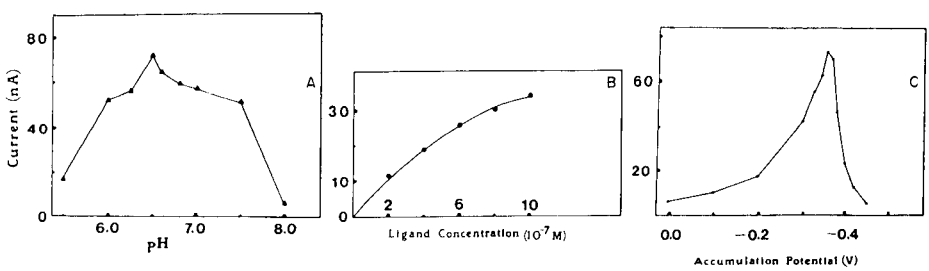

Fig. 3. Effects on the adsorptive stripping current: (A) pH; (B) Mordant Blue 9 concentration; (C) preconcentration potential. Thorium concentration, 20 $\mu g\ l^{-1}$; other conditions as in Fig. 2, except that in (A) the preconcentration potential was adjusted to 0.15 V more negative than the chelate peak potential (because of the shift in peak potential with the pH).

Response characteristics

Figure 4 shows voltammograms obtained after increasing the thorium concentration in 5 $\mu g\ l^{-1}$ (2.2×10^{-8} M) steps. Well defined stripping peaks are observed. These five measurements were part of seven concentration increments, up to 35 $\mu g\ l^{-1}$. Figure 4 (inset) shows the effect of different preconcentration periods. With preconcentration for 30 s and 60 s, the response is linear up to 30 and 20 $\mu g\ l^{-1}$ (1.3×10^{-7} and 8.6×10^{-8} M), respectively. The sensitivity then decreases as full surface coverage is approached. The slopes of the initial linear portions were 2.49 ± 0.05 (B) and 4.20 ± 0.63 (C) nA l μg^{-1} with intercepts of −1.26 ± 1.11 (B) and −3.49 ± 0.86 (C) nA and correlation coefficients of 0.999 (B, C). With shorter preconcentration times and/or unstirred solutions, saturation of the drop surface occurs at higher thorium levels, i.e., the linear range is extended.

Because of the effective accumulation of the thorium/Mordant Blue 9 chelate, very low detection limits were obtained following short preconcentration times. The detectability was estimated from measurements of 2 $\mu g\ l^{-1}$ (8.6×10^{-9} M) thorium, after 4-min preconcentration (other conditions as in Fig. 2). The limit of detection, calculated from 3 times the noise, was found to be 0.1 $\mu g\ l^{-1}$ (4×10^{-10} M). This value means that in the 10 ml of solution used, 1 ng of thorium can be detected. Ten successive measurements of 15 $\mu g\ l^{-1}$ thorium yielded a mean peak current of 60 nA, a range of 58—65 nA, and a relative standard deviation of 3.1% (conditions as in Fig. 2c).

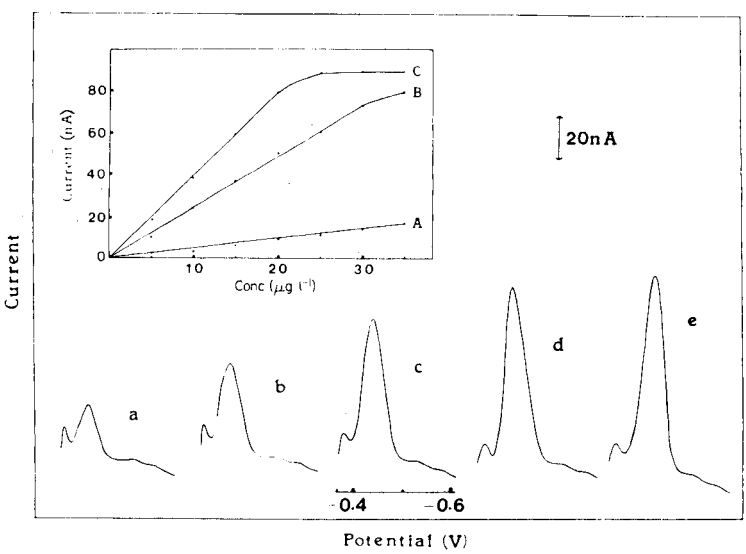

Fig. 4. Stripping voltammograms obtained for solutions of increasing thorium concentration in the range 5—25 $\mu g\ l^{-1}$ (a—e). Preconcentration for 60 s; other conditions as in Fig. 2. Also shown are calibration plots for different accumulation times: (A) 0 s; (B) 30 s; (C) 60 s.

Interferences

Interferences can be caused by metal ions that form reducible or nonreducible chelates with Mordant Blue 9. These may affect the thorium chelate response via an overlapping peak or may compete for adsorptive sites. Competition for surface sites can be caused also by organic surfactants. Such interfering effects were evaluated. No interferences were observed from Cu(II), Hg(II), Cd(II), Bi(III), Mn(II), Se(IV), Pb(II), Ni(II), Ca(II), or Ba(II). A slight decrease of the thorium stripping peak was observed in the presence of Fe(III) and Sb(III); Zn(II) caused a slight increase of the chelate response. Such changes did not affect the thorium quantitation. In contrast, a large overlapping response was observed in the presence of Ti(IV), Al(III), Ga(III) and U(IV). Hence, a separation step would be required in the presence of these metals. Such steps are common also to other methods for quantifying thorium [2, 3].

Additions of nickel(II) or iron(III) to thorium-containing solutions resulted in the appearance of new peaks (at −0.66 V and −0.59 V, respectively), associated with the reduction of the corresponding chelates with Mordant Blue 9. As a result, it is possible to quantify Th and Ni or Th and Fe(III) simultaneously in mixtures. For example, Fig. 5 shows adsorptive stripping voltammograms for 10 $\mu g\ l^{-1}$ thorium solutions containing increasing levels of nickel. The thorium response is not affected, while a well-defined concentration dependence is observed for nickel. The two chelate peaks were separated by 180 mV.

Interferences by organic surfactants were tested with model compounds, gelatin and dodecyl sodium sulfate. The 10 $\mu g\ l^{-1}$ thorium peak first increased

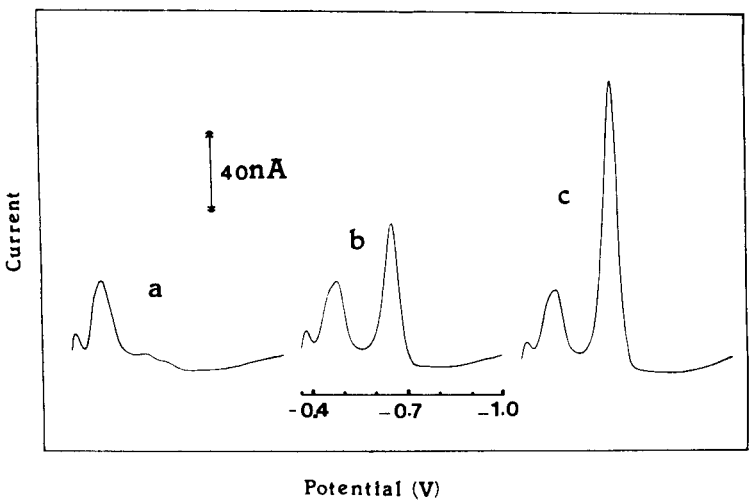

Fig. 5. Simultaneous adsorptive—stripping measurement of thorium and nickel: (a) 10 $\mu g\ l^{-1}$ thorium; (b) as (a) after addition of 10 $\mu g\ l^{-1}$ nickel; (c) as (b) after addition of 10 $\mu g\ l^{-1}$ nickel. Conditions as in Fig. 2(c).

(by about 50% and 10%) on addition of 2 and 4 mg l^{-1} gelatin, respectively. Further additions of gelatin caused a gradual and slow decrease of the chelate response, e.g., by about 30% and 50% in the presence of 100 and 200 mg l^{-1}, respectively. The anionic surfactant, dodecyl sodium sulfate, caused marked reductions in the peak height, by about 30% and 80% at 2 and 4 mg l^{-1} levels, respectively. Although the standard-additions procedure can be used for quantitation when the extent of peak depression is independent of the metal concentration, it is advisable to treat samples containing high levels of such surfactants by u.v. irradiation.

This work was supported in part by the National Institutes of Health (Grant No. GM 30913-03).

REFERENCES

1 See, e.g., C. A. Huh and M. P. Bacon, Anal. Chem., 57 (1985) 2138.
2 See, e.g., L. W. Green, N. L. Elliot and T. H. Longhurst, Anal. Chem., 55 (1983) 2394.
3 See, e.g., I. Roelandts, Anal. Chem., 55 (1983) 1637.
4 I. M. Kolthoff and J. J. Lingane, Polarography, Vol. II, Interscience, New York, 1952, p. 446.
5 F. Vydra, K. Stulik and E. Julakova, Electrochemical Stripping Analysis, Horwood, Chichester, 1976, p. 249.
6 D. S. Turnham, J. Electroanal. Chem., 7 (1964) 211.
7 R. Patzak and M. R. Zaki, Mikrochim. Acta, 2 (1959) 274.
8 See, e.g., J. Wang, Am. Lab., 17(5) (1985) 41.
9 B. Pihlar, P. Valenta and H. W. Nürnberg, Z. Anal. Chem., 307 (1981) 337.
10 M. Meyer and R. Neeb, Z. Anal. Chem., 315 (1983) 118.
11 C. M. G. van den Berg and Z. Q. Huang, Anal. Chem., 56 (1984) 2383.
12 N. K. Lam, R. Kalvoda and M. Kopanica, Anal. Chim. Acta, 154 (1983) 79.
13 C. M. G. van den Berg and Z. Q. Huang, J. Electroanal. Chem., 177 (1984) 269.
14 J. Wang, F. A. M. Farias and J. S. Mahmoud, Anal. Chim. Acta, 172 (1985) 57.
15 J. Wang and J. S. Mahmoud, J. Electroanal. Chem., 208 (1986) 383.
16 G. W. Latimer, Talanta, 15 (1968) 1.
17 T. M. Florence and W. L. Belew, J. Electroanal. Chem., 21 (1969) 157.

Analytica Chimica Acta, 188 (1986) 195—204
Elsevier Science Publishers B.V., Amsterdam — Printed in The Netherlands

PRINCIPAL COMPONENT ANALYSIS APPLIED TO COLLISIONALLY-ACTIVATED-DECOMPOSITION MASS SPECTRA OF ALKYLBENZENES

JUR J. WEBER*, JAN VAN THUIJL and HENK J. DE JONG[a]

Departments of Analytical and Organic Chemistry, Gorlaeus Laboratories, State University Leiden, P.O. Box 9502, 2300 RA Leiden (The Netherlands)

(Received 10th March 1986)

SUMMARY

Pattern recognition of the level-1 type is applied to collisionally-activated-decomposition (c.a.d.) mass spectra of eight isomeric C_9H_{12} alkylbenzenes. Principal component analysis is used for data compression. Only masses with a relative intensity above a variable threshold are selected; no autoscaling is used. Various criteria for deducing the number of factors are compared; because of the error structure, the 3*s*-misfit and chi-squared criteria are most suitable. The principal components technique produces three factors describing four different groups of c.a.d. mass spectra, those corresponding to n-propyl-, isopropyl-, ethylmethyl- and trimethyl-benzene molecular ions.

Since the early days of organic mass spectrometry, visual pattern recognition has been applied to extract information [1]. The analytical power of mass spectrometry has since been expanded by tremendous improvements in instrumentation, including gas chromatography/mass spectrometry, and by the use of dedicated computers. Two more recent techniques, tandem mass spectrometry (m.s./m.s.) [2] and computerized pattern recognition [3], have also assisted in the expansion of the analytical possibilities of mass spectrometry.

The aim of this study was to assess the analytical power of the combination of m.s./m.s. and computerized pattern recognition. The example used here involves the eight isomeric C_9H_{12} alkylbenzenes which have very similar mass spectra [4]. The m.s./m.s. technique applied was the constant parent ion scan. By collisionally activated decomposition (c.a.d.), a mass spectrum is obtained which is composed solely of daughter ions arising from the selected parent ion, in this case $C_9H_{12}^{+\cdot}$. To establish the number of significantly different spectra, pattern recognition was applied. Pattern recognition is often defined as the classification of observations into groups. As the goal of this study was to classify the c.a.d. mass spectra into eight predefined groups, (i.e., the isomers), the problem can be classified as level-1 pattern recognition

[a]Present address: Servier International Research Institute, 27 rue du Pont, 92202 Neuilly S-Seine, France.

0003-2670/86/$03.50

[5]. As the similarities between the c.a.d. mass spectra were not predictable, an assumption that the spectra can be classified into eight groups can lead to meaningless results [6]. Therefore, prior to classification, data compression is needed. This can best be done with principal components analysis (PCA) [7], in which all the measured intensities (the manifest variables) are considered as a dependent set. Their variation can be described by fewer principal components (latent variables). Thus PCA reduces the dimensionality of the observations. Another major feature is that the scores of the spectra on the components are not correlated, which facilitates decisions about which spectra are significantly different [8].

The data to be entered in PCA are the measured intensities at nominal masses which are not scaled. This is valid because all the intensities are measured on the same scale relative to a common standard [7]. Mathematically, this corresponds to a PCA of the "covariance about the origin" matrix, which is constructed from the raw data. Because each nominal mass represents a unique ionic formula, alkylbenzenes are especially appropriate as an example.

EXPERIMENTAL

Instrumentation and samples

Mass spectral data were obtained with a Kratos MS9/50 double-focussing mass spectrometer under the following conditions: ion source temperature, 400 K; trap current, 300 μA; accelerating voltage, 8 kV; electron energy, 70 eV. Samples were introduced either through an all-glass heated inlet system or through a direct insertion probe, both at a temperature of 400 K. The collision cell, built to a design of Maquestiau et al. [9], was situated near the focal point of the first field free region. Air was used as collision gas. The pressure of the collision gas, as measured in the introduction line by a MKS baratron type 170 capacitance manometer, was 0.036 torr. This attenuated the main beam intensity to ca. 35% of its original value. The c.a.d. spectra were recorded by using the B/E linked scan technique as described previously [10].

Calculations were done on an IBM 3083 mainframe computer by using SAS software (Version 5 edition; Statistical Analysis Systems Institute, Cary, NC) or by special programs written in APL, which is an interactive programming language especially suitable for matrix calculations (IBM, New York).

All compounds were commercial samples. Their purity, checked by n.m.r. and gas chromatography was $\geqslant$96%.

Principal component analysis

In PCA [8, 11], the data are assumed to have multivariate normal distribution with correlated variable scores; orthogonal rotation produces new variables, which are called principal components and are sorted in order of descending variance. The observations have uncorrelated scores on the principal components. In matrix notation, this is equivalent to

$$\mathbf{X} = \mathbf{Y}\mathbf{L}^{\mathrm{T}} \qquad (1)$$

where the T superscript denotes the transpose of the matrix, X is the data matrix, Y the score matrix and L the loading matrix. In both X and Y, each row is an observation. Each column of L is a normalized principal component with unit length. The principal components are the eigenvectors of the matrix of product moment coefficients. As the mass spectral intensities are not "autoscaled" to mean zero and unit variance here, that matrix takes the form of a "covariance about the origin" matrix, S:

$$S = X^T X/n \tag{2}$$

where n denotes the number of degrees of freedom, which is here equivalent to the number of observations, N. Eigenvectors are iteratively calculated in order of descending eigenvalue (i.e., variance). The scores of the observations are calculated from $Y = XL$.

As the data are correlated, the true number of eigenvectors is less than the number of variables, m, or the number of observations, N, whichever is smaller. To obtain stable estimates of the true dimensionality of the data, N should exceed m, and probably even exceed $3m$. But, because of experimental error, m eigenvectors are obtained [11]. In order to separate noise from structural information, the list of eigenvectors must be truncated. The first part (i.e., the primary set) consists of vectors with large eigenvalues describing structural information. The remainder (i.e., the secondary set) consists of vectors with nearly equal small eigenvalues describing noise. It is inevitable that some of the noise will mix into the primary set. Among the several criteria that exist to decide on p, the number of eigenvectors belonging to the primary set [11], the following are used here: (1) real error function, RE; (2) imbedded error function, IE; (3) factor indicator function, IND; (4) scree test; (5) $3s$ misfit; (6) chi-squared.

RE, IE and IND. Malinowski [12] established a Pythagorean relationship between the raw data, the data reproduced from the factors, and the "real" data, without experimental error. The real error (RE) estimates the difference between the raw and real data. It is composed of two terms: imbedded error, IE, and extracted error, XE. The latter estimates the difference between the data reproduced from the factors and the real data. In this study, the covariance matrix is divided by the number of its degrees of freedom (Eqn. 2), thus the RE and IE functions are given by

$$RE = [(\text{residual variance})/(m-p)]^{1/2}$$

$$IE = [p(\text{residual variance})/m(m-p)]^{1/2}$$

For the correct number of factors, agreement is expected between RE and an experimental estimate of the real error, while IE should reach a minimum value. Because PCA exaggerates the non-uniformity of error, this minimum may not be well defined. The factor indicator function (IND), defined as $IND = RE/(m-p)^2$, has a more pronounced minimum. Both the IE and IND functions can be used to test the suitability of factor analysis for the data involved. An increase of both IE and IND with increasing p which starts at $p = 1$ denotes that factor analysis is not appropriate for the case tested.

Scree test. When an increasing number of factors is used, the residual variance should first drop sharply and then level off in passing from the primary to the secondary set.

3s misfit, chi-squared. If the last $(m - p)$ columns from both Y and L are deleted, the data can be reproduced with p eigenvectors by using Eqn. 1. The difference between the measured and reproduced data can be related to the standard deviation per measurement. Reproduced data values for which this relative difference exceeds 3 are regarded as misfits. If p eigenvectors are sufficient, the residuals are entirely due to experimental error. Given a normal distribution for the experimental error, only 0.27% misfits are expected.

Alternatively, a chi-squared value can be calculated by summation of the squared differences between raw and reproduced data divided by the standard deviation per measurement [13]. This value is then compared to the expected value which is $(N - p)(m - p)$. For more or fewer than the true number of factors, the calculated value will be, respectively, less than or greater than expected. The cross-over point gives an estimate of p.

RESULTS AND DISCUSSION

The data set consisted of c.a.d. spectra of molecular ions of the eight isomeric C_9H_{12} alkylbenzenes listed in Table 1. Duplicate spectra were obtained and the procedure was repeated after several months, giving a total of 32 spectra. All spectra exhibited non-zero intensities for the same array of masses. Spectra of isomers 2—8 showed only slight differences; common features were a base peak at m/z 105, and other major peaks at m/z 119, 91, 103 and 77. Isomer 1 gave a base peak at m/z 91 and other peaks at m/z 105 and 78. As mass spectral intensities are the result of competing fragmentation processes, differences in relative intensity between various masses are important; and peaks with a low overall intensity have little weight in the PCA. Both these features favour the neglect of intensities below a certain threshold. When correctly applied, this will not reduce the true dimensionality of the data, whereas incorporation of small intensities would simply increase the error variance. Therefore, only masses with an overall average intensity of at least 1.5% of the total daughter ion current (TDIC) were selected. These masses are listed in Table 2.

TABLE 1

The eight isomeric C_9H_{12} alkylbenzenes examined

Isomer	Name	Isomer	Name
1	n-Propylbenzene	5	1-Ethyl-4-methylbenzene
2	Isopropylbenzene	6	1,2,3-Trimethylbenzene
3	1-Ethyl-2-methylbenzene	7	1,2,4-Trimethylbenzene
4	1-Ethyl-3-methylbenzene	8	1,3,5-Trimethylbenzene

TABLE 2

Average intensity and standard deviation for ten selected masses

m/z	Intensity[a]	Intensity (%TDIC)	Standard deviation[a]	m/z	Intensity[a]	Intensity (%TDIC)	Standard deviation[a]
119	28	6.8	3.2	103	20	4.8	2.8
117	15	3.8	2.1	91	49	14.0	5.7
115	13	3.2	2.5	79	6	1.5	1.4
105	184	44.2	21.1	78	7	1.9	1.8
104	15	3.8	2.3	77	16	3.8	3.3

[a]Arbitrary units.

Evaluation of the number of factors

Equation 2 was used to calculate the "covariance about the origin" matrix. The eigenvector solution produced the eigenvalues listed in Table 3. The number of factors has to be deduced by using the criteria discussed in the Experimental section.

The RE function. Table 2 gives the experimental estimate of the real error, i.e., the average standard deviation of the ten selected masses, which is 4.62. The value of RE closest to 4.62 is that obtained with two factors, 5.64, while three factors yield a RE of 2.12 (Table 3); thus two factors are present.

The IE function. The IE function also decreases when an increasing number of factors is used. Values obtained with three and four factors, however, are nearly equal, and the values level off for more than five factors. This indicates that the data are suitable for factor analysis, although no conclusion concerning the number of factors is possible.

The IND function. This function reaches a minimum for five factors but this minimum is very close to the values obtained for three and four factors. There is a sharp decrease from $n = 1$ to $n = 3$. Therefore, the data matrix is suitable for factor analysis but the number of factors remains uncertain.

Scree test. If the residual percent variance for zero factors is made equal

TABLE 3

Eigenvector solution of the 32 × 10 data matrix

p	Eigenvalue	Residual	RE	IE	100 × IND	3s misfit	Chi-squared	
							Calc.	Exp.
1	41857.22	4719.30	22.90	7.24	28.27	35	5360.84	279
2	4464.71	254.59	5.64	2.52	8.81	27	925.62	240
3	223.27	31.32	2.12	1.16	4.32	0	187.91	203
4	16.95	14.37	1.55	0.98	4.30	0	80.54	168
5	9.54	4.83	0.98	0.70	3.93	0	30.34	135
6	2.36	2.47	0.79	0.61	4.91	0	18.87	104
7	1.09	1.37	0.68	0.57	7.52	0	10.67	75

to the total variance, 46577, then the residual variance decreases by 90% for each successive extra eigenvector up to three factors. The fourth causes only a decrease of 50%. Therefore the number of factors is three.

The 3s misfit. The standard deviation is assumed to be constant throughout a data column and is taken from Table 2. As the data matrix contains 320 measurements an average of 0.27% × 320 = 0.86 misfits is to be expected, provided that the true number of factors is used for reproduction. Three factors cause zero misfits, so three must be the true number of factors.

The chi-squared test. The cross-over point lies between $p = 2$ and $p = 3$. Agreement between the calculated and experimental factors is far better for three factors.

It is concluded from the 3*s*-misfit and chi-squared criteria that three factors are present. The behaviour of the IE, RE and IND functions is not in agreement with three factors, but this can be accounted for by the structure of the measurement error. A principal component analysis of error can be done by first subtracting the average spectrum per isomer from the raw data. Then the pooled covariance matrix of error is calculated with Eqn. 2, with 32 − 8 as the number of degrees of freedom, because eight means were calculated (p. 137 [8]). The eigenvalues obtained from the error covariance matrix are presented in Table 4. The 3*s*-misfit and chi-squared criteria obviously do not apply here. The steady decrease of the IE function shows the data to be suitable for factor analysis. Not surprisingly, one factor estimates the RE to be less than the experimental estimate. Both the residual variance and IE criteria suggest the number of factors to be two or three. This is surprising because the number of factors present in a random error matrix equals the number of variables, which is ten here. It is concluded that the measurement errors are not random but highly correlated. Moreover, the dependence structure described by the factors is similar to that of the spectral data. The first error factor, PC1 error, is listed in Table 5 together with the three primary data factors, PC1, PC2 and PC3. From Table 5, it is clear that the PC1 error and PC1 are much the same. Thus it is concluded that PC1 also describes error and so the RE criterion failed to indicate the true number of factors.

TABLE 4

Eigenvalues resulting from PCA of error covariance

p	Eigenvalue	Residual	RE	IE	100 × IND
1	476.74	51.61	2.39	0.76	2.96
2	31.48	20.13	1.59	0.71	2.48
3	10.30	9.83	1.18	0.65	2.42
4	3.63	6.20	1.02	0.64	2.82
5	3.45	2.74	0.74	0.52	2.96
6	1.24	1.50	0.61	0.48	3.83
7	0.66	0.84	0.61	0.48	3.83

TABLE 5

Three eigenvectors of the 32 × 10 data matrix and one error vector

m/z	PC1	PC2	PC3	PC1 error
119	0.14	0.01	0.94	0.08
117	0.08	0.03	0.17	0.07
115	0.06	0.03	0.19	0.08
105	0.96	−0.17	−0.17	0.97
104	0.08	0.01	−0.02	0.08
103	0.10	0.01	0.08	0.10
91	0.16	0.98	−0.05	0.13
79	0.03	0.00	0.03	0.04
78	0.03	0.04	−0.01	0.05
77	0.08	0.02	0.08	0.11

When a p factor model is considered, the error already accounted for by the first $p - 1$ factors should be deleted from the experimental estimate. As m/z 105 produces most of both the PC1 error and PC1, the RE criterion can be improved by taking the average standard deviation of only nine masses, excluding m/z 105, as the experimental estimate of the real error. The value thus obtained is 2.78. Exclusion of m/z 91 as well (because this ion produces most of PC2) yields a value of 2.42. Both values are much closer to that of RE for $p = 3$, which is 2.12.

The fact that the error space is two- or three-dimensional explains the minimum of IND for $p = 5$. The steady decrease of the IE function can be explained by the existence of systematic or random errors, which may arise from the correction procedure that subtracts spontaneous metastable intensities from collisionally activated intensities [10]. Such spontaneous processes exist for few masses but include the base peak; inevitably, they contain a small component from collisionally-activated decomposition [14]. Omission of the correction procedure, however, will introduce other systematic errors.

The application of a threshold intensity for data selection assumes that the minor peaks do not contain extra information or, in terms of PCA, do not increase the true dimensionality of the data. To test this assumption, the threshold was lowered to 1.0% TDIC. Sixteen masses were then selected, i.e., those listed in Table 2 plus m/z 118, 102, 89, 65, 63 and 51. Eigenvalues obtained for this 32 × 16 data matrix are listed in Table 6. The experimental estimate of the real error, with the exclusion of m/z 105 and 91, is now 1.99. Again the number of primary factors is three, as indicated by the cross-over in the chi-squared test and the decrease of misfits to four, with $0.0027 \times 512 = 1.38$ misfits expected. The composition of the primary eigenvectors is essentially the same. The loadings in Table 4 are still valid, except for one 0.01 shift. Additional loadings for m/z 118, 102, 89, 65, 63 and 51 do not exceed 0.05. Given that an increase in the size of the data matrix tends to increase the number of primary factors [6], the application of a threshold intensity is valid.

TABLE 6

Eigenvector solution of the 32 × 16 data matrix

p	Eigenvalue	Residual	RE	IE	100 × IND	3s misfit	Chi-squared	
							Calc.	Exp.
1	41980.11	4745.97	17.79	4.45	7.91	50	5875.76	465
2	4476.95	269.02	4.38	1.55	2.24	36	1232.67	420
3	225.20	43.82	1.84	0.79	1.09	4	422.16	377
4	19.07	24.75	1.44	0.72	1.00	4	277.40	336
5	14.07	10.68	0.99	0.55	0.81	4	171.02	297
6	5.35	5.33	0.73	0.45	0.73	0	83.70	260
7	1.47	3.86	0.65	0.43	0.81	0	75.10	225

Distinction between spectra

The above discussion proves that PCA is appropriate for the problem and that the number of factors is three. The scores of the 32 spectra on these three factors are plotted in Fig. 1. Four well separated groups are present, representing the c.a.d. mass spectra of n-propyl-, isopropyl-, ethylmethyl- and trimethyl-benzene molecular ions. Within the last two groups, ring isomers are not separated.

As the scores are either high or nearly zero, rotation of factors [11, 15] is not needed to facilitate interpretation of differences between groups of spectra. The range of scores of isomers 2—8 on PC1 and that of isomer 1 on PC2 is rather broad. This confirms the suggestion that the primary factors describe error as well as structural information. Principal component 1 describes a spectrum typical of isomers 2—8 as well as differences in daughter-

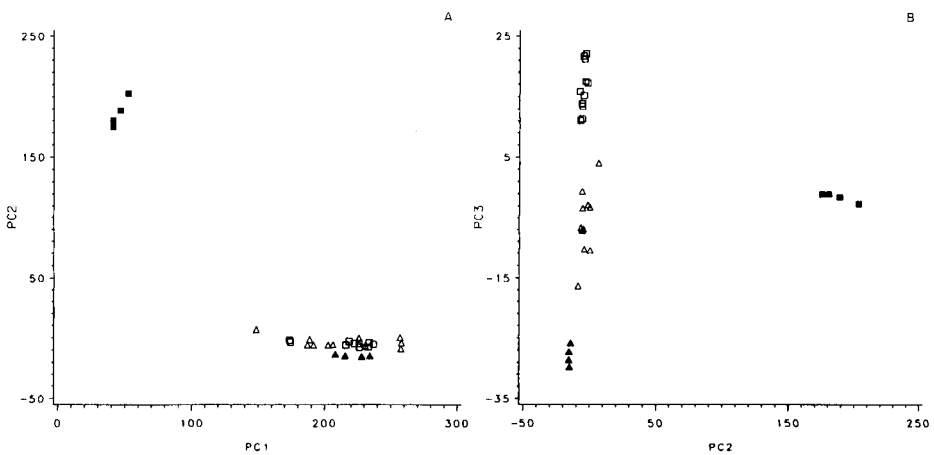

Fig. 1. Plot of scores on principal components 1 and 2 calculated from the 32 × 10 data matrix: (A) PC1 and 2; (B) PC2 and 3. Spectra are represented by the following symbols: (■) n-propylbenzene; (▲) isopropylbenzene; (△) ethylmethylbenzene; (□) trimethylbenzene.

ion yield at a given intensity of the molecular ion. An analogy holds for isomer 1 and PC2, whereas PC3 describes differences between the spectra of isomers 2, 3—5 and 6—8. Inspection of the loadings in Table 5 indicates that, in the order 2 > 3—5 > 6—8, the intensity of the ion with m/z 105 decreases whereas the intensities of the m/z 119, 117 and 115 ions increase. In mass spectrometric terms, PC3 describes the preference for loss of a methyl radical rather than loss of $H^{\bullet}$ followed by loss of one or two hydrogen molecules. The differences between isomers 1 and 2—8 described by PC1 and PC2 are obvious. Incorporation of isomer 1 into the data set, however, did not obscure the differences between isomers 2—8. This is not true for PCA of autoscaled data because this method is very sensitive to inhomogeneities in the data [8].

Conclusions

It is concluded that the information in the mass spectral intensities have been used optimally. The c.a.d. method is capable of recognizing different alkyl groups attached to an aromatic nucleus, but it cannot recognize the ring isomers. The difficulty in recognizing different alkylbenzenes on the basis of their 70-eV electron-impact mass spectra is probably due to inefficient use of these spectra. Therefore, the principal components technique was applied to such spectra obtained from isomers 1—8. This produced five groups of different mass spectra related to isomers 1, 2, 3—5, 6 and 7, and 8. The electron-impact method in conjunction with PCA is thus capable of recognizing different alkyl groups, even distinguishing isomer 8 from its ring isomers 6 and 7. The use of PCA can provide insight into small but significant differences between spectra and is to be recommended in mass spectrometry as a means of setting the limits of different techniques.

REFERENCES

1 A. Hood and M. J. O'Neal, in J. D. Waldron (Ed.), Advances in Mass Spectrometry, Pergamon Press, London, 1959, p. 175.
2 F. W. McLafferty (Ed.), Tandem Mass Spectrometry, Wiley, New York, 1983.
3 D. L. Massart, A. Dijkstra and L. Kaufmann, Evaluation and Optimization of Laboratory Methods and Analytical Procedures, Elsevier, Amsterdam, 1978, Chap. 16.
4 K. Biemann, Mass Spectrometry, McGraw-Hill, New York, 1962, p. 151.
5 C. Albano, W. Dunn III, U. Edlund, E. Johansson, B. Nordèn, M. Sjöström and S. Wold, Anal. Chim. Acta, 103 (1978) 429.
6 S. Wold, C. Albano, W. J. Dunn III, U. Edlund, K. Esbensen, P. Geladi, S. Hellberg, E. Johansson, W. Lindberg and M. Sjöström, in B. R. Kowalski (Ed.), Chemometrics, Mathematics and Statistics in Chemistry, D. Reidel, Dordrecht, 1984, pp. 89, 26.
7 R. W. Rozett and E. McLaughlin Petersen, Anal. Chem., 47 (1975) 1301.
8 D. F. Morrison, Multivariate Statistical Methods, 2nd edn., McGraw-Hill, New York, 1976.
9 A. Maquestiau, Y. van Haverbeke, C. de Meyer, R. Flammang and J. Perlaux, Bull. Soc. Chim. Belg., 85 (1976) 69.
10 M. W. E. M. van Tilborg and J. van Thuijl, Org. Mass Spectrom., 18 (1983) 331.
11 E. R. Malinowski and D. G. Howery, Factor Analysis in Chemistry, Wiley, New York, 1980.

12 E. R. Malinowski, Anal. Chem., 49 (1977) 612.
13 M. S. Bartlett, Br. J. Psychol., Stat. Sect., 3 (1950) 77.
14 J. E. Szulejko and M. M. Bursey, Org. Mass Spectrom., 20 (1985) 374.
15 R. W. Rozett and E. M. McLaughlin Petersen, Anal. Chem., 47 (1975) 2377; 48 (1976) 817.

Analytica Chimica Acta, 188 (1986) 205—217
Elsevier Science Publishers B.V., Amsterdam — Printed in The Netherlands

COMPUTERIZED SYSTEM WITH A HARD-WIRED DATA-ACQUISITION UNIT FOR POTENTIOMETRIC STRIPPING ANALYSIS

BOY HØYER, HANS JØRGEN SKOV and LARS KRYGER*

Department of Chemistry, Aarhus University, Langelandsgade 140, 8000 Aarhus C (Denmark)

(Received 24th March 1986)

SUMMARY

The system comprises an electrochemical module interfaced to and controlled by an Apple-IIe microcomputer. A high data-acquisition rate (660 kHz) is achieved by equipping the electrochemical module with a separate memory which is updated in hardware during recording of the stripping step. When a preset cut-off potential is exceeded, data acquisition is automatically terminated, and potentiostatic conditions are resumed. The electrochemical module also contains facilities for instrumental control. The controlling program for the microcomputer is written in assembler code, which can be linked to BASIC routines if necessary. Examples are given to illustrate the advantages of fast data acquisition in improving detection limits and reducing deposition times.

During recent years, potentiometric stripping analysis (p.s.a.) [1, 2] or chemical stripping analysis [3] have been widely studied for both new applications and instrumentation. The technique involves potentiostatic deposition of trace analytes on a working electrode, followed by stripping via chemical re-oxidation, the potential/time behaviour of the working electrode being monitored at open circuit. With a mercury-film electrode, traces of cadmium(II), copper(II), lead(II) and thallium(I) can be determined in a wide variety of materials and media [4—8]. In p.s.a., the quantitative signal is the duration of the re-oxidation process, i.e., the time during which the electrode potential remains near the conditional redox potential of the analyte concerned. Under properly defined hydrodynamic conditions, the stripping time is proportional to the analyte concentration and the attainable sensitivity may be limited by the time resolution with which the stripping signal can be recorded. Early instruments for p.s.a. [2] were based on analog recording of the potential/time signal on an x-t recorder which did not allow accurate measurement of signals lasting for $\leqslant 0.5$ s. The introduction of microcomputers [6, 9—11] for data logging and experimental control marked a major advance for the technique, particularly when fast computerized data acquisition of the stripping signal was provided [6, 10]. With this facility, the deposition times required are considerably reduced, and non-dearated samples can often be analyzed directly. The computer also facilitates reproducible termination of the stripping phase and resumption of potentiostatic control at a pre-

0003-2670/86/$03.50

selected potential, so that oxidation of the electrode material itself by strong oxidants can be avoided. In addition, computerized instrumentation allows implementation of multiple-scanning techniques [6, 12].

In this paper, a computerized instrument for p.s.a. is described which is an improvement over previous instruments in two ways. First, the commonly available Apple-IIe microcomputer is used for experimental control; this has its own operating system supporting a file system, and storage and retrieval of programs and data are rapid, without the need for a larger computer. Further, a large information base of software and literature is available [13], which is valuable for programming. Secondly, the electrochemical module is hard-wired in order to improve the time resolution in the recording of stripping transients. In earlier computerized potentiometric stripping instruments, the maximum data-acquisition frequency is dictated by the execution time of the program loop which handles input, storage and comparison of potentials. In the instrument described here, the signal recording and the check for overrun of the cut-off potential are implemented in hardware. After data acquisition has been completed, the recorded signal is transferred to the microcomputer. In this manner, a maximum data-acquisition rate of 660 kHz can be achieved.

The data-acquisition scheme is based on the multi-channel method [6], in which the potential axis is divided into intervals of equal width; each of these intervals is assigned to a location in the data memory. During the stripping phase, the electrode potential is monitored at constant frequency; if a potential reading falls within a given interval, the count in the corresponding memory location is incremented by one. In this manner, the number of clock counts accumulated while the cell voltage is fixed at each potential interval is recorded as a function of the electrode potential, and in the resulting potentiogram, the re-oxidation of an amalgamated analyte appears as a peak at the conditional redox potential of that analyte. This mode of data acquisition is particularly suitable for signal averaging and subtraction of background signals.

In computerized p.s.a., if the analog stripping transient is sufficiently reproducible, digitization can limit the precision obtained. If t_p denotes the duration of the primary signal, t_s the sampling interval and N_p the number of counts obtained, then $t_p = N_p t_s + e_p$ with $|e_p| \leqslant t_s$, where e_p is the error introduced by the discrete sampling. The same relation holds for the capacitance background signal: $t_b = N_b t_s + e_b$, with $|e_b| \leqslant t_s$. Both N_p and N_b are proportional to the sampling rate and so inversely proportional to t_s, assuming that t_s is considerably shorter than t_p and t_b, which must always be fulfilled in practice. For the background-corrected net signal, one obtains $t_n = t_p - t_b = (N_p - N_b)t_s + e_n$, with $|e_n| \leqslant 2t_s$. The relative error caused by the digital time measurement is then $|e_n|/t_n \leqslant 2/(N_p - N_b)$. Thus, if the net signal contains only a low number of counts, say $N_p - N_b = 20$, a substantial gain in precision can be obtained by increasing the sampling rate, but if $N_p - N_b$ is large, the analytical signal is already well resolved, and no noticeable improvement in precision is achieved.

EXPERIMENTAL

Hardware

A block diagram of the hardware is shown in Fig. 1.

Microcomputer. An Apple-IIe computer with 64 kbyte of RAM and a BASIC interpreter resident in ROM was used. The CPU is a Synertek 6502B microprocessor, running at a clock rate of 1 MHz; this CPU contains five eight-bit registers (one accumulator, two index registers, a stack pointer and a status register) and the data and address busses are 8 and 16 bits wide, respectively. Peripheral devices are interfaced by seven expansion slots in which all data, address and control signals are accessible. Programs and data can be displayed as text or as high-resolution graphics, on screen or on a matrix printer. Two floppy-disk drives provide storage of programs and data; they are controlled by the Apple disk-operating system (DOS version 3.3) which occupies 10.5 kbyte of RAM.

Data communication with electrochemical module. The microcomputer communicates with the electrochemical module through an optical fiber link at a transmission rate of 0.5 Mbit s^{-1}. The data transmission is supervised by two fiber-link controllers; one is connected to an expansion slot in the Apple-IIe and the other is built into the electrochemical module. In the construction of the electrochemical module, an internal bus compatible with a Motorola 68000 microprocessor was used; this necessitated a bus converter between the eight-bit data bus of the Apple and the sixteen-bit data bus of the electrochemical device. For data transference from the Apple, two data bytes are placed in the fiber-link controller by connecting to two successive memory locations in the I/O memory of the Apple. Then, data bytes are transferred to the electrochemical module together with an eight-bit address

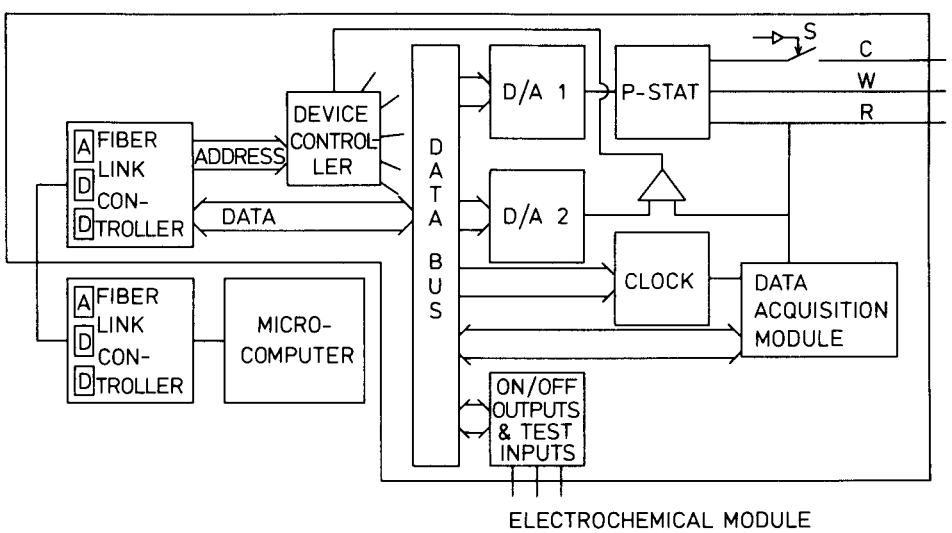

Fig. 1. Block diagram of the hardware configuration.

code which selects the destination device of the data (see Fig. 1). Functions not requiring data transfer (e.g., action of the clock) are activated similarly but without data bytes, whereas the address code is still used for device and function selection; only one write operation is needed. When the Apple receives data from the electrochemical device, the sixteen-bit word is placed in two successive memory locations in the I/O memory allocated to the fiber-link controller, from which the Apple can read and process the data.

The I/O addresses associated with the fiber-link controller are composed of a most significant byte selecting the appropriate expansion slot, while the least significant byte is the above address code used for device and function selection within the electrochemical module. The address code is subdivided into three fields, a three-bit device code, a three-bit function code, and one bit indicating whether data are sent to or read from the device in question. The least significant bit of the address code is used by the fiber-link controller to signal the transfer of data to the electrochemical device.

The data-transmission protocol is implemented by means of two status bits: ready send and ready receive. When the Apple-IIe is transferring information to the electrochemical module, the ready-send bit is pulled low for approximately 40 μs, whereafter the fiber link is again ready for transmission. The ready-receive bit is set when information is pending from the electrochemical module and indicates to the Apple whether the data requested has been transmitted. The ready-receive bit is also set when a clock pulse is received from the electrochemical module and when a stripping step ends, thus prompting further action from the computer. This status bit is reset by any read operation in the I/O memory associated with the fiber-link controller.

Electrochemical module. This module consists of several devices, each of which is described in detail below. All devices and functions under computer control are listed in Table 1. The device controller decodes the address signals output by the Apple-IIe, selects the appropriate device, and generates all signals necessary to synchronize the devices in the module. The D/A converter unit consists of two identical D/A converters (±2 V range, 12-bit resolution). The output of D/A 1 (Fig. 1) is fed to the potentiostat and fixes the cell potential during potentiostatic control. D/A 2 sets the cut-off potential, at which recording of the stripping signal is interrupted. The output of D/A 2 is fed to a comparator together with the cell voltage so that a switch in the relative polarity of these two potentials can be detected. The resulting control signal stops the A/D conversion in the data-acquisition module and reestablishes potentiostatic control of the cell by closure of the electronic switch S (Fig. 1). Also, the ready-receive status bit is set.

The programmable clock has a base frequency of 10 MHz. The clock period can be set with 16-bit resolution in two ranges: 0.1—6553.5 μs and 1—65535 μs. During recording of the stripping signal, the clock is used to trigger the A/D conversion in the data-acquisition module. When the electrochemical module is not in the stripping mode, the clock pulses are available for the computer through the ready-receive bit, and can be used for other purposes, e.g., timing of the periods with potentiostatic control of the cell.

TABLE 1

Functions under computer control in the electrochemical module

Device no.	Function no.	Description
0	0	Stop sending clock pulses to Apple
0	1	Start sending clock pulses to Apple
1	0	Set plating potential (D/A 1), within a range of 2 V
1	1	Set cut-of potential (D/A 2), within a range of 2 V
2	0	Set on/off switches for peripheral devices
2	0	Read test inputs
3	0	Set clock frequency in units of 0.1 μs
3	1	Set clock frequency in units of 1 μs
4	0	Read data from RAM address
4	0	Write data to RAM address
5	0	Select RAM address for subsequent read/write operation
6	0	Stop data acquisition
6	1	Start recording of primary signal
6	2	Start recording of background signal

Peripheral devices such as valves, stirrer motors and autosamplers can be controlled by means of ten on/off relays. Further, five test inputs sensitive to short-circuiting are available for monitoring the state of peripheral devices.

The data-acquisition unit (Fig. 2) comprises two identical 16-bit adders (A and B), an A/D converter (C) and a RAM module with 8K of 16-bit words (D). The A/D converter is of the successive approximation type (Burr-Brown ADC 803) with 12-bit resolution (±2 V) and a conversion time of 1.5 μs. In order to obtain equally fast updating of the RAM, the devices involved were supplemented with circuits allowing them to take control of the system data bus. When the A/D converter has taken a reading of the cell potential, the resulting binary number is simply the address of the RAM location which corresponds to the potential interval in which the reading falls. The data word in the memory cell is then transferred to the adder B, in which it is incremented by one. Subsequently, control of the data bus is transferred to the adder which writes the word back into the memory cell. This updating process lasts approximately 1 μs, and can thus be completed within the duration of the A/D conversion cycle.

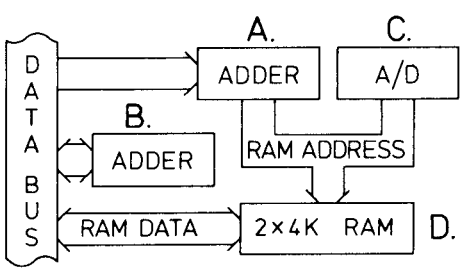

Fig. 2. Schematic diagram of the data-acquisition unit. See text for explanation.

The stripping signal is recorded with 1-mV resolution (±2 V), and the RAM can hold two signals simultaneously. The primary signal and the background signal can thus be recorded in rapid succession, and the computer need not read off the external memory between the scans.

The RAM can also be accessed directly by the computer. In practice, this situation occurs when the memory is zeroed before the recording of a stripping signal, and when the recorded signal is read into the Apple memory. First, adder A (Fig. 2) is loaded with the appropriate address, and in the subsequent read/write operation, the data word in the memory cell is transferred to the Apple-IIe or vice versa. The use of an adder for selecting the RAM address allows a useful auto-increment feature, so that the following read/write operation in the RAM will take place automatically in the following memory cell.

Apart from the potentiostat proper, the potentiostat unit comprises analog and digital meters for monitoring cell current and voltage. In order to minimize noise pick-up in the wires leading to the electrochemical cell, a preamplifier was built into a small box which can be placed close to the cell. Also, a low-pass filter with cut-off frequencies from 10 to 1000 Hz is provided for noise filtering.

Software

Programming considerations. The microcomputer program for experimental control and data handling was written in assembler code. Generally, the commercially available high-level languages (BASIC, PASCAL, etc.) do not provide routines for rapid I/O of data to/from experimental devices, and such specialized assembler routines are needed anyway. Owing to the relatively low computing power of the 6502B microprocessor, the gain in execution speed by programming in assembler is valuable when repetitive operations on large numbers of data are required. Moreover, assembler programming provides more efficient use of the computer memory which can be a decisive advantage given the limited RAM of the Apple-IIe.

Because standard subroutines for keyboard input and screen output are available in the Monitor ROM, as described in the Apple-IIe manual, assembler-coded programs need not be written from scratch. Also, many algorithms for number-base conversions, arithmetic operations, sorting of data, etc. are available for the 6502 microprocessor. In the program system described below, all such routines were taken from Scanlon [14].

Owing to the architecture of the 6502 microprocessor, the first 256 locations (page zero) of the Apple memory are particularly important. All 6502 instructions with an effective address on page zero occupy less memory and are executed about 30% faster than the corresponding instruction with an effective address anywhere else. Also, the indirect addressing modes of the 6502 must necessarily use page zero. In order to exploit these advantages, 24 consecutive page-zero locations are used extensively as scratch-pad locations throughout the assembler program; this also compensated for the low number of data registers in the 6502.

Programme description. The assembler-coded program is composed of a command interpreter, a general part for display and reduction of data, and a part which controls the electrochemical device. The most important commands are listed in Table 2.

The command interpreter accepts three-letter mnemonic commands, optionally followed by numerical arguments. After extensive error checking of the input line, program control is then transferred to the relevant subroutine. Some commands allow expected numerical arguments to be omitted, in which case the previous values are used as defaults. In this manner, frequent retyping of the same arguments is avoided. Although the Apple-IIe has no function keys, this feature was implemented by intercepting the first character on a new input line with the single-character input routine. The

TABLE 2

Summary of commands for p.s.a. control program

Group	Mnemonic	Parameters	Function
General	VID		Direct subsequent text output to video monitor
	HCO		Direct subsequent text output to printer
	TXT[a]		Display Apple text page
Graphical display	DIS		Display signal on graphics page
	EXP[a,b]	$n1, n2$	Display and expand channels $n1$—$n2$ of signal on graphics page
	ASC[a]		Enable autoscaling of signal
	LSF[a]		Lock scale factor to current value
	SCF	X	Set scale factor to X
	CLR		Clear graphics page
Cursor system	POS		Write out cursor position as (x,y)
	SCR	n	Move cursor to channel n
	CUT		Use channel no. of cursor as limit in integration window 1
Data handling	BFn[a]		Select data buffer n as default for subsequent commands
	LST	$n1, n2$	List contents of channels $n1$—$n2$
	SMn[b]	$n1, n2$	Set limits of integration window n to channels $n1$ and $n2$; write out sum
	ADD	n	Add channels n at a time
	MAV	n	Perform n-point moving average smoothing of data
Parameter handling	RPA	n	Display value of parameter n
	SPA	n, X	Set parameter n to X
	PLS		List all parameters
Other	PRT	$n1, n2$	Print channels $n1$—$n2$ as histogram on matrix printer
	RUN		Start p.s.a. experiment

[a]Command also implemented as function key. [b]Expected parameters may be omitted.

commands most frequently used were assigned a digit from 0 to 9, and so could be invoked by a single keystroke. Similarly, the cursor (see below) can be moved by pressing the left- or right-arrow keys of the computer.

Experimental data are stored in three data buffers, each holding 1024 two-byte signed integers. Because the electrochemical module records the potentiograms with 1-mV resolution, the size of the data buffers corresponds to a maximum potential range of 1.024 V, which is usually sufficient. If a larger potential range is required, the buffers can easily be expanded.

Recorded potentiograms can be displayed as histograms on the high-resolution graphics page (280 × 160 points), leaving four text lines at the bottom of the screen. The command DIS displays the entire signal, while smaller sections can be inspected by means of the EXP command. If the number of channels to be displayed exceeds 280, channel addition is performed; conversely, each channel can be expanded to several columns on the display if the number of channels needed is a fraction of 280. Vertically, the signal can be scaled automatically, or the scale factor can be set manually. With the PRT command, signals can be printed in histogram form on the matrix printer with higher resolution than the video screen permits.

On the video display, single channels of the potentiograms can be inspected by means of a cursor which appears as a small vertical bar above the signal. Also, the cursor can be used to set integration windows in conjunction with the CUT command. The cursor is moved through the data buffer with the left- and right-arrow keys of the Apple-IIe, while the SCR command transfers the cursor to a specific channel.

The program part that communicates with the electrochemical module was written as a hierarchical structure. At the lowest level, a set of subroutines performs basic tasks to control the electrochemical device. These routines, which use information stored in the parameter list (see below) are summarized in Table 3. On the next level, each routine performs a sequence of operations by several calls to the fundamental subroutines. For example, the routine POTTIME first sets the cell potential and clock rate used for the timing of the experiment. Then the CCOUNT waiting routine, in which the computer

TABLE 3

Summary of fundamental assembler-coded routines used in the control of the electrochemical module

Subroutine	Function
ZERO	Clears memory in electrochemical module
CSS	Sets the clock frequency used by the Apple-IIe for timing of the experiment
SPRATE	Sets data acquisition rate in p.s.a.
POTSET	Sets plating and cut-off potential
CCOUNT	Waiting routine counting of a specified number of clock pulses
MEMREAD	Reads a specified part of the recorded signal into the Apple memory

counts a specified number of clock pulses, is entered. Likewise, a STRIP routine sets the parameters for recording of the stripping potentiogram (data-acquisition rate and cut-off potential) after which the signal is recorded. Owing to this hierarchical structure, the main programme for experimental control becomes very short, and can easily be understood and altered by anyone without detailed knowledge of the program system. Table 4 shows the core of the simple program, in which a primary and a background p.s.a. signal are recorded, following a pre-electrolysis and a background electrolysis period, respectively. The routine POTTIME assumes that the cell potential to be set and the duration of the potential step are stored as two consecutive parameters in the list of experimental variables, and the Y-register must hold the index number of the first parameter. Thus, at the first call of POTTIME in Table 4, parameter 20 holds cell potential, while the next parameter contains the time count. The incorporation of a new potential/time step in the experiment then requires only two further lines in the assembler program. Recording of a stripping signal needs only two statements; first, the X-register is loaded with 0 or 1, indicating whether the main or background signal is to be recorded, and then the STRIP routine is called.

All arguments for the routines controlling the electrochemical module are stored in the parameter list, which consists of 128 signed two-byte integers. Parameter lists for different experimental conditions can rapidly be retrieved from floppy disk, and single parameters can be displayed and modified with the RPA and SPA commands. A hardcopy of all parameters is obtained with the PLS command in conjunction with the HCO command. This proved to be a useful feature in the documentation of experiments.

When repetitive measurements with identical instrumental parameters are needed, operation of the apparatus can be further simplified by the use of command files. The sequence of commands normally typed on the keyboard during the experiment is stored in a text file, which can then be executed with a single command line. Apart from the obvious automation advantage, this approach improves the reproducibility of timing and reduces the risk of typing error.

TABLE 4

Core of assembler program for a simple p.s.a. experiment

Instruction	Comments
LDY 20	Perform pre-electrolysis step
JSR POTTIME	
LDX 0	Record primary p.s.a. signal
JSR STRIP	
LDY 22	Perform background electrolysis step
JSR POTTIME	
LDX 1	Record background p.s.a. signal
JSR STRIP	

Generally, the assembler program performs integer calculations up to the level of the four basic arithmetic operations. Computations involving floating-point operations are too tedious to program in assembler code, and high-level languages are preferable. The assembler program can be incorporated efficiently as a subroutine in a program written in the built-in BASIC language of the Apple-IIe, because the language interpreter is present in a ROM. The built-in BASIC version is satisfactory for low-volume numerical calculations, but execution speed becomes a limiting factor if major computations are needed between experiments. A substantial gain in execution speed can be obtained by compiling the BASIC programs; several suitable compilers are available [15]. The combination of a language interpreter in ROM and a compiler for the same language proved useful for editing and debugging programs before compilation. Also, the compiled programs take advantage of machine-code routines in the interpreter ROM, thus reducing the size of the system library required at run-time.

Electrochemical procedures

A rotating glassy carbon electrode (Metrohm 628-50) at 1500 rpm was used. Solutions were prepared from triply distilled water and Suprapur (Merck) chemicals.

The base electrolyte for the model experiments was a non-deaerated 1.3×10^{-3} M acetate buffer prepared from sodium acetate and hydrochloric acid.

The fly-ash sample was decomposed and dissolved as previously described [7]; 2.5 ml of decomposed ash was diluted to 17.5 ml with water and adjusted to pH 4.8 with solid sodium acetate, and 50 μl of 2×10^{-2} M mercury(II) acetate was added. Sample solutions were not deaerated prior to measurements. The mercury film was plated onto the glassy carbon electrode in situ. The overlap of the thallium and lead peaks was negligible when a very thin mercury film was used. Consequently, the mercury film was renewed between determinations. A masking agent for lead (e.g., EDTA) was then unnecessary.

RESULTS AND DISCUSSION

To demonstrate the practical utility of the apparatus, thallium was determined in a certified coal fly ash (NBS SRM 1633a). This sample was chosen partly because of the low analyte concentration, and partly because of the very high content of oxidants in the decomposed ash (mainly iron(III), from 9.4% w/w iron in the fly ash), which causes rapid stripping of the amalgamated analytes. The thallium content of the coal fly ash was determined by standard addition to six subsamples drawn from the same decomposition solution. No significant blank value for thallium was observed. Figure 3 shows a typical stripping potentiogram of the digested ash. The thallium concentration found (5.6 ± 0.5 $\mu g\ g^{-1}$) is in good agreement with the certified value (5.7 ± 0.2 $\mu g\ g^{-1}$). The thallium content of the NBS fly ash was previously deter-

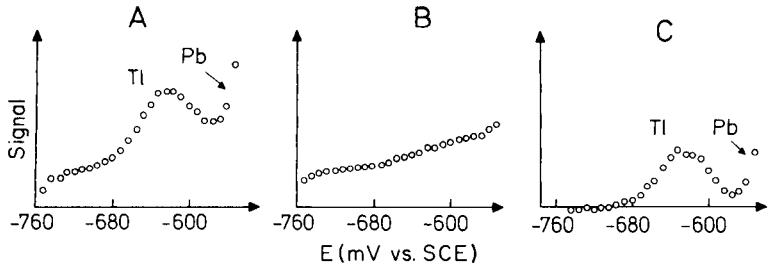

Fig. 3. Stripping potentiograms for a dissolved coal fly ash sample (NBS SRM 1633a). The thallium concentration in the sample solution is 8.1 ng g^{-1}. Electrolysis for 1 min at −900 mV vs. SCE; data-acquisition rate 660 kHz; channel width 8 mV. (A) Primary signal; (B) capacitance background signal; (C) background-corrected net signal.

mined at a data-acquisition frequency of 5 kHz. Accurate results were obtained [7], but a plating period of 8 min was needed to obtain sufficient sensitivity. In contrast, with the high data-acquisition rate of the present apparatus, a well-resolved thallium signal was obtained after only 1 min of pre-electrolysis.

In order to assess the improvement in sensitivity accruing from this high data-acquisition rate, model experiments with a buffer solution were conducted. The effect of the data-acquisition rate on the signal quality is illustrated in Fig. 4 for a solution containing 0.2 ng g^{-1} lead(II). Clearly, faster data acquisition improves the definition of the signal when short stripping transients are recorded. Alternatively, the increased rate can be utilized to maintain precision at shorter electrolysis times. From Fig. 5, the detection limit (taken as the concentration for which the relative standard deviation of the background corrected signal was 0.50) after 60 s of pre-electrolysis can be estimated as 0.1 ng g^{-1} lead(II) or cadmium(II). The stripping time vs.

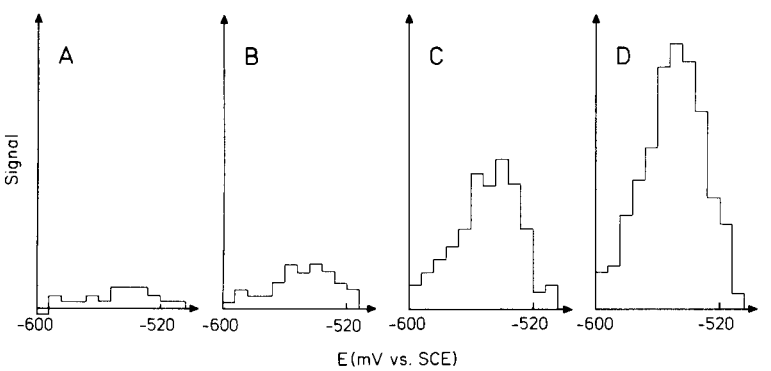

Fig. 4. Effect of data-acquisition rate on the signal quality in p.s.a. Potentiograms were recorded in a solution containing 0.2 ng g^{-1} lead(II) with pre-electrolysis at −900 mV vs. SCE for 30 s. Channel width 8 mV. The data-acquisition rate and the number of clock counts obtained during recording of the signal were: (A) 44.4 kHz, 19; (B) 88.5 kHz, 45; (C) 345 kHz, 147; (D) 660 kHz, 261.

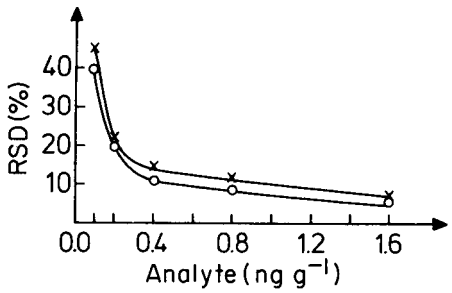

Fig. 5. Relative standard deviation of background-corrected signals (n = 10) as a function of analyte concentration: (×) lead; (○) cadmium. Pre-electrolysis for 60 s at −900 mV vs. SCE; data-acquisition rate 660 kHz.

concentration relation remained linear even in this range; with 60 s of pre-electrolysis, the correlation coefficients were 0.998 and 0.999 for lead(II) and cadmium(II), respectively, for concentrations in the range 0.1—1.6 ng g^{-1}.

The use of fast data acquisition in p.s.a. does not, of course, affect the analog signal and other factors can influence the precision ultimately obtained. Figure 6 illustrates the typical quality of signals near the detection limit. Although fast data acquisition improves the definition of the analytical signal, it does not change the signal/background ratio and so the background-subtraction procedure remains critical. The capacitance signal recorded after a short electrolysis period generally provides a good fit to the background function in the primary signal but, with small signals, the precision will obviously be reduced. However, the background signal in p.s.a. is caused mainly by a well-defined and reproducible physicochemical process rather than random noise. Consequently, if the capacitance signal is not distorted (e.g., by surfactants), the background curve lends itself to curve-fitting techniques.

In p.s.a., the amalgamated analytes are re-oxidized by transport of oxidizing agent to the working electrode. Small fluctuations in the transport rate cannot be avoided, but the effect on the analytical signal will tend to

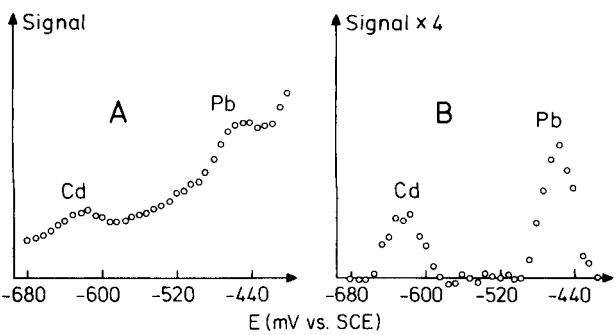

Fig. 6. P.s.a. signals obtained for a solution containing 0.4 ng g^{-1} cadmium(II) and 0.4 ng g^{-1} lead(II) with pre-electrolysis for 60 s at −900 mV vs. SCE (data-acquisition rate 660 kHz; channel width 8 mV): (A) primary signal; (B) background-corrected signal.

cancel out if the stripping time is long compared with the time scale of the fluctuations. When short stripping transients are detected, short-term variations in the transport of oxidant become an important source of imprecision. Stripping in stationary solutions should thus be avoided because diffusion-controlled transport is sensitive to random convection, e.g., caused mechanical disturbances [16]. A reproducible hydrodynamic pattern can be obtained around the working electrode when stripping is done under convective conditions. In batch p.s.a., this is best achieved with a high-precision rotating disk electrode; in flow p.s.a., cells must be designed with regard to elimination of turbulent conditions [17].

With short stripping transients, the analytical signal becomes more sensitive to electrical noise because the period over which the noise is averaged (i.e., the stripping time) is shorter, and so possible interfering noise is extended towards higher frequencies. Some precautions against electrical noise were taken in the design of the described apparatus (e.g., keeping the signal preamplifier close to the cell), but enclosing the cell in a Faraday cage might improve matters further.

The above results show that advantages can be gained by using data-acquisition rates as high as 660 kHz. Although it would be possible, at moderate cost, to produce an even faster data-acquisition unit for p.s.a., this would be of limited utility until the factors limiting the reproducibility of the analog stripping transient have been optimized.

The authors are indebted to J. K. Christensen for assistance with the preparation of the coal fly ash samples. A research fellowship (B. H.) from the Danish Technical Research Council (16-3499. K-810) is gratefully acknowledged.

REFERENCES

1 D. Jagner and A. Graneli, Anal. Chim. Acta, 83 (1976) 19.
2 D. Jagner, Anal. Chem., 50 (1978) 1924.
3 S. Bruckenstein and J. W. Bixler, Anal. Chem., 37 (1965) 786.
4 D. Jagner, M. Josefson and S. Westerlund, Anal. Chim. Acta, 129 (1981) 153.
5 D. Jagner, M. Josefson, S. Westerlund and K. Årén, Anal. Chem., 53 (1981) 1406.
6 J. Mortensen, E. Ouziel, H. J. Skov and L. Kryger, Anal. Chim. Acta, 112 (1979) 297.
7 J. K. Christensen, L. Kryger and N. Pind, Anal. Chim. Acta, 141 (1982) 131.
8 N. Pind, Talanta, 31 (1984) 1118.
9 T. Anfält and M. Strandberg, Anal. Chim. Acta, 103 (1978) 379.
10 H. J. Skov and L. Kryger, Anal. Chim. Acta, 122 (1980) 179.
11 A. Graneli, D. Jagner and M. Josefson, Anal. Chem., 52 (1980) 2220.
12 L. Kryger, Anal. Chim. Acta, 120 (1980) 19.
13 V. Karanassios and G. Horlick, Talanta, 32 (1985) 601.
14 L. J. Scanlon, 6502 Software Development, H. W. Sams & Co., IN, 1980.
15 J. H. Taylor and J. S. Taylor, Byte 7, no. 9 (1982) 440.
16 M. Josefson, Ph.D. Thesis, University of Goteborg, 1983.
17 L. Anderson, D. Jagner and M. Josefson, Anal. Chem., 54 (1982) 1371.

Analytica Chimica Acta, 188 (1986) 219—227
Elsevier Science Publishers B.V., Amsterdam — Printed in The Netherlands

INTERPRETATION OF INFRARED SPECTRA BASED ON STATISTICAL APPROACHES

J. SEIL, I. KÖHLER, C. W. v. d. LIETH and H. J. OPFERKUCH*

Deutsches Krebsforschungszentrum, Zentrale Arbeitsgruppe Spektroskopie, Im Neuenheimer Feld, 6900 Heidelberg (Federal Republic of Germany)

(Received 3rd March 1986)

SUMMARY

A computer procedure is presented for deriving classification rules automatically from a given set of i.r. spectra. The percentage of peaks belonging to a cluster within a set of spectra is used as a measure to train classification rules and define families of spectra. The algorithm obtains information from the fingerprint region of the i.r. spectra and is tested for natural products in different ways. The information is used for fast preliminary interpretation of spectra and the search time is decreased considerably. The study is based on the SPEKTREN information system of the German Cancer Research Center.

The rapid development of infrared (i.r.) techniques in recent years has produced wider interest in i.r. spectroscopy and various major and minor data collections with "full" spectroscopic information are already available or are being created. As the interpretation of an entire spectrum is usually difficult, computer methods have been devised to aid in the evaluation of i.r. spectral data. Library-search systems [1—5] are well established for the identification of i.r. spectra and function successfully provided that the unknown spectrum is in the data file. Substructural information for an unknown compound is often available by means of a substructure-abundance histogram for the best hits of a match. Nevertheless, the time required to search through a large data file can be prohibitively long [6]. Therefore it is desirable to develop new approaches to automatic interpretation of i.r. information: both pattern recognition [7—12] and rule-based algorithms [13—18] have been investigated with respect to spectral interpretations and classifications. Most of this work was done on functional groups and relatively small molecules. This traditional application of i.r. spectroscopy is often successful by visual examination alone. Therefore, it is of interest to develop methods which also evaluate the fingerprint region of the spectrum and thus provide quick and automatic classification of chemically similar skeletons. This could be used for preliminary interpretation of series of spectra.

The development of classification rules should be automatic, because rule finding is often the most laborious and time-consuming step in the classification procedure. Yet the rule trainer must be able to follow any single step.

0003-2670/86/$03.50

Both possibilities can help to condense spectral information for new interpretation rules. No special statistical model was used in this attempt. The main idea was to condense spectral and structural information from a data bank in order to attain a new quality. In an attempt to reach this goal, the problem arose of how structural similarity is encoded by the corresponding set of spectra and vice versa.

EXPERIMENTAL

This study is based on the i.r. data bank of the SPEKTREN information system of the German Cancer Research Center. The data bank currently contains about 2500 spectra of organic molecules and natural products which were recorded with a dispersive i.r. spectrometer. The peak positions are automatically calculated from a digitized spectrum with 1 point per wavenumber and stored together with structural information on the molecule (e.g., chemical name, connection table, HOSE code) for each spectrum. The SPEKTREN retrieval system allows the user to define sets of molecules by chemical names, HOSE code, molecular formula or library search runs. For the investigation presented here, only the 1600 solid compounds recorded in potassium bromide were used. The wavenumber range investigated was 1700—300 cm^{-1}.

Investigation of band distributions

Sets containing spectra of compounds with similar skeletons (Fig. 1) were generated. For each set, the distribution of all bands of the corresponding spectra was calculated. For many sets, the band distribution observed was far from uniform (e.g., estrans, Fig. 2), but most of the bands were bundled within the range of wavenumbers considered. It was assumed that such a set of similar skeletons could readily be encoded by the sequence of the more powerful bundles of bands called clusters. Therefore, the clusters had to be detected in order to verify the assumption.

Definition of clusters

Because of their varying broadness, the bundles of bands determine a variable raster within the wavenumber range considered; this raster consists of an alternating sequence of regions with high and low spectral information content.

An algorithm was developed in order to find such a raster. It is based on the concept of bundles and clusters (see Table 1) and is similar to the procedure described earlier [18]. An example is shown in Fig. 3. The upper and lower limits of the detected clusters are stored together with the number of bands which comprise the corresponding cluster (see Fig. 4). The differences in the number and the density of bands comprising the clusters are described by a measure called the cluster weight (see Table 1). This quantity connects the amount and the density of spectral information within a cluster. The

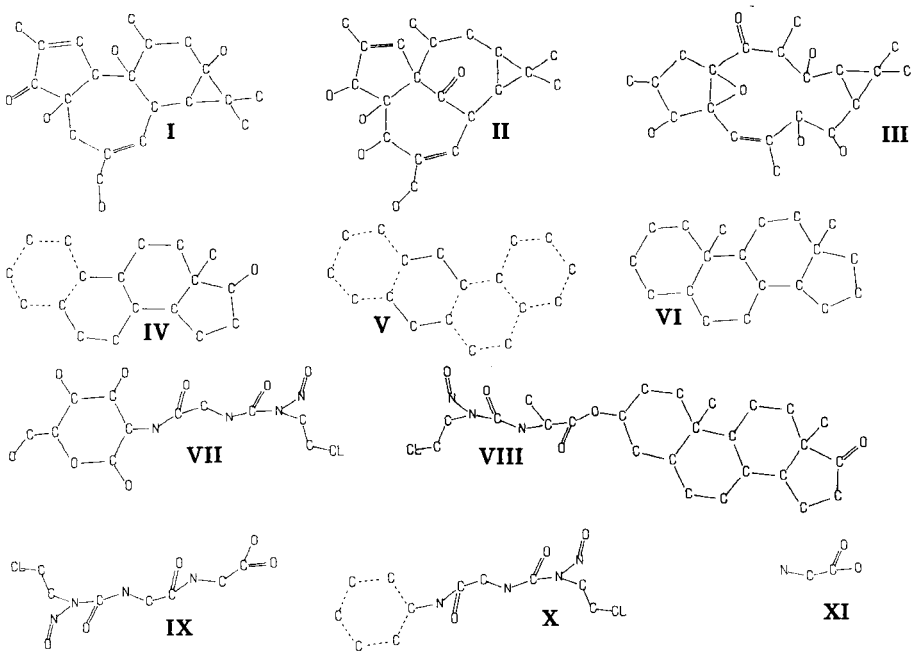

Fig. 1. Structures I—XI of the skeletons considered.

percentage of bands which belong to a cluster is taken as the measure of spectral similarity and is designated PDB (percentage of detected bands).

Classification procedure

A cluster sequence score is calculated for each spectrum and each cluster sequence. Essentially, this score consists of the number of bands which lie within a cluster, with addition of the respective cluster weights (see Table 1). The scores for all the sets of spectra used are calculated and a hit list of sets is generated. The spectrum is considered correctly classified if the set of spectra to which the spectrum belongs is at the top of a hit list of descending scores.

RESULTS

Classification

Table 2 shows the results of the classification for the eleven groups of spectra involved in this test. The numbers in column 1 refer to the skeletons given in Fig. 1. Classification is nearly always successful for sets with a PDB $>50\%$. Most such spectra are well represented by the cluster sequence of their respective group (completeness of information) and rather badly encoded by sequences of other groups (exclusiveness of information). These observations lead to the following definitions: (1) a set of spectra shows

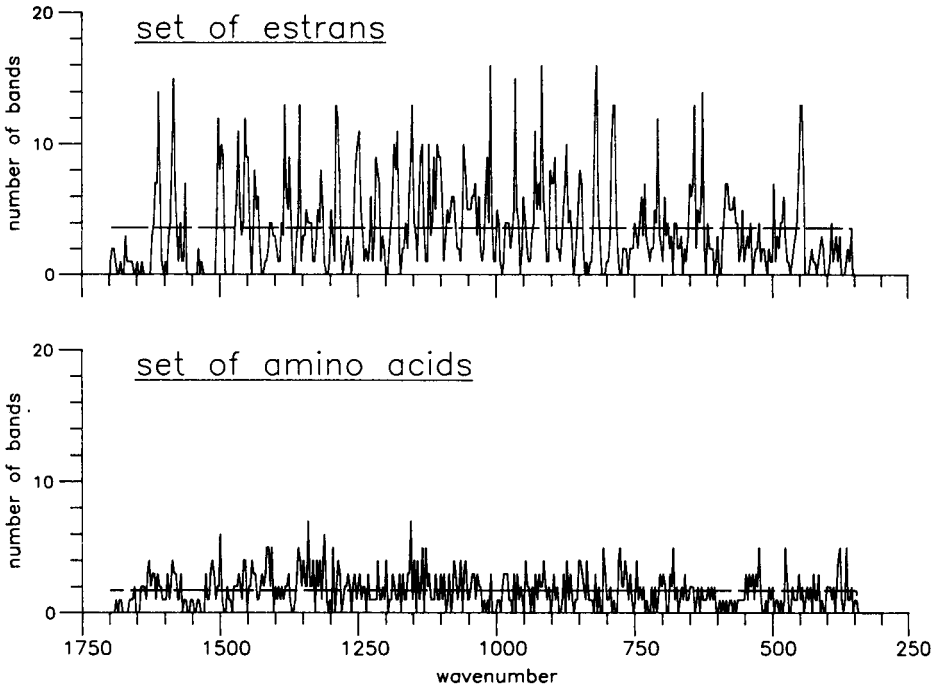

Fig. 2. Band distributions for two sets of compounds. The dashed horizontal line corresponds to uniform distribution (noise; see Table 1). For many sets of spectra, the distribution of bands differs greatly from uniform distribution, as in the set for estrans. For amino acids, band distribution is much more uniform.

similarity if its PDB is larger than a certain percentage (e.g., 50%) and is then called a group; (2) a group of spectra is called a family if the corresponding compounds have similar skeletons.

Training sets of spectra

The PDB can be used to search sets of spectra for subsets which constitute a group, or to reject mismatches from a set in order to attain a family. The procedure is based on rejection of spectra with relatively low scores and evaluation of the PDB for the remainder. As shown in the last column of Table 3, the PDB can collapse: no group can be found by this method. In contrast, the PDB for a sequence of subsets with steroids increases from 45% to 60%. The remaining 33 spectra form a group after the set has been trained. The result of classification training sets is shown in Table 3.

Defining new sets of spectra

The training procedure for sets of spectra can also be used to generate semi-automatically new groups of spectra from a data bank. A set comprising, for example, the 30 best-matched spectra of a library search can be treated

TABLE 1

Definitions

Term	Definition
1 Noise	NB/WRD[a]
2 Bundle	Group of nearby bands, the number of which is greater than that expected for uniform distribution.
3 Cluster	A bundle is called a cluster if the number of bands which belong to it is (A) >30% of the number of compounds which are members of the corresponding set, or (B) >1.5 times the expected value for uniform distribution.
4 Percentage of detected bands (PDB)	Percentage of those bands which belong to a cluster sequence.
5 Cluster weight (CW)[b]	(NBC/NSP) × (NBC/EXPECT)$^{1/2}$.
6 Cluster sequence score (CSS)	Sum of the weights of all matched clusters (with regard of multiple matchings) multiplied by the percentage of hits.

[a]NB is the number of all bands within the considered range which are part of a set of spectra. WRD is the width of its range of elevation. [b]NBC is the number of bands within a cluster. NSP is the number of spectra within the corresponding set. EXPECT is the number of bands to be expected within the cluster underlying uniform distribution.

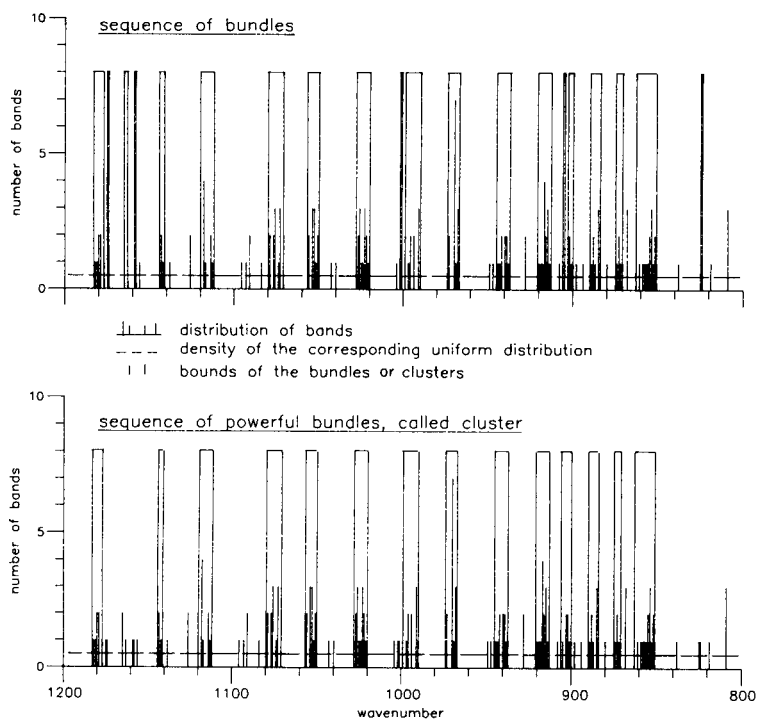

Fig. 3. Detection of bundles and clusters (part of the wavenumber range).

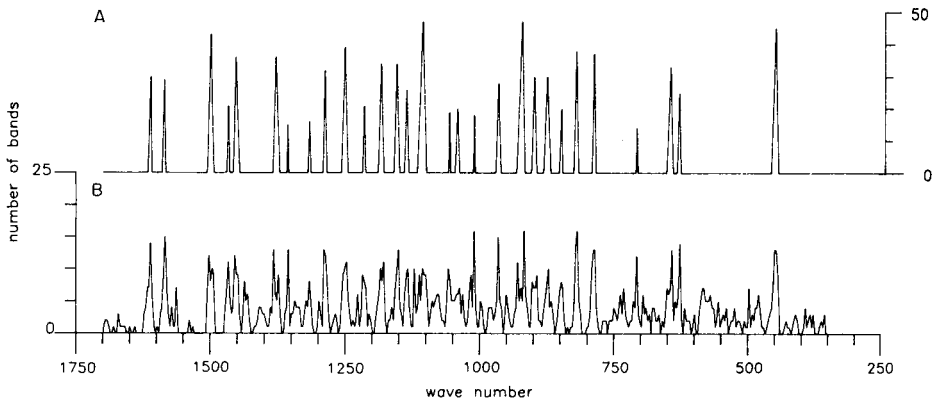

Fig. 4. Result of a cluster analysis (set of estrans): (A) positions and limits of the clusters and number of bands within each cluster; (B) distribution of bands (resolution is 1 point per 4 wavenumbers).

TABLE 2

Cluster analysis and classification of compounds on which the analysis depends

Set of compounds[a]	Number of compounds	Number of correctly classified compounds	PDB (%)
I	22	21	54
II	39	38	72
III	15	15	69
IV	44	44	54
V	27	27	53
VI	58	40	45
VII	11	11	65
VIII	30	28	60
IX	30	20	45
X	22	21	61
XI	28	0	18

[a]See Fig. 1.

in the way described above. Figure 5 describes graphically how this procedure functions. If a group of spectra can be extracted from the data bank, the spectroscopist has to decide whether it indeed represents a meaningful family of spectra. The family number VII was generated in this way.

Completeness and unambiguity of information

In order to test the completeness of information of the classification rules, training sets were created randomly from the existing groups of spectra and classification rules were derived as described above. Then the remaining test spectra were classified with these rules. The results are given in Table 4.

TABLE 3

Cluster analysis and classification of compounds after training

Set of compounds[a]	Number of compounds	Number of correctly classified compounds	PDB (%)
I	19	19	63
II	33	33	75
III	15	15	69
IV	39	38	54
V	21	19	53
VI	33	33	60
VII	11	11	65
VIII	27	27	61
IX	24	18	50
X	19	19	61
XI	0	—	—

[a]See Fig. 1.

Depending on the group of spectra, 70% of the test compounds were classified correctly. In more than 90% of the cases, the "correct" set is in position 1, 2 or 3 on the hit list (last columns). Several spectra of unknown compounds could also be classified. These observations suggest that the bands related to a skeleton are well represented within the respective cluster sequence.

In order to test unambiguity of the information compressed in a cluster sequence, the number of hits and the scores were calculated for all spectra in the data bank. Only a few spectra were found which exhibited scores similar to those of members of a particular family but which did not belong to that family.

Conclusion

The concept of clusters proved to be quite efficient for both classification of compounds and for the generation of groups of spectra. It should be emphasized that earlier attempts with constant rasters produced unsatisfactory results compared with those described above. The semi-automatic procedure for generating sets of spectra by a library search, and subsequent training to form a group of spectra is shown to be helpful in condensing spectral information to provide better knowledge about the skeleton region of i.r. spectra.

The algorithm was developed mainly to obtain information from the skeleton region of an i.r. spectrum and was tested on natural products, so that further investigations of other regions of an i.r. spectrum and other categories of compounds are required.

The algorithm can be used interactively for preliminary interpretation of series of spectra; it needed less than one second of computing time for the eleven families of compounds examined here.

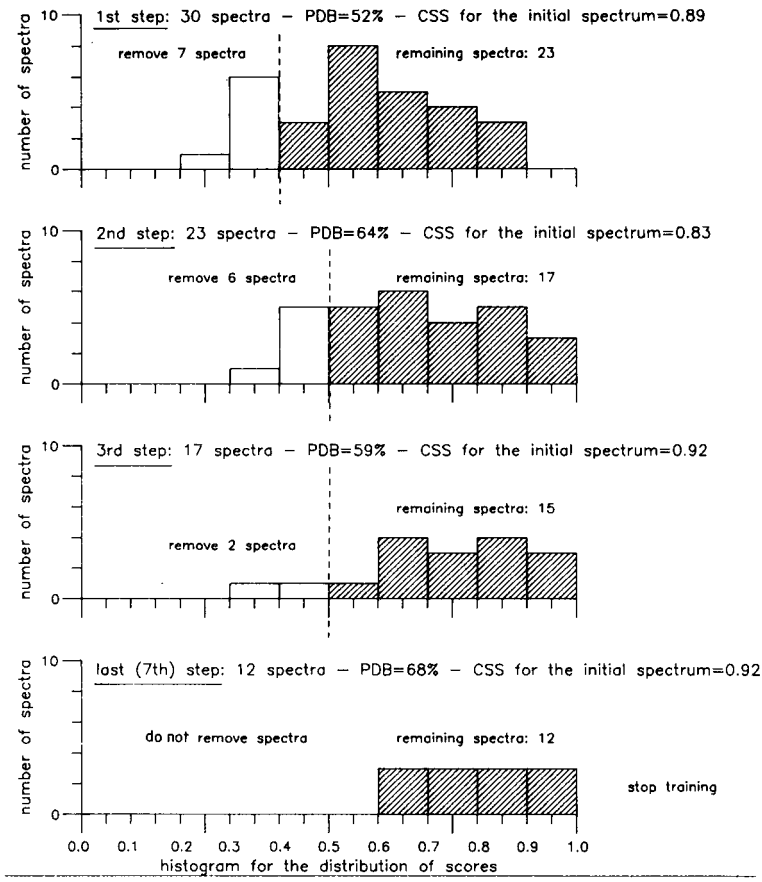

Fig. 5. Procedure for generating a group of spectra semi-automatically as follows. (1) Choose an initial spectrum and search for identity through the i.r. data base. (2) Store the n (e.g., 30) best-matched spectra. (3) Train the classification rule on this set; to do this, specify the cluster sequence, evaluate the CSS (cluster sequence score) for all spectra, and then remove spectra which have low CSS with respect to the others. Stop, if the CSS of the initial spectrum decreases remarkably, or if the PDB collapses, or if the number of the remaining spectra is <10, or if the PDB and all scores of the remaining spectra are high. Else go to 3. As a result, a group of 12 spectra was found, eleven of them represent compounds containing structure VII and one of them structure X. The 18 spectra removed do not represent compounds containing structure VII.

TABLE 4

Classification of "unknown" compounds (generally "unknown" compounds were obtained by excluding them randomly from the sets before training)

Set of compounds[a]	Number of compounds taken for analysis	Number of new compounds	Number of correctly classified compounds	Second or third scored
I	11	11	7	4
II	19	19	15	2
III	11	4	4	—
IV	22	22	22	—
V	13	12	3	4
VI	24	23	16	7
VII	8	3	3	—
VIII	15	15	9	3
IX	24	18	15	3
X	11	11	7	3

[a]See Fig. 1.

REFERENCES

1 Z. Hippe and R. Hippe, Appl. Spectrosc. Rev., 16 (1980) 135.
2 M. Zippel, J. Mowitz, I. Köhler and H. J. Opferkuch, Anal. Chim. Acta, 140 (1982) 123.
3 I. Köhler, M. Zippel, C. W. v. d. Lieth and H. J. Opferkuch, Fresenius Z. Anal. Chem., 315 (1983) 334.
4 S. R. Lowry and T. L. Isenhour, J. Chem. Inf. Comput. Sci., 15 (1975) 212.
5 S. R. Lowry, D. A. Huppler and C. R. Anderson, J. Chem. Inf. Comput. Sci., 25 (1985) 235.
6 M. Ruprecht and J. T. Clerc, J. Chem. Inf. Comput. Sci., 25 (1985) 241.
7 K. Varmuza, Pattern Recognition in Chemistry, Springer, Berlin, 1980.
8 K. Varmuza, Anal. Chim. Acta, 122 (1980) 273.
9 G. Hangac, R. C. Wieboldt, R. B. Lam and T. L. Isenhour, Appl. Spectrosc., 36 (1982) 40.
10 S. S. Williams, R. B. Lam and T. L. Isenhour, Anal. Chem., 55 (1983) 1117.
11 J. C. W. G. Bink and H. A. Van'T Klooster, Anal. Chim. Acta, 150 (1983) 53.
12 N. A. B. Gray, Anal. Chem., 47 (1975) 2426.
13 H. B. Woodruff and G. M. Smith, Anal. Chem., 52 (1980) 2221.
14 H. B. Woodruff and G. M. Smith, Anal. Chim. Acta, 133 (1981) 545.
15 S. A. Tomellini, D. D. Saperstein, J. M. Stevenson, G. M. Smith, H. B. Woodruff and P. F. Seelig, Anal. Chem., 53 (1981) 2367.
16 S. A. Tomellini, J. M. Stevenson and H. B. Woodruff, Anal. Chem., 56 (1984) 67.
17 M. O. Trulson and M. E. Munk, Anal. Chem., 55 (1983) 2137.
18 C. W. v. d. Lieth, J. Seil, I. Köhler and H. J. Opferkuch, Org. Magn. Reson., 23 (1985) 1048.

Analytica Chimica Acta, 188 (1986) 229—238
Elsevier Science Publishers B.V., Amsterdam — Printed in The Netherlands

THE DETERMINATION OF INDIVIDUAL GASEOUS IONIC ALKYLLEAD SPECIES IN THE ATMOSPHERE

C. N. HEWITT*

Department of Environmental Science, University of Lancaster, Lancaster LA1 4YQ (Great Britain)

ROY M. HARRISON and M. RADOJEVIC

Department of Chemistry, University of Essex, Colchester CO4 3SQ (Great Britain)

(Received 8th May 1986)

SUMMARY

Gaseous ionic alkyllead species (in the ng Pb m^{-3} range) are collected from air by absorption in water. After extraction into n-hexane, they are propylated or butylated and quantified by gas chromatography/electrothermal atomic absorption spectrometry. Interference from inorganic lead compounds and aerosol-phase alkyllead compounds is entirely absent, whilst that from tetraalkyllead compounds is small and generally negligible. This method allows the unequivocal identification of gaseous ionic alkyllead species in the atmosphere.

The determination of organic lead compounds in the atmosphere, arising from the world-wide use of tetraalkyllead (TAL) as gasoline additives and possibly from the natural alkylation of inorganic lead, has attracted much attention in recent years. Considerable advances in the determination of the various compounds have been made since the first practical method for the determination of total organic lead in air was reported by Snyder and Henderson in 1961 [1].

To date, two differing methodologies have been developed for this purpose. First, those utilizing iodine monochloride as an absorbing reagent followed by a selective extraction procedure and determination by atomic absorption spectrometry (a.a.s.) which gives a measure of the total gas-phase alkyllead in the sample (see, e.g. [2, 3]). Secondly, those based upon a chromatographic separation followed by an element-specific detector, which allows the determination of each tetraalkyllead compound in the sample. Several such methods have been reported based either on collection and preconcentration of the analytes on a porous polymer at ambient temperature (see, e.g. [4, 5]) or by cryogenic trapping at −80°C or lower (see, e.g. [6—9]).

Although it has been postulated that tetraalkyllead (R_4Pb) decomposes in the environment to give inorganic lead according to the following simplified scheme:

0003-2670/86/$03.50

$R_4Pb \rightarrow R_3Pb^+ \rightarrow R_2Pb^{2+} \rightarrow Pb^{2+}$

neither of the methodologies outlined above allows the determination of the suggested ionic alkyllead intermediate products. Whilst these species have been identified in aqueous samples (e.g., by spectrophotometry [10] or anodic stripping voltammetry [11]), no attempt had been made to identify them in the atmosphere. However, their presence in the atmosphere has been inferred from indirect evidence obtained from comparative studies based on simultaneous sampling with a species-specific gas chromatographic (g.c./a.a.s.) method and a non-specific (iodine monochloride) method [12, 13]. In an earlier study [5], it was found that the TAL concentration at a rural site was invariably lower than the total gas-phase organic lead concentration during a 50-day sampling period. It was postulated that this difference in concentrations (with a minimum of ca. 1 ng Pb m^{-3} for these samples) was due to the presence of some other (non-TAL) alkyllead species in the gas phase which would be detected by the iodine monochloride method but not by the TAL-specific g.c./a.a.s. method. It was suggested that the excess (non-TAL) alkyllead is probably trialkyllead or dialkyllead or both in the gas phase, arising from the decomposition of TAL in the atmosphere. Aerosol-associated alkyllead compounds can be separated by filtration and determined separately [13].

Concurrent with the development of these methods for the determination of tetraalkyllead in the atmosphere, a method for the determination of ionic organic lead species in aqueous and biological samples was reported [14]. In this elegant method, the ionic alkyllead species are extracted into an organic solvent with sodium diethyldithiocarbamate (NaDDC) followed by butylation to form the tetraalkyl derivatives of the ionic compounds. These derivatives are then amenable to analysis by g.c./a.a.s. This method has been modified in our laboratories where the use of benzene is discouraged [15] and has recently been refined to give better chromatographic separation and a faster procedure by using a propylating (rather than a butylating) Grignard reagent [16].

Once a suitable derivatization and analytical technique had been developed for the ionic alkyllead species, it became feasible to develop a method for their collection and quantification in air samples [17]. This paper describes the technique in detail.

EXPERIMENTAL

Chemicals and instrumentation

Pure tetramethyllead (TML), pure tetraethyllead (TEL) and a mixed solution containing all five tetraalkyllead compounds in diisopropyl ether, together with the chloride salts of trimethyllead (TriML), triethyllead (TriEL), dimethyllead (DiML) and diethyllead (DiEL) were kindly supplied by the Associated Octel Company (Ellesmere Port, Great Britain). They were all stored in the dark at 4°C and handled according to the Company's safety

instructions. Propylmagnesium chloride (Aldrich) and butylmagnesium chloride (Alfa Products) were used. All other chemicals were from BDH.

The g.c./a.a.s. system used was described in detail elsewhere [5], and is based on the system developed by Ebdon et al. [18]. Briefly, a Perkin-Elmer F17 gas chromatograph with a glass column (1 m long, 6-mm o.d., 2-mm i.d.) containing 3% OV-101 on Gaschrom-Q was interfaced with an Evans Electroselenium 240 Mk. 2 flame atomic absorption spectrometer by a 1/16-in. o.d. stainless-steel transfer line heated to 150° C. The g.c. eluate was mixed with hydrogen and fed into a ceramic tube of recrystallized alumina (150 mm long, 14-mm o.d., 9-mm i.d.) suspended in the air/acetylene flame along the light path. As an alternative to the flame-heated ceramic tube, an electrothermal atomization cell can be used, with enhanced resolution and sensitivity [16].

Procedures

Generation of ionic alkyllead vapour. For the development work described, it was necessary to generate an air stream containing the ionic alkyllead species in the gas phase. This was done with the vapour generator shown in Fig. 1. A small quantity (ca. 0.1 g) of the solid alkyllead salt (TriALCl) was placed in a stainless-steel tube with glass wool plugs at each end. Charcoal-filtered air was pumped through the tube and the output was filtered through a 0.45-μm pore diameter Millipore membrane placed in a stainless-steel holder with a teflon gasket. Charcoal-filtered secondary diluent air was added and the resultant air stream was sampled with use of another pump.

The total gas-phase lead content of the filtered output of the generator was quantified by bubbling it through iodine monochloride solution followed by a.a.s. measurement [3]. The volatility of the salts was found to be much higher than expected and high vapour concentrations were found at ambient temperatures (e.g., 450 μg m^{-3} for TriML with no secondary diluent air).

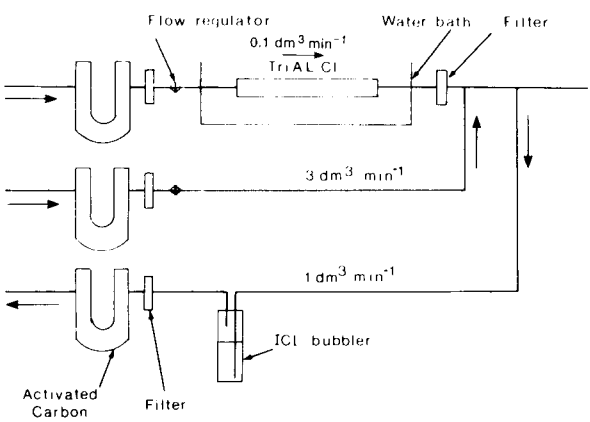

Fig. 1. Vapour generator for ionic tri- and di-alkyllead species.

Subsequently, the tube containing the salt was immersed in a ice/water slush bath and ten times the amount of diluent air shown in the figure was used. In this way, low vapour concentrations were achievable, approaching the same order of magnitude as those expected in polluted ambient air.

The alkyllead produced by the generator was also sampled by use of a cryogenic trap. This was a glass U-tube (20 cm long, 1 cm diameter) containing 2-mm glass beads and immersed in a liquid nitrogen/ethanol slush bath at −130° C. The collection efficiency of the trap was evaluated by placing an iodine monochloride bubbler after it. Provided that sufficient time was allowed for the trap to cool to the slush bath temperature before sampling began (ca. 1 min), then no alkyllead was found to pass through the trap. The efficiency of removal of the ionic lead species and TML and TEL from spiked glass beads (using the method detailed below) was found to be quantitative. After sampling, the trap was removed from the slush bath, 10 cm^3 of deionized double-distilled water and 2.5 cm^3 of n-hexane were carefully added and the trap was allowed to warm to room temperature. The beads and liquid were transferred to a glass tube and 1.5 g of sodium chloride and 1.5 cm^3 of aqueous 0.1 M NaDDC were added. The tube was mechanically shaken for 30 min and the contents were transferred to a glass separating funnel which had a teflon tap. The organic phase was removed, the ionic alkyllead compounds were butylated or propylated as previously described [15, 16] and used for g.c./a.a.s.

This method showed that the gas-phase output of lead from the vapour generator was not exclusively as the ionic alkyllead species; the analogous tetraalkyl compound was also produced. For example, TriML solid produced both TriML and TML in the gas-phase. This may be explained by disproportionation reactions [19]. This production of TAL had to be taken into account in calculating the collection efficiency of the method described below because TAL interfered slightly.

Generation of tetraalkyllead vapour. A pre-requisite to any method for the sampling of gas-phase TriAL or DiAL in air is that any TAL present in the air should not interfere. For this reason, a constant-temperature diffusion cell, shown in Fig. 2, was used to generate low concentrations of TML and TEL vapour in an air stream. For some experiments, charcoal-filtered secondary diluent air was added to the air stream and samples were taken with a separate pump in the same manner as shown in Fig. 1.

Collection efficiency tests. Two 125-cm^3 gas bubblers were modified by extending their central tubes to within 2—3 mm of the base of the bottles with 0.5-mm capillary tubing. The bubblers were charged with 80 cm^3 of deionized double-distilled water and connected in series. A third bubbler containing 80 cm^3 of 0.1 M iodine monochloride solution was connected in series behind these. The output of the alkyllead vapour generator was sampled by drawing a known volume of air (as determined by a GAP rotameter and stopwatch) through the sampling train. This was repeated three times using fresh solutions for each of the four alkyllead salts. After sampling was

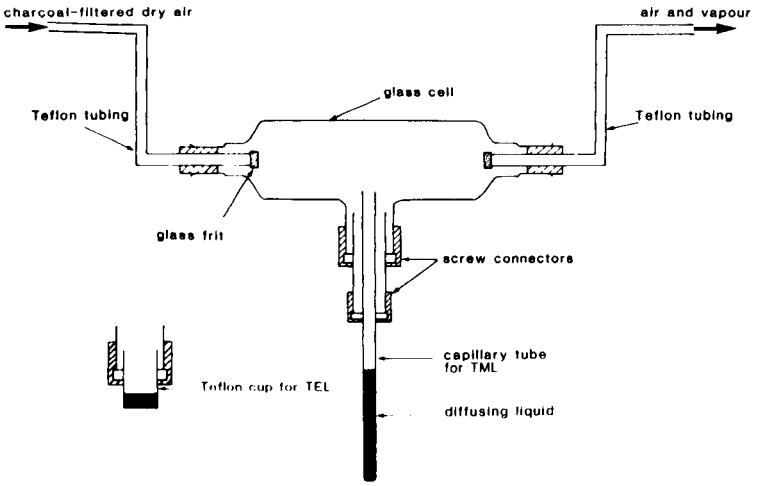

Fig. 2. Vapour generator for tetraalkyllead.

completed, any alkyllead present in the iodine monochloride solution was selectively extracted by dithizone in carbon tetrachloride in the presence of EDTA, back-extracted into 1% nitric acid/1% hydrogen peroxide and analysed by graphite-furnace a.a.s. [3]. The contents of the two water bubblers were combined, transferred to a 250-cm^3 glass bottle and extracted, alkylated and examined by g.c./a.a.s. [15].

Sampling of ambient air. Air was drawn at 1—5 dm^3 min^{-1} through two modified 125-cm^3 gas bubblers in series, each charged with 80 cm^3 of de-ionized double-distilled water and preceded by a 0.45-μm membrane filter. Upon completion of sampling (24—48 h), the contents of the bubblers were combined, extracted and processed as above by the propylation procedure [16]. All sampling was done in the dark or in darkened bottles and exposure of prepared samples to light was kept to a minimum.

RESULTS AND DISCUSSION

Interference from TAL

The recoveries of TML and TEL vapours obtained by the various procedures are shown in Table 1. Less than 4% of the TML and less than 1% of the TEL bubbled through the water was recovered. Furthermore, in all cases it was found not as TAL but as the alkylated trialkyl derivative. Given the aqueous solubility of TAL (15 $\mu g\ dm^{-3}$ for TML and ca. 0.3 $\mu g\ dm^{-3}$ for TEL at 30°C) [19], it was expected that some TAL would be recovered as such. However, decomposition to TriAL must have occurred, either during sampling or storage, and any remaining TAL was removed in the air stream or by adsorption on the bottle walls. This indicates that interference from any TAL present in the air sample is slight, and is negligible in most ambient air sampling applications.

TABLE 1

Recovery of tetraalkyllead vapour by absorption in water

Method of analysis	Concentration in air (ng dm^{-3})[a]			
	TML		TEL	
Iodine monochloride	3.5	199	16	320
Cryogenic trap/ g.c./a.a.s.	3.5	190	16	303
Water/butylation/ g.c./a.a.s.	0.14	7.2	<d.l.[b]	1.0
Recovery in water (%)	4.0	3.7	<0.1	0.3

[a]All values are the mean of three determinations with two absorption bottles used in series. [b]Detection limit (absolute d.l. = 30 pg Pb).

Recovery of ionic alkyllead compounds

Table 2 shows the collection efficiencies for the gas-phase ionic alkyllead species from water. These were calculated after allowance had been made for the known extraction and propylation efficiencies for the various compounds from aqueous solutions [16]. Whilst butylation is an acceptable derivatization method for the TriAL compounds with similar near-quantitative efficiencies to those obtained by propylation, it proved an unsatisfactory method for DiAL. Butylation efficiencies of only 29 ± 4% (DiML) and 21 ± 5% (DiEL) were found compared with propylation efficiencies of 95 ± 10% (DiML) and 98 ± 12% (DiEL).

Collection efficiencies for the various compounds range from 79% for TriML to 46% for DiEL. The corresponding detection limits for the various compounds in air depend on the absolute detection limits of the detector used. These are shown in Table 3. It can be seen that g.c./flame a.a.s. [5] has rather modest detection limits, especially for the butylated DiAL compounds, giving detection limits in air ranging from 0.25 ng Pb m^{-3} for TriML to 8.7 ng Pb m^{-3} for DiEL, based on a 5-m^3 air sample. However, improvements are obtained when propylation is used for derivatization, followed by g.c./electrothermal a.a.s. [16]. A further improvement can be achieved by concentrating the propylated extract from 5 cm^3 to 0.5 cm^3 by slowly purging with nitrogen (80% recovery) [16]. Detection limits in air of 0.06—0.44 ng Pb m^{-3} are then obtained (for TriML and DiEL, respectively).

The efficiency of collection of the compounds in water at various ionic alkyllead vapour concentrations was investigated by adding varying amounts of diluent air to the vapour generator. The results are given in Table 2. For TriML, concentrations of 260 and 230 ng Pb m^{-3} gave collection efficiencies of 79 and 76%, respectively. Decreasing the concentration of TriML to 0.1 ng Pb m^{-3} did not affect the collection efficiency. Similarly, decreasing the TriEL, DiML and DiEL concentrations did not significantly alter the collection efficiency for these compounds.

TABLE 2

Collection efficiencies of ionic alkyllead vapours by water

Species	TriML			TriEL			DiML			DiEL		
Vapour concn. (ng Pb m^{-3})	260	230	0.1	550	150	3	2100	270	7	2700	260	20
Efficiency (%)[a]	79	76	79	75	67	69	67	66	65	46	48	45

[a]Calculated after allowing for non-quantitative recovery and propylation efficiencies (TriML 104%, TriEL 100%, DiML 95%, DiEL 98%, [15]). Each value is the mean of three determinations.

TABLE 3

Detection limits for alkyllead chlorides by different methods

Method	Detection limit[a]			
	TriML	TriEL	DiML	DiEL
G.c./flame a.a.s. after butylation	0.025	0.044	0.210	0.500
Corresponding d.l. in air	0.25	0.47	2.75	8.7
G.c./electrothermal a.a.s. after propylation and N_2 concentration	0.02	0.05	0.03	0.08
Corresponding d.l. in air	0.06	0.17	0.13	0.44

[a]Detection limit is defined as 3 × standard deviation of the noise. The absolute limits are given as ng Pb; the limits for air are given as ng Pb m^{-3}, based on a 5-m^3 air sample with a 50-μl injection.

Sample storage and loss

Loss of the various TriAL and DiAL compounds during sampling was investigated by spiking water with known amounts of the chlorides. Carbon-filtered air was bubbled through the solutions at 2 dm^3 min^{-1}, the rate normally used for air sampling. After passage of ca. 3 m^3 of air, the solutions were analysed. No loss of alkyllead was observed. Similarly, spiked solutions of TriAL and DiAL (50 ng Pb dm^{-3}), which correspond to an air concentration of 1 ng Pb m^{-3} for a 5-m^3 air sample were found to be stable when stored in the dark for 72 h.

The possible redistribution of alkyl groups between compounds during sampling and storage was investigated by spiking water with known amounts of TriML and TriEL chlorides. Carbon-filtered air (3 m^3 at 2 dm^3 min^{-1}) was bubbled through the water in the dark and the solution then analysed. No evidence of the formation of mixed alkyllead compounds was seen in the resultant chromatogram.

TABLE 4

Results obtained for TAL, TriAL and DiAL in air at a background urban site (ng Pb m^{-3})[a]

Inorganic lead	TML	TMEL	DMDEL	MTEL	TEL	TriML	DiMEL	DiEML	TriEL	DiML	DiEL
145	3.2	—	—	1.8	6.6	—	—	—	—	—	—
148	6.1	1.0	1.6	3.3	—	0.4	—	—	—	—	5.1
111	3.2	—	—	—	—	—	1.2	—	—	2.6	—
103	1.0	—	—	—	1.9	—	—	—	1.1	—	0.7
274	10.9	2.6	—	—	2.6	19.8	—	—	—	—	—
167	2.0	—	—	1.7	—	0.3	—	—	—	0.5	—

[a]A dash indicates that the concentration was below the detection limit. TAL species were determined as described earlier [5].

Results of ambient air sampling

Some results from sampling at a background urban roof-top site in Colchester are listed in Table 4, which includes results for TAL obtained simultaneously. The only compound to appear in all samples is tetramethyllead. The TAL composition of these samples and inorganic lead levels are more typical of rural than urban sites [5]. Trialkyllead and dialkyllead species are rather variable both in relative and absolute concentrations, but clearly may comprise an appreciable proportion of total gas phase alkyllead.

Conclusions

Collection from the atmosphere of gas-phase ionic alkyllead compounds was achieved by bubbling filtered air through water. Collection efficiencies of 46—79% were found for the various compounds. The subsequent extraction and alkylation followed by g.c./a.a.s. allows their simultaneous, specific determination. Whilst the collection efficiencies found are not quantitative, this method appears to be the only one presently available which allows the gaseous ionic alkyllead species to be determined in an air sample. If the samples are propylated, concentrated by purging with nitrogen, and examined by g.c./electrothermal a.a.s., then the method is very sensitive, allowing these species to be determined in ambient air. Both inorganic lead and solid-phase alkyllead species are excluded from the determination by the use of a highly efficient particle filter. Gas-phase tetraalkyllead compounds give a slight interference (<4%).

The fact that variations in ionic alkyllead vapour concentrations do not significantly alter their collection efficiencies in water indicates that the method is suitable for the collection of the species from the ambient atmosphere. The techniques described have been successfully applied to a variety of atmospheric samples.

The Natural Environment Research Council is thanked for provision of a research studentship (to C.N.H.). The staff of the Associated Octel Co., Ellesmere Port are thanked for helpful discussions and the provision of chemicals.

REFERENCES

1 L. J. Snyder and R. S. Henderson, Anal. Chem., 33 (1961) 1175.
2 S. Hancock and A. Slater, Analyst, 100 (1975) 422.
3 J. Birch, R. M. Harrison and D. P. H. Laxen, Sci. Total Environ., 14 (1980) 31.
4 T. Nielsen, H. Egsgaard, E. Larsen and G. Schroll, Anal. Chim. Acta, 124 (1981) 1.
5 C. N. Hewitt and R. M. Harrison, Anal. Chim. Acta, 17 (1985) 277.
6 Y. K. Chau, P. T. S. Wong and P. D. Goulden, Anal. Chim. Acta, 85 (1976) 421.
7 D. C. Reamer, W. H. Zoller and T. C. O'Haver, Anal. Chem., 50 (1978) 1449.
8 W. R. A. De Jonghe, D. Chakraborti and F. C. Adams, Anal. Chem., 52 (1980) 1974.
9 B. Radziuk, Y. Thomassen, J. C. Van Loon and Y. K. Chau, Anal. Chim. Acta, 105 (1979) 255.

10 H. R. Potter, A. W. P. Jarvie and R. N. Markall, Water Pollut. Control, 53 (1977) 123.
11 S. E. Birnie and D. J. Hodges, Environ. Technol. Lett., 2 (1981) 433.
12 W. R. A. De Jonghe, D. Chakraborti and F. C. Adams, Environ. Sci. Technol., 15 (1981) 1217.
13 R. M. Harrison, C. N. Hewitt and M. Radojevic, Sci. Total Environ., 44 (1985) 235.
14 Y. K. Chau, P. T. S. Wong and O. Kramar, Anal. Chim. Acta, 146 (1983) 21.
15 R. M. Harrison and M. Radojevic, Environ. Technol. Lett., 6 (1985) 129.
16 M. Radojevic, A. Allen, S. Rapsomanikis and R. M. Harrison, Anal. Chem., 58 (1986) 658.
17 C. N. Hewitt and R. M. Harrison, Proc. Int. Conf. Heavy Metals Environ., 1985, C.E.P. Edinburgh, pp. 171.
18 L. Ebdon, R. W. Ward and D. A. Leathard, Analyst, 107 (1982) 129.
19 H. Shapiro and F. W. Frey, The Organic Compounds of Lead, Wiley, New York, 1968.

Analytica Chimica Acta, 188 (1986) 239—245
Elsevier Science Publishers B.V., Amsterdam — Printed in The Netherlands

LIQUID—LIQUID EXTRACTION OF METAL IONS BY THE SULFIDE PODAND 1,12-DI-2-THIENYL-2,5,8,11-TETRATHIADODECANE

ELWIRA LACHOWICZ* and ANDRZEJ KRAJEWSKI

Department of Analytical Chemistry, Warsaw University of Technology, PL-00-664 Warsaw (Poland)

MIROSŁAW GOLIŃSKI

Institute of Organic Chemistry, Polish Academy of Sciences, PL-01-224 Warsaw (Poland)

(Received 11th November 1985)

SUMMARY

The sulfide podand (an open-chain neutral multidentate ligand with six sulfur donor atoms) 1,12-di-2-thienyl-2,5,8,11-tetrathiadodecane (TTD) was synthesized. Its extracting properties were examined with 1,2-dichloroethane and 4-methylpentan-2-one as solvents. The reagent showed high selectivity for silver(I) and copper(I) ions; mercury(II) was extracted (ca. 97%) under certain conditions. Extraction of silver(I) was studied in detail with ^{110m}Ag tracer. Log D values $\geqslant 2$ were obtained for the range from pH 6 (with perchlorate as counter-ion) to 2 M perchloric acid or 6 M nitric acid. The ratio of Ag:TTD in the complex was 1:1. Silver could be back-extracted with 4—6 M hydrochloric acid.

Polythioethers are neutral sulfur-containing reagents. Both bidentate [1—4] and polydentate cyclic [3, 5—10] thioethers have been used for the extraction of soft metal ions. Cyclic ligands (with S, O or N donor atoms) belong to the class of reagents which form so-called host-guest complexes with metal ions. In Vögtle and Weber's classification and nomenclature of "host" ligands [11, 12], coronands (monocyclic ligands), cryptands (bi- and poly-cyclic) and podands (their acyclic, open-chain analogs) are distinguished. Podands have some advantages over cyclic compounds: they are easier to synthesize, their structure is more flexible and their complexation rate is greater. It has been observed that the macrocyclic ligand containing four thioether donor atoms forms only a slightly more stable complex with nickel(II) in nitromethane than does the corresponding open-chain ligand [13]. Thus the large macrocyclic effect occurring in the cyclic vs. acyclic tetramine complexes in aqueous solution [14] was not found in that case. Spherical wrapping of podands around a metal ion [11, 12] (confirmed by x-ray structural analysis of crystalline complexes) creates a pseudocavity similar to that possessed by cyclic compounds such as crown ethers. Rigid donor terminal groups bearing donor centres facilitate complex formation with these pseudocyclic species and increase the stability constants (the effect being called the "terminal groups concept").

0003-2670/86/$03.50

Here a new reagent is presented, the podand 1,12-di-2-thienyl-2,5,8,11-tetrathiadodecane containing six sulfur donor atoms. Its extracting abilities towards a group of metal ions, mainly silver, are described.

EXPERIMENTAL

Synthesis of 1,12-di-2-thienyl-2,5,8,11-tetrathiadodecane

The 1,12-di-2-thienyl-2,5-8,11-tetrathiadodecane (TTD) was prepared from 1,4,7,10-tetrathiadecane [15] and 2-chloromethylthiophene [16]. The reaction proceeded in a catalytic two-phase system [17] as follows: 2-chloromethylthiophene (72.9 g, 0.55 mol) was added dropwise during 10 min to an efficiently stirred mixture of 1,4,7,10-tetrathiadecane (53.6 g, 0.25 mol), aqueous 50% (w/v) sodium hydroxide (600 ml), tetrabutylammonium bromide (8.1 g, 0.025 mol) and toluene (1000 ml). Slight cooling was necessary to keep the temperature below 25°C. After the addition was complete, stirring was continued for 1 h. Then the mixture was diluted with water, the organic layer was separated and the aqueous phase was extracted with 100 ml of toluene. The combined toluene extracts were washed with water and dried with sodium sulfate. Evaporation of solvent (under reduced pressure) and two recrystallizations from a 1:3 tetrachloromethane/hexane mixture gave 1,12-di-2-thienyl-2,5,8,11-tetrathiadodecane (yield 60—64%). The product had m.p. 50.8—51.6°. The ^{1}H-n.m.r. (60 MHz, $CDCl_3$, δ in ppm) data were: 2.74 (12 H, s); 4.03 (4H, s); 6.96—7.54 (6H, m). Elemental data: calcd. for $C_{16}H_{22}S_6$, 47.25% C, 5.45% H, 47.3% S; found 46.8% C, 5.3% H, 47.45% S.

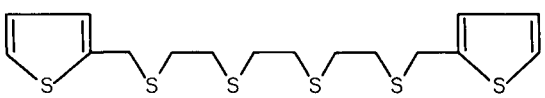

Reagents and equipment

The solutions of 1,12-di-2-thienyl-2,5,8,11-tetrathiadodecane (TTD) used were 1×10^{-3} M, prepared in 1,2-dichloroethane or methyl isobutyl ketone (MIBK). 1,2-Dichloroethane was shaken three times with 2 M potassium hydroxide and distilled water [8], dried with molecular sieves and distilled.

The radioactive tracers ^{110m}Ag (as silver nitrate in 1 M nitric acid) and ^{197}Hg were produced by the ORiPI (Swierk near Warsaw). The total silver and mercury concentrations in the initial solutions were adjusted without taking into account the isotope concentrations (ca. 10^{-8} M). Stock solutions of silver and mercury (1×10^{-2} M) were prepared from silver nitrate and mercury sulfate dissolved in nitric acid. Stock solutions of other ions (1 mg ml^{-1}) were prepared from the appropriate sulfates or nitrates. Sodium perchlorate was recrystallized twice from distilled water. Other reagents were of analytical purity.

A NaI(Tl) scintillation detector was used to measure the activity of the ^{110m}Ag and ^{197}Hg isotopes. A Pye-Unicam SP90 Series 2 atomic absorption spectrometer was used for the determination of other metal ions.

Procedures

Extraction of silver and mercury. An aqueous solution containing 1×10^{-5} M silver(I), an appropriate volume of ^{110m}Ag solution (or 5×10^{-6} M mercury(II) and ^{197}Hg) and any other reagents required was prepared. Buffer solutions (pH 3—6) were made with 1 M acetic acid and 1 M sodium acetate. In some experiments, the ionic strength was kept at 0.3 with sodium sulfate. An aliquot (10 ml) of this solution was shaken with a solution (10 ml) of the TTD in 1,2-dichloroethane or MIBK for 5 min and then allowed to stand for 15 min. After phase separation, 2-ml portions of each phase were transferred to polyethylene ampoules and the isotope activity was measured.

The pH of the aqueous phase after extraction was measured when required. Distribution coefficients were evaluated as a mean from the results of duplicate experiments. The isotope balance, checked for each experiment, ranged from 96 to 104% (any exceptions are mentioned below).

Extraction of other ions. These experiments were done in the same way. The concentration of test ion was 10 $\mu g\ ml^{-1}$. In order to obtain copper(I) ion, an appropriate amount of hydroxylammonium sulfate was added to give a 0.1 M solution. After separation, the aqueous phase was transferred to a beaker and evaporated to a small volume; 2 ml of concentrated nitric acid was added, the contents were evaporated again and the solution was diluted to 10 ml with water. The metal ion was quantified by atomic absorption spectrometry.

RESULTS AND DISCUSSION

Extraction of various ions with TTD

The TTD reagent is easily soluble in 1,2-dichloroethane, MIBK and toluene. The absorption spectrum of 5×10^{-5} M TTD in 1,2-dichloroethane, which gives a molar absorptivity of $1.7 \times 10^4\ l\ mol^{-1}\ cm^{-1}$ at 238 nm, does not show any changes when the solution is equilibrated with 0.1 M perchloric acid, acetate buffer solution pH 4.7, or 0.1 M sodium hydroxide. Storage for 2 weeks does not alter the solution, as judged by the spectra.

Extractions were studied for various "soft" metal ions, i.e., Ag(I), Cu(I), Hg(II) and Cd(II), as well as intermediate ions, i.e., Cu(II), Ni(II), Co(II), Zn(II) and Pb(II), and "hard" Fe(III) ions, according to Pearson's classification [18]. In these experiments, two solutions (pH 4.7 with perchlorate as counter-ion, and 1 M perchloric acid) were extracted with TTD in 1,2-dichloroethane or MIBK. Results are summarized in Table 1.

Silver(I) are extracted very well under the two sets of conditions tested (I and II). Extraction of mercury(II) is relatively good only in 1 M perchloric acid medium. The percentage extraction of mercury(II) separated under I and II conditions does not depend on the time of extraction in the range 2—15 min. Copper(I) is separated quantitatively at pH 4.7, but in 1 M perchloric acid no extraction was observed probably because copper(II) was not reduced to copper(I) in that solution. Extraction of cadmium(II) (also "soft"

TABLE 1

Extraction of metal ions with TTD under different conditions

Metal ion	Extraction (%)		Metal ion	Extraction (%)	
	I[a]	II[b]		I[a]	II[b]
Hg(II)	21.8	96.9	Ni(II)	2.0	0
	48.8[c]	—	Co(II)	2.0	0
Cu(I)	99.5	0	Zn(II)	1.0	0
Ag(I)	99.0	99.2	Pb(II)	1.0	0
Cd(II)	0.5	0	Fe(III)	1.0	—
Cu(II)	1.0	0			

[a]Conditions: pH 4.7, 2×10^{-3} M $NaClO_4$, 1×10^{-3} M TTD in 1,2-dichloroethane. [b]Conditions: 1 M $HClO_4$, 1×10^{-3} M TTD in MIBK. [c]2×10^{-2} M sodium perchlorate.

but with a low value of softness parameter [19]), as well as intermediate and "hard" metal ions is negligible or zero. The relationship observed here for TTD between the extractability of ions and their assignment to the various Pearson classes agrees with the results obtained for the cyclic thiacrown, 1,4,8,11-tetrathiacyclotetradecane [8].

Extraction of silver in various pH and acid concentrations

The values of the distribution coefficient for silver (under the conditions with pH 4.7, 2×10^{-3} M perchlorate, 1×10^{-3} M TTD in 1,2-dichloroethane) did not depend on the time of shaking in the range 2—20 min, so extraction for 5 min was used.

Extraction of silver from the following aqueous phases was examined: acetate-buffered solutions of pH 3—6 containing perchlorate as counter-ion, and sulfuric (with perchlorate), perchloric and nitric acid solutions. The values of the distribution coefficients for silver obtained with TTD in 1,2-dichloroethane, MIBK and toluene are summarized in Fig. 1. The range of acidity in which extraction was high was very wide. The best results ($\log D \geqslant 2$, $E \geqslant 99.0\%$) were achieved in the case of MIBK at pH 2—6 (with 2×10^{-3} M perchlorate present) and in 0.1—1 M perchloric acid; with 1,2-dichloroethane, best results were obtained with solutions containing 0.1—2 M perchloric acid or 1—6 M nitric acid. Toluene was not a suitable solvent. Increase in the sulfuric acid concentration caused decreased silver extraction and ^{110m}Ag isotope balance (to 90% in 3 M sulfuric acid). For concentrations of nitric acid exceeding 6 M or perchloric acid exceeding 2 M, the solutions of TTD in 1,2-dichloroethane and MIBK became yellow, probably because of reagent oxidation. The extraction of silver from nitric acid with TTD in MIBK gave inferior results (curve 3, Fig. 1), compared to extractions in the presence of perchlorate or small concentration of perchloric acid (curves 1 and 4, Fig. 1). As is shown in Table 2, the addition of perchlorate or perchloric acid did not improve the extractions sufficiently.

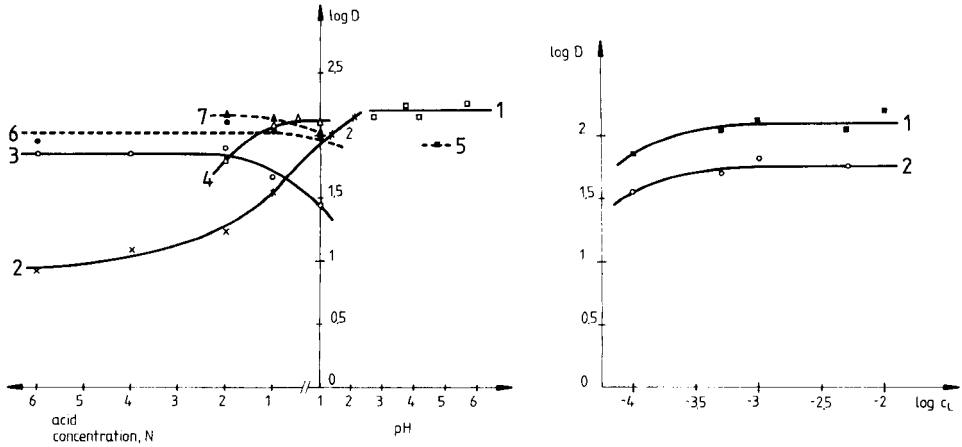

Fig. 1. Plots of log D vs. pH and acid concentration for silver. Media for extractions with 1×10^{-3} M TTD in MIBK: (1) 2×10^{-3} M $NaClO_4$, acetic buffers; (2) 2×10^{-3} M $NaClO_4$, H_2SO_4; (3) HNO_3; (4) $HClO_4$. Media for extractions with 1×10^{-3} M TTD in 1,2-dichloroethane: (5) 2×10^{-3} M $NaClO_4$, acetic buffer; (6) HNO_3; (7) $HClO_4$.

Fig. 2. Effect of initial TTD concentration in MIBK on log D for silver: (1) 1 M $HClO_4$; (2) 2 M HNO_3.

TABLE 2

Extraction of silver from nitric acid/sodium perchlorate or nitric acid/perchloric acid with 1×10^{-3} M TTD in MIBK

HNO_3 (M)	$NaClO_4$ (M)	log D	HNO_3 (M)	$HClO_4$ (M)	log D
1	—	1.66	2	0.1	1.87
1	0.01	1.64	2	1	1.98
2	—	1.80	—	1	2.09

The value of log D for silver extracted from 2 M nitric acid with 1×10^{-3} M TTD in MIBK was independent of silver concentration in the range 10^{-7}—10^{-4} M silver(I). For 1×10^{-5} M silver, a change in the initial TTD concentration, C_L, in MIBK from 5×10^{-4} to 5×10^{-3} M had no influence on the log D for silver separated from 1 M perchloric acid or 2 M nitric acid (Fig. 2).

Equilibrium study of the extraction of silver with TTD and perchlorate

In order to examine the composition of the ion-associate of silver with TTD and perchlorate extracted into 1,2-dichloroethane or MIBK, plots of log D vs. log $[L]_0$ and log D vs. log $[ClO_4^-]$ were prepared (Figs. 3 and 4); here $[L]_0$ and $[ClO_4^-]$ denote equilibrium concentration of TTD in organic phase and ClO_4^- in aqueous phase, respectively.

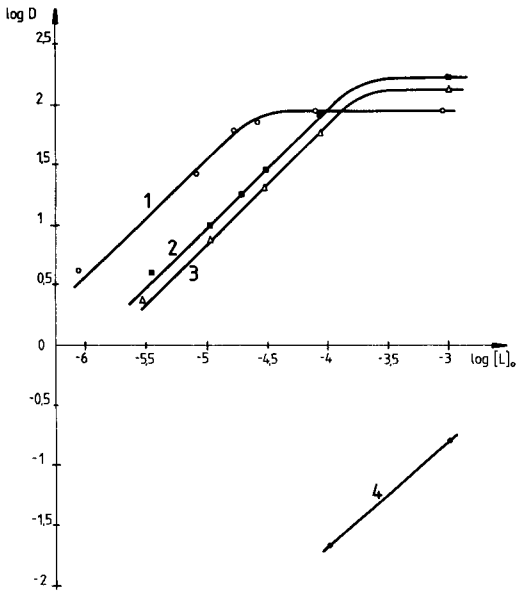

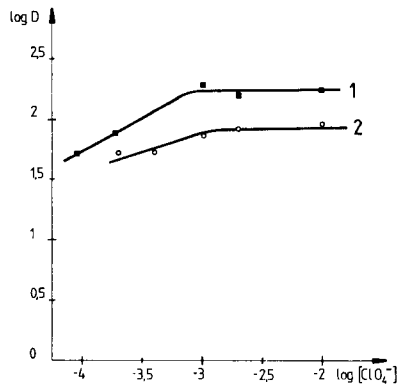

Fig. 3. Plots of log D for silver vs. log $[L]_0$. Solvent: (1) 1,2-dichloroethane; (2) MIBK; (3) MIBK, ionic strength 0.3 M; (4) toluene. Conditions: 2×10^{-3} M $NaClO_4$ in all cases; 0.2 M acetate buffer pH 4.7 for curves 1, 2 and 4, and 0.02 M for curve 3.

Fig. 4. Plots of log D for silver vs. log $[ClO_4^-]$: (1) 1×10^{-3} M TTD in MIBK, 0.02 M acetate buffer, ionic strength 0.3 M; (2) 1×10^{-3} M TTD in 1,2-dichloroethane, 0.2 M acetate buffer.

As can be seen in Fig. 3, slopes of ca. 1 were obtained for both solvents, indicating that Ag:TTD = 1:1 in the cation complex. The experiments done to confirm the amounts of perchlorate counter-ion in the ion-associate (Fig. 4) did not give the expected effect of diminishing the log D value with decreased of perchlorate concentration. Possibly both acetate and perchlorate can act as counter-ions. The extractions done without perchlorate, but otherwise under the conditions used for Fig. 4, gave log D values of 1.2 and 0.7 for 1,2-dichloroethane and MIBK, respectively; however, the isotope balance did not then exceed 90%.

Back-extraction

The results of back-extraction of silver from the organic solutions by hydrochloric acid solutions are shown in Table 3.

Conclusion

The sulfide podand examined here, an open-chain ligand possessing four thioether groups and two thiophene-sulfur atoms providing further coordination, gave highly selective extractions of silver and mercury ions. Reagents of

TABLE 3

Percentage back-extraction (R, %) of silver with different concentrations of hydrochloric acid for a shaking time of 5 min

Extraction conditions	R (%) for different HCl concs.		
	1 M	4 M	6 M
I[a]	95.3	98.4	98.5
		98.3[c]	
II[b]		96.8	

[a]Conditions: 0.5 M $HClO_4$, 1×10^{-3} M TTD in MIBK. [b]Conditions: 1 M HNO_3, 1×10^{-3} M TTD in 1,2-dichloroethane. [c]15-min shaking time.

this type may be suitable for other purposes, offering equivalents to the thia-crown compounds. The podands are much more economic to prepare.

This work was supported by the Scientific Programme M.R. I.32.

REFERENCES

1 V. A. Pronin, M. V. Usoltseva and S. M. Shostakovskij, Izv. Akad. Nauk SSSR, Ser. Khim., (1971) 2371.
2 V. A. Pronin, M. V. Usoltseva, Z. N. Shastina, N. K. Gusarova, E. P. Vyalykh, S. V. Amosova and B. A. Trofimov, Russ. J. Inorg. Chem., 18 (1973) 1921.
3 A. Ohki, M. Takagi and K. Ueno, Anal. Chim. Acta, 159 (1984) 245.
4 Y. Baba, Y. Ikeda and K. Inoue, Bull. Chem. Soc. Jpn., 58 (1985) 881.
5 D. Sevdić, Lj. Jovanovac and H. Meider-Goričan, Mikrochim. Acta (Wien), II (1975) 235.
6 D. Sevdić and H. Meider, J. Inorg. Nucl. Chem., 39 (1977) 1403, 1409; 43 (1981) 153.
7 D. Sevdić, L. Fekete and H. Meider, J. Inorg. Nucl. Chem., 42 (1980) 885.
8 K. Saito, Y. Masuda and E. Sekido, Anal. Chim. Acta, 151 (1983) 447.
9 K. Saito, Y. Masuda and E. Sekido, Bull. Chem. Soc. Jpn., 57 (1984) 189.
10 E. Sekido, K. Chayama and M. Muroi, Talanta, 32 (1985) 797.
11 F. Vögtle and E. Weber, Angew. Chem. Int. Ed. Engl., 18 (1979) 753.
12 E. Weber and F. Vögtle, in F. L. Bosche (Ed.), Host-guest Complex Chemistry, Vol. I, Akademie-Verlag, Berlin, 1982, p. 1.
13 G. F. Smith and D. W. Margerum, J. Chem. Soc. Chem. Commun., (1975) 807.
14 F. P. Hinz and D. W. Margerum, Inorg. Chem., 13 (1974) 2941.
15 J. S. Bradshaw, J. Y. Hui, Y. Chan, B. L. Haymore, R. M. Izatt and J. J. Christensen, J. Heterocycl. Chem., 11 (1974) 45.
16 K. B. Wiberg and H. F. McShane, in E. C. Horning (Ed.), Organic Syntheses, Coll. Vol. 3, J. Wiley, New York, 1955, p. 197.
17 M. Mąkosza, in A. F. Scott (Ed.), Survey of Progress in Chemistry, Vol. IX, Academic Press, New York, 1979, p. 1.
18 R. G. Pearson, J. Am. Chem. Soc., 85 (1963) 3533.
19 S. Yamada and M. Tanaka, J. Inorg. Nucl. Chem., 37 (1975) 587.

Analytica Chimica Acta, 188 (1986) 247—255
Elsevier Science Publishers B.V., Amsterdam — Printed in The Netherlands

ACTIVATED CARBON AS ADSORBENT FOR ALKYLLEAD IN AIR

ODDVAR RØYSET[a]
Department of Chemistry, University of Oslo, Blindern, Oslo (Norway)
YNGVAR THOMASSEN
Institute of Occupational Health, P.O. Box 8149 Dep., N-0033 Oslo 1 (Norway)
(Received 3rd May 1986)

SUMMARY

A method is described for the determination of alkyllead in air with activated carbon as adsorbent. The main factor affecting the adsorption capacity of the activated carbon for alkyllead was the concentration of hydrocarbons in the sampled air, as these were also adsorbed. Particulate inorganic lead was collected on a membrane filter in front of the adsorbent. The alkyllead was extracted from the adsorbent into hot nitric acid, and the concentration determined by electrothermal atomic absorption spectrometry. The detection limit was 0.002 μg Pb m^{-3} (sample volume 1 m^3), and precision was 9.5% r.s.d. at 2.1 μg Pb m^{-3} alkyllead. The method was used to monitor exposure of gasoline tank truck drivers to alkyllead. During the filling of tank trucks with leaded gasoline, alkyllead concentrations from 1 to 750 μg Pb m^{-3} were found in the drivers' breathing zone, but most were well below the Norwegian TLV of 75 μg Pb m^{-3}.

Alkyllead compounds, added to increase the octane rating of gasoline, have long been a source of air pollution, particularly in working areas where gasoline is produced and handled. The different methods used for the collection of alkyllead compounds in air and for the determination of the concentration, have been reviewed thoroughly by De Jonghe and Adams [1]. One procedure commonly used is the trapping of the alkyllead compounds in a reactive solution of iodine monochloride in hydrochloric acid. Another makes use of various types of solids in narrow columns but the adsorption capacity is low at ambient temperatures, thus the adsorbents must be cooled to liquid air temperature. The disadvantage of this technique is that the adsorbent rapidly becomes clogged by ice forming from condensed water from the air. The trapping technique has the advantage of being non-destructive, and the concentrations of the five commonest tetraalkyllead compounds can be determined by gas chromatography; but the sampling equipment is complicated, and therefore this method is not widely used for routine work.

Although well established as an adsorbent for organic compounds in air, activated carbon has been used relatively little for alkyllead compounds.

[a]Present address: Norwegian Forest Research Institute, Box 61, N-1432 Ås-NLH.

0003-2670/86/$03.50

Snyder [2] reported that the high lead content of the carbon caused difficulties in monitoring alkyllead compounds in air. However, for monitoring occupational exposure to alkyllead compounds [3, 4], the problem can be avoided by using an organic solvent to extract the alkyllead from the activated carbon. As the threshold limits for alkyllead compounds refer to total lead (as alkyllead) present in the work atmosphere, speciation of the alkyllead compounds is of secondary interest. This paper is concerned with a method suitable for the determination of the total concentration of alkyllead in the work environment, and the application of this method to the monitoring of occupational exposure. Electrothermal atomic absorption spectrometry (a.a.s.) is used to quantify lead.

EXPERIMENTAL

Reagents

Commercial adsorbent tubes (SKC, Pittsburgh, PA), packed with either activated carbon or the synthetic adsorbent XAD-4 were used. In the front and back sections were 100 mg and 50 mg of adsorbent, respectively. Activated carbon (Fluka) was ground and the 0.6—1.2-mm fraction was boiled with 65% nitric acid for 1 h, four times successively. The carbon was then washed with demineralized water, air-dried and reactivated in air at 450°C for 30 min. The anti-knock agents tetramethyllead (TML) and tetraethyllead (TEL) (Ethyl Corporation, Baton Rouge, LA) were dissolved in 53% xylene/18% heptane which also contained 1,2-dibromoethane and 1,2-dichloroethane as scavengers. All gas mixtures were prepared shortly before use by injecting these alkyllead standards or gasoline into a 10-l high-pressure gas container filled with compressed pure nitrogen to a pressure of about 100—150 atm.

Apparatus

The Perkin-Elmer (PE) 5000 atomic absorption spectrometers used were equipped with a PE HGA 500 graphite furnace, an AS-40 autosampler, PR-10 printers, model 56 recorders and standard flame atomizer. The 283.3-nm lead resonance line was used with deuterium background correction for the measurements with the graphite furnace. Pyrolytically coated graphite tubes and L'vov platforms (Perkin-Elmer) were used.

For the determination of the absorption capacity and breakthrough time for the adsorption tubes, a manifold was built in which up to ten tubes could be exposed simultaneously to a gas mixture. At fixed time intervals, single tubes were removed and the amounts of alkyllead in the front and back sections were determined. The breakthrough time was calculated from the breakthrough curves.

Procedure for the determination of alkyllead

A cellulose acetate filter (0.80-μm pore size; Millipore AAWG) in a Millipore filter holder was placed in front of the adsorption tube which was

connected to the pump. For the determination of alkyllead in air near tanks being filled with gasoline, a flow rate of 0.2 ml min^{-1} and sample volumes less than 10 l proved to be useful, whereas the sample volumes had to be less than 0.2 l for saturated gasoline vapour. Exposed tubes were capped immediately and refrigerated until further treatment. The cellulose acetate filter was dissolved in 2.0 ml of 65% nitric acid (p.a.) by digestion at 70° C for 1 h, and the solution was diluted to 10 ml with demineralized water. The front and back sections of the adsorption tube were each placed in 0.4 ml of 65% nitric acid (p.a.) at 70° C for 30 min. Each extract was diluted to 2.0 ml with demineralized water. If the amount of alkyllead adsorbed was above 100 ng, the sample was further diluted. The lead in the extracts was determined by electrothermal a.a.s. (as in Table 1); the best precision and recovery were obtained with the L'vov platform. All extraction equipment was soaked in dilute nitric acid before use. The results were corrected for the volume of activated carbon in the solution.

If the amount of lead found in the back section of a tube was less than 10% of the amount found in the front section (i.e., breakthrough value <10%), the data were accepted. For breakthrough values between 10 and 25%, the results were considered "minimum values"; and above 25%, the data were discarded.

RESULTS AND DISCUSSION

Investigations of activated carbon as adsorbent

Adsorption capacity. In addition to the commercial SKC tubes containing activated carbon or XAD-4, activated carbon from Fluka (washed with hot nitric acid or heated in an argon atmosphere to 2200° C to reduce the lead concentrations) was tested. For most of these tests, a hydrocarbon concentration of ca. 1000 mg m^{-3} was used (300 ppm calculated as hexane),

TABLE 1

Temperature program for graphite-furnace a.a.s. of lead in the nitric acid extracts of the absorbent

	Wall atomization[a]				L'vov platform[a]			
	Ramp	Hold	Temp.	Internal gas flow	Ramp	Hold	Temp.	Internal gas flow
Dry	5	25	130	300	—	—	—	—
Dry	1	5	200	300	10	30	300	300
Ash	1	15	500	300	1	15	500	300
Atomize	1	5	2200	20	0	5	2000	20
Clean	1	1	2500	200	0	2	2500	300
Cool	—	—	—	—	0	20	25	300

[a]Ramp and hold given in seconds, temperature in ° C, and internal gas flow in ml min^{-1}.

corresponding to that found in the vicinity of tanks while they are being filled with gasoline [5].

The data listed in Table 2 show that the adsorption capacity of the acid-washed reactivated carbon (Fluka) for alkyllead was very high, while that for the SKC carbon was somewhat lower but acceptable. The acid-washing/reactivation of the Fluka carbon had a positive effect, as is evident from the much shorter 1% breakthrough time of the untreated Fluka carbon. In contrast, the heating treatment significantly reduced the absorption capacity of the Fluka carbon. The SKC XAD-4 was also found to be unsuitable as an adsorbent for alkyllead under the conditions used in these experiments.

Breakthrough time, hydrocarbon concentration and flow rate. The breakthrough time for the alkyllead compounds depends on the hydrocarbon concentrations because both types of compounds are adsorbed. The relationship between 1% breakthrough time (t_b) and hydrocarbon concentration (C) for tests III and IV in Table 2 was found to be defined by: $\log t_b = 5.1 - 0.81 \log C$. The derived slope is close to that found for a number of hydrocarbons [6], and confirms the influence of the hydrocarbon concentration on the breakthrough time.

The relation for 1% breakthrough time (t_b) and flow (F) for tests I, II and III in Table 1 was found to be: $\log t_b = 1.4 - 1.24 \log F$ ($r = -0.999$). The breakthrough time is inversely proportional to the flow, in agreement with gas adsorption theory [7].

Co-adsorption effects and breakthrough volume. The effect of co-adsorption of hydrocarbons was investigated by measuring the distribution of adsorbed alkyllead between the front and back sections of SKC tubes, with increasing volume of samples containing high concentrations of hydrocarbons. As can be seen in Fig. 1, with sample volumes exceeding 50 l, some of the alkyllead on the front section migrates to the back section, which results in significant breakthrough losses.

To examine breakthrough volumes, standards containing TML and TEL were injected into the front section of SKC tubes and 150 l of filtered air was pumped through. There was no redistribution of the compounds from the front to the back section. In preliminary tests, no redistribution of TML itself occurred even with 5000 l of air. This confirms that the migration described above was caused by the co-adsorption of the hydrocarbons. Therefore, breakthrough losses will be small under normal sampling conditions but may be significant if the hydrocarbon concentration is high. Similar tests were done with the SKC XAD-4 adsorbent; more than 95% of the added TML was lost from the front section of the tube after 150 l of air had passed, whereas the less volatile TEL was completely retained on the front section.

Recovery of alkyllead from activated carbon. The front sections of SKC activated carbon tubes were spiked with alkyllead by injecting standard solutions of both TML and TEL and by injecting gasoline containing TML and TEL. Up to 50 µl of gasoline was injected, corresponding to about 38 mg of hydrocarbons or, according to the results listed in Table 2, saturation of the

TABLE 2

Adsorption capacity data for various active carbon adsorbents and XAD-4 under different experimental conditions[a]

Test no.	I	II	III	IV	V	VI	VII	VIII
Adsorbent type	SKC standard	SKC standard	SKC standard	SKC standard	Fluka untreated	Fluka acid-washed[b]	Fluka heated[c]	SKC XAD-4
Flow (l min^{-1})	0.11	0.40	2.0	0.10	1.85	1.85	1.80	1.80
Gasoline (mg m^{-3})	1260	1070	1090	12000	1000	1000	900	1000
Alkyllead (mg Pb m^{-3})	0.57	0.48	0.49	4.6	0.45	0.45	0.41	0.45
Breakthrough time (min) 1% *t*	400	95	11	65	5	40	<5	<10
10% *t*	460	110	19	95	13	>40	<5	<10
25% *t*	500	120	25	100	31	>40	<5	<10
Breakthrough volume (l) 1% *V*	44	38	22	6.5	10	74	<9	<18
10% *V*	51	44	37	9.5	25	>74	<9	<18
25% *V*	55	48	50	10.0	57	>74	<9	<18
1% Breakthrough, mg gasoline per 100 mg adsorbent	55	41	24	78	10	74	<5	<10

[a]All tubes contained 100 mg adsorbent in the front section. The gas mixtures were prepared using gasoline containing only TML (0.4 g Pb l^{-1}). [b]Washed with nitric acid as explained in Experimental. [c]Heated in argon atmosphere for 10 s at 2000°C to evaporate the contaminating lead from the carbon.

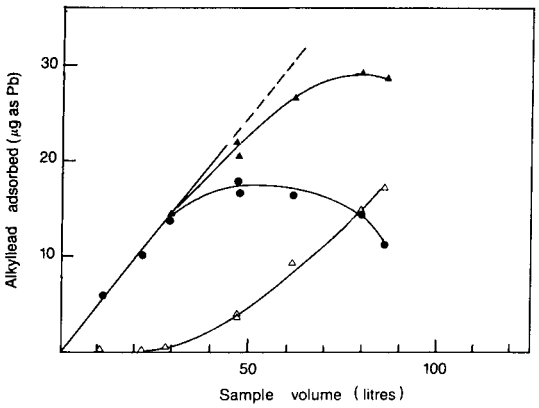

Fig. 1. The amount of alkyllead adsorbed in an SKC tube with increasing sample volume. The experimental conditions were the same as for test III, Table 1. (•) Front section; (△) back section; (▲) front plus back section; (———) total amount of alkyllead passed through the tube.

front section by hydrocarbons. The spiked tubes were stored at both 4 and 25° C for up to 10 weeks. These were no losses of alkyllead and no migration even at that time. Recovery of the alkyllead was between 95 and 105% for all tubes.

While TML was quantitatively desorbed by ethanol, propanol, isobutanol or methyl isobutyl ketone, TEL was not, indicating that some of the TEL may have decomposed on the adsorbent to alkyllead salts or to inorganic lead. Therefore, the desorption method of choice was not by means of organic solvents but by extraction and decomposition of the adsorbed alkyllead as described in the experimental section. The recovery of both TML and TEL from spiked tubes was between 98 and 102%.

Lead contamination in the activated carbon. Table 3 shows that the blank values were between 5 and 15 ng of lead per 100 mg of adsorbent for SKC tubes. Because of these large variations in the blank, the detection limit obtainable was high. Methods for reducing the lead content of the carbon were investigated. Boiling the adsorbent in nitric acid (as described under Experimental) reduced the concentration of extractable lead significantly and made the concentration more reproducible; the detection limit decreased by about one order of magnitude (Table 3).

Filter collection efficiency. For sampling of particulate matter in air, 0.80-μm pore-size cellulose acetate membrane filters were used. This type of filter was tested by placing a second filter of pore size 0.22 μm behind the first in the same cartridge. The filters were used for sampling particulate lead in a parking garage where the inorganic lead concentration in the air was in the range 1—10 μg Pb m^{-3}. For sampling periods of 12—24 h at 100 l h^{-1}, the maximum breakthrough of inorganic particulate lead to the second filter was 0.02—0.04%. The alkyllead concentration in air is usually more than 1%

TABLE 3

Lead extractable from two types of activated carbon adsorbents and detection limits of the method

Type of activated carbon	Extractable lead[a] (ng Pb/100 mg ads.)		Detection limit[b] (μg Pb m^{-3})	
	Mean	S.d.	1 l	1000 l
SKC (untreated)	10.4	4.2	13	0.013
Fluka (acid-washed)	2.6	0.6	1.8	0.002

[a]Front sections (100 mg) were extracted with 0.4 ml of nitric acid as in the procedure for determination of alkyllead (see Experimental). Data are the means of 10 determinations. [b]The detection limit is calculated as 3 times the standard deviation of the blank value divided by the sample volume (1 l or 1000 l).

of that of inorganic particulate lead, thus possible contamination of the adsorbent by breakthrough of particulate lead is negligible.

Precision of the method. At an alkyllead concentration of 2.1 μg Pb m^{-3}, a total precision of 9.5% relative standard deviation (n = 10) was obtained for the method including sampling, extraction and a.a.s. determination.

Alkyllead in working environments

The exposure of tank truck drivers to alkyllead was investigated at a central gasoline storage plant in Oslo. While the tanks were being filled, which normally takes 20—30 min, air was sampled in the breathing zone through pumps worn by the drivers, and also directly over the tank opening. The results of these measurements are shown in Table 4. Three were above the Norwegian alkyllead TLV of 75 μg Pb m^{-3}. The alkyllead concentration in the gasoline vapour forced out of the tank during filling was from 100 to 500 times above the TLV. During the same experiment, hydrocarbons in the air were collected on additional activated carbon tubes and determined (Table 4). In the determination of alkyllead in saturated gasoline vapour, the tubes were quickly saturated by hydrocarbons (breakthrough 50%, concentration for alkanes given only to indicate a minimum level), and significant breakthrough of alkyllead also occurred.

Conclusion

The adsorption capacity of activated carbon for alkyllead (and hydrocarbons) is high, and the adsorption tubes are easily coupled to standard sampling equipment. The hydrocarbon concentrations in most samples are not high enough to cause significant breakthrough losses for sample volumes below 10 l. For samples in which the hydrocarbon concentrations are above 1000 ppm, as in undiluted gasoline vapour, breakthrough may occur at volumes below 0.2 l.

The method described was developed for monitoring occupational exposure to alkyllead compounds. It is sensitive enough for the determination of

TABLE 4

Determination of alkyllead, inorganic lead and hydrocarbons in the air while tank trucks were being filled with gasoline at Sjursøya, Oslo (June 1983)

Sample	Alkyllead (μg Pb m^{-3})	Particulate lead (μg Pb m^{-3})	Benzene[a] (ppm)	Toluene[a] (ppm)	Total alkanes (ppm)
Pumps worn	113	26	—	—	—
by drivers[b]	764	<2.0	—	—	—
	30	6.2	—	—	—
	43	<2.0	5.4	4.2	126
	116	3.1	14	9.5	214
	37	43	5.4	4.5	115
	<2.0	6.6	0.1	0.1	10
	14	6.9	5.1	6.9	137
	2.7	10	1.2	1.5	44
	5.8	4.2	3.0	3.3	85
	5.9	<1.2	1.2	2.3	50
	<4.0	0.8	0.3	0.5	4
	13	<2.7	6.5	7.3	102
	13	<1.7	2.3	2.1	89
Pumps over	3200(30%)	3	—	—	—
tank opening[c]	36300(20%)	100	—	—	—
	18800(25%)	280	—	—	—
	18700(20%)	95	3090(30%)	2190(12%)	14400(50
	21900(21%)	<44	2980(25%)	2460(13%)	25100(50
	3690(6%)	<3	1950(9%)	1780(3%)	34000(50
[TLV	75	50	5	75	–]

[a]Benzene, toluene and alkanes were determined by gas chromatography as described by Fjeldstad and Holterman [5]. [b]Sample volume 2—6 l at 0.2 ml min^{-1}. [c]Sample volume 0.2 l at 0.2 ml min^{-1}. The numbers in parentheses are breakthrough values.

alkyllead concentrations in air below 1 μg Pb m^{-3}. For such samples, the hydrocarbon concentrations are low, thus it is possible to sample at least 1000 l with small risk of breakthrough losses. The method has been applied with good results to the determination of alkyllead concentrations in urban and non-urban air at different locations in Oslo, as discussed elsewhere [8].

REFERENCES

1 W. R. A. De Jonghe and F. C. Adams, Talanta, 29 (1982) 1057.
2 L. J. Snyder, Anal. Chem., 39 (1967) 591.
3 R. F. Cope, B. P. Pancamo, W. E. Rinehart and G. L. ter Haar, J. Am. Ind. Hyg. Assoc., 40 (1979) 372.
4 K. Andersson, J. O. Levin, C. A. Nilsson, C. Sødermark and O. Westermark, Report 1981:35, Arbetarsskyddsstyrelsen, Umeå, Sweden, 1981.

5 P. Fjeldstad and E. Holterman, Benzene Exposure in the Gasoline Branch, Rep. HD 872/82, Institute of Occupational Health, Oslo, Norway, 1982.
6 I. G. O. Nelson, J. Am. Ind. Hyg. Assoc., 37 (1976) 205.
7 R. G. Melcher, R. R. Langher and R. D. Kagel, J. Am. Ind. Hyg. Assoc., 39 (1978) 349.
8 O. Røyset and Y. Thomassen, Atmos. Environ., 20 (1986) in press.

Analytica Chimica Acta, 188 (1986) 257—261
Elsevier Science Publishers B.V., Amsterdam — Printed in The Netherlands

Short Communication

PIEZOELECTRIC IMMUNO SENSOR FOR THE DETECTION OF *Candida albicans* MICROBES

H. MURAMATSU

Seiko Instruments Inc., Research and Development Dept., Takatsuka-shinden, Matsudo-shi, Chiba 271 (Japan)

K. KAJIWARA, E. TAMIYA and I. KARUBE*

Research Laboratory of Resources Utilization, Tokyo Institute of Technology, Nagatsuta-cho, Midori-ku, Yokohama 227 (Japan)

(Received 16 May 1986)

Summary. The system consists of an AT-cut quartz piezoelectric crystal, oscillator and frequency counter. The surface of the palladium-plated electrodes is oxidized anodically, and anti-*Candida* antibody is immobilized onto the surface. The crystal sensor is dipped into *Candida* suspension and the surface mass increase, caused by immuno-adsorption of *Candida*, is measured by the decrease in the resonant frequency of the crystal. The frequency shift is correlated with *C. albicans* concentration in the range 10^6—5×10^8 cells cm^{-3}. The crystal sensor showed no response to *Saccharomyces cerevisiae*.

The determination of *Candida albicans* has become important in clinical analysis [1—3]; *C. albicans* is found in the human body even under normal conditions, but an increase in cell population can induce infection and disease. Presently, *C. albicans* is conventionally assayed by visual inspection of antibody-antigen (*Candida* species) aggregate formation. This method, however, requires technical skill, is time-consuming and gives only a semiquantitative assessment of the *C. albicans* concentration. Matsuoka et al. [4] showed that a potentiometric method could be applied to a *C. albicans* immunoassay. In this method, the negatively charged *C. albicans* is adsorbed onto an antibody-bound membrane, inducing a considerable change in the membrane potential (linear in the range 10^4—5×10^5 cells cm^{-3}). Another immunoassay based on an electric pulse technique was also proposed and applied to the *C. albicans* immunoassay (linear in the range 10^7—6×10^7 cells cm^{-3}) [5]. This communication reports the development of a new technique based on piezoelectric crystals, the piezoelectric immuno sensor.

Piezoelectric sensors are based on the measurement of small mass changes on the surface of a piezoelectric crystal caused by the specific adsorption of molecules onto a specially modified surface [6, 7]. The relationship between surface mass change, Δm (g), resonant frequency, F (Hz) and frequency change (ΔF), is given by the Sauebrey equation: $\Delta F/F = -\Delta m/A\rho t$, where A is the crystal area covered by the adsorbed materials (cm^2), ρ is the density

0003-2670/86/$03.50

of the quartz (g cm^{-3}) and t is the thickness of the uncoated crystal (cm). Piezoelectric crystals have been applied to the detection of water in gases, several organic compounds in air [8–10] and traces of metals in solution [11, 12]. Clinical applications include a surface acoustic-wave device for the detection of Human IgG [13].

In this study, piezoelectric immuno crystals, coated with immobilized anti-*Candida* antibody, are applied to the immunoassay of *C. albicans*. This appears to be the first reported application of piezoelectric crystals to the determination of micro-organism concentration. The feasibility of the sensor for the detection of *C. albicans* is described.

Experimental

Apparatus and materials. The piezoelectric crystals used were AT-cut quartz, 8 mm × 8 mm × 0.18 mm, with a basic resonant frequency of 9 MHz (Seiko Electronic Components, and Yakumo Tsushin Kogyo). Silver electrodes were formed on the crystal by vacuum deposition and were plated with palladium. The palladium electrodes were treated by anodic oxidation at +1.4 V vs. Ag/AgCl in 0.5 M sodium hydroxide. The silver electrodes were also coated with silicon dioxide by a sputtering technique. An oscillator circuit was constructed from a TTL-IC SN7400 [12] and the crystal frequency was monitored with a universal counter (Iwatsu SC7201).

Anti-*Candida* antibody (*Candida* check no. 4) was obtained from Iatoron Laboratories (Tokyo). *Candida albicans* was cultured in a medium containing glucose (2%), peptone (2%) and yeast extract (1%) at pH 7.0 for 48 h at 30° C. The cells were collected and suspended in phosphate buffer (pH 7.0, 0.05 M) after being washed twice with distilled water.

Immobilization of antibody. Electrodes were treated with γ-aminopropyltriethoxysilane (APTES) (2% in acetone) for 1 h at 25°C. They were air-dried and the resonant frequency of the crystal was measured (F_1). The electrodes were placed in aqueous glutaraldehyde (5%, pH 7.0) for 3 h. Anti-*Candida* antibody was immobilized on the electrodes via the surface aldehyde groups by dipping into the antibody preparation (10 mg protein cm^{-3}) for 30 min. The unreacted aldehyde was then blocked with 0.1 M glycine. Prior to use, sensors were rinsed with 0.5 M sodium chloride to remove any effect resulting from non-specific adsorption.

Assay of C. albicans. The treated piezoelectric crystals were dipped in the microbial suspension for 30 min to allow reaction to occur between the immobilized antibody and the microbe. The crystals were then rinsed with 0.5 M sodium chloride and water and dried in air. The resonant frequency, F_2, was measured. The frequency difference $\Delta F = F_1 - F_2$ was calculated.

Cell number was measured, for comparison, with a hemacytometer. Microbes adsorbed onto the electrodes were labelled with 4,6-diamidino-2-phenylindole dihydrochloride and observed by fluorescence microscopy [14].

Results and discussion

Effect of surface-modification procedure on the density of adsorbed cells. A prerequisite for the electrode surface is that it should be chemically stable during the measurement process, and that a high density of antibody should be immobilized onto it. Therefore, four surfaces were assessed for their cell-binding ability, as shown in Table 1. Silver does not possess long-term stability in aqueous environment, so the electrodes were either plated with palladium or sputtered with silicon dioxide. Of the four electrode pretreatments, palladium anodically oxidized at +1.4 V vs. Ag/AgCl adsorbed the most *C. albicans* cells (3.7×10^7 cells cm^{-2}). The anodic oxidation peak of the palladium electrode was confirmed by cyclic voltammetry. This reaction can be considered as follows [15]:

$$Pd + 2OH^- \rightleftharpoons Pd(OH_2) + 2e^-$$

Thus it is likely that the anodically oxidized palladium electrode has a more highly hydroxylated surface than untreated palladium. Consequently, a larger number of antibodies was immobilized on the anodically oxidized surface when γ-APTES and glutaraldehyde were used. The silicon dioxide surface also adsorbed a large number of *C. albicans* cells but its surface was not stable during oscillation, causing the measured resonant frequency gradually to increase. Based on these results, all further experiments were done with anodically oxidized palladium as the surface material.

Relationship between antigen-antibody reaction time and the frequency change. Figure 1 shows the relationship between antigen-antibody reaction time and the resonant frequency change. After the piezoelectric crystal sensor had been dipped into the microbe suspension, the sensor was dried in air and the resonant frequency was measured; F_2 became stable within 5 min. The change in resonant frequency (ΔF) increased with increasing immersion time. The frequency change caused by the immobilization of antibody was ca. 150 Hz. The antibody molecular weight is ca. 15 000 daltons, thus 150 Hz corresponds, according to the Sauebrey equation, to about 9×10^{11} adsorbed antibody molecules. After a 30-min immersion in the microbe suspension, sufficient microbes had reacted to allow measurement of the *C. albicans* concentration. Contact times greater than 30 min allowed more microbes to

TABLE 1

Effect of electrode surface and pretreatment on the number of bound cells for a *C. albicans* concentration of 2×10^8 cells cm^{-3} and a 30-min contact time

Surface	Number of bound cells (cm^{-2})
Pd	1.3×10^7
Pd with anodic oxidation	3.7×10^7
Ag paste	7.2×10^6
SiO_2 sputtered	1.5×10^7

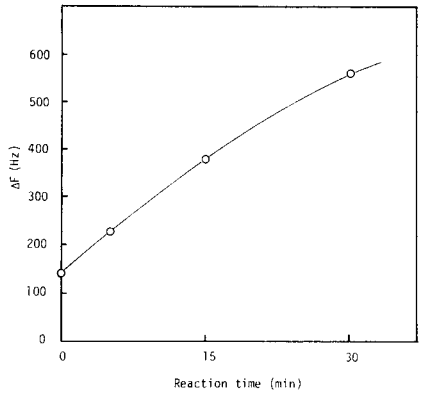

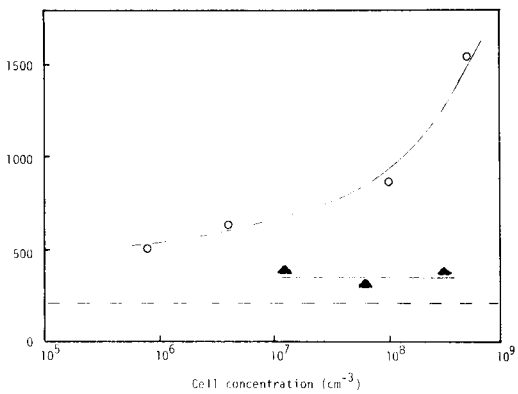

Fig. 1. Relationship between antigen—antibody contact time and resonant frequency change (*C. albicans* concentration) 5×10^6 cells cm^{-3}).

Fig. 2. Correlation between cell concentration and resonant frequency change (30-min contact time) for *C. albicans* (○) and *S. cerevisiae* (▲). The dashed line indicates the change in frequency when the anodized Pd electrode is coated with antibody.

be adsorbed, but for practical measurements, 30 min was considered to be adequate.

Correlation between cell concentration and frequency change. Figure 2 shows the correlation between the cell concentration and the resonant frequency shift resulting from binding of *C. albicans* in the range 1×10^6—5×10^8 cells cm^{-3}. In other tests, the number of microbes adsorbed on the electrode was also measured by microscopy; these tests confirmed that the magnitude of ΔF was related to the actual number of adsorbed microbes. The sensor showed no increase in response with microbe concentration for another yeast species, *Saccharomyces cerevisiae* (Fig. 2); the small constant increase in ΔF is caused by non-specific adsorption.

Although the piezoelectric immuno sensor is not as sensitive as the potentiometric method, it has greater advantages in both its convenience of use and its wider effective concentration range. Improvement in the techniques used for antibody immobilization may better the sensor sensitivity. Further studies are aimed at developing a flow system combined with the piezoelectric immuno sensor for the continuous determination of *C. albicans* concentration.

We thank Mr. J. M. Dicks and Mr. M. Kimura (Seiko Electronic Components Ltd.) for helpful discussions.

REFERENCES

1 T. J. Roger and E. Bulish, Microb. Rev., 44 (1980) 660.
2 T. E. Kiehn, Science, 206 (1979) 577.
3 M. A. Persi and J. C. Burnham, Appl. Environ. Microbiol., 42 (1981) 364.
4 H. Matsuoka, I. Karube, N. T. K. Nhung and S. Suzuki, Denki Kagaku, 50 (1982) 946.

5 H. Matsuoka, E. Tamiya and I. Karube, Anal. Chem., 57 (1985) 2002.
6 W. H. King, Jr., Anal. Chem., 36 (1964) 1735.
7 W. H. King, Jr. and L. W. Corbett, Anal. Chem., 41 (1969) 580.
8 K. H. Karmarkar and G. G. Guilbault, Anal. Chim. Acta, 75 (1975) 111.
9 G. G. Guilbault, Anal. Chem., 55 (1983) 1682.
10 W. P. Carry, K. R. Beebe and B. R. Kowalski, Anal. Chem., 58 (1986) 149.
11 T. Nomura and M. Iijima, Anal. Chim. Acta, 131 (1981) 97.
12 T. Nomura and K. Tsuge, Anal. Chim. Acta, 169 (1985) 257.
13 J. E. Roederer and G. J. Bastiaans, Anal. Chem., 55 (1983) 2333.
14 D. H. Williamson and D. J. Fennell, in D. M. Prescott (Ed.), Methods in Cell Biology, Vol. 12, Academic Press, New York, 1975, p. 355.
15 M. S. Antelman and F. J. Harris, Jr., The Encyclopedia of Chemical Electrode Potentials, Plenum Press, New York, 1982, p. 168.

Analytica Chimica Acta, 188 (1986) 263—267
Elsevier Science Publishers B.V., Amsterdam — Printed in The Netherlands

Short Communication

VOLTAMMETRIC/AMPEROMETRIC DETECTION FOR FLOW-INJECTION SYSTEMS

CRAIG E. LUNTE, SY-WEN WONG, THOMAS H. RIDGWAY and WILLIAM R. HEINEMAN*

Department of Chemistry, University of Cincinnati, Cincinnati, OH 45221 (U.S.A.)

KENNETH W. CHAN

Department of Chemistry, California State University, Fresno, CA 93740 (U.S.A.)

(Received 9th May 1986)

Summary. A dual-electrode voltammetric/amperometric detector for flow-injection systems is described. The detector provides qualitative voltammetric information without the charging currents associated with scanning the potential. Selectivity is enhanced relative to direct voltammetric detection at a single electrode because only chemically reversible redox couples are detected. A preliminary evaluation with hexacyanoferrate(III) and ascorbic acid is presented.

Electrochemical detection in combination with liquid chromatography or flow-injection systems has become widely used for trace organic determinations because of the low detection limits and high selectivity which can be achieved [1]. Amperometric detectors are currently the most widely used electrochemical detectors because they provide the lowest detection limits. However, voltammetric detectors offer the advantage of qualitative as well as quantitative information. Several voltammetric detectors for liquid chromatography and flow-injection systems have been described [2—7]. These detectors typically use a pulsed waveform such as a staircase or square wave to overcome the large charging currents associated with potential-scanning techniques. Even with these pulse techniques, it has not been possible to achieve the detection limits readily obtained by simple amperometric detectors. A voltammetric detector with a fiber microelectrode has recently been described which exhibited greatly reduced charging currents permitting scan rates of up to 1 V s^{-1} [7]. However, this detector is limited to use with open-tubular chromatographic systems.

In this communication, an alternative to direct voltammetric detection at a single electrode is described. This method, named voltammetric/amperometric detection, is based on a dual-electrode thin-layer transducer in a series configuration. The potential at the upstream electrode is scanned while the downstream electrode is maintained at a constant potential. The downstream electrode is used to monitor the redox reaction occurring at the upstream electrode without the charging current associated with scanning the poten-

0003-2670/86/$03.50

tial. Therefore, voltammetric information can be obtained at an electrode operated in an amperometric mode. The theory for this mode of detection is the same as for the more classical rotating ring-disk electrode [8, 9]. A similar concept has been used for anodic stripping voltammetry with collection in flow streams [10]. This report describes the operational principles of this detector when the downstream electrode is operated at a potential to reverse the reaction observed at the upstream electrode.

Experimental

Reagents. All solutions were prepared from reagent-grade chemicals and distilled, deionized water. Potassium hexacyanoferrate(III) (Mallinckrodt) and ascorbic acid (Sigma Chemical Co.) were used. The supporting electrolyte was 0.1 M sodium acetate buffer, pH 5.

Flow-injection system. The flow injection system consisted of a Model 396 Minipump (Milton Roy, Riviera Beach, FL), a pulse damper, and a Model 7010 injection valve (Rheodyne). A 100-μl sample loop was used. The flow rate was 50 μl min^{-1}.

Electrochemical apparatus. The bipotentiostat used was controlled with an MC-6809 microprocessor. The construction of this instrument and its application to anodic stripping voltammetry of indium have been described [11—13]. This instrument can independently apply various potential waveforms and measure the resulting currents at two working electrodes. The thin-layer electrochemical cell used was built inhouse (Fig. 1) but is similar in design to those available from Bioanalytical Systems. The working electrodes

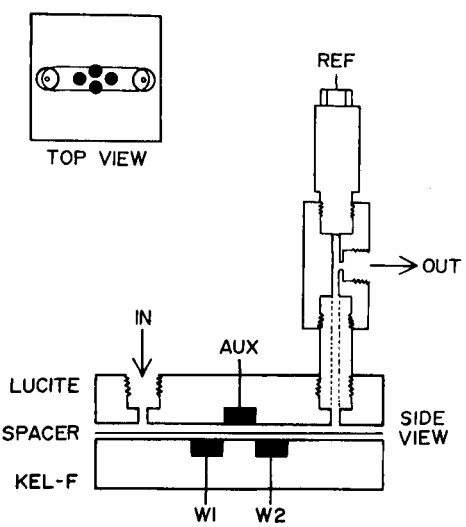

Fig. 1. Dual-electrode thin-layer flow cell for voltammetric/amperometric detection. W1, upstream scanned electrode; W2, downstream amperometric electrode; AUX, auxiliary electrode; REF, reference electrode. Spacer thickness was 0.127 mm.

and the auxiliary electrodes were glassy carbon and the reference electrode was Ag/AgCl. All potentials are reported vs. the Ag/AgCl electrode.

Results and discussion

Cell characterization. Two characteristics of the thin-layer cell are critical to successful operation of the voltammetric/amperometric detector; these are the cell resistance and the collection efficiency of the downstream electrode. Preliminary experiments were designed to evaluate these parameters. As for any scanned potential technique, the cell resistance is critical for good potential control. The cell resistance was estimated by evaluating the dependence of peak current and peak potential on scan rate. Cyclic voltammetry with the hexacyanoferrate(II)/(III) couple as the probe showed that the cell resistance was ca. 2 kohm. This produces an insignificant iR drop of about 15 mV at the currents typically encountered (ca. 10 μA).

The collection efficiency of the cell was evaluated by operating both electrodes at a constant potential. The upstream electrode was operated at a potential sufficient to reduce hexacyanoferrate(III) at a mass transport-limited rate (+0.15 V) while the downstream electrode was operated at a potential (+0.55 V) sufficient to oxidize the hexacyanoferrate(II) produced. Table 1 lists the collection efficiencies observed at flow rates of 25—400 μl min^{-1}. As can be seen, the collection efficiency is almost independent of flow rate.

Voltammetric/amperometric detection. The voltammetric behavior of the analyte is probed at the upstream electrode by scanning the applied potential. This is followed at the downstream electrode by collection of the redox product from the upstream electrode. The downstream electrode is maintained at a constant potential sufficient to reverse the upstream electrode process. Because the downstream electrode is maintained at a constant potential, there is no interference from charging current in the voltammetric response. The detector therefore should be capable of providing voltammetric information which maintaining the low detection limits associated with amperometric detection.

Figure 2A shows the responses at both the upstream and downstream electrodes for the injection of 100 μl of 10^{-5} M hexacyanoferrate(III) at 50 μl min^{-1}. The upstream electrode was scanned from +0.55 V to +0.15 V at a rate of 1.0 V s^{-1}, while the downstream electrode was operated at a constant +0.55 V. The well-defined voltammetric response at the downstream electrode mirrors the direct voltammetric response observed at the upstream electrode, indicating that the voltammetry of a compound can be followed

TABLE 1

Effect of flow rate on collection efficiency

Flow rate (μl min^{-1})	25	50	100	200	400
Collection efficiency	0.165	0.190	0.182	0.159	0.174

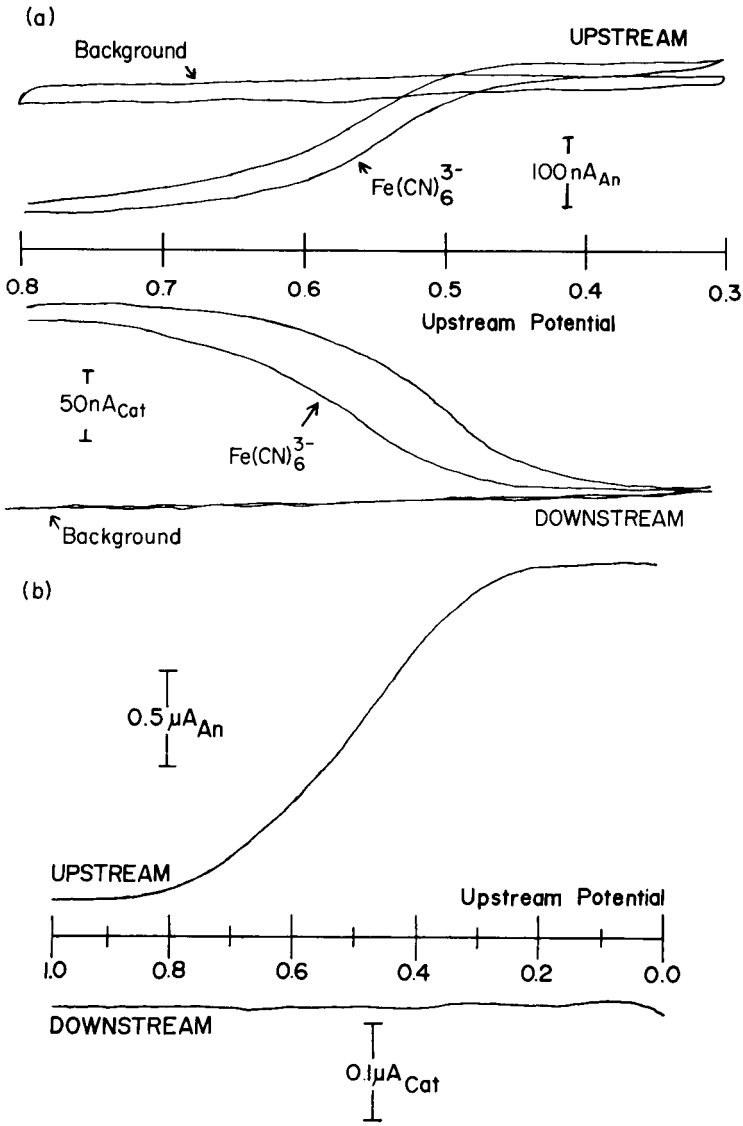

Fig. 2. Voltammetric/amperometric detection: (a) 10^{-5} M potassium hexacyanoferrate(III) at a flow rate of 50 μl min^{-1}; (b) 10^{-5} M ascorbic acid at a flow rate of 1.0 ml min^{-1}. In both case, scan rate was 1.0 V s^{-1}.

amperometrically. The hysteresis seen is from the time delay between the upstream and downstream electrodes. The voltammogram is a plot of downstream current vs. upstream potential; because of the time delay, the downstream current actually corresponds to an earlier upstream potential. Optimization of this detector will provide software compensation for this time delay to eliminate the hysteresis.

It has been shown that the series configuration of the dual-electrode detector used in an amperometric mode can greatly increase selectivity because only chemically reversible redox couples are detected [14]. This same selectivity occurs in the voltammetric/amperometric mode. Figure 2B shows the upstream and downstream responses for 10^{-5} M ascorbic acid. Because the oxidation of ascorbic acid is irreversible, the large voltammetric signal at the upstream electrode is not accompanied by a response at the downstream electrode. The voltammetric/amperometric detector is thus capable of resolving electrochemically reversible from irreversible compounds.

Conclusions

Preliminary work on the characterization of a dual-electrode voltammetric/amperometric detector proved satisfactory. Further work will involve fuller characterization of the controlling parameters in order to design a better bipotentiostat and thin-layer cell. The detection limits that can be achieved with this detector can then be evaluated. It is expected that detection limits will be similar to those attainable with direct amperometric detection and that the detector will be useful in liquid chromatography.

REFERENCES

1 R. E. Shoup (Ed.), Bibliography of Recent Reports of Electrochemical Detection, BAS Press, West Lafayette, IN, 1982.
2 J. Wang and H. D. DeWald, Anal. Chim. Acta, 153 (1983) 325.
3 J. J. Scanlon, P. A. Flaquer, G. W. Robinson, G. E. O'Brien and P. E. Sturrock, Anal. Chim. Acta, 158 (1984) 169.
4 T. A. Last, Anal. Chem., 55 (1983) 1509.
5 W. L. Caudill, A. G. Ewing, S. Jones and R. M. Wightman, Anal. Chem., 55 (1983) 1877.
6 R. Samuelsson, J. O'Dea and J. Osteryoung, Anal. Chem., 52 (1980) 2215.
7 J. G. White, R. L. St. Claire III and J. W. Jorgenson, Anal. Chem., 58 (1986) 293.
8 G. W. Schieffer and W. J. Blaedel, Anal. Chem., 49 (1977) 49.
9 W. J. Albery and M. L. Hitchman, Ring-Disc Electrodes, Clarendon Press, Oxford, 1971.
10 F. Opekar and P. Beran, J. Electroanal. Chem., 69 (1976) 1.
11 J. Wise, Ph.D. Dissertation, University of Cincinnati, OH, 1983.
12 M. Oth, Ph.D. Dissertation, University of Cincinnati, OH, 1983.
13 J. A. Wise, W. R. Heineman and P. T. Kissinger, Anal. Chim. Acta, 172 (1985) 1.
14 D. A. Roston, R. E. Shoup and P. T. Kissinger, Anal. Chem., 54 (1982) 1417A.

Analytica Chimica Acta, 188 (1986) 269—274
Elsevier Science Publishers B.V., Amsterdam — Printed in The Netherlands

Short Communication

DETERMINATION OF TRIAZINE PESTICIDES BY HIGH-PERFORMANCE LIQUID CHROMATOGRAPHY WITH SWEPT-POTENTIAL ELECTROCHEMICAL DETECTION

DALE S. OWENS and PETER E. STURROCK*

School of Chemistry, Georgia Institute of Technology, Atlanta, Georgia 30332-0400 (U.S.A.)

(Received 16th May 1986)

Summary. A swept-potential electrochemical detector, operating in the square-wave voltammetric mode, is used to detect a mixture of five triazine pesticides separated on a reverse-phase resin column. Limits of detection are below 1 ng injected. Two compounds, not completely separated by the column, are resolved on the potential axis.

Triazine pesticides are used commonly in the control of weeds in food crops. These compounds are reported to have a long persistence and to have contaminated wells and streams [1—4]. Traces of some triazines have been found in human urine [5]. A common method of quantifying triazine pesticides is gas chromatography, but this is not suitable for some of the higher-molecular-weight compounds and those with polar side-chains. Liquid chromatography with ultraviolet (u.v.) detection has been advocated. Beilstein et al. [6] determined seventeen s-triazine herbicides and derivatives by reverse-phase high-performance liquid chromatography (h.p.l.c.); the best limit of detection reported was about 18 ng. Burrows et al. [7] reported limits of detection 4—5 ng (200 μl of 21 and 28 μg l^{-1} solution) for two s-triazines. Parker et al. [8] studied 21 triazines by reverse-phase h.p.l.c. and mass spectrometry; their sensitivity was very poor, with limits of detection on the order of 1 μg. When the present study was nearing completion, the Supelco Company reported the separation of ten triazines by reverse-phase h.p.l.c. [9]; they did not report limits of detection, but these appeared to be about 1 ng.

The electrochemistry of triazine compounds has been studied. Benadikova and Kalvoda [10] reported the determination of triazines by adsorptive stripping voltammetry; this approach is sensitive but must be combined with a separation step for real applications. Their reduction voltammograms at pH 3.5 showed the waves for the triazines on the toe of the solvent decomposition wave. Pacakova and Nemec [11] discussed the oxidations of triazines on platinum in anhydrous acetonitrile. They reported half-wave potentials ranging from 1.8 to 2.1 V vs. the saturated calomel reference

0003-2670/86/$03.50

electrode (SCE). These are extremely positive potentials, and pure anhydrous acetonitrile is not a satisfactory mobile phase for most chromatographic separations. These oxidation potentials appear to correlate with the environmental persistence of these compounds because most natural decomposition pathways are oxidative.

In this study, a swept-potential electrochemical detector was applied to the detection of triazine pesticides. This detector, and other applications of it, have been reported by Sturrock and co-workers [12—14].

Experimental

The instrument has been described in detail [13]. The isocratic h.p.l.c. system was the same as before [12], except that a Hamilton PRP-1 column (4.6 × 150 mm) was used. For most experiments, a Spectra-Physics 8770 pump was used; for other experiments a pneumatic-amplifier pump (Haskel No. 26740 as modified by DuPont for the Model 830 chromatograph) was used.

A supply of Hamilton PRP-1 reverse-phase resin (10-μm mesh) was obtained and two columns (4.6 × 150 mm) were slurry-packed as recommended by the manufacturer; the Haskel pump and a Micromeritics slurry packer were used for the packing operation. The advantage of this resin is that it can be used safely from pH 1 to pH 13. The resin beads are not as hard as silica, and, therefore, the packed columns do not have as high a theoretical plate count as silica-based columns of similar mesh size. One of the columns had a plate count of 4500, which corresponds to the manufacturer's claim of 30 000 plates per meter; the other column was slightly inferior. The manufacturer now markets prepacked columns with a 5-μm mesh size of this resin and a claim of 50 000 plates per meter.

The flow cell used was a model 310 (Princeton Applied Research) which is a wall-jet cell with a mercury-drop working electrode and a silver/silver chloride reference electrode. The mercury drop was replaced before each voltammetric sweep to avoid the problem of a fouled electrode surface, which is so common with solid electrodes such as graphite. For all experiments, the medium-size drop was used.

Five 2-chloro-1,3,5-triazines were obtained from the U.S. Environmental Protection Agency (Research Triangle Park, North Carolina). The compounds were used as received.

Results and discussion

Initial experiments with square-wave voltammetry confirmed the observations of Benadikova and Kalvoda [10]. Repeat experiments at different pH values showed that as the pH decreased, the reduction waves of the triazines became better separated from the wave of the solvent decomposition. However, the optimum pH values were clearly below the lower pH limit for the usual reverse-phase chromatographic columns with aliphatic side-chains bonded to a silica support. Thus, effective electrochemical detection for

these compounds requires a stationary phase which can be used at low pH values, such as the Hamilton PRP-1 reverse-phase resin.

For such PRP-1 resin columns, initial chromatographic separations were tested with a u.v. detector and large amounts of the triazines injected. The chromatographic capacity factors and electrochemical reduction peak potentials for the five triazines are listed in Table 1. The compounds are well separated chromatographically except for Atrazine and Cyanazine, which overlap partially. The capacity factor for Cyanizine is a function of pH, being lower at higher pH values.

After the preliminary tests, the swept-potential electrochemical detector was connected to the PRP-1 resin column for further experiments. The optimum mobile phase was 60:40 (v/v) acetonitrile/water with a final pH of 1.02. This ratio of acetonitrile to water was dictated by the reduction peak of oxygen in the injected sample. The oxygen peak does not move as much with mobile phase composition as the peaks of the triazines, and at this composition of mobile phase, the oxygen peak falls between the peaks for Simazine and Atrazine.

Figure 1 shows a section of the chromatogram containing the first four peaks. This figure was obtained by summing the points of each voltammetric sweep to give a pseudo-d.c. chromatogram which has the same appearance as a chromatogram obtained with a conventional d.c. amperometric detector set at −0.95 V. Figure 2 shows a three-dimensional projection of the swept-potential chromatogram from which Fig. 1 was generated. It is obvious in Fig. 2 that peak B (Atrazine) and peak C (Cyanazine) are resolved on a potential basis even though they overlap significantly in Fig. 1. The section of parallel straight lines corresponds to the oxygen peak where the amplifiers have been forced to their limits. Other than this section, only raw data with no filtering or smoothing are shown in the figures.

Figure 3 further clarifies the situation.Figure 3(a) was generated from the same data as the previous figures by plotting only one point per voltammetric

TABLE 1

Experimental factors for 2-chloro-1,3,5-triazines[a]

Compound	Peak potential (V)	Capacity factor	Limit of detection (ng)
Simazine	−0.81	1.94	0.26
Atrazine	−0.82	3.11	0.31
Cyanazine	−0.92	3.68	0.35
Propazine	−0.83	5.04	0.37
Anilazine	−0.71	10.8	0.71

[a]Conditions: Hamilton PRP-1 column (4.6 × 150 mm); 60% acetonitrile/40% water (pH 1.02) as mobile phase; square-wave voltammetry (30 Hz, pulse −50 mV, step −10 mV, potentials vs. Ag/AgCl).

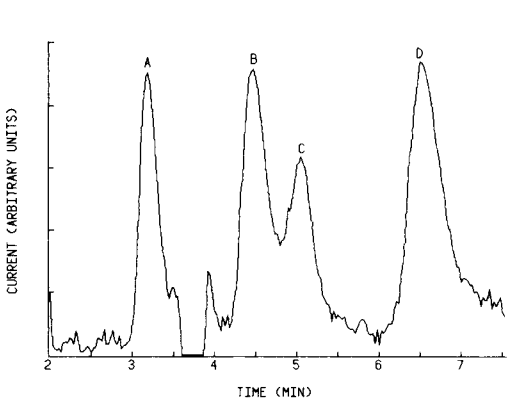

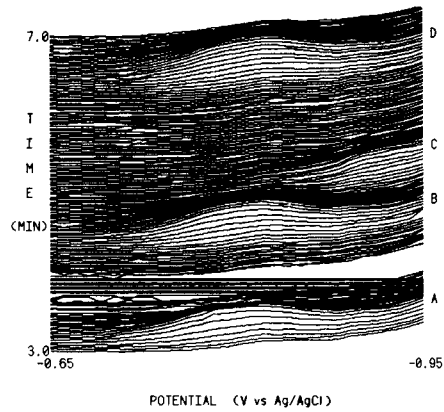

Fig. 1. Pseudo-d.c. chromatogram of four triazine pesticides. Summation of all points in each voltammetric sweep from −0.63 to −0.95 V. Square-wave voltammetry with steps of −10 mV and pulses of −50 mV at 30 Hz. Peaks: (A) simazine, 78 ng; (B) atrazine, 65 ng; (C) cyanazine, 100 ng; (D) propazine, 112 ng.

Fig. 2. Swept-potential chromatogram of the four triazine pesticides. Same data as Fig. 1.

sweep, specifically the points with a base potential of −0.82 V. Thus, components with reduction peaks at more positive or more negative potentials do not appear in this chromatogram. It can be seen that the peak for Cyanazine does not appear in this figure, and thus the overlap with Atrazine has been resolved. Figure 3(b) was generated similarly but only the points with a base potential of −0.93 V were used. Here, the peak for Cyanazine is very pronounced with much smaller peaks for the other three compounds.

Over the range from 0 to 480 ng injected, the detector sensitivity was 0.5759 ± 0.0076 nA ng^{-1} with a Pearson correlation coefficient of 0.9996 and a standard error of 2.9 nA. The limits of detection suffer from the fact that at the potentials required for the reduction of these compounds, the background current from decomposition of the solvent is significant. However, the limits of detection, which are summarized in Table 1, are somewhat better than those claimed by other workers for u.v. detection. These limits of detection were calculated after the raw data had been smoothed with a Fourier smoothing program reported by Aubanel and Oldham [15]. Considering that the best limits of detection of triazine compounds claimed for the u.v. detector are around 1 ng [9], and that this previous work used a column of at least 20,000 theoretical plates as compared to the 4500 plates in our column, it is clear that the swept-potential detector has a lower detection limit than the u.v. detector for the quantitation of triazine pesticides. In addition, this group of compounds serves to demonstrate the power of the swept-potential mode of operation in the resolution of overlapping peaks.

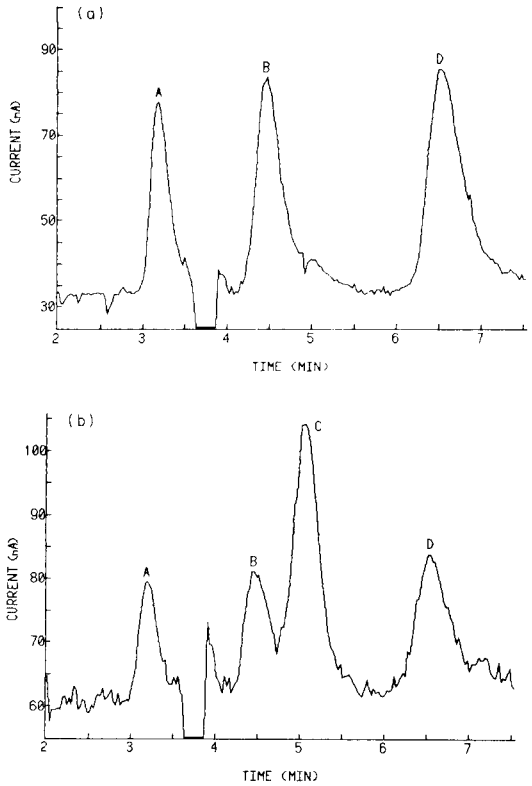

Fig. 3. Constant-base-potential chromatograms of triazines from the same data as Figs. 1 and 2. (a) Only current responses from the base potential of —0.82 V are plotted; (b) only current responses from base potential of —0.93 V are plotted.

The research on which this paper is based was financed in part by the United States Department of the Interior, Geological Survey, through the State of Georgia Water Resources Research Institute (project USGS G-900 (06)).

REFERENCES

1 R. Frank, G. Sirons, R. Thomas and K. McMillan, J. Great Lakes Res., 5 (1979) 131.
2 R. Frank, G. Sirons and B. Ripley, Pestic. Monit. J., 13 (1979) 120.
3 R. Frank and G. Sirons, Sci. Total Environ., 12 (1979) 223.
4 W. Hormann, J. Tournayre and H. Egli, Pestic. Monit. J., 13 (1979) 128.
5 M. Erickson, C. Frank and D. Morgan, J. Agr. Food Chem., 27 (1979) 740.
6 P. Beilstein, A. M. Cook and R. Hutter, J. Agric. Food Chem., 29 (1981) 1132.
7 E. Burrows, E. Brueggeman and S. Hoke, J. Chromatogr., 294 (1984) 494.
8 C. E. Parker, C. A. Haney, D. J. Harvan and J. R. Hass, J. Chromatogr., 242 (1982) 77.
9 Supelco Reporter, Vol. IV, No. 3, May 1985.
10 H. Benadikova and R. Kalvoda, Anal. Lett., 17(A13) (1984) 1519.
11 V. Pacakova and I. Nemec, J. Chromatogr., 148 (1978) 273.

12 J. Scanlon, P. Flaquer, G. O'Brien, G. Robinson and P. Sturrock, Anal. Chim. Acta, 158 (1984) 169.
13 P. Reardon, G. O'Brien and P. Sturrock, Anal. Chim. Acta, 162 (1984) 175.
14 M. Thomas, H. Msimanga and P. Sturrock, Anal. Chim. Acta, 174 (1985) 287.
15 E. Aubanel and K. Oldham, Byte, 10 (1985) 207.

Analytica Chimica Acta, 188 (1986) 275—280
Elsevier Science Publishers B.V., Amsterdam — Printed in The Netherlands

Short Communication

DETERMINATION OF SOLUBLE CYANIDE IN SOIL SAMPLES BY DIFFERENTIAL PULSE POLAROGRAPHY

S. B. ADELOJU* and K. M. GAWNE

Trace Analysis Unit, Division of Chemical and Physical Sciences, Deakin University, Victoria 3217 (Australia)

(Received 12th June 1986)

Summary. Soluble cyanide can be determined in soil samples by differential pulse polarography. Interference from sulphide is avoided by treating the alkali-stabilized sample solutions with lead carbonate prior to distillation of cyanide from the soil extract. Less than 10 $\mu g\ l^{-1}$ cyanide can be determined accurately, depending on the weight of sample taken and the final collection volume. For a 100-g soil sample, the detection limit is 5 ng g^{-1}, which is similar to the limit of a standard spectrophotometric method. Relative standard deviations are 1—3%.

The determination of cyanide is needed routinely in waste treatment and pollution control, particularly in connection with metal finishing processes, blast furnace operations, etc. [1]. As little as 0.2 $mg\ l^{-1}$ cyanide is considered to be fatal to many fish species [2]. In soils, cyanide may be present as free soluble species and as stable insoluble complexes. Soluble species are obviously the greater danger, as they can spread readily through spillage, run-off or clean-up operations. Seepage of cyanide through the ground can also affect the nutrient balance of the soil and so affect plant growth. Regular monitoring of soluble cyanide in possibly polluted soils is essential.

Several methods exist for the determination of cyanide in natural waters [3—5], waste waters [3, 6, 7] and biological materials [8], but little has been reported about cyanide levels in soil samples [9]. In most available methods, distillation is used to separate and preconcentrate cyanide from the bulk matrix and spectrophotometry is applied to the distillate [3—9]. Despite the unpleasant reagents used in most spectrophotometric procedures for cyanide, other available techniques [4, 10] have been little used. Voltammetric methods [11—15], which are suitable for ultratrace levels of cyanide, do not appear to have been applied to soils.

In this communication, differential pulse polarography (d.p.p.) is used to quantify free soluble cyanide in soils after distillation to achieve preconcentration and separation. The reliability of the method is examined.

Experimental

Reagents and standard solutions. Analytical-grade reagents and distilled/deionized water were used throughout. Hydroxide solutions were prepared

0003-2670/86/$03.50

by dissolving appropriate amounts of sodium hydroxide in water. Cyanide standards were prepared daily by dissolving potassium cyanide in the appropriate hydroxide solution. Acetate buffer, chloramine-T and pyridine/barbituric acid reagent were prepared as described for the ASTM standard spectrophotometric method [1].

Instrumentation. An EG & G Princeton Applied Research microprocessor-controlled polarographic analyzer (PAR Model 384) was used with a PAR Model 303 static mercury drop electrode. All potentials cited are referred to the silver/silver chloride (saturated KCl) reference electrode; the auxiliary electrode was a platinum wire. A medium-size mercury drop (surface area 0.015 cm^2) was used, unless indicated otherwise.

All solutions were deoxygenated with purified nitrogen for 5 min before polarography and nitrogen was passed over the solution during measurements. Standard solutions of cyanide were added to the polarographic cell with fixed-volume Socorex micropipettes with disposable tips. The solution was deoxygenated for 30 s after each addition.

A Pye-Unican SP600 u.v. spectrophotometer was used with 1-cm cells to measure absorbances.

Soil samples. Samples of soil were collected at depths of 0, 20 and 50 cm from a land area used for storage disposal of waste from coke oven and blast furnace operations. The waste in storage drums had been stored for a long period to a depth of 50 cm from the surface, and corrosion had caused concern about soil contamination. The collected samples were sieved through a coarse mesh (ca. 5 mm) and then through a finer mesh (ca. 2 mm) to remove stones, metal pieces and other debris. The moisture content of selected depth samples was measured by recording weight loss after oven drying and cyanide concentrations were corrected to dry weight. The pH of each sample was measured after shaking a portion of the soil in distilled/deionized water. Ideally, acidic samples will not contain free soluble cyanide, owing to its loss as HCN.

Extraction of cyanide from soil samples. Accurately weigh 5—100 g of sample (depending on cyanide concentration) into a 250-ml conical flask and add 100—200 ml of 0.01 M sodium hydroxide. Stopper the flask tightly and shake vigorously (mechanical agitator) for 2 h. Then, after 15—30 min, filter through a 0.45-μm filter (HA type) to remove precipitated or colloidal material. If necessary, warm the solution and allow the precipitate to age before filtering. Remove sulphide from this solution by precipitation (as PbS) after addition of 50 mg of lead carbonate. Repeat this addition until no more lead sulphide forms and then filter through a Whatman No. 541 hardened ashless filter paper. Such removal of sulphide prior to distillation is generally recommended [1, 16], to avoid any possibility of conversion of cyanide to thiocyanate in the absorption vessel. Canterford [12] indicated that sulphide can interfere with the polarographic determination of cyanide.

Separation and preconcentration of cyanide. Transfer the extracted soil sample solution to a 500-ml or a 1-l, three-neck distillation (round bottom)

flask, fitted with a vertical 25-cm Liebig condenser and attached to two 100-ml gas bubblers [1]. The first bubbler contains water (to collect acid fumes) and the second contains 0.01 M sodium hydroxide. Distil, with the aid of nitrogen stream and suction, after adding sulphuric acid (1 + 1) and copper chloride reagent [1]. Collect the hydrogen cyanide in 10 ml 0.01 M sodium hydroxide to ensure quantitative retention [1, 10, 12]. Distillation time depended on the content of cyanide in the sample, but 2 h was found to be adequate for all the soils considered. The efficiency of collection depended on the gas flow and on the size of bubbles formed in the bubblers; the frit generally recommended [1] was essential.

Polarographic determinations. Pipette 5 ml of the cyanide solution into the cell, deoxygenate for 5 min and determine cyanide by d.p.p., scanning from −0.50 V to −0.15 V at a rate of 4 mV s^{-1} (pulse amplitude 50 mV, drop time 1 s). Quantify the cyanide by two or three standard additions, taking into consideration the weight of sample, final volume and moisture content.

Spectrophotometric determinations. The ASTM standard method with chloramine-T and barbituric acid [1] was used.

Results and discussion

The polarography of cyanide at mercury electrodes has been studied extensively [12, 13, 17]. The pH of the solution is a critical factor. Karchmer and Walker [18] recommended a pH of 10.8 for d.c. polarography, but Canterford [12] later demonstrated that better separation of the cyanide and hydroxide waves was obtained at pH 9—10. In the present work, it was found that the resolution and sensitivity of the d.p.p. peaks for cyanide deteriorated rapidly with increasing concentration of sodium hydroxide; the optimum sodium hydroxide concentration was 0.01 M. Relative standard deviations were then 1—2%. Lower hydroxide concentrations were not considered because they could lead to losses in the acid distillation step.

Figure 1 shows that the cyanide peak diminished with increasing scan rate and was better resolved at slower scan rates (1—4 mV s^{-1}). In terms of speed of analysis and the levels of cyanide likely in polluted soil samples, a scan rate of 4 mV s^{-1} was considered appropriate, but the slower scan rate was used for relatively low concentrations of cyanide. The cyanide peak height increased with pulse amplitude up to 50 mV but then decreased significantly so that 50 mV was selected for routine use.

Under the chosen experimental conditions, the peak current increased linearly with increasing concentration of cyanide over the range 0—2610 $\mu g\ l^{-1}$. The peak shifted to more negative potentials with increasing concentration, but adequate peak resolution was maintained within the concentration range considered. The limit of detection for cyanide depended somewhat on the chosen scan rate, being 50 $\mu g\ l^{-1}$ at 1 or 2 mV s^{-1} and 65 $\mu g\ l^{-1}$ at 4 mV s^{-1}.

Distillation time. The required distillation time for complete recovery of soluble cyanide was investigated with alkaline standard solutions of cyanide

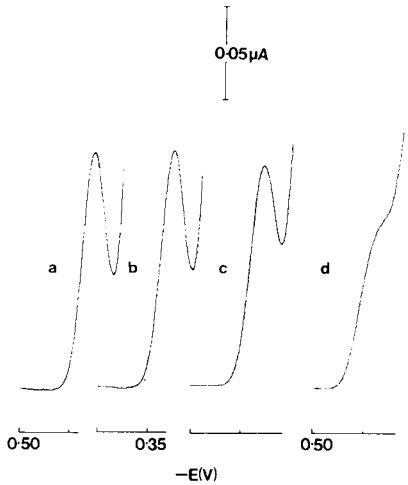

Fig. 1. Influence of scan rate (mV s^{-1}) on the resolution and sensitivity of the cyanide peak: (a) 1, (b) 2, (c) 4, (d) 8 mV s^{-1}. Drop time 1 s; 295 μg CN^- l^{-1}; 0.01 M NaOH; other conditions as given in experimental section.

(1 mg l^{-1}). Recoveries were only around 60% after distillation for 1 h but were complete (⩾95%) after distillation for ⩾2 h. A distillation time of 2 h was therefore chosen and up to 6 samples were distilled simultaneously. This distillation time was checked for the soluble soil extracts. The colouration of the soil extract was found to affect the required distillation time. Generally, clear pale yellow filtrates required only a 2-h distillation for complete removal of cyanide, whereas cloudy brown filtrates required more than 4 h. The brown cloudy filtrates probably contained complexed cyanide which often requires a longer period for release as hydrogen cyanide [1]. For some samples, the amount of hydrogen cyanide evolved at hourly intervals increased up to the third hour, but was still fairly high at the fourth hour of distillation. On this basis, it was considered necessary to ensure that the soil extract (filtrate) was clear pale yellow or colourless (as was the case in some of the soil samples), prior to distillation.

Recovery of distillation method. The efficiency of the distillation method after 2 h was checked further. The recoveries from alkaline standard solutions of cyanide (10—200 μg l^{-1}) were in the range 95—98%, which is satisfactory for routine analysis. It was, of course, vital to ensure that the distillation apparatus was leak-free.

The recovery of cyanide was also investigated with an unpolluted surface soil sample. Soluble cyanide (0—100 ng g^{-1}) was added to 100-g portions of the soil, which were then taken through the extraction/distillation procedure. Excellent recoveries of the cyanide were obtained from the soil sample based on the polarographic measurements, and these results agreed with those obtained by the spectrophotometric method (Table 1). It can therefore be

TABLE 1

Recovery of soluble cyanide from spiked unpolluted soil samples (100 g)

Cyanide added (ng g^{-1})	Cyanide found (ng g^{-1})[a]	
	D.p.p.	Spectrophotometry
0	n.d.[b]	n.d.[b]
10	9.6 ± 0.3 (96 ± 3%)	9.5 ± 0.2 (95 ± 2%)
25	24.3 ± 0.3 (97 ± 1%)	24.6 ± 0.5 (98 ± 2%)
50	49.2 ± 0.8 (98 ± 2%)	49.1 ± 1.2 (98 ± 2%)
100	97.8 ± 1.6 (98 ± 2%)	98.2 ± 2.6 (98 ± 3%)

[a]Error is based on the mean deviation for triplicate determinations. Percentage recovery is given in parentheses. [b]Not detectable.

concluded that the polarographic method described is as reliable as the commonly recommended spectrophotometric method.

The distillation method is useful for the preconcentration of relatively low concentration of cyanide. As little as 10 $\mu g\ l^{-1}$ cyanide can be preconcentrated by a factor of 10—100 for determination by d.p.p. With the extraction/distillation procedure, 5.0 ng g^{-1} cyanide can be quantified based on the use of a 100-g soil sample; this is similar to the limit of detection of 3.5 ng g^{-1} obtained with the more tedious spectrophotometric method.

Levels of cyanide in soil samples. Of 27 samples obtained from the storage site for the coke blast furnace wastes, only four showed detectable level of soluble cyanide. These were all 20-cm depth samples from four of the nine sampling sites. The soluble cyanide level found in these sites ranged from 6 to 2,402 ng g^{-1} and it was recommended that the contaminated soil from

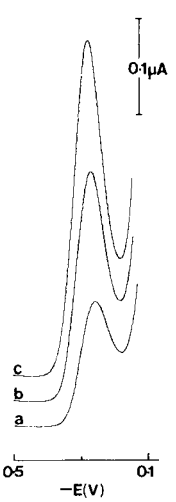

Fig. 2. Determination of soluble cyanide in soil extract by standard additions: (a) sample only; (b) +260 $\mu g\ CN^-\ l^{-1}$; (c) +520 $\mu g\ CN^-\ l^{-1}$. Conditions: 100 g of soil; distillation time, 2 h; mercury drop size, 0.025 cm^2; other conditions as in experimental part.

these sites be removed and replaced in line with the Environmental Protection Authority Guidelines (Victoria, Australia). Figure 2 illustrates the suitability of the d.p.p. method for quantifying soluble cyanide in one of the 20-cm depth samples by standard additions. As would be expected, the surface samples contained no detectable soluble cyanide. The 50-cm depth samples also contained no detectable level of cyanide, which suggests that the loss of cyanide from the surface samples occurs by volatilization or oxidation rather than seepage through the soil. The pH of the samples varied from 6.7 to 9.2, but there was no direct relationship with the levels of soluble cyanide in the four samples.

The authors are grateful to the Geelong Regional Commission for providing the funds for this research.

REFERENCES

1 Annual Book of ASTM Standards, D 2036—81, 1984, pp. 713—734.
2 Quality Criteria for Water, U.S. Environmental Protection Agency, 1976, NTIS Report No. EPA-440/9-76-023, p. 133.
3 M. S. Shuman, J. Water Pollut. Control Fed., 52 (1980) 1083.
4 G. T. Hefter and A. R. Longmore, Int. J. Environ. Anal. Chem., 16 (1984) 315.
5 G. T. F. Wong and P. G. Brewer, Anal. Chim. Acta, 81 (1976) 81.
6 D. Owerbach, J. Water Pollut. Control Fed., 52 (1980) 2647.
7 Standard Methods for the Examination of Water and Waste Water, 14th edn., American Public Health Association, Washington, 1976.
8 J. O. Egekeze and F. W. Oehme, J. Anal. Toxicol., 3 (1979) 119.
9 M. J. 't Hart and R. P. van den Geugten, Stud. Env. Sci., 17 (1981) 523.
10 B. Pihlar, L. Kosta and B. Hristovski, Talanta, 26 (1979) 805.
11 B. Pihlar and L. Kosta, Anal. Chim. Acta, 114 (1980) 275.
12 D. R. Canterford, Anal. Chem., 47 (1975) 88.
13 E. Kirowa-Eisner, D. Talmor and J. Osteryoung, Anal. Chem., 53 (1981) 581.
14 R. D. Rocklin and E. L. Johnson, Anal. Chem., 55 (1983) 4.
15 R. E. Humphrey and S. W. Sharp, Anal. Chem., 48 (1976) 222.
16 Methods for Chemical Analysis of Water and Wastes, EPA-600/4-79-020, Storet No. 00720, EPA, Cincinnati, 1979.
17 I. M. Kolthoff and C. S. Miller, J. Am. Chem. Soc., 63 (1941) 1405.
18 J. H. Karchmer and M. T. Walker, Anal. Chem., 27 (1955) 37.

Analytica Chimica Acta, 188 (1986) 281—283
Elsevier Science Publishers B.V., Amsterdam — Printed in The Netherlands

Short Communication

AUTOMATED FLOW-INJECTION PROCEDURES FOR GLYCEROL AND TRIGLYCERIDES

M. MASOOM
Institute of Biochemistry, University of Baluchistan, Quetta (Pakistan)
P. J. WORSFOLD*
Department of Chemistry, University of Hull, Hull HU6 7RX (Great Britain)
(Received 18th June 1986)

Summary. An automated flow-injection manifold with stopped flow and merging zones is reported for the determination of triglycerides (50—250 mg dl^{-1}) and glycerol (5.0×10^{-6}—1.0×10^{-2} M). In each case, a single reagent cocktail (20 μl) is synchronously merged with sample (20 μl) and the rate of formation of NADH monitored spectrophotometrically at 340 nm. For glycerol, the reagent contains glycerol dehydrogenase and NAD in Tris buffer, pH 8.0; for triglycerides, lipase is also included. The correlation coefficient for triglycerides over the range 50—250 mg dl^{-1} was 0.971.

Serum triglyceride and cholesterol levels are important diagnostic indicators for various forms of hyperlipoproteinaemia [1]. The two sources of triglycerides in serum are dietary intake (exogenous triglycerides) and synthesis in fatty tissue (endogenous triglycerides); both sources are metabolized by a variety of lipases to form free fatty acids and glycerol. This reaction forms the basis of several spectrophotometric [2, 3], fluorimetric [4] and enzymatic [5, 6] procedures for the determination of serum triglycerides.

This communication describes an automated flow-injection manifold, based on merging zones, for the determination of glycerol and triglycerides according to the following reactions;

$$\text{Triglycerides} + 3H_2O \xrightarrow{\text{lipase}} \text{glycerol} + 3 \text{ fatty acids}$$

$$\text{Glycerol} + NAD^+ \xrightarrow{\text{glycerol dehydrogenase}} \text{dihydroxyacetone} + NADH + H^+$$

The formation of NADH is monitored at 340 nm and, under appropriate conditions, the rate of reaction is proportional to the concentration of glycerol or triglycerides.

Experimental

Reagents and standards. Aqueous glycerol standards covering the range 5.0×10^{-6}—1.0×10^{-2} M were prepared in 0.05 M Tris buffer at pH 8.0.

0003-2670/86/$03.50

Triglyceride standards covering the range 50—250 mg dl^{-1} were prepared from a lyophilized lipid control serum (Lipid Control-E; Sigma) reconstituted in 0.05 M Tris buffer at pH 8.0. Glycerol dehydrogenase (glycerol:NAD^+2-oxidoreductase; E.C. 1.1.1.6., from *Enterobacter aerogenese*; Boehringer) was obtained as a lyophilized powder with an activity of 250 U mg^{-1}. Lipase (triacylglycerol acylhydrolase; E.C. 3.1.1.3., from *Candida cylindracea*; Boehringer) was obtained as a lyophilized powder with an activity of 670 U mg^{-1}. The reagent used for the direct determination of glycerol contained glycerol dehydrogenase (2 U ml^{-1}), ammonium chloride (8.0×10^{-3} M) and NAD (0.012 M) in Tris buffer (0.05 M) at pH 8.0. The reagent used for the determination of triglycerides was the same with the addition of lipase (670 U ml^{-1}).

Instrumentation and procedures. An automated merging-zones manifold was used as described previously [7]. The detector was a single-beam spectrophotometer (LKB Ultrospec) equipped with an 8-μl flow cell. Standard solutions (20 μl) and reagent (20 μl) were simultaneously injected into separate streams of Tris buffer (0.05 M) at pH 8.0, each pumped at 2.5 ml min^{-1} using a peristaltic pump (Ismatec Mini S-820). The zones were merged 12 cm downstream, passed through a 50-cm, 0.5-mm i.d. reaction coil and a packed reactor (2.5 cm × 1.5 mm i.d.) containing glass beads (0.50—0.75 mm diameter) and then into the flow cell. The merged zones were stopped in the flow cell for 120 s and the absorbance was monitored at 340 nm. All standards and reagents were prepared daily and all standards were injected in triplicate.

Results and discussion

The use of an automated flow-injection manifold with merging zones for the fluorimetric determination of enzyme activity levels in serum has been reported [7]. The results presented here show that the substrates can be determined in a similar fashion and that spectrophotometric detection can also be used. The calibration data for glycerol (5×10^{-6}—1×10^{-2} M) and

TABLE 1

Calibration data for glycerol and triglycerides

Glycerol		Triglycerides	
Concentration (M)	Rate[a] (abs. min^{-1})	Concentration (mg dl^{-1})	Rate[a] (abs. min^{-1})
0	0.0035	—	—
5.0×10^{-6}	0.0038	50	0.016
1.0×10^{-5}	0.0065	100	0.056
1.0×10^{-4}	0.0110	150	0.140
1.0×10^{-3}	0.0280	200	0.277
1.0×10^{-2}	0.0506	250	0.398

[a]Mean of 3 readings.

triglycerides (50—250 mg dl^{-1}) are given in Table 1. The correlation coefficient for the triglycerides calibration graph was 0.971 (n = 5), with the standards covering the range of clinical interest.

The hydrolysis of triglycerides by lipase is relatively slow [8] and therefore a high lipase activity was maintained in the reagent cocktail. The sampling rate for quantitative purposes was still only 25 h^{-1}, however, because of the 120-s stop time in the flow cell. The sampling rate could be considerably improved if the technique was used for semi-quantitative screening purposes. For diagnostic use, the procedure could be used in conjunction with a previously reported flow-injection method for the determination of cholesterol [9].

REFERENCES

1 R. Richterich and J. P. Colombo, Clinical Chemistry, Wiley, Chichester, 1981, pp. 439—450.
2 L. A. Carlson and L. B. Wadström, Clin. Chim. Acta, 4 (1959) 197.
3 F. G. Soloni, Clin. Chem., 17 (1971) 529.
4 D. Mendelson and A. Antonis, J. Lipid Res., 2 (1961) 45.
5 G. Bucolo and H. David, Clin. Chem., 19 (1973) 476.
6 J. E. Wakayama and R. J. Swanson, Clin. Chem., 23 (1977) 223.
7 M. Masoom and P. J. Worsfold, Anal. Chim. Acta, 179 (1986) 217.
8 P. Desnuelle and P. Savary, J. Lipid Res., 4 (1963) 369.
9 M. Masoom and A. Townshend, Anal. Chim. Acta, 174 (1985) 293.

Analytica Chimica Acta, 188 (1986) 285—288
Elsevier Science Publishers B.V., Amsterdam — Printed in The Netherlands

Short Communication

SPECTROPHOTOMETRIC FLOW-INJECTION DETERMINATION OF CELLOBIOSE DEHYDROGENASE ACTIVITY IN FERMENTATION SAMPLES WITH 2,6-DICHLOROPHENOLINDOPHENOL

KAJ ANDRÉ HOLM

Enzyme Microbiological Laboratory, NOVO Research Institute, Novo Allé, DK-2880 Bagsvaerd (Denmark)

(Received 4th March 1986)

Summary. Cellobiose dehydrogenase activity (0.25—1 U ml^{-1}) is monitored by oxidation of cellobiose to cellobionolactone, thus reducing 2,6-dichlorophenolindophenol to a colourless compound. To prevent any β-glucosidase from reacting, gluconolactone is added as inhibitor. The sample throughput is 120 h^{-1}.

Cellobiose dehydrogenase (CBDH) is an extracellular oxidoreductase formed by a number of micro-organisms, e.g., different species of *Sporotrichum* [1, 2]. When grown on cellulosic substrates, CBDH is normally produced together with a number of cellulolytic enzymes [1, 3, 4]. It is highly selective to cellobiose and oligosaccharides, catalyzing the oxidation to the corresponding aldonic acid in the presence of a suitable hydrogen or electron acceptor. However, molecular oxygen cannot be used as oxidizing agent [2]. CBDH may be involved in the enzymatic degradation of cellulose and lignin in wood by minimizing the end-product inhibition of cellulase enzymes by cellobiose. Quinone radicals produced by the action of wood-root fungal laccase on lignin may accept the electrons produced on oxidation of cellobiose [3, 5]. These reduced phenols must play an important role in the breakdown of the aromatic nucleus. Further ring-splitting enzymes are able to catalyze the breakdown of aromatic substances in most fungi [6].

Dekker [5] has reported a manual spectrophotometric method for the determination of CBDH activity, using cellobiose as substrate and dichlorophenolindophenol as electron acceptor. This communication describes a flow-injection analysis (f.i.a.) procedure based on this method. To prevent any β-glucosidase present from reacting, fluconolactone is added as an inhibitor [5].

Experimental

Apparatus. The f.i.a. system consisted of a sampler (Tecator 5007), analyzer (Tecator 5020), heating bath unit (NOVO design), spectrophotometer (Tecator 5022 + 5023), printer (Alphacom 40), and recorder (BBC Servogor 120).

0003-2670/86/$03.50

Reagents. All chemicals used were of analytical-reagent grade. Tris buffer (pH 7.5, 0.2 M) was prepared by dissolving 24.22 g of Tris and 14 ml of concentrated hydrochloric acid in a final volume of 1 l of demineralized water. Cellobiose reagent (4.3 mM) was prepared by dissolving 148 mg of D-cellobiose (Fluka) and 3.25 g of magnesium sulphate heptahydrate in 100 ml of the Tris buffer. Gluconolactone (4.3 mM) was prepared by dissolving 19.2 mg of gluconolactone in 25 ml of pH 5.0 acetate buffer (0.1 M). The 2,6-dichlorophenolindophenol (DCPIP) solution (0.21 mM) was prepared by dissolving 6 mg of DCPIP in 100 ml of the Tris buffer. Enzyme standards, 0.25, 0.5, 0.75, and 1 U ml^{-1} of spray-dried NOVO enzyme, were prepared in the Tris buffer. (One cellobiose dehydrogenase unit is the amount of enzyme which under the standard conditions [2] reduces 1 μmol DCPIP per minute.)

Procedure. The flow diagram used is shown in Fig. 1. The cellobiose substrate, the DCPIP reagent, and the gluconolactone solution are mixed before addition of the enzyme (range 0.25—1 U ml^{-1}). For incubation, the temperature is 50°C and the time 20 s. Absorbance is measured at 605 nm. The decrease in absorbance is a measure of the enzyme activity. When filtered culture broths are analyzed, a sample blank has to be included. This is obtained by replacing the cellobiose reagent by Tris buffer, pH 7.5, 0.2 M.

Results

The f.i.a. procedure was optimized with regard to both the manifold design and the general analytical conditions. Regarding the selectivity of the electron acceptor, it should have a standard redox potential, E'_0, of ca. +0.22 V [5]. The two most obvious artificial electron acceptors which might be used were methylene blue and 2,6-dichlorophenolindophenol (DCPIP). Of these, at pH 7.5 DCPIP is the only possibility [2]. The autoxidation of DCPIP at pH 7 is slow and does not interfere. It is known that DCPIP can inhibit CBDH. Peel [7] found 40% inhibition by 0.4 mM DCPIP. With 0.05 mM DCPIP as used in the present method no inhibition could be detected. As DCPIP is also a pH indicator, 0.2 M Tris buffer, pH 7.5, was used to prevent changes in the dye absorbance resulting from pH changes. DCPIP has an absorbance maximum at 605 nm.

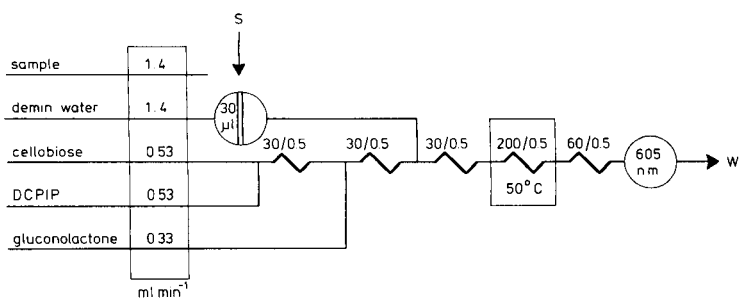

Fig. 1. Flow-injection manifold for CBDH assay. Numbers without units indicate length (cm) and inner diameter (mm) of tubing.

As β-glucosidase can interfere by hydrolyzing the substrate cellobiose to glucose, it is necessary to inhibit the β-glucosidase to achieve accurate results. This can be achieved by the addition of 1 mM gluconolactone [5] in 0.1 M acetate buffer, pH 5.0.

In order to increase the sensitivity of the f.i.a. method, the incubation temperature was changed from 40°C in the manual method to 50°C, which is still well below the optimum for the enzyme (70°C with 5 min incubation); no problem with the stability of the enzyme was experienced. In this way the sensitivity of the f.i.a. method was increased by 72%. For the f.i.a. method, the incubation time (time from addition of the enzyme to the reaction mixture until the peak appears on the recorder) at 50°C is only 20 s. Figure 2 shows that a longer reaction time gives greater sensitivity, as was shown by using the stop-flow facility of the FIA 5020. By increasing the incubation time from 20 s to 45 s, a gain in sensitivity of 214% can be obtained. However, for routine use an incubation time of 20 s is retained.

The pH optimum for the enzyme was found to be pH 7.0. The maximum sensitivity for DCPIP is reached at pH 7.0—7.5. The 0.2 M Tris buffer applied has greatest buffer capacity at pH 7.0—9.2, so pH 7.5 was selected for routine use. Tris is more suitable than a phosphate buffer, as the latter has a weak inhibiting effect on CBDH [2].

Under the established standard conditions, for 0.25, 0.5, and 1 U ml^{-1} CBDH and 0.19, 0.75, and 1.5 g l^{-1} cellobiose, the Michaelis-Menten constant was found to be 16 mg l^{-1} cellobiose (≈47 μM cellobiose) as shown by the Hanes plot [8] (Fig. 3). Substrate inhibition appears at >15 g l^{-1} cellobiose.

Different substrates were tested to investigate the selectivity of CBDH. When the activity of CBDH with 2.5 mM cellobiose was taken as 100%, the following activities were found for a number of other substrates, all at 2.5 mM: glucose, 12%; lactose, 94%; glycerol, 0%; carboxymethylcellulose (Hercules 7 LFD 4 g l^{-1}), 46%.

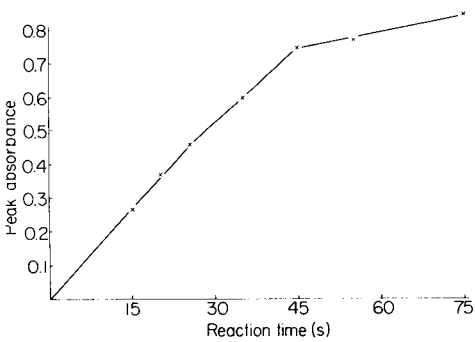

Fig. 2. Peak absorbance of DCPIP at 605 nm as a function of incubation time.

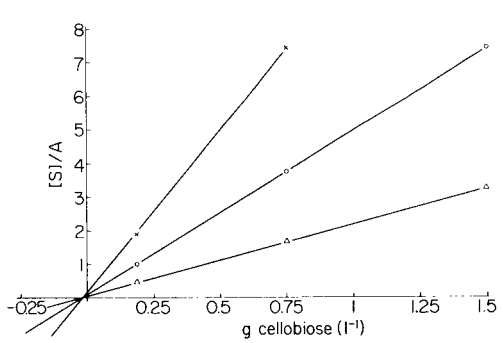

Fig. 3. Determination of the Michaelis constant using Hanes plots. The CBDH concentrations are: (×) 0.25; (○) 0.5; (△) 1.0 U ml^{-1}. [S] = substrate conc., A = peak absorbance.

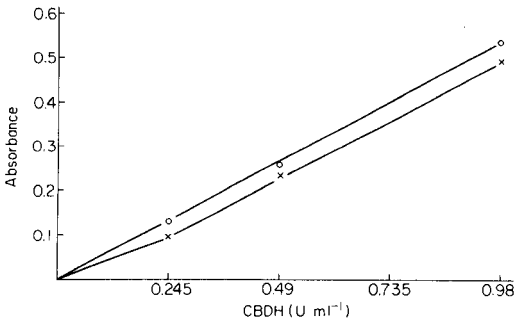

Fig. 4. Calibration plots for CBDH dissolved in: (×) demineralized water; (○) Tris buffer, pH 7.5.

The results described so far were achieved in the absence of magnesium. According to Coudray et al. [2], magnesium enhances CBDH activity. In the present experiments, optimal conditions were obtained with 0.05 M magnesium sulphate in the cellobiose solution, the sensitivity being increased by 18%.

Figure 4 compares the calibration graphs obtained when CBDH was dissolved in demineralized water and in pH 7.5 Tris buffer. A rectilinear graph was obtained only when the enzyme was dissolved in the buffer. Therefore, standards and fermentation broth samples were diluted with Tris buffer before injection.

For a given series of 25 identical fermentation samples analyzed on the same day, the mean peak absorbance was 0.584 (s.d. = 0.0056, r.s.d. = 0.97%). The correlation coefficient between the flow and manual procedure results was 0.96 (N = 40). With the flow procedure, the sample throughput is 120 h^{-1}, compared to about 10 h^{-1} with the manual method.

The author is obliged to G. Skøt for discussions regarding the preparation of this manuscript.

REFERENCES

1 U. Westermark and K. E. Eriksson, Acta Chem. Scand., Ser. B, 28 (1974) 209.
2 M. R. Coudray, G. Canevascini and H. Meier, Biochem. J., 203 (1982) 277.
3 U. Westermark and K. E. Eriksson, Acta Chem. Scand., Ser. B, 28 (1974) 204.
4 U. Westermark and K. E. Eriksson, Acta Chem. Scand., Ser. B, 29 (1975) 419.
5 R. F. H. Dekker, J. Gen. Microbiol., 120 (1980) 309.
6 R. B. Cain, Biochem. J., 108 (1968) 797.
7 J. L. Peel, in J. R. Norris and D. W. Ribbons (Eds.), Methods in Microbiology, Academic Press, London and New York, Vol. 6B, 1972, p. 1.
8 H. Bisswanger, Theorie und Methoden der Enzym Kinetik, Verlag Chemie, Weinheim, 1979, p. 81.

Analytica Chimica Acta, 188 (1986) 289—294
Elsevier Science Publishers B.V., Amsterdam — Printed in The Netherlands

Short Communication

EXTRACTION AND SPECTROPHOTOMETRIC DETERMINATION OF ZINC IN COAL FLY ASH AND POND SEDIMENTS WITH 2-[2-(3,5-DIBROMOPYRIDYL)AZO]-5-DIMETHYLAMINOBENZOIC ACID

TAKEO KATAMI* and TOMOKUNI HAYAKAWA

Gifu Prefectural Research Institute for Environmental Pollution, 8 Chome, Yabuta, Gifu 500 (Japan)

MASAMICHI FURUKAWA and SHOZO SHIBATA

Government Industrial Research Institute, Nagoya, Kita-ku, Nagoya 462 (Japan)

TADASHI HARA

Department of Chemical Engineering, Faculty of Engineering, Doshisha University, Karasuma Imadegawa, Kamigyo-ku, Kyoto 602 (Japan)

(Received 15th April 1986)

Summary. An extraction-spectrophotometric method is described for the determination of traces of zinc with 2-[2-(3,5-dibromopyridyl)azo]-5-dimethylaminobenzoic acid. The reagent forms a stable, blue 1:2 zinc/reagent complex that can be extracted into chloroform. The apparent molar absorptivity of the zinc(II) complex is 1.26×10^5 l mol^{-1} cm^{-1} at 610 nm in chloroform. The reagent is relatively selective; interferences from cobalt, copper and nickel can be masked with dimethylglyoxime and aluminium and iron with a mixture of sodium fluoride and triethanolamine. The method is applied to the determination of zinc in coal fly ash and pond sediments with good precision and accuracy.

Among the numerous spectrophotometric reagents for the determination of zinc, dithizone, di-β-naphthylthiocarbazone and 1-(2-pyridylazo)-2-naphthol are widely used, but they are not sensitive [1]. In studies of organic reagents that provide molar absorptivities of the order of 10^5 l mol^{-1} cm^{-1} for different metals, 2-[2-(3,5-dibromopyridyl)-azo]-5-dimethylaminobenzoic acid (diBr-PAMB) was synthesized and evaluated as a very sensitive chromogenic reagent for cobalt [2] and nickel [3]. Recently, it was shown that diBr-PAMB reacts with zinc in aqueous dioxane solution [4].

In the present communication, an extraction-spectrophotometric method is reported for the determination of zinc with diBr-PAMB. The compound reacts with several metal ions, but most of these do not interfere when sodium fluoride, triethanolamine and dimethylglyoxime are added as masking agents. The zinc complex is readily extracted into chloroform. The proposed method is applied to the determination of microgram amounts of zinc in coal fly ashes and pond sediments.

0003-2670/86/$03.50

Experimental

Apparatus. A Hitachi Model 124 spectrophotometer with 1-cm cells was used for recording spectra and absorbance measurements. Extractions were done with an Iwaki Model KM shaker. The pH was measured with a Denki–Kagaku Model HG-2 pH meter.

Reagents. A 0.05% (w/v) diBr-PAMB solution in *N,N*-dimethylformamide was prepared from pure materials; diBr-PAMB is available commercially (Dojindo Laboratories, Kumamoto). This solution was stable for several months when stored in an amber-coloured bottle.

A standard zinc solution (1.00 g l^{-1}) was prepared by dissolving 99.99% zinc in distilled hydrochloric acid and diluting with redistilled water. Working solutions were prepared by accurate dilution.

Buffer solution, pH 8.5, was made from equal volumes of 0.2 M potassium chloride and 0.2 M boric acid, the pH being adjusted with 0.2 M sodium hydroxide. Organic solvents were purified by conventional methods. The reagents were of analytical grade.

Recommended general procedure. Transfer an aliquot of the slightly acidic sample solution containing 0.4—4.0 μg of zinc to a 100-ml separatory funnel, and dilute to about 20 ml with redistilled water. Add 5 ml of pH 8.5 buffer solution and 0.5 ml of 0.05% (w/v) diBr-PAMB solution. Mix the solution by stirring, add 10 ml of chloroform, and shake vigorously for 1 min. Allow the phases to separate and then transfer the organic layer to a 1-cm glass cell after removing the water by passage through cotton fiber. Measure the absorbance at 610 nm against a reagent blank taken through the same procedure.

Procedure with masking. Transfer an aliquot of sample solution to a 50-ml beaker. Add 2 ml of 10% (w/v) triethanolamine, 1 ml of 10% (w/v) sodium fluoride. Adjust the pH to 8.5 with 4% (w/v) sodium hydroxide, and dilute to about 20 ml with redistilled water. Transfer the solution into a 100-ml separatory funnel and proceed as described above.

Determination of zinc in coal fly ash. Heat a 0.2-g sample of the ash in a 100-ml platinum dish with 1 ml of sulfuric acid, 10 ml of nitric acid, 5 ml of perchloric acid and 10 ml of hydrofluoric acid (all concentrated acids). Evaporate almost to dryness. Dissolve the residue in 20 ml of 1 M hydrochloric acid with heating for 30 min, and then cool to room temperature, transfer to a 100-ml calibrated flask and dilute with redistilled water. Complete the procedure with masking, as described above.

Determination of zinc in pond and sea sediments. Dry a 0.2-g sample of sediment at 110°C for 4 h, transfer the dried sample to a PTFE beaker and add 20 ml of nitric acid (1 + 1). After heating for 1 h, add 5 ml of concentrated nitric acid and 15 ml of hydrofluoric acid and evaporate the solution to 10 ml. Cool, add 20 ml of perchloric acid and 10 ml of hydrofluoric acid and evaporate to 5 ml. Add 20 ml of redistilled water and filter through a 5A filter-paper. Wash the residue with 10 ml of 0.1 M perchloric acid and transfer the filtrate to a 100-ml calibrated flask. Continue the procedure as described for the fly ash.

Results and discussion

Absorption spectra, organic solvent and molar absorptivity. Zinc(II) and diBr-PAMB form a blue complex that can be extracted into chloroform, dichloromethane, 1,2-dichloroethane or nitrobenzene. Of the solvents investigated, chloroform was the best because the extracts exhibited the highest absorbance. The absorption spectra of the zinc/diBr-PAMB complex and the reagent blank in chloroform are shown in Fig. 1. The zinc(II) complex in chloroform exhibits an absorption maximum at 610 nm, where the apparent molar absorptivity of the complex was found to be 1.26×10^5 l mol^{-1} cm^{-1}.

Effect of pH, reagent concentration and shaking time. The effect of varying pH on the extraction of the zinc complex was examined according to the recommended procedure. The final pH of each aqueous solution was measured after extraction. The absorbance was maximum and constant over the pH range 7.0—10.5. Subsequent determinations were done at pH 8.5. The effect of an excess of the chromogenic reagent was examined. It was found that 0.3 ml of 0.05% (w/v) diBr-PAMB solution sufficed to complex 3.5 μg of zinc; with higher concentrations, the absorbance was essentially constant. The minimum shaking time for complete extraction of the zinc complex with chloroform was 20 s at room temperature. The absorbance at 610 nm was stable for at least 24 h.

Nature of the complex and calibration graph. It was previously reported [4] that zinc(II) reacted with diBr-PAMB to form a blue 1:1 (Zn/reagent) complex in 40% (v/v) dioxane solution over the pH range 6–8; the molar absorptivity of the complex was 5.8×10^4 l mol^{-1} cm^{-1} at 605 nm. The absorption spectrum of the zinc complex is shown in Fig. 1 (curve B). The absorbance of this 1:1 complex in aqueous solution above pH 7 decreased

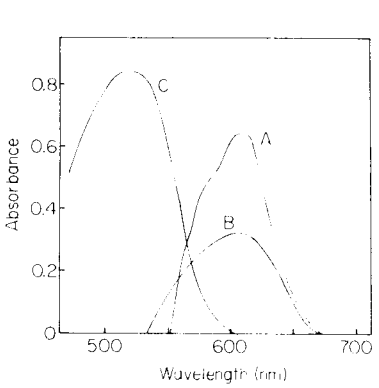

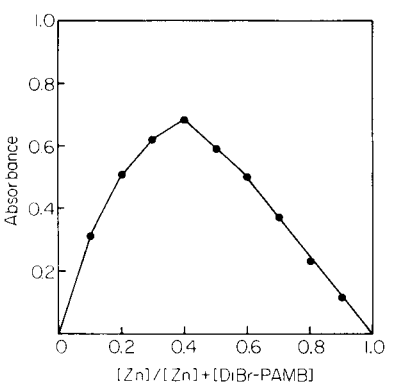

Fig. 1. Absorption spectra of zinc complex against reagent blank: (A) zinc(II) complex extracted into chloroform; (B) zinc(II) complex in 40% (v/v) dioxane solution; (C) reagent blank (2×10^{-5} M) measured against chloroform. Conditions: 5×10^{-6} M zinc(II), 5×10^{-5} M diBr-PAMB, pH 7.0.

Fig. 2. Continuous variation plots of the Zn/diBr-PAMB complex. Wavelength, 610 nm; pH, 8.5; concentration, 3×10^{-5} M.

considerably with increasing pH. Zinc(II) and diBr-PAMB formed only the 1:1 complex in aqueous or 40% (v/v) dioxane solution at pH 6.5, when the reagent added was in a 5–20-fold mole ratio to zinc. However, the stoichiometry of the zinc complex in chloroform was different. The continuous variations method (Fig. 2) showed unequivocally that a 1:2 Zn/reagent complex was formed at pH 8.5, and the molar absorptivity of this 1:2 complex was twice that of the 1:1 complex. Therefore, it seems that the 1:1 complex in aqueous solution is extracted into chloroform to form a 1:2 complex.

The calibration graph obtained by the recommended procedure showed good linearity over the range 0–4.0 μg of zinc per 10 ml of chloroform. Reproducibility tests for 15 results at the 2.5 μg zinc level showed a relative standard deviation of 0.8%. The Sandell sensitivity was 0.5 ng Zn cm^{-2} at 610 nm.

Effect of diverse ions. The selectivity of diBr-PAMB is relatively good compared with that of other reagents [1]. Numerous ions were examined by applying the method to 2.5 μg of zinc in the presence of increasing amounts of the ion tested. The tolerance limit was taken as the amount giving an error of ±2% in the absorbance. For the determination of 2.5 μg of zinc by the recommended procedure, foreign ions and compounds can be tolerated at the levels listed in Table 1. As can be seen, many cations can be tolerated at levels of 1 mg. However, cobalt(II), copper(II), nickel(II) and palladium(II) form intensely coloured complexes with diBr-PAMB, and aluminium(III), cadmium(II), iron(III), manganese(II), tin(IV) and titanium(IV) interfere. These interferences can be decreased by the addition of appropriate masking agents (Table 2). Cobalt, copper and nickel can be masked with dimethylglyoxime and aluminium and iron with sodium fluoride and triethanolamine. For the determination of zinc in a synthetic aqueous sample (20 ml) that contained 2.5 μg of zinc, 2 mg of aluminium, 1 mg of iron, 100 μg of

TABLE 1

Tolerance limits for the determination of zinc (2.5 μg)

Amount tolerated (mg)	Ion or compound added
500	Cl^-, NO_3^-, ClO_4^-, SO_4^{2-}
200	Triethanolamine
100	Sodium fluoride
50	Dimethylglyoxime, potassium iodide, phenol, sodium thiosulfate
20	Sodium citrate
10	Sodium tartrate, thiourea
1	As(III), Ca(II), Hg(II), Li(I), Mg(II), Mo(VI), Rb(I), Sb(III), Se(IV), Si(IV), Sr(II), W(VI)
0.5	Pb(II), V(V)
0.1	Ba(II)
0.05	Ag(I), Bi(III), Cr(VI)

TABLE 2

Elimination of interferences on zinc (2.5 μg) by addition of masking agents

Ion	Masking agent[a] and amount (mg)	Amount tolerated (μg)	
		Without masking agent	With masking agent
Al(III)	NaF (100)/TEA (200)	5	2000
Cd(II)	$Na_2S_2O_3$ (50)	5	100
Co(II)	DMG (20)	0.5	50
Cu(II)	DMG (20)	1	500
Fe(III)	NaF (100)/TEA (200)	5	1000
Ni(II)	DMG (20)	0.2	100
	NaF (100)/TEA (200)	–	1
Mn(II)	Na citrate (20)	5	30
Pd(II)	$Na_2S_2O_3$ (50)	5	1000
Sn(IV)	TEA (200)	2	100
Ti(IV)	NaF (100)/TEA (200)	1	100

[a]TEA, triethanolamine. DMG, dimethylglyoxime.

titanium, and 1 μg of nickel, sodium fluoride and triethanolamine were used for masking, as described under Experimental, and satisfactory results were obtained.

Applications. Zinc was determined in coal fly ash and in sediments as described under Experimental. The results for some standards and samples (Table 3) show good agreement with the certified values of the standard reference materials and also with the results obtained by an atomic-absorption spectrometric method.

TABLE 3

Determination of zinc in coal fly ash and in sediments

Sample	Zinc content (μg g^{-1})			
	Proposed method		Atomic-absorption spectrometry	
	Mean[a]	Range	Mean[a]	Range
NBS SRM-1633a[b]	220	212–228	219	213–229
Coal fly ash A	140	128–149	138	124–147
Coal fly ash B	74	71–78	75	70–78
Pond sediment[c]	339	333–348	338	325–346
Sea sediment	401	393–413	404	395–420

[a]Mean of five determinations. [b]Certified value, 220 ± 10 μg g^{-1}. [c]NIES SRM No. 2, certified value 343 ± 17 μg g^{-1}.

In conclusion, the extraction-spectrophotometric method with diBr-PAMB is simple and convenient to use for the determination of zinc in coal fly ash and pond sediments.

REFERENCES

1 See, e.g., Z. Marczenko, Spectrophotometric Determination of Elements, Horwood, Chichester, 1976.
2 T. Katami, T. Hayakawa, M. Furukawa and S. Shibata, Analyst, 108 (1983) 864.
3 T. Katami, T. Hayakawa, M. Furukawa and S. Shibata, Analyst, 109 (1984) 731.
4 T. Katami, T. Hayakawa, M. Furukawa, S. Shibata and T. Hara, Anal. Sci., 2 (1986) 169.

Analytica Chimica Acta, 188 (1986) 295—300
Elsevier Science Publishers B.V., Amsterdam — Printed in The Netherlands

Short Communication

ASSAY OF MIXTURES OF CHLORPHENIRAMINE MALEATE, PYRILAMINE MALEATE AND PHENYLPROPANOLAMINE HYDROCHLORIDE IN COLD-ALLERGY TABLETS BY DIFFERENCE SPECTROPHOTOMETRY

HENRY S. I. TAN* and GERALDINE C. SALVADOR

College of Pharmacy, University of Cincinnati-Medical Center, Cincinnati, OH 45267 (U.S.A.)

(Received 28th April 1986)

Summary. Mixtures of chlorpheniramine maleate (CPM) and phenylpropanolamine hydrochloride (PPA), with and without pyrilamine maleate (PRM), are assayed by u.v. difference spectrophotometry without prior separation. The spectra for CPM and PRM in solutions at pH 1 and pH 6 show differences whereas the spectra for PPA remain the same at pH 1 and 6. For PPA, quantitation is based on the spectral change on oxidation to benzaldehyde with metaperiodate; this oxidation does not affect CPM and PRM. Calibration plots are linear for 6.7—99.6 $\mu g\ ml^{-1}$ CPM (r = 0.9992), 12.7—50.6 $\mu g\ ml^{-1}$ PRM (r = 0.9997) and 25—115.3 $\mu g\ ml^{-1}$ PPA (r = 0.9980) in the presence of one another. Average recoveries (± RSD) from simulated PPA/CPM tablets were: PPA, 98.4 ± 0.4% (without PRM, n = 3), 99.8 ± 0.4% (with PRM, n = 5); CPM, 99.3 ± 0.6% (without PRM, n = 3), 99.2 ± 0.4% (with PRM, n = 5); and PRM, 99.5 ± 0.2% (in PPA/CPM/PRM tablets, n = 5). The method was successfully applied to commercial cold-allergy tablets containing these compounds.

Many cold and allergy tablets contain mixtures of chlorpheniramine maleate and phenylpropanolamine hydrochloride with and without pyrilamine maleate. Because of interferences, there were no easy methods of quantifying these three compounds in tablets. A simple and reliable assay was needed for quality control. Mixtures of chlorpheniramine maleate and phenylpropanolamine hydrochloride have been assayed by gas chromatography [1, 2]. The phenylpropanolamine content in mixtures with chlorpheniramine has been determined by spectrophotometry after reaction with ninhydrin [3] and by fluorimetry with the fluorescamine derivative [4]; the chlorpheniramine content was not quantified in these studies. High-performance liquid chromatography has been applied to the determination of mixtures of phenylpropanolamine hydrochloride and chlorpheniramine maleate [5] and mixtures of phenylpropanolamine hydrochloride with pyrilamine maleate [5—7]. Doyle and Fazzari [8] suggested the possibility of assaying mixtures of pyrilamine maleate and chlorpheniramine maleate by difference spectrophotometry but did not report experimental conditions or results. Fabrizio [9] developed a programmed-temperature gas-chromatographic method for

0003-2670/86/$03.50

the assay of mixtures of phenylpropanolamine, chlorpheniramine, and pyrilamine with other drugs after formation of the acetyl derivatives.

In an earlier assay [10], mixtures of phenylpropanolamine hydrochloride with guaifenesin or dextromethorphan hydrobromide were determined without prior separation. The phenylpropanolamine content was quantified by difference spectrophotometry and the guaifenesin and dextromethorphan hydrobromide by ordinary absorbance measurements. Difference spectrophotometry avoids interferences by some other active and/or inactive ingredients, provided that the latter components do not undergo spectral changes with change in the sample medium [8]. In this communication, chlorpheniramine, pyrilamine and phenylpropanolamine are assayed by a difference-spectrophotometric method in the presence of each other. Quantitation of chlorpheniramine and pyrilamine is based on the differences in their absorption spectra at pH 1 and pH 6, conditions for which the spectrum of phenylpropanolamine remains unchanged. The assay of phenylpropanolamine is based on a spectral change produced by oxidation to benzaldehyde by metaperiodate [10—12].

Experimental

Drugs and reagents. The drugs used were phenylpropanolamine hydrochloride (Sigma Chemical Co.), chlorpheniramine maleate (Amend Drug and Chemical Co.) and pyrilamine maleate (International Chemical Laboratories). Solutions were aqueous 2.0% (w/v) sodium metaperiodate (Fisher Scientific), aqueous 10.0% (w/v) sodium metabisulfite (Matheson, Coleman and Bell), aqueous 1.5% (w/v) disodium hydrogenphosphate, pH 1 buffer (25 ml of 0.2 M KCl and 54.2 ml of 0.2 M HCl diluted to 100 ml with water) and pH 6.0 buffer (88.9 ml of 0.0667 M monopotassium dihydrogenphosphate and 11.1 ml of 0.0667 M of disodium hydrogenphosphate dihydrate).

Instruments. A DMS-100 u.v.-visible double-beam spectrophotometer (Varian Instruments) with a band width of 1.0 nm or an Acta-V double-beam spectrophotometer (Beckman) with a slit width of 7 mm was used; 1-cm cells were used throughout.

Procedure for chlorpheniramine maleate and phenylpropanolamine hydrochloride mixtures. A standard solution was prepared by dissolving 12 mg of chlorpheniramine maleate and 75 mg of phenylpropanolamine hydrochloride in methanol in a 100-ml volumetric flask and diluting to volume with methanol.

To quantify chlorpheniramine maleate, two 3.0-ml aliquots of the standard solution were transferred to separate 10-ml volumetric flasks; one was diluted to volume with pH 1 solution and the other with pH 6 buffer. The solution at pH 1 was scanned against that at pH 6 and the absorbance was measured at 273 nm.

To quantify phenylpropanolamine hydrochloride, a 10-ml aliquot of the standard solution was transferred to a 50-ml volumetric flask and diluted to volume with methanol. Two 4.0-ml aliquots of this solution were transferred

to separate 10-ml volumetric flasks and treated with aqueous solutions of disodium phosphate, sodium metaperiodate and sodium metabisulfite in the specified order. The absorbance was measured at 251 nm as described previously [10].

Procedure for chlorpheniramine maleate, pyrilamine maleate and phenylpropanolamine hydrochloride mixtures. A standard solution was prepared by dissolving 10 mg of chlorpheniramine maleate, 65 mg of pyrilamine maleate and 125 mg of phenylpropanolamine hydrochloride in methanol in a 100-ml volumetric flask and diluting to volume with methanol.

To quantify chlorpheniramine maleate, two 3.0-ml aliquots of the standard solution were treated exactly as described above.

To quantify pyrilamine maleate, a 10-ml aliquot of the standard solution was diluted to 50.0 ml with methanol. Two 3.0-ml aliquots of this solution were transferred to separate 10-ml volumetric flasks; one aliquot was diluted to volume with pH 1 solution and the other with pH 6 buffer. The solution at pH 1 was measured at 323 nm against the solution in pH 6 buffer.

To quantify phenylpropanolamine hydrochloride, a 10-ml aliquot of the standard solution was diluted to 50.0 ml with methanol. Two 3.0-ml aliquots of this solution were transferred to separate 10-ml volumetric flasks and treated with solutions of disodium phosphate, sodium metaperiodate and sodium metabisulfite and measured at 251 nm as described previously [10].

Procedure for chlorpheniramine maleate/phenylpropanolamine hydrochloride tablets with or without pyrilamine maleate. Twenty tablets were weighed and finely powdered. An aliquot equivalent to about 12 mg of chlorpheniramine (or 2 mg in mixtures containing also pyrilamine maleate) was transferred to a 100-ml volumetric flask. After addition of about 20 ml of methanol and sonication for about 10 s, the mixture was diluted to volume with methanol, shaken and filtered, with the first 5 ml of filtrate being discarded.

To quantify chlorpheniramine maleate, two 3.0-ml aliquots (5.0 ml for mixtures with pyrilamine maleate) of the filtrate were taken to prepare the solutions at pH 1 and pH 6 for measurement as described above.

To quantify phenylpropanolamine hydrochloride in mixtures without pyrilamine maleate, 10.0 ml of the filtrate was diluted to 50.0 ml with methanol. Two 4.0-ml aliquots of this solution were transferred to separate 10-ml volumetric flasks and each was treated as described above with phosphate, metaperiodate, etc. For mixtures with pyrilamine, two 3.0-ml aliquots of the filtrate were treated in the same way without prior dilution.

To quantify pyrilamine maleate, two 3.0-ml aliquots of the filtrate were taken to prepare the solutions at pH 1 and pH 6 for subsequent measurement as described above for pyrilamine maleate.

Results and discussion

To obtain positive difference spectra, the solution at pH 1 is measured against that at pH 6. (All comparison spectra shown below are of equimolar concentrations of the species.) Figure 1 shows the absorption spectra of chlor-

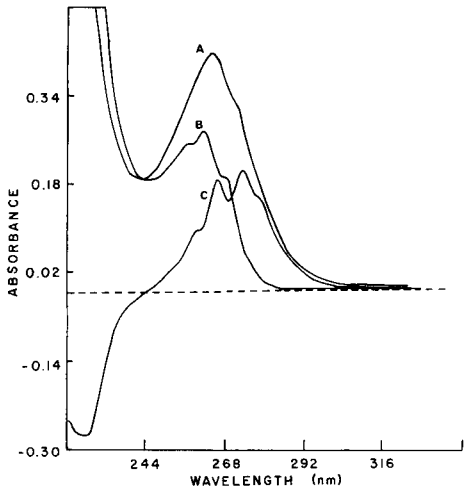

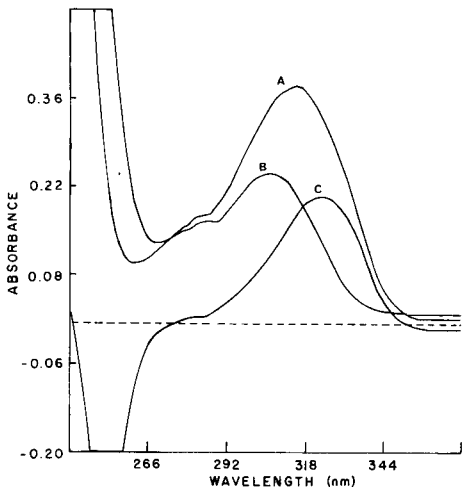

Fig. 1. Absorption spectra of chlorpheniramine maleate: (A) at pH 1; (B) at pH 6; (C) difference spectrum of pH 1 vs. pH 6 solutions.

Fig. 2. Absorption spectra of pyrilamine maleate: (A) at pH 1; (B) at pH 6; (C) difference spectrum of pH 1 vs. pH 6 solutions.

pheniramine in the presence of phenylpropanolamine at pH 1 (λ_{max} = 264 nm) and pH 6 (λ_{max} = 260 nm). The difference spectrum shows maxima at 265.5 and 273 nm and crosses the baseline at the isosbestic wavelength (242 nm). The difference spectrum of chlorpheniramine in the presence of phenylpropanolamine and pyrilamine exhibits absorption maxima at 273 and 280 nm, and an isosbestic point at 264.5 nm.

Pyrilamine maleate shows absorption maxima at 314 nm at pH 1 and at 306 nm at pH 6 with an isosbestic wavelength at 273 nm (Fig. 2). The difference spectrum of pyrilamine shows an absorption maximum at 323 nm. The wavelength selected for quantitation of pyrilamine (323 nm) is not affected by chlorpheniramine because the difference spectrum of the latter is negligible above 300 nm. The isosbestic wavelength of pyrilamine coincides with one of the absorption maxima in the difference spectrum of chlorpheniramine with or without pyrilamine. Accordingly, the wavelength selected for chlorpheniramine is 273 nm. Figure 3 gives the difference spectrum of a mixture of chlorpheniramine and pyrilamine which is overlaid with difference spectra for the same concentrations of these compounds, showing how the individual spectra produce the difference spectrum. The spectrum of phenylpropanolamine is the same at pH 1 and 6; accordingly, this compound does not interfere with the assay of chlorpheniramine and pyrilamine.

The assay of phenylpropanolamine hydrochloride was based on the spectral shift obtained after oxidation of this compound to benzaldehyde by metaperiodate in alkaline solution [10]. Chlorpheniramine and pyrilamine, lacking the —CHOH—CH—NHR structural unit [13], did not react with metaperiodate.

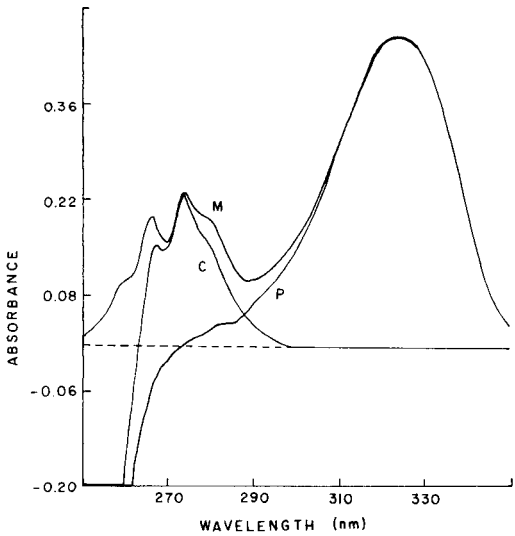

Fig. 3. Difference absorption spectra (pH 1 vs. pH 6) of chlorpheniramine maleate (C), pyrilamine maleate (P), and a mixture (M) containing the two components at similar concentrations as in the individual solutions.

Data presented for chlorpheniramine and pyrilamine maleate were obtained in the presence of phenylpropanolamine hydrochloride. For chlorpheniramine, linearity was established for 6.7—99.6 μg ml^{-1}. Typical regression equations were $A = 11.45\ C - 0.015$ ($r = 0.9998$) in the absence of pyrilamine maleate, and $A = 11.64\ C - 0.007$ ($r = 0.9992$) in the presence of pyrilamine maleate. Linear calibration was obtained for 12.7—50.6 μg ml^{-1} pyrilamine maleate in the presence of chlorpheniramine maleate and phenylpropanolamine hydrochloride with a typical regression equation of $A = 12.21\ C - 0.009$ ($r = 0.9997$). Under these conditions, the following log ϵ ($\pm$ SD) values were obtained from the difference spectra ($n = 4$): chlorpheniramine maleate, 3.639 $\pm$ 0.009 (without pyrilamine maleate) and 3.771 $\pm$ 0.012 (with pyrilamine maleate); pyrilamine maleate, 3.678 $\pm$ 0.006.

Difference spectra for various concentrations of chlorpheniramine maleate with or without pyrilamine maleate and those of various concentrations of pyrilamine maleate. Linear calibration was obtained for 12.7—50.6 μg ml^{-1} at the isosbestic wavelength of each compound. This is an indication that any interferences present have cancelled at this point and therefore, most likely have cancelled also at other wavelengths. For phenylpropanolamine hydrochloride in the presence of chlorpheniramine and pyrilamine maleate, linearity was obtained for 25.0—115.3 μg ml^{-1} with a typical regression equation of $A = 7.59\ C - 0.067$ ($r = 0.9980$) and a log ϵ value of 3.095 $\pm$ 0.034 ($n = 4$).

The difference spectrum for phenylpropanolamine hydrochloride was the same as shown previously [10]. The difference spectra for different concentrations of phenylpropanolamine in the presence of chlorpheniramine and pyrilamine maleate also cross the baseline at its isosbestic point so that the

latter two compounds and other components do not interfere with the assay of phenylpropanolamine.

Validation studies were done by spiking tablet placebos, containing mannitol, starch, magnesium stearate and hydrated soy oil, with accurately weighed quantities of the compounds. Three simulated tablets were prepared containing 11.2—23.1 mg of chlorpheniramine maleate and 74.6—119.8 mg of phenylpropanolamine hydrochloride in each tablet. Recoveries of 98.9—100.0% of chlorpheniramine maleate and 98.0—98.3% of phenylpropanolamine hydrochloride were obtained. This corresponds to average recoveries (± RSD, n = 3) of 99.3 ± 0.6% for chlorpheniramine maleate and 98.4 ± 0.4% for phenylpropanolamine hydrochloride. Five simulated tablets, containing 7.7—11.2 mg of chlorpheniramine maleate, 57.5—64.7 mg of pyrilamine maleate and 117.6—122.3 mg of phenylpropanolamine hydrochloride per tablet, gave recoveries of 98.7—100.0%, 99.3—99.8% and 99.5—100.3%, respectively, resulting in average recoveries (n = 5) of 99.2 ± 0.4%, 99.5 ± 0.2% and 99.8 ± 0.4%, respectively.

Several commercial cold and allergy tablets containing the compounds of interest were selected for assay by the proposed method. Assay of tablets with a label claim of 12 mg of chlorpheniramine maleate and 75 mg of phenylpropanolamine hydrochloride per tablet yielded recoveries of 97.5—99.2% and 96.9—98.4% of label claim, respectively, resulting in average percent recoveries (n = 5) of 98.5 ± 0.7% and 97.9 ± 0.6%, respectively. The recoveries in commercial tablets with label claims of 2.0 mg of chlorpheniramine maleate, 12.5 mg of pyrilamine maleate and 25.0 mg of phenylpropanolamine hydrochloride were 96.5—99.5%, 99.2—100.0% and 97.6—102.8%, respectively, corresponding to average recoveries (n = 4) of 98.4 ± 1.5%, 99.6 ± 0.5% and 100.0 ± 2.3%, respectively. The proposed method is suitable for single dose assay of tablets containing the usual dosages of the compounds.

This paper was presented at the 132nd Annual Meeting of the APhA Academy of Pharmaceutical Sciences, Pharmaceutical Analysis and Control Section, San Antonio, TX, February 1985.

REFERENCES

1 H. Kinsun, M. A. Moulin and E. C. Savini, J. Pharm. Sci., 67 (1978) 118.
2 R. E. Madsen and D. F. Magnin, J. Pharm. Sci., 65 (1976) 924.
3 D. Burke, V. S. Venturella and B. Z. Senkowski, J. Pharm. Sci., 63 (1974) 269.
4 L. S. Shankle, J. Pharm. Sci., 67 (1978) 1635.
5 T. L. Sprieck, J. Pharm. Sci., 63 (1974) 591.
6 V. Das Gupta and A. G. Glanekar, J. Pharm. Sci., 66 (1977) 895.
7 D. R. Heidemann, J. Pharm. Sci., 70 (1981) 820.
8 T. D. Doyle and F. R. Fazzari, J. Pharm. Sci., 63 (1974) 1921.
9 F. De Fabrizio, J. Pharm. Sci., 69 (1980) 855.
10 H. S. I. Tan and G. C. Salvador, Anal. Chim. Acta, 176 (1985) 71.
11 L. Chafetz, J. Pharm. Sci., 60 (1971) 291.
12 H. S. I. Tan and G. C. Salvador, J. Chromatogr., 261 (1983) 111.
13 S. L. Tompsett, Analyst, 92 (1967) 534.

Analytica Chimica Acta, 188 (1986) 301—305
Elsevier Science Publishers B.V., Amsterdam — Printed in The Netherlands

Short Communication

EFFECT OF CROWN-ETHER SURFACTANTS ON FLAME ATOMIC ABSORPTION AND FLAME EMISSION SIGNALS OF SOME MONOVALENT CATIONS

TIMOTHY J. WARD, DANIEL W. ARMSTRONG*, BRONISLAW P. CZECH[a], JACEK F. KOSZUK and RICHARD A. BARTSCH

Department of Chemistry and Biochemistry, Texas Tech University, Lubbock, TX 79406 (U.S.A.)

(Received 30th May 1986)

Summary. Two surface-active and one surface-inactive 18-crown-6 derivatives were synthesized and evaluated for their abilities to enhance flame atomic absorption and flame emission signals of monovalent cations. Enhancements of potassium signals were noted for the surface-active compounds but not for the surface-inactive compound. The critical micelle concentration was determined and compared to the degree of enhancement. Surfactant-induced signal enhancements are not due to the slight or moderate decrease in the size of the aerosol first produced in the nebulizing chamber. Additional mechanistic considerations are discussed.

The use of surfactants to improve the sensitivity in flame atomic spectrometry has been evaluated by several groups [1—6] but there is no consensus as to their effectiveness in enhancing signals or agreement on a cohesive model. Dean [1] observed that "a trace of surfactant" enhanced emission signals obtained in experiments with a premix burner, but later studies contradicted this observation, prompting Dean to discount his previous data and conclude that in premix burners, the vigorous agitation process of aspiration and nebulization impedes the accumulation of detergents at droplet surfaces [2, 6, 7].

Kodama et al. [4] used sodium dodecyl sulfate (SDS) in an improved method for chromium quantitation by atomic absorption spectrometry (a.a.s.) with a premix burner. They observed that the absorbance more than doubled as SDS concentrations were increased up to the critical micelle concentration (c.m.c.) but did not increase further beyond the c.m.c. This enhancement was attributed to the production of smaller droplets during nebulization as a result of reduced surface tension. In a subsequent study of droplet size distribution, Kodama and Miyagawa [5] concluded that surfactants produced aerosols 20—50% finer than those attainable in normal aqueous systems. Venable and Ballard [3] also reported that SDS increased signal intensity in a.a.s.

[a]Current address: Technicon Instruments Corporation, Tarrytown, NY 10591, U.S.A.

0003-2670/86/$03.50

The mechanism of surfactant-induced enhancements in flame atomic spectrometry has been described [7]. Different surfactants and analytes were examined as well as the effects of aspiration rates, fuel/oxidant ratios, burner height, surface tension, viscosity, diffusion rates, etc. It was concluded that the reduction in aerosol droplet size (which resulted from decreased surface tension) was not an important factor in signal enhancements. The role of the surfactant seems to involve interaction with the analyte ion, which concentrates it on the surface of the aerosol. Secondary and tertiary processes can then take place. For example, the surface layers of the primary aerosol can be stripped to form a smaller secondary aerosol enriched in analyte and surfactant. This is akin to aerosol ionic redistribution [8]. The surfactant may also affect desolvation, atomization, etc. Subsequent studies were done by Farino and Browner [9] and Kirkman [10] on surfactant-induced enhancements in flame atomic spectrometry and inductively-coupled plasma emission spectrometry. Again, similarities as well as contradictions were reported. It is also evident that the reported enhancements are not particularly impressive in any of the studies (a maximum of about 2-fold, while 20—90% enhancements are typical). It also seems that it is beneficial to have an attraction or close association between the added surfactant and the metal ion analyte. Also, system variations, particularly in the nebulizing chamber, can have a substantial effect on the observed results.

In this work, three aspects of this phenomenon will be examined which have not been considered previously: (1) the possibility of enhancements being produced by surfactants that complex metal ions rather than attract them electrostatically; (2) possible enhancements for monovalent metal ions; and (3) a comparison of conditions for enhancement of flame emission and atomic absorption signals.

Experimental

Materials. Stock metal ion solutions (0.5 mg l^{-1}) were prepared from analytical-grade reagents. Sodium chloride and potassium chloride (Baker) were dried for 2 h at 110°C before use. Silver nitrate (Fisher Scientific) was used as received. Unless specified otherwise, reagent-grade chemicals and solvents used in synthesis were obtained from commercial suppliers and used as received.

Synthesis of a quaternary ammonium crown ether (1). Triethylamine (0.20 g, 2.0 mmol) and 2-(9-bromononyl)-18-crown-6 [11] (0.30 g, 0.6 mmol) were dissolved in 0.5 ml of ethanol and the solution was stirred in a stoppered flask at 85°C for 24 h. The excess of triethylamine and solvent were removed in vacuo to yield 0.35 g (96%) of **1** as an extremely hygroscopic, white solid (m.p. 35—37°C). Characteristic data are: ^{1}H-n.m.r. ($CDCl_3$) 1.1—1.9 (m, 25), 3.1—4.1 (m, 31); calculated for $C_{27}H_{56}BrNO_6 \cdot 2.5\,H_2O$, 52.7% C, 9.96% H; found, 52.8% C, 9.66% H.

Synthesis of a phosphonic acid crown ether (2). Triethyl phosphite (1.90 g, 11.4 mmol) and 2-(9-bromononyl)-18-crown-6 (0.80 g, 1.7 mmol) were

mixed under nitrogen and heated at 155—160°C (oil bath) for 24 h. The excess of triethyl phosphite was removed in vacuo and the residue was purified by column chromatography on alumina with ethyl acetate as eluent to give a diester (0.86 g, 96%) as a hygroscopic, colorless liquid. The diester (1.6 mmol) was heated with 0.5 ml of trimethylbromosilane at 95°C in a stoppered flask for 1 h. The volatile components were removed in vacuo, 5 ml of methanol was added, and the evaporation was repeated. The crude product was purified on a short alumina column with successive elutions with ethyl acetate, methanol and methanol/HCl (100:3). The last fractions were evaporated to dryness. Chloroform was added, and the mixture was washed with water and dried over magnesium sulfate. Evaporation of the solvent in vacuo gave 0.25 g (31%) of the phosphonic acid as an extremely hygroscopic, pale yellow oil. Characteristic data are: i.r. (neat) 2314 cm^{-1} (POH), 1294 cm^{-1} (P=O), 1119 cm^{-1} (C—O); ^{1}H-n.m.r. ($(CD_3)_2CO$) 0.6- 2.0 (m,18), 2.9—4.3 (m,25); calculated for $C_{21}H_{43}O_9P \cdot 0.25\ H_2O$, 53.0% C, 9.1% H; found, 53.1% C, 9.2% H.

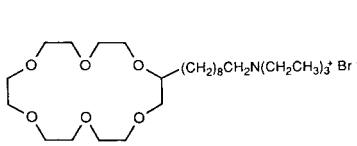

(1)

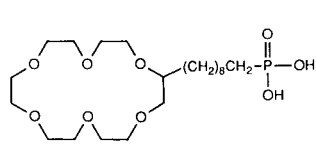

(2)

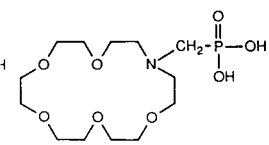

(3)

Synthesis of a phosphonic acid monoaza crown ether (3). This compound was prepared by [12] in 83% yield.

Instrumentation. Atomic absorption and emission measurements were made on a Perkin-Elmer Model 5000 atomic absorption spectrometer with a premix burner. An air/acetylene flame was used for all studies and readings are the average of ten replicate 0.5-s integrations. The flame condition giving the maximum signal was optimized by varying the height of the optical path above the burner. Surface tension was measured with a du Nouy tensiometer with a platinum ring.

Results and discussion

Two of the synthesized crown-ether derivatives were surface-active (**1** and **2**) and one was surface-inactive (**3**). It is well known that 18-crown-6 complexes monovalent cations, in particular potassium [13]. Figure 1 shows the relationship between the surface tension and concentration of compound **1**; a break point indicating the c.m.c. appears at 1.3×10^{-2} M. Previous work suggested that the greatest atomic absorption enhancements usually occur around the c.m.c. for most surfactants. In this work, absorbance was enhanced with increasing surfactant concentration up to and slightly beyond the c.m.c. At a concentration of ca. 3×10^{-2} M, compound **1** gave a maximum enhancement of nearly 80% for potassium absorbance (Fig. 2). At higher surfactant concentrations, the enhancement was less. Under similar conditions,

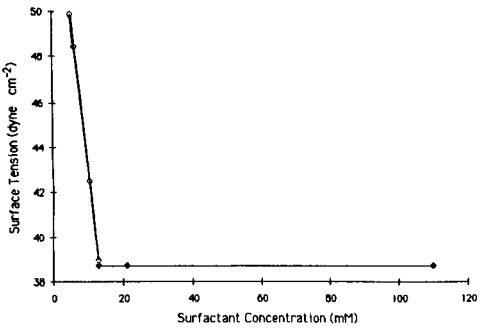

Fig. 1. Surface tension vs. concentration of quaternary ammonium crown surfactant 1.

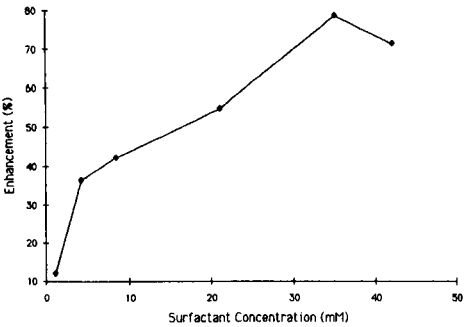

Fig. 2. Percent enhancement of absorbance by potassium (0.5 mg l^{-1}) vs. concentration of quaternary ammonium crown surfactant 1.

the phosphonic acid crown ether, **2**, gave results analogous to those obtained with compound **1**. It is significant that the charge on these surfactants did not affect appreciably the signal enhancement, presumably because complexation is a function of the crown moiety and that electrostatic attraction plays little role in the association of potassium ion and surfactant. Studies conducted with potassium standards at higher concentrations (2, 5, 10 mg l^{-1}) also showed increased sensitivity, but the degree of enhancement was somewhat lower. The experimentally found c.m.c. (based on surface tension) is slightly lower than the surfactant concentration at which the maximum absorbance occurs. Because surfactant aggregation actually occurs over a narrow range of concentrations and c.m.c. values can depend on the method of measurement [14], it is not certain if the aforementioned difference is real or an artifact of the technique used to evaluate the c.m.c.

It could be argued that the observed enhancements were not due to complexation of the metal ion by the surfactant but rather to suppression of ionization or some other effect of compounds **1** and **2**. To investigate this, a related phosphonic acid monoaza crown ether, **3**, without the aliphatic C_8 chain was synthesized. If ionization suppression were significant, some enhancement should still be observed even when the surface-active properties of the crown have been eliminated, as in compound **3**. In no case were any enhancements observed when compound **3** was added to the standard solution. Apparently both surface activity and a close association between the surfactant and analyte are necessary for signal enhancements.

Under identical experimental conditions, surfactant **1** had no apparent effect on the absorbance of silver or sodium ion. The binding of silver and sodium to 18-crown-6 is less than that of potassium. The binding constant of potassium to 18-crown-6 in water is 115 while those of silver and sodium are 39 and <2, respectively [13]. A small enhancement might have been expected for silver, but the bromide present may have prevented this by the formation of silver bromide.

Emission studies were also conducted with surfactant **1** and potassium. After burner height and aspiration rates had been optimized, an enhancement of 45% was observed. Kirkman [10] also noted enhancements for various metals in emission studies with a d.c. plasma spectrometer. For example, cetyltrimethylammonium bromide at a concentration of 4×10^{-3} M gave an enhancement of 50% for cobalt.

It is interesting that the flame emission enhancement for potassium was about half that of the flame absorption enhancement. The solution matrix, conditions and nebulizing chamber were analogous for both experiments. Increasing the relative concentration of analyte in the flame is one way of producing signal enhancements. However, other factors that affect vaporization, desolvation and atomization rates can modify signal intensities. Many of the enhancements observed in this study seem to be consistent with the aerosol ionic redistribution model [8]. The surfactant is undoubtedly present at the air/water interface of the aerosol and is known to complex potassium ion. Any surface stripping of the primary aerosol would produce a smaller, secondary aerosol which would be more likely to reach the flame. However, a comparison of absorption and emission results, as well as enhancements for potassium vs. silver ion indicate that a number of other factors can, and very likely are, affecting these surfactant systems. The roles of other complex equilibria and desolvation and atomization effects have yet to be thoroughly investigated and reported. Such studies would help to elucidate what currently appears to be a very complex multifaceted phenomenon.

We gratefully acknowledge the support of the Division of Basic Chemical Sciences of the Department of Energy (DE-AS058ER13159).

REFERENCES

1 J. A. Dean, Flame Photometry, McGraw-Hill, New York, 1960.
2 E. Pungor and M. Mahr, Talanta, 10 (1963) 537.
3 R. L. Venable and R. V. Ballard, Anal. Chem., 46 (1974) 131.
4 M. Kodama, S. Shimizu, M. Sato and T. Tominaga, Anal. Lett., 10 (1977) 591.
5 M. Kodama and S. Miyagawa, Anal. Chem., 52 (1980) 2358.
6 J. A. Dean and T. C. Rains (Eds.), Flame Emission and Atomic Absorption Spectrometry, M. Dekker, New York, 1969.
7 H. Kornahrens, K. Cook and D. W. Armstrong, Anal. Chem., 54 (1982) 1325.
8 J. A. Boroweic, A. W. Boorn, J. H. Dillard, M. S. Cresser and R. F. Browner, Anal. Chem., 52 (1980) 1054.
9 J. Farino and R. F. Browner, Anal. Chem., 56 (1984) 2709.
10 C. M. Kirkman, Ph.D. dissertation, University of Massachusetts, 1985.
11 B. P. Czech, M. J. Pugia and R. A. Bartsch, Tetrahedron, 41 (1985) 5439.
12 M. Tazaki, K. Nita, M. Takagi and K. Ueno, Chem. Lett., (4) (1982) 571.
13 H. K. Frensdorff, J. Am. Chem. Soc., 93 (1970) 600.
14 D. W. Armstrong, Separation and Purification Methods, 14 (1985) 213.

Analytica Chimica Acta, 188 (1986) 307—310
Elsevier Science Publishers B.V., Amsterdam — Printed in The Netherlands

Short Communication

DETERMINATION OF SELECTED TRACE METALS IN SCALLOPS BY FLAME ATOMIC ABSORPTION SPECTROMETRY AFTER REMOVAL OF SODIUM ON HYDRATED ANTIMONY PENTOXIDE

S. K. NYARKU*, MARK DELMAGE and KATHY SZTURM
Chemistry Department, Brandon University, Brandon, Manitoba R7A 6A9 (Canada)
(Received 28th April 1986)

Summary. Hydrated antimony pentoxide is used to remove sodium ion for the determination of trace metals in scallop specimens of *Plactopecten magellanicus*. The concentrations of Cd, Cr, Co, Cu, Au, Fe, Pb, Mn, Hg, Ni, Ag and Zn were determined in the samples and in a standard reference material. This method yields improved detection limits with simple apparatus.

Marine organisms are known to contain relatively high concentrations of trace metals in some organs. These concentrations are much greater than those found in the marine environment. High levels of manganese and zinc are found in the kidneys and cadmium is concentrated in the digestive glands [1, 2]. The ability of the kidneys to concentrate manganese has been used as a biological indicator to monitor contamination by manganese-54 from atmospheric fall-out [3]; some organs such as the kidneys and the digestive glands appear to be reliable indicators of stable trace metals in the environment.

Hydrated antimony pentoxide (HAP) was used here to obtain improved detection limits in a project designed to follow the seasonal changes in the trace metal concentrations in the scallop species, *Plactopecten magellanicus*, which is common in the waters off the coast of Newfoundland. Hydrated antimony pentoxide is known to remove sodium from strong acid solutions with a retention capacity of 31 mg g^{-1} of HAP [4]. This capacity is fairly independent of the type or concentration of the acid medium, and has been utilized to avoid sodium interference in the determination of trace elements in various matrices by neutron activation [5, 6]. This use of HAP in the determination of trace elements in scallops is effective in removing interferences of sodium and improves the determination of many elements by atomic absorption spectrometry. It is thus possible to determine whether there are significant correlations between elements other than nickel and cobalt [7] in the species.

0003-2670/86/$03.50

Experimental

Sample collection and preparation. The scallop samples were collected in Strawberry Cove, Port Saunders, Newfoundland, in about 5 m of water. They were freeze-dried, placed in plastic vials and weighed. The samples were transferred to a glass Potter-Elvehjem homogenizer fitted with a motorized teflon pestle and metals of interest were quantified in portions of the homogenized samples by neutron activation at the Dalhousie University Slowpoke Reactor facility in Halifax, Nova Scotia. There were no detectable differences in the elemental concentrations between the homogenized and ordinary samples which showed that there was no contamination during the process of homogenization.

Procedures. Approximately 0.75-g samples of the homogenized materials were digested in 5.0 ml of Ultrex nitric acid for about 20 min. This was sufficient for the complete digestion of the scallop samples, but with the Bovine Liver standard reference material, the addition of 30% hydrogen peroxide was necessary to effect complete digestion. About 2.0 ml of the hydrogen peroxide solution was added dropwise to the acid suspension of the scallops. After digestion, the solutions were diluted to 10.0 ml with 3 M nitric acid and quantitatively transferred to previously conditioned disposable polyethylene columns (10-mm i.d., Vermor, Italy, with a 15-ml reservoir) containing 5 g of HAP, which was held in position with quartz wool plugs; the HAP was slurried with water before packing. The effluent was collected at a flow rate of 2.0 ml min^{-1} in a 25.00-ml volumetric flask and the column was washed with 3 M nitric acid to give a total of 25 ml of solution. This solution was aspirated directly into the air/acetylene flame of an atomic absorption spectrometer (Model IL-251, Instrumentation Laboratories), which was used as recommended by the manufacturer.

Calibration. During the initial stages of this study, the method of standard additions was used. Results showed that there were no losses of the added elements during digestion and passage through the column. The addition of 2.0 μg, 4.0 μg and 8.0 μg of each element of interest gave quantitative recoveries in each case. Single-element standards were used subsequently for the determination of trace elements in the NBS SRM-1577 Bovine Liver.

Radiotracer studies were done to evaluate the sodium reduction factor and losses of selected elements during the HAP preconcentration process. The nuclides of interest were added to the digested solutions just before transfer to the HAP column in a total volume of 10 ml. After passage through the column, the effluent was collected and evaporated to 10 ml, and the activities of the nuclides were measured in a well-type sodium iodide detector.

Results and discussion

Table 1 shows the concentrations of trace elements in the Bovine Liver standard reference material by the above procedure. The results agree within the limits of experimental error and indicate that the use of HAP is reliable for the determination of trace elements in biological materials. In the absence of

TABLE 1

Concentrations of trace elements in a standard reference material (SRM-1577 Bovine Liver)

Metal	Metal content ($\mu g\ g^{-1}$)		Metal	Metal content ($\mu g\ g^{-1}$)	
	Certified	This work		Certified	This work
Cadmium	0.27	0.30	Lead	0.34	0.30
Chromium	0.088	<0.1	Manganese	10.3	9.78
Cobalt	(0.18)[a]	0.20	Mercury	0.016	<0.1
Copper	193	190	Nickel	—	2.85
Gold	—	0.38	Silver	0.06	<0.1
Iron	268	261	Zinc	130	128

[a]Tentative value.

HAP, the resulting solutions produced intense yellow flames which prevented the detection of some elements at these low concentrations.

Significant differences in the levels of trace metals were found in samples with different freeze-dried weights. Smaller samples had lower concentrations of trace elements. This observation may account for the fact that samples of scallops from the same area showed variations in the levels of trace metals [1, 2]. The weights, or the ages and sizes, of the samples appear to be important.

Radiotracer studies with ^{22}Na, ^{54}Mn, ^{57}Co and ^{65}Zn showed that >99% of sodium was retained on the HAP column and the percentage retention of the other nuclides was negligible. It was observed that large quantities of HAP were leached from the column during the process and thus the flow rate must be carefully controlled to obtain optimum results. The main factors which are important for the successful application of this method are thorough washing of the HAP column with 3 M nitric acid before use, careful control of the flow rate and acid concentrations greater than 3 M.

The authors acknowledge a Research Grant from Brandon University. We thank Dr. A. Chatt and the staff at the Dalhousie University Slowpoke Reactor Facility for help in the preliminary studies, Len Vassalo, Fisheries Department, St. John's, Newfoundland, for the supply of scallops, and G. Rayner-Canham, Sir Wilfred Grenfell College, Corner Brook, Newfoundland, for his interest.

REFERENCES

1 R. R. Brooks and M. G. Rumsby, Limnol. Oceanogr., 10 (1965) 521.
2 H. M. Fox and H. Ramage, Proc. R. Soc. London, Ser. B., 108 (1931) 157.
3 C. L. Schelske, W. D. C. Smith and J. A. Lewis, Annu. Rep. Bur. Commer. Fish. Radiobiol. Lab., Branfort, NC, 1965; Circ. Fish Wildlife Serv., Washington, 255 (1966).
4 F. Girardi and E. Sabbioni, J. Radioanal. Chem., 1 (1968) 169.

5 F. Girardi, R. Pietra and E. Sabbioni, Proc. 2nd Int. Conf. Mod. Trends Act. Anal., NBS Spec. Publ. 312, 1 (1969) 639.
6 S. K. Nyarku and A. Chatt, J. Radioanal. Chem., 71 (1982) 129.
7 G. W. Rayner Canham, M. Van Roode and J. Burke, Inorg. Chim. Acta, 106 (1985) L37.

Analytica Chimica Acta, 188 (1986) 311—315
Elsevier Science Publishers B.V., Amsterdam — Printed in The Netherlands

Short Communication

DETERMINATION OF MICROGRAM AMOUNTS OF ARSENIC IN GEOLOGICAL MATERIALS AND WATERS BY WAVELENGTH-DISPERSIVE X-RAY FLUORESCENCE SPECTROMETRY

C. M. HEMENS and C. M. ELSON*

Department of Chemistry, Saint Mary's University, Halifax, Nova Scotia B3H 3C3 (Canada)

(Received 24th June 1986)

Summary. Microgram quantities of arsenic are determined in geological materials or water samples by coprecipitating the analyte with elemental selenium and using x-ray fluorescence directly on the precipitate. The coprecipitation step removes elemental interferences and converts the sample to a thin film. The selenium matrix enhances the fluorescent emission of arsenic which enables 0.2 $\mu g\ g^{-1}$ to be determined. The method is applied to a series of geological reference materials and a seawater sample.

The arsenic content of geological materials and natural waters usually cannot be quantified directly by instrumental techniques because of either interferences or the insensitivity of the instruments. Hence, isolation and preconcentration steps form a vital part of the overall determination. Brooks et al. [1] recently listed the instrumental techniques that are presently used along with their detection limits and the accompanying methods of separation. The most popular method for determining arsenic was atomic absorption spectrometry coupled with the hydride-generation procedure and x-ray fluorescence spectrometry (x.r.f.) was the sixth most common technique.

Because geochemists routinely use x.r.f. for major element determinations, it was of interest to develop a separation procedure which, when combined with x.r.f., would quantify microgram amounts of arsenic in rocks and also have a wider application. Recently, selenium was used as a selective and quantitative precipitating agent for arsenic, antimony and gold [2]. The combination of coprecipitation with selenium and quantitation via neutron activation provided a sensitive method of determining arsenic. Since that report, a method of determining arsenic in natural waters has been published based on coprecipitation of magnesium ammonium arsenate along with magnesium ammonium phosphate, and x.r.f. [3]. This latter procedure requires the addition of several reagents, pH adjustments and considerable time. Here, a method to determine microgram quantities of arsenic based on the collection of arsenic by elemental selenium and the direct quantitation of arsenic in the precipitate by wavelength-dispersive x.r.f. is described. The

0003-2670/86/$03.50

method requires the addition of only two reagents following sample digestion and 30 min to complete.

Experimental

Reagents. All chemicals were reagent grade unless otherwise specified. Glassware and teflon-ware were cleaned with warm (1 + 1) nitric acid. Arsenic standard solutions (100 mg l^{-1}) were prepared by dissolving dried arsenic pentoxide (0.1533 g) in 7 ml of 10% (w/v) sodium hydroxide and adjusting the volume to 1 l with 1 M nitric acid. Selenium reagent solutions (500 mg l^{-1}) were prepared by dissolving 0.4081 g of selenous acid in 500 ml of (1 + 9) hydrochloric acid. Tin(II) chloride solutions were prepared by dissolving 20 g of tin(II) chloride dihydrate in 25 ml of warm concentrated hydrochloric acid and diluting to 100 ml.

The rock reference standards were obtained from the U.S. Geological Survey, the Department of Energy, Mines & Resources Canada, the U.S. National Bureau of Standards and the Centre de Recherches Petrographiques et Geochimiques of France.

Procedures. Ground rock samples (0.5—1.0 g) were weighed into teflon beakers and wetted with 10 ml of nitric acid and 10 ml of perchloric acid. The volume was reduced to a thick paste (2—3 ml) by heating on a sandbath and then an additional 3 ml of perchloric acid and 10 ml of hydrofluoric acid were added. The mixture was evaporated to near dryness overnight. The residues were dissolved in (1 + 9) hydrochloric acid, transferred to a volumetric flask and diluted to 100 ml. Two 25-ml aliquots of the sample solutions were pipetted into two 150-ml beakers which contained 25 ml of (1 + 9) hydrochloric acid. A 10-ml aliquot of the selenium reagent solution was then added to each beaker, and a standard spike of 10 μg of arsenic was added to one of the beakers. The solutions were warmed and stirred with a glass rod. A 5-ml aliquot of the tin(II) chloride solution was added to the warm solutions. An additional 3 ml of the tin(II) solution was added after 5 min. The solutions were left to cool and then filtered through the central portion of 1.2-μm filters (Sartorius, 47-mm diameter). The filters were dried at 50° C for 10 min and then mounted for x.r.f. spectrometry.

Water samples were acidified (1 ml HCl/100 ml), filtered and stored in polyethylene bottles after collection. Samples weighing 0.2—0.5 kg were transferred to 600-ml beakers and 20—50 g of concentrated hydrochloric acid was added. The samples were then treated identically to the rock digests commencing with the addition of 10 ml of selenium reagent solution. Reagent blanks were treated in the same way.

Sample mounting and measurements. After drying, the filters were wrapped in a single thickness of plastic tape (3M, Highland Tape, 48-mm wide) ensuring that they remained flat. Excess tape was trimmed off and the filters were placed in modified x.r.f. sample cups which had been machined to accept 47-mm diameter samples. For x.r.f., a Philips PW1400 x-ray fluorescence spectrometry was used with a rhodium-anode tube operated at 60 kV and

40 mA. A 35-mm diameter mask was inserted between the sample and primary collimator. The primary collimator had spacings of 150 μm; the diffracting crystal was LiF(200). Two detectors were used in tandem: a thallium-doped NaI scintillation counter and an argon-filled flow proportional counter. The spectrometer was controlled by a Micro PDP11 computer.

Arsenic concentrations were quantified by using net intensities (average of three readings) of the As K_α x-rays, 2θ angle of 33.985°, and the method of standard additions. Typical counting times were 10 s.

Results and discussion

The acid digestion of the rock samples was done in two stages: the HNO_3/$HClO_4$ stage oxidized As(III) to As(V) prior to the addition of hydrofluoric acid. In this manner, the loss of analyte by volatilization of arsenic trifluoride [4] during the digestion was prevented.

Because the addition of tin(II) reduced iron(III) as well as the selenous acid, a second portion of tin(II) was added to ensure complete precipitation of selenium. The precipitate was easily filtered. On the filter, the precipitate formed a circular patch 25—30 mm in diameter which corresponded to a film thickness of $\leqslant 1$ mg cm^{-2}.

The selenium coprecipitation step is quantitative and highly selective for arsenic, antimony and gold [2]. These elements are believed to be isomorphously included in the selenium matrix. In the present study, the arsenic K_α emission (2θ angle of 33.99°) appeared as a simple, symmetrical peak free from interferences. The emission intensity was a linear function of the amount of arsenic present in the sample. Attempts to quantify arsenic in pressed powder discs were unsuccessful because of a major interference from Lead L_1 emission at 2θ = 33.93° [5]. The present method not only yields the analyte in a thin film format, which increases the sensitivity of the x.r.f. technique, but also eliminates elemental interferences. Furthermore, the intensity of the K_α emission from 10 μg of arsenic(V) spotted on filter papers which were coated with 5 mg of selenium was three times higher than that for a similar amount of arsenic on a plain filter. This enhancement of the arsenic fluorescence is due to the photoelectric absorption of the selenium K_{β_1} and K_{β_2} emissions by the analyte. These selenium emissions have wavelengths (0.0992 and 0.0993 nm) that fall just below the arsenic K edge at 0.1045 nm. Because the sample matrix consists of 5 mg of pure selenium, the intensity of the two Se K_β emissions will be significant. It was observed that the enhancement remained constant as the amount of selenium in the matrix was varied from 1 to 5 mg.

Results for a series of reference geological materials and a seawater sample are presented in Table 1 together with published values. The error limits represent one standard deviation based on 2—4 determinations. In general, the present results are in agreement with published values; the Halifax harbour sample was collected 5 years after the earlier study but the agreement is still reasonable. The detection limits, based on Currie's definition [11], were

TABLE 1

Concentration of arsenic in geological materials and a water sample

Sample	Arsenic concentration ($\mu g\ g^{-1}$)	
	Present work	Published values
BX-N	117 ± 4[a]	120 [7]
NBS-1645	71 ± 2	66[b], 71 [8], 62.6 [2]
SGR-1	68 ± 2	63 [7], 71 [8], 66.7 [2], 74.5 [9], 66 [10]
SY-3	20 ± 3	20 [7]
SY-2	18 ± 0.3	18 [7]
SCO-1	11 ± 2	15 [7], 12.4 [8], 12.2 [2], 10.8 [9], 54.3 [10]
UB-N	13 ± 1	12 [7]
MAG-1	11 ± 1	9.6 [8], 6.0 [10], 8.8 [2]
DR-N	2.5 ± 0.6	3 [7]
Seawater[c]	2 ± 1	0.95 [2]

[a]One standard deviation. [b]NBS recommended value. [c]From Halifax Harbour; results in $\mu g\ l^{-1}$.

0.6 $\mu g\ g^{-1}$ for rocks and 1 $\mu g\ l^{-1}$ for water samples for 10-s counting times. When the counting time was extended to 100 s, the limits were 0.2 $\mu g\ g^{-1}$ and 0.4 $\mu g\ l^{-1}$, respectively. It should be mentioned that these detection limits are based on the results of the x.r.f. measurement step only and do not include the variations that occur as individual samples are processed but they do offer a means of comparing different methods which have similar precisions. These detection limits are similar to those published by Becker et al. [3] but are 22 times higher than those for the selenium coprecipitation with quantitation by neutron activation [2]. Nevertheless, the present method is fast and is easily used to determine microgram quantities of arsenic in rocks and waters.

The authors acknowledge the assistance and cooperation of the X-ray Fluorescence Facility, Saint Mary's University, in particular Mr. Kevin Cameron, and the Natural Sciences and Engineering Research Council of Canada for financial support.

REFERENCES

1 R. R. Brooks, D. E. Ryan and H. Zhang, Anal. Chim. Acta, 131 (1981) 1.
2 C. M. Elson, J. Milley and A. Chatt, Anal. Chim. Acta, 142 (1982) 269.
3 N. S. C. Becker, V. M. McRae and J. D. Smith, Anal. Chim. Acta, 173 (1985) 361.
4 S. Bajo, Anal. Chem., 50 (1978) 649.
5 L. Leoni and M. Saitta, Rend. Soc. Ital. Mineral. Petrol., 32 (1976) 497.
6 R. Jenkins and J. L. DeVries, Practical X-ray Spectrometry, Springer-Verlag, New York, 1967, p. 132.

7 S. Abbey, Studies in Standard Samples of Silicate Rocks and Minerals 1969—1982, Canadian Government Publishing Centre Supply and Services, Quebec, Canada, 1983, p. 78.
8 H. A. van der Sloot, D. Hoede, T. J. L. Klinkers and H. A. Das, J. Radioanal. Chem., 71 (1982) 463.
9 B. P. Fabbi and L. F. Espos, U.S. Geol. Surv. Prof. Pap., 840 (1976) 89.
10 H. A. van der Sloot and J. Zonderhuis, Geostand. Newsl., 3 (1979) 185.
11 L. A. Currie, Anal. Chem., 40 (1968) 586.

Analytica Chimica Acta, 188 (1986) 317—319
Elsevier Science Publishers B.V., Amsterdam — Printed in The Netherlands

Short Communication

SEPARATION OF INORGANIC ANIONS BY UNSUPPRESSED ION CHROMATOGRAPHY

ENRICO BORGARELLO, NICK SERPONE* and SANDRO TORCINI[a]

Department of Chemistry, Concordia University, 1455 deMaisonneuve Blvd. West, Montréal, Québec H3G 1M8 (Canada)

CLAUDIO MINERO and EZIO PELIZZETTI*

Dipartimento di Chimica Analitica, Università di Torino, Via Giuria 5, Torino I-10125 (Italy)

(Received 16th May 1986)

Summary. The elution behaviour of 11 inorganic anions is investigated by unsuppressed ion chromatography with PRP-X100, a macroporous poly(styrene-divinylbenzene) strong-base anion-exchanger. Weak acids (cyanide and sulfide) can be separated and detected at pH 9 with sodium *p*-hydroxybenzoate as the eluent.

Ion chromatography is an attractive technique for the determination of ions in solutions [1]. The method was first developed with conductometric detection to monitor ion-exchange separation. Typically, ions are separated on a column containing a low-capacity ion-exchange resin; the effluent is then passed through a second column (suppressor column) to reduce the equivalent conductance of the eluent [2]. Later, methods were developed which do not require the suppressor column [3]. A low-capacity ion-exchange column is combined with a low-conductivity eluent which can be passed directly through the conductometric detector. Whereas weak acids with $pK_a > 7$ cannot be detected with suppressed ion chromatography, the unsuppressed procedure does permit the detection of such acids when an alkaline eluent is used.

In the present communication, a single-column ion-chromatographic technique is applied to the determination of a series of inorganic anions.

Experimental

All chemicals were used as received from the vendor(s). Stock solutions of each analyte (2000 mg l^{-1}) were prepared and diluted with water as appropriate. The eluents were prepared by dissolving the required amount of substance in water and the pH was adjusted with sodium or potassium hydroxide. Water was distilled, boiled and purged with argon.

[a]Permanent address: CRE/ENEA Casacia Laboratories, Rome, Italy.

0003-2670/86/$03.50

The Wescan liquid chromatograph used was equipped with a 430 Wescan conductivity detector. Separations were done with a Hamilton column (4.1 mm i.d., 10 cm long) packed with PRP-X100 resin; the characteristics of this resin have been reported [4]. The flow rate was 1.5 ml min^{-1}, unless otherwise noted.

Results and discussion

Table 1 summarizes the different retention times for a series of simple inorganic anions at different pH's and with different eluents. Perusal of these data indicates that, for the same eluent and increasing pH, the retention time for any given anion decreases. For a given pH, an increase in the eluent concentration leads to a decrease in retention time. Linearity of the calibration plots was verified for fluoride and chloride over the range 20—100 mg l^{-1}.

It is interesting to note that very weak acids such as hydrogen cyanide and hydrogen sulfide can be detected under appropriately selected conditions. In as much as sulfide and cyanide are dissolved as monovalent anions in the pH range 9—11 (pK_a = 9.3 for HCN and thus partial ionization occurs in this range), the sodium salt of *p*-hydroxybenzoic acid as eluent at pH 8.95 permits both ion exchange and conductometric detection. This separation was recently reported on other columns and with other eluents, as well as with other detection techniques [4—6]. However, the present results demonstrate

TABLE 1

Retention times for various anions at different pH with several eluents

Ion	Retention time (min)[a]									
	4 mM KHP 4.6	4 mM KHP 3.7	2 mM KHP 4.4	2 mM KHP 3.7	2 mM KHP 3.5	1 mM KHP 3.5	1 mM KHP 3.0	6 mM NaBz 6.9	4 mM HBA 8.9	4 mM HBA 8.0
F^-	—	—	—	—	2.8	4.0	—	2.4	—	—
Cl^-	—	3.0	—	—	3.8	5.1	4.9	2.9	2.7	5.2 4.3[b]
NO_2^-	—	3.7	—	—	4.2	5.6	—	3.2	-	6.4[b]
NO_3^-	—	4.35	3.3	4.85	5.4	7.6	—	4.2	5.6	8.4[b] 10.4
Br^-	—	4.0	3.0	4.3	4.8	6.8	—	3.6	4.3	6.8[b] 8.4
SO_4^{2-}	4.0	—	6.5	16.7	—	—	—	8.9	6.6	—
$S_2O_3^{2-}$	—	—	10.6	—	—	—	—	15.2	13.5	—
HS^-	—	—	—	—	—	—	—	—	3.3	—
SCN^-	—	—	15.1	—	—	—	—	21.8	—	—
CN^-	—	—	—	—	—	—	—	—	15.3	—
I^-	—	—	—	—	—	—	—	10.2[c]	—	—

[a]Eluents are KHP (potassium hydrogenphthalate), NaBz (sodium benzoate), HBA (*p*-hydroxybenzoic acid, sodium salt). The numbers underneath are the pH values of the eluents. [b]1.8 ml min^{-1}. [c]Broad peak.

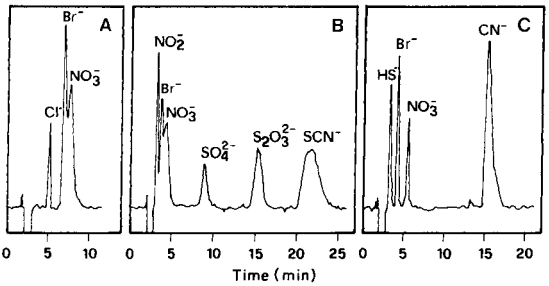

Fig. 1. Separation of various anions at 1.5 ml min^{-1} with different eluents: (A) chloride, nitrate, and bromide at pH 3.5 with 1 mM KHP; (b) nitrite, bromide, nitrate, sulfate, thiosulfate and thiocyanate at pH 6.9 with 6 mM sodium benzoate; (C) sulfide, bromide, nitrate, and cyanide at pH 8.95 with 4 mM sodium *p*-hydroxybenzoate. The 100-μl of injected solution contained each ion noted at the 20 mg l^{-1} level.

that quantitative chromatograms can be obtained for thiocyanate and iodide at reasonable speed compared to earlier data [5].

The separation capability of the column was verified for several different mixtures. Figure 1 illustrates some of the fast and effective separations that can be obtained.

The PRP-X100 resin is a macroporous poly(styrene-divinylbenzene) strong-base anion-exchanger. As shown above, it performs well even at high pH values. The sodium salt of *p*-hydroxybenzoic acid is an excellent eluent even at high pH, while potassium hydrogenphthalate provides good performance in the pH range 3.0—4.6. It is noteworthy that ions such as cyanide and sulfide can be detected under appropriate conditions; because of the toxicity of these anions, numerous methods have been proposed for their determination but many suffer from interferences. Elution with *p*-hydroxybenzoic acid at pH 8.95 provides separation of cyanide and sulfide from each other and from interfering ions.

Support of this work by the Natural Science and Engineering Research Council of Canada and by the Consiglio Nazionale delle Ricerche and the Ministero della Publica Istruzione, Roma, is gratefully acknowledged. S. T. thanks CRE/ENEA for leave. We are also grateful to NATO (grant no. 843/84) for exchange support and to Mr. B. Patterson for lending the chromatograph.

REFERENCES

1 F. C. Smith, Jr. and R. C. Chang, The Practice of Ion Chromatography, J. Wiley, New York, 1983.
2 H. Small, T. S. Stevens and W. C. Bauman, Anal. Chem., 47 (1975) 1801.
3 D. T. Gjerde, J. S. Fritz and G. Schmuckler, J. Chromatogr., 186 (1979) 509.
4 D. P. Lee, J. Chromatogr. Sci., 22 (1984) 327.
5 T. Okada and T. Kuwamoto, Anal. Chem., 57 (1985) 829.
6 J. Weiss and M. Gobl, Frezenius Z. Anal. Chem., 320 (1985) 439.

Analytica Chimica Acta, 188 (1986) 321—327
Elsevier Science Publishers B.V., Amsterdam — Printed in The Netherlands

Book Reviews

K. Grob, *Classical Split and Splitless Injection in Capillary Gas Chromatography*. Hüthig, Heidelberg, 1986 (ISBN 3-7785-1142-4), xv + 324 pp. Price DM 112.

Although capillary gas chromatography has been widely applied for many years, to many users the techniques of sample introduction are still shrouded in mystery. Even experienced practitioners can falter when a familiar approach, being applied successfully in routine work, fails completely with a different type of sample. This is the book to lift the shroud on split and splitless injection! No previous text has attempted such a comprehensive account of these important topics.

The book is divided into four parts; the first two involve detailed discussions of split and splitless injection, respectively, including descriptions of injection devices and the mechanisms involved, along with numerous practical guidelines. Particular emphasis is given to the difficulties of quantitative analysis. Part three is devoted to the problems associated with the syringe in both split and splitless injection, including the evaporation of the sample inside the needle and losses through adsorption. The fact that over 60 pages are given over to this topic emphasises that the handling of the syringe during injection is much more significant than might be expected. The final part of the book deals with programmed-temperature vaporization injection where the sample is introduced into a cold vaporizing chamber which is then rapidly heated. Here the author points out that this relatively new approach has not yet been thoroughly tested and the conclusions drawn are only provisional.

Throughout the book the text is well presented in the usual manner of the Chromatographic Methods Series from Hüthig, with clear paragraph numbering and with important sections highlighted in bold type. Further, the text is strikingly illustrated with numerous line diagrams of the type familiar to those who have read the author's research papers. Being written by a single author, the book presents an integrated approach throughout, being easy to follow and exceptionally well cross-referenced. No one was better equipped to write such a book, and Dr. Grob has produced an important reference work. In the preface he states that a second book is in preparation dealing with on-column injection — I look forward to a further de-mystifying account!

Richard Gill

H. A. M. de Kruijf and H. J. Kool (Eds.), *Organic Micropollutants in Drinking Water and Health*. Elsevier, Amsterdam, 1985 (ISBN 0-444-42583-7). xx + 507 pp. Price Dfl. 360.

It is a sobering thought that over two thousand different organic micropollutants have been detected in potable waters but that less than 20% of these micropollutants have currently been identified. To add to the problem, it has been suggested that the uncertainties in the toxicological data for many of these identified substances may be in the range of one to three orders of magnitude, whilst the uncertainties in the choice of model to assess lifetime risk from these substances may exceed six orders of magnitude.

This book addresses these and related problems and contains contributions from the foremost authorities on the various aspects of organic micropollutants in potable waters. There are 39 papers covering a wide range of topics relating to organic micropollutants including identification techniques, control, legislation, setting of standards, toxicological considerations, effect of treatment processes, chemical and biological removal techniques, effect of disinfectants, alternatives to chlorination, taste and odour considerations, mutagenicity testing and epidemiological studies. The book is highly recommended, not only to research workers in these areas, but to all interested environmental scientists. The only criticisms are that the papers are not grouped into logical sections and that for a book of 507 pages the subject index only occupies one and a half pages. Also, in the reviewer's opinion, the high price will restrict the number of personal copies purchased.

In the U.S.A./Canada, the book is available from Elsevier Science Publishers Co. Inc., P.O. Box 1663, Grand Central Station, New York, NY 10163.

K. C. Thompson

H. Engelhardt (Ed.), *Practice of High Performance Liquid Chromatography. Applications, Equipment and Quantitative Analysis*. Springer-Verlag, Berlin, 1986 (ISBN 3-540-12589-2). xii + 461 pp. Price DM 198.

Rather than attempting a comprehensive coverage, the editor of this compilation of 15 review articles has taken selected topics as illustrations of the applications, equipment, and methods of high performance liquid chromatography as it is currently practised. The articles on equipment include a general survey of instrumentation and discussions of preparative separations and column switching. One of the most useful articles is a detailed review of quantitative analysis in HPLC by Asshauser and Ullner, an important topic which is often ignored in texts on chromatographic methods. Other articles on the methods of HPLC consider liquid—liquid chromatography, ion-pair chromatography, and sample pretreatment methods.

Much of the book covers the applications of HPLC in selected areas including forensic drug analysis, the determination of psychotropic drugs, and the

analysis of natural and synthetic drugs including medicinal herbs. In contrast, there are articles on inorganic analyses and the examination of coal and oil products. The spread of HPLC into biochemistry is represented by articles on the separation of nucleic acids, lipids, and amino-acids and proteins.

Generally, the articles are well written by recognised authorities in their fields and provide an interesting survey of the wide role of HPLC. The coverage is mainly up to mid-1983 with very few later references; "a recent survey" is dated 1982. Overall, this compilation will be a worthwhile addition to any library, where it should be useful to both the practical chromatographer and as a guide to possible applications of the technique.

Roger M. Smith

I. M. Kolthoff and P. J. Elving (Eds.), *Treatise on Analytical Chemistry: Part 1. Theory and Practice, Vol. 10, Section 1. Magnetic Field and Related Methods of Analysis.* Wiley, New York, 1984. 533 pp. Price £61.75.

The first edition of this series appeared around 1959, when most of the techniques dealt with in this volume were either in their infancy or not even conceived. Thus, this second edition has to introduce the techniques of NMR, NQR, ESR and Mössbauer spectroscopy and to elaborate their applicability to modern analytical chemistry against a background of an enormous number of other books and review articles covering these areas. This task is accomplished well, but unevenly. In addition to the spectroscopic methods detailed above, this volume also includes a chapter on secondary-ion mass spectrometry (SIMS), a curious combination.

Chapter one is a standard introduction to the principles of NMR presented in a lucid manner with the minimum of mathematical material. The discussion of structural influences on chemical shifts and coupling constants is supported with tables of typical data. This material could serve as a useful starting point for any chemistry undergraduate, but will be particularly suitable for students of analytical chemistry with the emphasis on quantitative analysis based on thorough appreciation of fundamentals. Two-dimensional techniques are delat with only briefly, but that is relatively unimportant in this case.

The second chapter deals with ^{13}C-NMR in a rather brief fashion. No developments after 1980 are referred to and this presentation has been somewhat overtaken by the growth in the use of complex pulse sequences in heteronuclear NMR.

ESR is not usually regarded as a technique of significant application to analytical problems, but a variety of typical procedures are described in Chapter three. However, there is little reference to analytical problems in medicinal biochemistry, an area which could have been usefully expanded at the expense of the overelaborate detail of instrument structure.

Neither Nuclear Quadrupole Resonance nor Mössbauer spectroscopy are techniques of great value in analytical chemistry and this is confirmed by the

lack of applications in Chapters four and six. However, both articles are excellent introductions to the broader chemical significance of these spectroscopies and might serve to stimulate novel analytical application.

Investigation of the composition of surfaces or thin films by secondary-ion mass spectrometry has expanded vigorously in the last ten years and is becoming an analytical technique of some value in this special area. The experimental and theoretical aspects of SIMS are described in Chapter five, in a superb introduction to this topic. In contrast, the survey of analytical applications is rather brief and is likely to do little more than whet the appetite. Fortunately abundant references are given.

On the whole, this volume meets the objectives of the Editors, to do justice to theory and practice of contemporary analytical chemistry, and should be available to all undergraduates and postgraduates with a need to understand the application of magnetic spectroscopies to analytical chemistry. The book is very well produced and includes a useful general index to all chapters.

D. F. Ewing

A. C. Moffatt, J. V. Jackson, M. S. Moss and B. Widdop (Eds.), *Clarke's Isolation and Identification of Drugs in Pharmaceuticals, Body Fluids and Post-mortem Material, 2nd edn.* The Pharmaceutical Press, London, 1986 (ISBN 0-85-369-166-5). xix + 1223 pp. Price £88.00.

The power and rapid development of analytical science is nowhere better illustrated than in the identification and determination of drugs and other organic compounds, and their metabolites, in body fluids and tissues and in pharmaceutical products. The concentrations involved are often below 1 ng ml^{-1}, and the matrices exceedingly complex. Nowhere are the strategies for such analyses and the relevant properties of such compounds presented in such painstaking detail than in this completely rewritten, second edition of Clarke's much used text.

The book is in four parts. The first (305 pp.) is a collection of 18 chapters, dealing with strategies for analysis in clinical, forensic and sporting situations, quality control, detection of inorganic species and pesticides, and concise descriptions of TLC, GC, HPLC, MS, colour tests, immunoassays, UV/visible spectrophotometry and spectrofluorimetry, IR and NMR. The list of authors reads like a "Who's who" of UK clinical and toxicological analysts, and the information provides a comprehensive account of modern analytical procedures for drugs, pesticides and other compounds, from the sampling and separation stages to the instrumental measurement and interpretation of the results.

Part 2 (763 pp.) is an alphabetical list of compounds with those properties considered relevant. These include the type of activity of the compound, full name and other names, CASE registry number, structural and molecular formula, molecular weight, dissociation constant(s), colour tests, TLC, GC,

HPLC, IR, MS and UV parameters (including UV and IR spectra), references to methods of quantitation, and pharmacokinetics and dose details. Perhaps some spectrofluorimetric information would also have been useful, but the vast amount of data already included should be sufficient for most users. In Part 3, the compounds are tabulated in various ways: in order of increasing molecular weight, melting point, *Rf* values in more than 20 systems, GC retention indices and HPLC k' values also in numerous systems, UV absorption maxima in various aqueous solutions, IR peaks (the 6 with greatest absorbance) and MS peaks (the 8 most intense). Such compilations are well suited to computerization and automated search procedures, and perhaps appropriate software will one day form a useful companion to this book. Part 4 comprises 5 pages detailing the composition of reagents and sources of test materials used in the earlier parts, and is followed by a comprehensive, 51-page index.

This is undoubtedly a very important publication. It is an essential text for laboratories engaged in drug analysis or in analysis of body fluids for toxic materials. Like its predecessor, it will undoubtedly become well thumbed, at the bench as well as in the library, and should serve as the standard reference work on the subject for many years. Dr. Moffatt and his team are to be congratulated on their sustained effort in producing such an excellent compilation.

Alan Townshend

J. G. Nikelly (Ed.), *Advances in Capillary Chromatography*. Hüthig, Heidelberg, 1986 (ISBN 3-7785-1143-2). 138 pp. Price DM 56.00.

Advances in Capillary Chromatography is a most welcome and useful contribution to any library. Not so much a grouping of chapters (edited by J. G. Nikelly), it is more a collection of plenary lectures. The development of an analytical technique is usually characterised by a series of significant developments each of which provides a major leap forward. In this respect it can be argued that the introduction of fused silica capillary columns marks the coming of age of capillary GLC. However, several significant developments have taken place subsequently and these are included in this book.

Amongst the areas reviewed are supercritical fluid chromatography, still an academic pursuit but becoming an accepted research technique, particularly in conjunction with mass spectrometry. Progress in this area is summarised in chapters by Markides and Lee, and Smith, Wright and Udseth. A second tandem technique which is covered is GC/FTIR, an area where progress has been rapid now that FTIR instruments are readily available. Finally, a brief but interesting chapter reviewing the economic aspects of a particular technique (in this case quantitative GC/MS) points the way to future trends.

A very readable and useful little book.

M. Cooke

C. F. Poole and S. A. Schuette, *Contemporary Practice of Chromatography*. Elsevier, Amsterdam, 1984 (ISBN 0-444-424105-5). x + 708 pp. Price Dfl. 159.00 (paperback, ISBN 0-444-42506-3).

The authors' aim is to provide a book which reviews modern gas, liquid and thin-layer chromatography at the first degree and postgraduate level, and which also serves as an overall text for the practising chromatographer. They see the need for this because of the increasing specialisation shown in the literature which covers these techniques. Poole and Schuette have succeeded admirably; their review is as concise as is needed in a very extensive subject, and yet is sufficiently detailed when detail is required. The coverage is extensive, with chapters on basic theory, instrumental requirements for GC, and for HPLC, the column in each technique, and sample preparation. A chapter on "hyphenated methods" describes the coupling of GC and HPLC with MS, FTIR, NMR and optical emission spectroscopy. The final chapter deals with high performance thin-layer chromatography. Careful use is made of the literature, with a reference list at the end of each chapter. The text is illustrated with a large number of instructive figures.

Inevitably, this is a "snapshot" of chromatography as it was at the time of writing and it will date, hopefully not too rapidly! The book is to be welcomed as a comprehensive review of these areas, useful for students and a starting point for practising professionals. Some effort should be made in later editions to correct the many typographical errors which mar the otherwise fine presentation.

In the U.S.A./Canada the book is available from Elsevier Science Publishers Co. Inc., P.O. Box 1663, Grand Central Station, New York, NY 10163.

R. B. Moyes

J. C. Touchstone and M. F. Dobbins, *Practice of Thin Layer Chromatography, 2nd edn.* Wiley, New York, 1983 (ISBN 0-471-09766-7). xxiii + 405 pp. Price £38.00.

This is a revised and updated edition of the earlier invaluable guide to the basic theory and above all to practical aspects of classical TLC which, despite the growth of HPLC, still remains of major importance in chemical, biochemical and pharmaceutical research and quality control. The chapters are detailed and follow a progressive pattern. They deal comprehensively, in a self contained format, with material topic by topic. Early chapters deal with basic concepts, preparation of thin-layer plates, commercial precoated plates, preparation and application of the sample, the mobile phase, developing techniques, visualization procedures, documenting, quantitation and reproducibility of results. These are followed by procedures for use of radioactivity in TLC, discussions of preparative, reversed phase and high performance TLC, special development techniques, e.g. vapour programmed development and

the hot plate method, and finally the combination of TLC with other analytical techniques.

The book is a well illustrated and practical guide to established technologies. The level is at the advanced postgraduate—serious practitioner level. Beginners will find the chapter on the selection of mobile phase to separate specific components of a mixture most helpful. This is an excellent book and is worthy of better than the normal camera-ready typeface format provided.

D. T. Burns

S. Gorog (Ed.), *Advances in Steroid Analysis '84. (Analytical Chemistry Symposium Series, Vol. 23).* Elsevier, Amsterdam, 1985 (ISBN 0-444-99533-1). xii + 604 pp. Price Dfl. 375.00.

Steroid analysis is common in clinical, pharmaceutical and food laboratories, as well as an unfortunate requirement in sports medicine (human and animal). The wide range of compounds that have to be identified and quantified, and the elegant methods of achieving this goal, are clearly demonstrated in this volume. It contains the papers presented at the 2nd Symposium on the Analysis of Steroids, held at Szeged, Hungary in 1984, reproduced from camera-ready copy.

The bulk of the contents concentrate on the techniques used for steroid analysis, mainly radio- and enzyme immunoassays, GC, GC/MS, HPLC, and some spectral and other procedures. There are also some non-technique papers such as structure-function relationships, pharmacokinetics, sport performance and some protein- and receptor binding studies. Finally, there is a good subject index.

The papers, although in a variety of typefaces, are clearly reproduced, and the Figures, often a problem in such publications, are of a high standard. Overall, the book indicates that the methods of steroid analysis have developed markedly over the last decade, and the present text gives a good account of the present state of the art.

In the U.S.A./Canada the book is available from Elsevier Science Publishers Co. Inc., P.O. Box 1663, Grand Central Station, New York, NY 10163.

ANALYTICA CHIMICA ACTA, VOL. 188 (1986)

AUTHOR INDEX

Adeloju, S. B.
— and Gawne, K. M.
Determination of soluble cyanide in soil samples by differential pulse polarography 275
Agterdenbos, J.
— and Bax, D.
A study on the generation of hydrogen selenide and decomposition of tetrahydroborate in hydride-generation atomic absorption spectrometry 127
Armstrong, D. W., see Ward, T. J. 301
Augustyniak, W., see Trojanowicz, M. 165

Bartsch, R. A., see Ward, T. J. 301
Bax, D., see Agterdenbos, J. 127
Berglund, R., see Renman, L. 137
Bergmark, B., see Lundberg, E. 111
Borgarello, E.
—, Serpone, N., Torcini, S., Minero, C. and Pelizzetti, E.
Separation of inorganic anions by unsuppressed ion chromatography 317
Brätter, P., see Chisela, F. 85
Brätter, P., see Frenzel, W. 151
Bryson, L. J., see McCamey, D. A. 119

Chan, K. W., see Lunte, C. E. 263
Chisela, F.
— and Brätter, P.
Determination of trace elements in biological materials by instrumental epithermal neutron activation analysis 85
Christensen, L. H.
— and Drabaek, I.
Energy-dispersive x-ray fluorescence spectrometry of industrial paint samples 15
Czech, B. P., see Ward, T. J. 301

De Jong, H. J., see Weber, J. J. 195
Delmage, M., see Nyarku, S. K. 307
Dowe, R. J., see Pesek, J. J. 101
Drabaek, I., see Christensen, L. H. 15

Ellis, A. T., see Wegscheider, W. 59
Elson, D. M., see Hemens, C. M. 311

Frenzel, W.
— and Brätter, P.
The fluoride ion-selective electrode in flow injection analysis. Part 3. Applications 151
Fuksiewicz, A., see Trojanowicz, M. 165
Furukawa, M., see Katami, T. 289

Gawne, K. M., see Adeloju, S. B. 275
Gilfrich, J. V.
Multilayered structures as dispersing devices in x-ray spectrometry 51
Goldbach, K., see Wegscheider, W. 59
Goliński, M., see Lachowicz, E. 239

Hara, T., see Katami, T. 289
Harrison, R. M., see Hewitt, C. N. 229
Hayakawa, T., see Katami, T. 289
Hayashi, Y., see Taniguchi, A. 95
Heineman, W. R., see Lunte, C. E. 263
Hemens, C. M.
— and Elson, D. M.
Determination of microgram amounts of arsenic in geological materials and waters by wavelength-dispersive x-ray fluorescence spectrometry 311
Hewitt, C. N.
—, Harrison, R. M. and Radojevic, M.
The determination of individual gaseous ionic alkyllead species in the atmosphere 229
Hirayama, K.
— and Leyden, D. E.
Determination of trace amounts of vanadium(IV) and (V) in water by energy-dispersive x-ray fluorescence spectrometry combined with preconcentration and separation 1
Holm, K. A.
—, Spectrophotometric flow-injection determination of cellobiose dehydrogenase activity in fermentation samples with 2,6-dichlorophenolindophenol 285
Houk, R. S., see Serfass, R. E. 73
Høyer, B.
—, Skov, H. J. and Kryger, L.
Computerized system with a hard-wired

data-acquisition unit for potentiometric stripping analysis 205
Hulanicka-Michalak, T., see Trojanowicz, M. 165
Hulanicki, A., see Trojanowicz, M. 165

Iannelli, D. P., see McCamey, D. A. 119
Imakuma, K., see Salvador, V. L. R. 67

Jagner, D., see Renman, L. 137

Kajiwara, K., see Muramatsu, H. 257
Karube, I., see Muramatsu, H. 257
Katami, T.
—, Hayakawa, T., Furukawa, M., Shibata, S. and Hara, T.
Extraction and spectrophotometric determination of zinc in coal fly ash and pond sediments with 2-[2-(3,5-dibromopyridyl)azo]-5-dimethylaminobenzoic acid 289
Köhler, I., see Seil, J. 219
Koszuk, J. F., see Ward, T. J. 301
Krajewski, A., see Lachowicz, E. 239
Kryger, L., see Høyer, B. 205

Labrecque, J. J.
—, Rosales, P. A. and Mejías, G.
Simultaneous determination of lanthanides by radioisotope x-ray fluorescence spectrometry based on characteristic *K*-radiation 9
Lachowicz, E.
—, Krajewski, A. and Goliński, M.
Liquid—liquid extraction of metal ions by the sulfide podand 1,12-di-2-thienyl-2,5,8,11-tetrathiadodecane 239
Leyden, D. E., see Hirayama, K. 1
Leyden, D. E., see Wegscheider, W. 59
Lieth, C. W. v. d., see Seil, J. 219
Lundberg, E.
— and Bergmark, B.
Determination of total tin in geological materials by electrothermal atomic absorption spectrometry 111
Lunte, C. E.
—, Sy-Wen Wong, Ridgway, T. H., Heineman, W. R. and Chan, K. W.
Voltammetric/amperometric detection for flow-injection systems 263

Mahan, K. I., see Wegscheider, W. 59
Mantler, M.
X-ray fluorescence analysis of multiple-layer films 25
Masoom, M.
— and Worsfold, P. J.
Automated flow-injection procedures for glycerol and triglycerides 281
Matuszewski, W., see Trojanowicz, M. 165
McCamey, D. A.
—, Iannelli, D. P., Bryson, L. J. and Thorpe, T. M.
Determination of silicone in fats and oils by electrothermal atomic absorption spectrometry with in-furnace air oxidation 119
Mejías, G., see Labrecque, J. J. 9
Minero, C., see Borgarello, E. 317
Muramatsu, H.
—, Kajiwara, K., Tamiya, E. and Karube, I.
Piezoelectric immuno sensor for the detection of *Canadida albicans* microbes 257
Murphy, K., see Van den Berg, C. M. G. 177

Nyarku, S. K.
—, Delmage, M. and Szturm, K.
Determination of selected trace metals in scallops by flame atomic absorption spectrometry after removal of sodium on hydrated antimony pentoxide 307

Opferkuch, H. J., see Seil, J. 219
Owens, D. S.
— and Sturrock, P. E.
Determination of triazine pesticides by high-performance liquid chromatography with swept-potential electrochemical detection 269

Pałys, M., see Trojanowicz, M. 165
Pelizzetti, E., see Borgarello, E. 317
Pesek, J. J.
—, Rosser, G. L., Dowe, R. J. and Schneider, J. F.
Fluorescence studies of the kinetics of binding and removal of metal ions in proteins 101

Rachetti, A.
— and Wegscheider, W.
A fundamental parameters approach including scattered radiation for monoenergetically excited samples in energy-dispersive x-ray fluorescence spectrometry 37
Radojevic, M., see Hewitt, C. N. 229

Raszewski, S., see Trojanowicz, M. 165
Renman, L.
—, Jagner, D. and Berglund, R.
Computer system and flow cell for automated potentiometric and constant-current stripping analysis 137
Ridgway, T. H., see Lunte, C. E. 263
Riley, J. P., see Van den Berg, C. M. G. 177
Rosales, P. A., see Labrecque, J. J. 9
Rosser, G. L., see Pesek, J. J. 101
Røyset, O.
— and Thomassen, Y.
Activated carbon as adsorbent for alkyl-lead in air 247

Salvador, G. C., see Tan, H. S. I. 295
Salvador, V. L. R.
— and Imakuma, K.
Determination of trace metals in nuclear-grade uranium dioxide by x-ray fluorescence spectrometry 67
Schneider, J. F., see Pesek, J. J. 101
Seil, J.
—, Köhler, I., Lieth, C. W. v. d. and Opferkuch, H. J.
Interpretation of infrared spectra based on statistical approaches 219
Serfass, R. E.
—, Thompson, J. J. and Houk, R. S.
Isotope ratio determinations by inductively-coupled plasma/mass spectrometry for zinc bioavailability studies 73
Serpone, N., see Borgarello, E. 317
Shibata, S., see Katami, T. 289
Skov, H. J., see Høyer, B. 205
Sturrock, P. E., see Owens, D. S. 269
Sy-Wen Wong, see Lunte, C. E. 263
Szturm, K., see Nyarku, S. K. 307
Szyller, J., see Trojanowicz, M. 165

Tamiya, E., see Murgmatsu, H. 257
Tan, H. S. I.
— and Salvador, G. C.
Assay of mixtures of chlorpheniramine maleate, pyrilamine maleate and phenylpropanolamine hydrochloride in cold-allergy tablets by difference spectrophotometry 295
Taniguchi, A.
—, Hayashi, Y. and Yuki, H.
Determination of cholesterol with a laboratory-built chemiluminescence system 95
Thomassen, Y., see Røyset, O. 247
Thompson, J. J., see Serfass, R. E. 73
Thorpe, T. M., see McCamey, D. A. 119
Torcini, S., see Borgarello, E. 317
Trojanowicz, M.
—, Hulanicki, A., Matuszewski, W., Pałys, M., Fuksiewicz, A., Hulanicka-Michalak, T., Raszewski, S., Szyller, J. and Augustyniak, W.
Flow-injection catalytic determination of molybdenum with biamperometric detection in a microprocessor-controlled system 165

Van den Berg, C. M. G.
—, Murphy, K. and Riley, J. P.
The determination of aluminium in seawater and freshwater by cathodic stripping voltammetry 177
Van Thuijl, J., see Weber, J. J. 195

Wang, J.
— and Zadeii, J. M.
Stripping voltammetry of thorium based on adsorptive accumulation 187
Ward, T. J.
—, Armstrong, D. W., Czech, B. P., Koszuk, J. F. and Bartsch, R. A.
Effect of crown-ether surfactants on flame atomic absorption and flame emission signals of some monovalent cations 301
Weber, J. J.
—, Van Thuijl, J. and De Jong, H. J.
Principal component analysis applied to collisionally-activated-decomposition mass spectra of alkylbenzenes 195
Wegscheider, W., see Rachetti, A. 37
Wegscheider, W.
—, Ellis, A. T., Goldbach, K., Leyden, D. E. and Mahan, K. I.
Use of sensitivity as a function of fluorescent x-ray energy in energy-dispersive x-ray spectrometry 59
Worsfold, P. J., see Masoom, M. 281

Yuki, H., see Taniguchi, A. 95

Zadeii, J. M., see Wang, J. 187

ontinued from outside back cover)

ripping voltammetry of thorium based on adsorptive accumulation
J. Wang and J. M. Zadeii (Las Cruces, NM, U.S.A.) 187

mputer Methods and Applications
incipal component analysis applied to collisionally-activated-decomposition mass spectra of alkylbenzenes
J. J. Weber, J. van Thuijl and H. J. de Jong (Leiden, The Netherlands) 195
omputerized system with a hard-wired data-acquisition unit for potentiometric stripping analysis
B. Høyer, H. J. Skov and L. Kryger (Aarhus, Denmark) 205
terpretation of infrared spectra based on statistical approaches
J. Seil, I. Köhler, C. W. v. d. Lieth and H. J. Opferkuch (Heidelberg, F.R.G.) 219

parations
ne determination of individual gaseous ionic alkyllead species in the atmosphere
C. N. Hewitt (Lancaster, Gt. Britain), R. M. Harrison and M. Radojevic (Colchester, Gt. Britain) 229
quid—liquid extraction of metal ions by the sulfide podand 1,12-di-2-thienyl-2,5,8,11-tetrathiadodecane
E. Lachowicz, A. Krajewski and M. Goliński (Warsaw, Poland) 239
ctivated carbon as adsorbent for alkyllead in air
O. Røyset and Y. Thomassen (Oslo, Norway) 247

ort Communications
ezoelectric immuno sensor for the detection of *Candida albicans* microbes
H. Muramatsu (Chiba, Japan), K. Kajiwara, E. Tamiya and I. Karube (Yokohama, Japan) 257
oltammetric/amperometric detection for flow-injection systems
C. E. Lunte, Sy-Wen Wong, T. H. Ridgway, W. R. Heineman (Cincinnati, OH, U.S.A.) and K. W. Chan (Fresno, CA, U.S.A.) 263
etermination of triazine pesticides by high-performance liquid chromatography with swept-potential electrochemical detection
D. S. Owens and P. E. Sturrock (Atlanta, GA, U.S.A.) 269
etermination of soluble cyanide in soil samples by differential pulse polarography
S. B. Adeloju and K. M. Gawne (Victoria, Australia) 275
utomated flow-injection procedures for glycerol and triglycerides
M. Masoom (Quetta, Pakistan) and P. J. Worsfold (Hull, Gt. Britain) 281
ectrophotometric flow-injection determination of cellobiose dehydrogenase activity in fermentation samples with 2,6-dichlorophenolindophenol
K. A. Holm (Bagsvaerd, Denmark) 285
traction and spectrophotometric determination of zinc in coal fly ash and pond sediments with 2-[2-(3,5-dibromopyridyl)azo]-5-dimethylaminobenzoic acid
T. Katami, T. Hayakawa (Gifu, Japan), M. Furukawa, S. Shibata (Nagoya, Japan) and T. Hara (Kyoto, Japan) 289
ssay of mixtures of chlorpheniramine maleate, pyrilamine maleate and phenylpropanolamine hydrochloride in cold-allergy tablets by difference spectrophotometry
H. S. I. Tan and G. C. Salvador (Cincinnati, OH, U.S.A.) 295
ffect of crown-ether surfactants on flame atomic absorption and flame emission signals of some monovalent cations
T. J. Ward, D. W. Armstrong, B. P. Czech, J. F. Koszuk and R. A. Bartsch (Lubbock, TX, U.S.A.) 301
etermination of selected trace metals in scallops by flame atomic absorption spectrometry after removal of sodium on hydrated antimony pentoxide
S. K. Nyarku, M. Delmage and K. Szturm (Brandom, Man., Canada) 307
etermination of microgram amounts of arsenic in geological materials and waters by wavelength-dispersive x-ray fluorescence spectrometry
C. M. Hemens and D. M. Elson (Halifax, Nova Scotia, Canada) 311
paration of inorganic anions by unsuppressed ion chromatography
E. Borgarello, N. Serpone, S. Torcini (Montreal, Que., Canada), C. Minero and E. Pelizzetti (Torino, Italy) . . 317

ook Reviews 321

uthor Index 329

CONTENTS

(Abstracted, Indexed in: Anal. Abstr.; Biol. Abstr.; Chem. Abstr.; Curr. Contents Phys. Chem. Earth Sci.; Life Sci.; Index Med.; Mass Spectrom. Bull.; Sci Citation Index; Excerpta Med.)

X-Ray Fluorescence Spectrometry

Determination of trace amounts of vanadium(IV) and (V) in water by energy-dispersive x-ray fluorescence spectrometry combined with preconcentration and separation
K. Hirayama and D. E. Leyden (Fort Collins, CO, U.S.A.) 1

Simultaneous determination of lanthanides by radioisotope x-ray fluorescence spectrometry based on characteristic *K*-radiation
J. J. Labrecque, P. A. Rosales and G. Mejías (Caracas, Venezuela) 9

Energy-dispersive x-ray fluorescence spectrometry of industrial paint samples
L. H. Christensen (Roskilde, Denmark) and I. Drabaek (Copenhagen, Denmark) 15

X-ray fluorescence analysis of multiple-layer films
M. Mantler (San Jose, CA, U.S.A.) 25

A fundamental parameters approach including scattered radiation for monoenergetically excited samples in energy-dispersive x-ray fluorescence spectrometry
A. Rachetti and W. Wegscheider (Graz, Austria) 37

Multilayered structures as dispersing devices in x-ray spectrometry
J. V. Gilfrich (Washington, DC, U.S.A.) 51

Use of sensitivity as a function of fluorescent x-ray energy in energy-dispersive x-ray spectrometry
W. Wegscheider (Graz, Austria), A. T. Ellis, K. Goldbach, D. E. Leyden (Fort Collins, CO, U.S.A.) and K. I. Mahan (Pueblo, CO, U.S.A.) 59

Determination of trace metals in nuclear-grade uranium dioxide by x-ray fluorescence spectrometry
V. L. R. Salvador and K. Imakuma (São Paulo, Brasil) 67

Other Spectrometric Methods

Isotope ratio determinations by inductively-coupled plasma/mass spectrometry for zinc bioavailability studies
R. E. Serfass, J. J. Thompson and R. S. Houk (Ames, IA, U.S.A.) 73

Determination of trace elements in biological materials by instrumental epithermal neutron activation analysis
F. Chisela and P. Brätter (Berlin, F.R.G.) 85

Determination of cholesterol with a laboratory-built chemiluminescence system
A. Taniguchi, Y. Hayashi and H. Yuki (Chiba, Japan) 95

Fluorescence studies of the kinetics of binding and removal of metal ions in proteins
J. J. Pesek, G. L. Rosser (San Jose, CA, U.S.A.), R. J. Dowe and J. F. Schneider (Dekalb, IL, U.S.A.) 101

Determination of total tin in geological materials by electrothermal atomic absorption spectrometry
E. Lundberg and B. Bergmark (Umeå, Sweden) 111

Determination of silicone in fats and oils by electrothermal atomic absorption spectrometry with in-furnace air oxidation
D. A. McCamey, D. P. Iannelli, L. J. Bryson and T. M. Thorpe (Cincinnati, OH, U.S.A.) 119

A study on the generation of hydrogen selenide and decomposition of tetrahydroborate in hydride-generation atomic absorption spectrometry
J. Agterdenbos and D. Bax (Utrecht, The Netherlands) 127

Electrometric Methods

Computer system and flow cell for automated potentiometric and constant-current stripping analysis
L. Renman, D. Jagner and R. Berglund (Lund, Sweden) 137

The fluoride ion-selective electrode in flow injection analysis. Part 3. Applications
W. Frenzel and P. Brätter (Berlin, F.R.G.) 151

Flow-injection catalytic determination of molybdenum with biamperometric detection in a microprocessor-controlled system
M. Trojanowicz, A. Hulanicki, W. Matuszewski, M. Pałys, A. Fuksiewicz, T. Hulanicka-Michalak, S. Raszewski, J. Szyller and W. Augustyniak (Warsaw, Poland) 161

The determination of aluminium in seawater and freshwater by cathodic stripping voltammetry
C. M. G. van den Berg, K. Murphy and J. P. Riley (Liverpool, Gt. Britain) 177

(Continued on inside back cover)